University of Bielefeld

Department of Cell Biology

Targeting of MYC- and NF-κB-signaling in primary human cancer stem-like cells

Cumulative Dissertation

Submitted for the fulfilment of the requirements

for the doctoral degree of natural science

Doctor rerum naturalis (Dr. rer. nat.)

By Beatrice Ariane Windmöller

2021

Supervised by

Prof. Dr. Christian Kaltschmidt

Following publications originated within the scope of this PhD Thesis:
(* included in the dissertation)

Original research articles:

1.) *

"A typical carcinoid of the lung - a case report with pathological correlation and propagation of the cancer stem cell line BKZ1 with synaptophysin expression"

Beatrice A. Windmöller, Johannes F. W. Greiner, Christine Förster, Ludwig Wilkens, Fritz Mertzlufft, Jan Schulte Am Esch, Barbara Kaltschmidt, Christian Kaltschmidt, Morris Beshay

Medicine (Baltimore). 2019 Dec; 98(49): e18174. Published online 2019 Dec 10. doi:10.1097/MD.0000000000018174

2.) *

"Isolation and Characterization of Two Novel Colorectal Cancer Cell Lines, Containing a Subpopulation with Potential Stem-Like Properties: Treatment Options by MYC/NMYC Inhibition"

Jan Schulte Am Esch*, **Beatrice A. Windmöller*,** Johannes Hanewinkel, Jonathan Storm, Christine Förster, Ludwig Wilkens, Martin Krüger, Barbara Kaltschmidt, Christian Kaltschmidt

Cancers (Basel). 2020 Sep; 12(9): 2582. Published online 2020 Sep 10. doi:10.3390/cancers12092582; (*: equal contribution)

3.) *

"Nanopore Sequencing reveals global Transcriptome Signatures of mitochondrial and ribosomal Gene Expressions in various human Cancer Stem-like Cell Populations"

Kaya E. Witte*, Oliver Hertel*, **Beatrice A. Windmöller**, Laureen P. Helweg, Anna L. Höving, Cornelius Knabbe, Tobias Busche, Johannes F. W. Greiner, Jörn Kalinowski, Thomas Noll, Fritz Mertzlufft, Morris Beshay, Jesco Pfitzenmaier, Barbara Kaltschmidt, Christian Kaltschmidt, Constanze Banz-Jansen* and Matthias Simon*

Cancers (Basel). 2021 Mar; 13(5): 1136. Published online 2021 Mar 6. doi:10.3390/cancers13051136; (*: equal contribution)

4.) *

"Novel primary human Cancer Stem-like Cell Populations from Non-small Cell Lung Cancer: Inhibition of Cell Survival by targeting NF-κB- and MYC-Signaling"

Beatrice A. Windmöller*, Morris Beshay*, Laureen P. Helweg, Clara Flottmann, Miriam Beermann, Christine Förster, Ludwig Wilkens, Johannes F. W. Greiner, Christian Kaltschmidt and Barbara Kaltschmidt

Cells. 2021 Apr 27; 10(5): 1024. Published online 2021 Apr 27. doi:10.3390/cells10051024;. (*: equal contribution)

5.) *

"Diminishment of novel endometrial carcinoma-derived stem-like cells by targeting mitochondrial bioenergetics and MYC"

Beatrice A. Windmöller*, Laureen P. Helweg*, Leonie Burghardt, Jonathan Storm, Christine Förster, Ludwig Wilkens, Barbara Kaltschmidt, Constanze Banz-Jansen* and Christian Kaltschmidt*

Under review at Gynecologic Oncology; (*: equal contribution)

6.)

"NF-κB p65 directs sex-specific neuroprotection in human neurons"

Lucia M Ruiz-Perera, Lennart Schneider, **Beatrice A. Windmöller**, Janine Müller, Johannes F. W. Greiner, Christian Kaltschmidt, Barbara Kaltschmidt

Sci Rep. 2018; 8: 16012. Published online 2018 Oct 30. doi:10.1038/s41598-018-34394-8

7.)

"Huge typical pulmonary carcinoid presented with gigantism syndrome"

Morris Beshay, Federico Gutierrez, **Beatrice A. Windmöller**, Christine Förster, Fritz Mertzlufft

Gen Thorac Cardiovasc Surg. 2021; 69(2): 371–374. Published online 2020 Jul 28. doi:10.1007/s11748-020-01445-9

8.)

"Platelets Boost Recruitment of CD133 + Bone Marrow Stem Cells to Endothelium and the Rodent Liver-The Role of P-Selectin/PSGL-1 Interactions"

Nadja Lehwald, Constanze Duhme, Iryna Pinchuk, Julian Kirchner, Kristina Wieferich, Moritz Schmelzle, Kerstin Jurk, **Beatrice A. Windmöller**, Wolfgang Hübner, Bernhard Homey, Johannes Bode, Ralf Kubitz, Tahar Benhidjeb, Martin Krüger Simon C. Robson, Wolfram T. Knoefel, Beate E. Kehrel, Jan Schulte Am Esch

Int J Mol Sci. 2020 Sep; 21(17): 6431. Published online 2020 Sep 3. doi:10.3390/ijms21176431

9.)

"Hepatic Vasculopathy and Regenerative Responses of the Liver in Fatal Cases of COVID-19"

Barbara Kaltschmidt*, Antonia D. E. Fitzek*, Julia Schaedler*, Christine Förster*, Christian Kaltschmidt, Thorsten Hansen, Fabian Steinfurth, **Beatrice A. Windmöller**, Christian Pilger, Cihang Kong, Kashika Singh, Axel Nierhaus, Dominic Wichmann, Jan Sperhake, Klaus Püschel, Thomas Huser, Martin Krüger*, Simon C. Robson*, Ludwig Wilkens*, Jan Schulte Am Esch*

Clin Gastroenterol Hepatol. 2021 Jan 29. doi: 10.1016/j.cgh.2021.01.044 [Epub ahead of print]; (*: equal contribution)

10.)

"Inter- and intra-populational heterogeneity of characteristic markers in adult human neural crest-derived stem cells"

Beatrice A. Windmöller*, Anna L. Höving*, Johannes F. W. Greiner

Under review at Stem Cell Reviews and Reports; Preprint on bioRxiv https://doi.org/10.1101/2021.06.25.449886; (*: equal contribution)

Reviews:

1.)

"Between fate choice and self-renewal - Heterogeneity of adult neural crest-derived stem cells"

Anna L. Höving*, **Beatrice A. Windmöller***, Cornelius Knabbe, Barbara Kaltschmidt, Christian Kaltschmidt, Johannes F. W. Greiner

Front Cell Dev Biol. 2021; 9: 662754. Published online 2021 Apr 8. doi: 10.3389/fcell.2021.662754; (*: equal contribution)

Table of Content

Abbreviations

AC	Adenocarcinoma
ALDH1	Aldehyde dehydrogenase 1
CCND1	Cyclin D1
CCSC	Colorectal cancer stem cell
CD133	Prominin-1
CD44	CD44-antigen
CLSII	Collagenase type II
COX7C	Cytochrome c oxidase subunit 7C
CRC	Colorectal cancer
CSC	Cancer stem cell
Dexa	Dexamethasone
DNA	Deoxyribonucleic acid
EC	Endometrial carcinoma
ECSC	Endometrial cancer stem cell
EGF	Epidermal growth factor
EMT	Epithelial to mesenchymal transition
EPCAM	Epithelial cell adhesion molecule
FCCP	Carbonyl cyanide 4-(trifluoromethoxy) phenylhydrazone
FCS	Fetal calf serum
FGF-2	Fibroblast growth factor 2
GO	Gene ontology
GSC	Glioblastoma stem cell-like cell
IC_{50}	Half maximal inhibitory concentrations
IKK	IκB kinase
IκB	inhibitor of nuclear factor kappa B
LCSC	Lung cancer stem cell
LGR5	Leucine-rich repeat-containing G protein-coupled receptor 5
MAX	MYC-associated factor X
mRNA	messenger ribonucleic acid
MYC	MYC proto-oncogene
NF-κB	Nuclear factor kappa-light-chain-enhancer of activated B-cells
NMYC	NMYC proto-oncogene
NSCLC	Non-small cell lung cancer
OXPHOS	Oxidative phosphorylation
PCSC	Prostate cancer stem cell
PDTC	Pyrrolidinedithiocarbamate
RPL28	Ribosomal protein L28
RPLP1	Ribosomal protein lateral stalk subunit P1
SCC	Squamous cell carcinoma
TMRE	Tetramethylrhodamine ethyl ester
TNF-α	Tumor necrosis factor α
USA	United States of America

List of Figures

Abstract

Cancer is one of the leading causes of death worldwide, while the disease is driven by abnormal growth of cells from particular parts of the body that may invade or spread to heathy tissue. On molecular level, deregulations of various signaling pathways are involved in the process of carcinogenesis particularly including signaling mediated by the transcription factors nuclear factor kappa-light-chain-enhancer of activated B-cells (NF-κB) and MYC. On cellular level, especially a small subpopulation of self-renewing cancer cells, known as cancer stem cells (CSCs), plays a crucial role in carcinogenesis and was reported to mediate tumor growth, treatment resistance, metastasis, immune evasion as well as cancer relapse. Thus, CSCs are of enormous clinical interest and their propagation *in vitro* is a highly promising tool for investigating the molecular biology and evolving novel cancer therapeutics to overcome CSC-mediated treatment failures.

Considering the high relevance of CSCs, this thesis shows the successful establishment of 12 novel primary CSC-like populations derived from colorectal, pulmonary and endometrial carcinogenic tissue. CSC-like populations were successfully isolated from one pulmonary (BKZ-1) and one rectal (BKZ-2) neuroendocrine neoplasm as well as from one colorectal adenocarcinoma (BKZ-3). In addition, CSC-like populations were generated from three pulmonary squamous cell carcinomas (BKZ-4, BKZ-5 and BKZ-6), three pulmonary adenocarcinomas (BKZ-7, BKZ-8 and BKZ-9) and three endometrial carcinomas (BKZ-10, BKZ-11 and BKZ-12). The CSC-phenotype of these 12 BKZ-populations was confirmed by their capacity to form spheres and by the expression of several well-established stemness marker proteins including Prominin-1 (CD133), CD44-antigen (CD44) and Nestin. In addition, nuclear Synaptophysin expression was observable in every CSC-like BKZ-population even independent to a neuroendocrine origin of the tumor, indicating nuclear Synaptophysin as a novel CSC-marker. On mechanistic level, the NF-κB subunit RelA was found to be localized in the cytosol in every BKZ-population, suggesting a crucial function of NF-κB in primary human CSCs. Accordingly, inhibition of NF-κB-signaling resulted in significant reductions in cell survival for pulmonary squamous cell carcinoma- (BKZ-4, BKZ-5 and BKZ-6) and adenocarcinoma-derived (BKZ-7, BKZ-8 and BKZ-9) CSC-like populations. Next to NF-κB, MYC family proteins were shown to be ubiquitously present in all BKZ-populations, with MYC protein being localized within the nucleus and NMYC in the cytosol. Notably, a significant decrease in cell survival was observable in all BKZ-populations after application of the MYC/NMYC inhibitor KJ-Pyr-9. Inhibition of MYC

was further found to be more effectively impairing survival of lung CSC-like populations (BKZ-4 – BKZ-9) in comparison to the application of NF-κB inhibitors, strongly suggesting MYC as promising therapeutic target. Global gene expression profiling of six of the 12 BKZ-populations using RNA-sequencing supported this eminent role of MYC and NF-κB in the here identified CSC-like cells. In particular, almost all investigated BKZ-populations (BKZ-7 – BKZ-12) showed MYC gene expression next to an enrichment of the gene ontology-term "NF-κB binding". Further, ribosome- and mitochondria-associated genes were observed to be expressed in the six BKZ-populations, suggesting a MYC-dependent regulation of mitochondrial and ribosomal biogenesis in CSCs. Accordingly, inhibition of MYC/NMYC using KJ-Pyr-9 reduced the mRNA expression levels of ribosomal protein L28 and ribosomal protein lateral stalk subunit P1 in BKZ-8. Impairment of the mitochondrial function using metformin further significantly decreased survival of endometrial CSC-like populations (BKZ-10 – BKZ-12), emphasizing a role of increased mitochondrial biogenesis in CSC-like populations.

In summary, this thesis shows the successful isolation of 12 novel primary CSC-like populations derived from colorectal, pulmonary and endometrial carcinogenic tissue and their application for studying CSC biology *in vitro*. On mechanistic level, this work provides evidence for NF-κB and especially MYC being promising targets to impair survival of CSCs from colorectal, pulmonary and endometrial origin, which may build the basis to overcome CSC-driven therapeutic failures.

Zusammenfassung

Krebs ist eine der häufigsten Todesursachen weltweit, wobei sich die Krankheit durch die unkontrollierte Vermehrung von Zellen auszeichnet, die in gesundes Gewebe eindringen und sich dort ausbreiten können. An diesem Prozess sind auf molekularer Ebene Veränderungen verschiedenster Signalwege beteiligt, darunter die Familien der Transkriptionsfaktoren *nuclear factor kappa-light-chain-enhancer of activated B-cells* (NF-κB) und MYC. Auf zellulärer Ebene spielt vor allem eine Subpopulation selbsterneuernder Krebszellen, die als Krebsstammzellen (CSCs) bezeichnet werden, eine entscheidende Rolle in der Karzinogenes. Studien zeigten, dass CSCs höchst wahrscheinlich für Tumorwachstum, Therapieresistenz, Metastasierung, Immunevasion sowie Rezidive verantwortlich sind. Ferner sind CSCs von enormem klinischen Interesse und ihre Etablierung *in vitro* ist essentiell für die Untersuchung der molekularen Biologie sowie für die Entwicklung von CSC-spezifischer Krebstherapien.

In Anbetracht der enormen Relevanz von CSCs wird in dieser Doktorarbeit die erfolgreiche Etablierung von 12 neuartigen primären CSC-ähnliche Populationen aus kolorektalem, pulmonalem und endometrialem karzinogenem Gewebe vorgestellt. CSC-ähnliche Populationen wurden erfolgreich aus einem pulmonalen (BKZ-1) und einem rektalen (BKZ-2) neuroendokrinen Tumor, sowie aus einem kolorektalen Adenokarzinom (BKZ-3) isoliert. Darüber hinaus wurden CSC-ähnliche Populationen aus drei pulmonalen Plattenepithelkarzinomen (BKZ-4, BKZ-5 und BKZ-6), drei pulmonalen Adenokarzinomen (BKZ-7, BKZ-8 und BKZ-9) und drei Endometriumkarzinomen (BKZ-10, BKZ-11 und BKZ-12) generiert. Der CSC-Phänotyp der 12 etablierten BKZ-Populationen wurde durch ihre Fähigkeit zur Sphärenbildung und durch die Expression mehrerer etablierter Stammzellmarkerproteine wie Prominin-1 (CD133), CD44-Antigen (CD44) und Nestin bestätigt. Zusätzlich konnte Synaptophysin als Protein in den Zellkernen aller CSC-ähnlichen BKZ-Population unabhängig von einem neuroendokrinen Ursprung des Tumors nachgewiesen werden. Somit scheint die nukleäre Expression von Synaptophysin potenziell als neuer CSC-Marker genutzt werden zu können. Auf mechanistischer Ebene wurde die NF-κB-Untereinheit RelA im Zytosol aller BKZ-Populationen nachgewiesen, was auf eine entscheidende Funktion von NF-κB in primären humanen CSCs hindeutet. Dementsprechend führte die Inhibierung des NF-κB-Signalweges zu einer signifikanten Reduktion des Zellüberlebens für CSC-ähnliche Population isoliert aus pulmonale Plattenepithelkarzinomen (BKZ-4, BKZ-5 und BKZ-6) und Adenokarzinomen (BKZ-7,

BKZ-8 und BKZ-9). Neben NF-κB wurde gezeigt, dass Proteine der MYC-Familie ubiquitär in allen BKZ-Populationen vorhanden sind, wobei MYC im Zellkern und NMYC im Zytosol lokalisiert war. Entsprechend hat die Anwendung des MYC/NMYC-Inhibitors KJ-Pyr-9 in allen BKZ-Populationen zu einer signifikanten Reduktion der Überlebensrate geführt. Weiterhin wurde festgestellt, dass die Inhibierung von MYC im Vergleich zur Inhibierung von NF-κB das Überleben der pulmonalen CSC-ähnlichen Populationen (BKZ-4 - BKZ-9) stärker beeinträchtigt. Ferner scheinen NF-κB aber vor allem MYC vielversprechende therapeutische Ziele zu sein. Die globale Genexpressionsanalyse von sechs der 12 BKZ-Populationen (BKZ-7 - BKZ-12) mittels RNA-Sequenzierung bestätigte eine wichtige Rolle von MYC und NF-κB in den hier identifizierten CSC-ähnlichen Zellen. Hier wurde in fast allen untersuchten BKZ-Populationen eine MYC-Genexpression, sowie eine Anreicherung von Genen im Zusammenhang mit dem *gene ontology term* "*NF-κB binding* " festgestellt. Weiterhin wurde in den sechs BKZ-Populationen ein Anstieg von Ribosomen- und Mitochondrien-assoziierten Genen detektiert, was auf eine MYC-abhängige Regulation der mitochondrialen und ribosomalen Biogenese in CSCs hinweist. Dementsprechend reduzierte die Inhibierung des MYC/NMYC Signalweges mittels KJ-Pyr-9 die mRNA-Level der ribosomalen Proteine *ribosomal protein L28* und *ribosomal protein lateral stalk subunit P1* in BKZ-8. Zusätzlich führte die Inhibierung der mitochondrialen Funktion mittels Metformin zu einer signifikanten Reduktion des Überlebens der endometrialen CSC-ähnlichen Populationen (BKZ-10 - BKZ-12), was auf eine wichtige Rolle der erhöhten mitochondrialen Biogenese in CSC-ähnlichen Populationen schließen lässt.

Zusammenfassend präsentiert die vorliegende Arbeit die erfolgreiche Isolierung von 12 neuartigen primären CSC-ähnlichen Populationen aus kolorektalem, pulmonalem und endometrialem karzinogenem Gewebe sowie deren Anwendung in Studien zur Untersuchungen der CSC-Biologie *in vitro*. Auf mechanistischer Ebene liefert diese Arbeit Beweise dafür, dass NF-κB und insbesondere MYC vielversprechende therapeutische Ziele sind, um CSC-Populationen aus kolorektalem, pulmonalem und endometrialem karzinogenem Gewebe zu dezimieren und somit CSC-bedingte therapeutische Misserfolge zu minimieren.

1 Aim and Objectives

CSCs are self-renewing cells that are highly relevant in cancer research as they drive carcinogenesis as well as therapeutic failures. Thus, extensive research regarding their molecular biology and specific characteristics is inevitable for the improvement of current cancer therapeutics as well as for the development of novel targeted therapies.

Aim:

This thesis aims the establishment of primary CSC-like cells derived from colorectal, pulmonary and endometrial carcinogenic tissue as novel *in vitro* models for the investigation of molecular regulators of CSC-like cell survival.

Objectives:

- Cell culture protocols will be adapted for the establishment of primary human CSC-like populations originating from colorectal, pulmonary and endometrial carcinogenic tissue.
- Generated cell populations will be investigated for their marker profile using immunocytochemistry and other molecular assays including quantitative polymerase chain reactions and flow cytometry.
- Analysis of CSC-related signal transduction including NF-κB, MYC and other relevant pathways will be performed.

2 Introduction

2.1. The architecture of cancer

2.1.1. Advances in the Fight against Cancer

Cancer is one of the leading causes of death worldwide, with incidence increasing steadily in recent decades (Bray et al. 2018; Ferlay et al. 2021). For 2020, 19.3 million new cancer cases and 10.0 million cancer deaths worldwide were reported (Ferlay et al. 2021), with lung cancer being the leading cause of cancer-related deaths (Ferlay et al. 2021; Bray et al. 2018). In several states of the United States of America (USA), the age standardized cancer mortality even exceeded that for heart diseases, which was the leading cause of death since 1910 in the USA (Harding et al. 2018). Nevertheless, increased research in the field of cancer biology led to clinical advances in the last decades, too. In the very beginning of cancer treatment, first surgery, then also radiation and chemotherapy represented the basis of therapies for patients who suffered from cancer (Sigerist 1932). However, systemic chemotherapy often reveals severe side effects as these drugs not only target the diseased area, but also healthy tissue. Nowadays these fundamental approaches are still first-line therapies for several cancer types, but are often combined with therapies using targeted drugs that revolutionized the field of cancer treatment (Markham et al. 2020; West et al. 2019; Zhang et al. 2017). These therapies are based on the identification of appropriate targets involved in cancer progression (reviewed in (Sawyers 2004), making the understanding of molecular biology of carcinogenesis essential for their development.

Tumorigenesis is a multistep process in which genetic alterations of oncogenes and tumor-suppressor genes drive the progressive transformation of normal human cells into highly malignant derivates (Vogelstein et al. 2013). Nevertheless, Hanahan and Weinberg elucidated in their updated comprehensive review “Hallmarks of Cancer: The Next Generation” that tumor biology is far more complex than initially assumed. Years of investigation depicted that carcinogenesis and tumor invasion are regulated by a multitude of intrinsic characteristics as well as by the tumor-microenvironment (Hanahan and Weinberg 2000; Hanahan and Weinberg 2011). Hallmarks like sustaining proliferative signaling, evading growth suppressors, avoiding immune destruction, resting cell death and deregulating cellular energetics are only extracts of the mosaic of several capabilities acquired by cancer cells (Hanahan and Weinberg 2011). Even though the ongoing increase

in the knowledge of cancer biology led to improvements in clinical diagnosis and cancer treatments, effectiveness of therapeutic drugs is still not satisfactory. Treatments frequently only lead to short-term success with subsequent tumor relapse and/or metastasis most likely based on intratumoral heterogeneity (Gerlinger et al. 2012). These genetic variations of distinct regions of the same tumor are drivers of aggressive disease progression as exposure to extrinsic factors, including the microenvironment, therapeutic drugs and the immune system results in the selection of the most resistant subpopulation of cancer cells (reviewed in (Vitale et al. 2021)). By now there is growing evidence that cancer stem cells (CSCs), a small subpopulation of self-renewing cancer cells, play a crucial role in driving intratumoral heterogeneity and therapeutic failures, emphasizing CSCs as highly promising target for the development of novel cancer therapeutics.

2.1.2. Cancer stem-like cells and their cellular hallmarks

CSCs are highly plastic self-renewing cells at the top of hierarchically organized tumors sustaining the long-term maintenance and heterogeneity of neoplasms (reviewed in (Reya et al. 2001; van Neerven et al. 2016)). While the existence of CSCs was already discussed in 1877 based on the embryonic character of a population of cancer cells (reviewed in (Cooper 2009)), strong experimental evidences were firstly published in the 1990s by identifying a self-renewing subpopulation of acute myeloid leukemia cells owning tumor-initiating abilities (Bonnet and Dick 1997; Lapidot et al. 1994). Few years later the first identification of CSCs in solid tumors by Michael Clarks group in breast cancer followed (Al-Hajj et al. 2003). Nowadays, the plastic CSC model partly considers both of the main discussed theories for intratumoral heterogeneity, which are the clonal evolution model and the classic hierarchical CSC model. The clonal evolution model posits the transformation of single cells leading to unlimited proliferation capability causing uncontrolled tumor growth resulting in accumulation of diverse mutations and intratumoral heterogeneity. In this model it is believed that over a tumors lifespan every cancer cell is able to initiate a tumor, become resistant or cause recurrence (Nowell 1976). The classic CSC model postulates the existence of single mutated cells with unlimited proliferative potential, too. However, those cells with stem cell characteristics are thought to exclusively drive tumor growth, recurrence and resistance, while heterogeneity of the tumor is assumed to be based on symmetric or asymmetric division of CSCs giving rise to more differentiated cancer cells not owning tumor initiating features (Reya et al. 2001; Pardal et al. 2003). The current plastic CSC theory

comprises both models as it assumed that CSCs behave dynamically by giving rise to different subclones of cancer cells with mature progeny. Nevertheless, those differentiated cancer cells harbor the capacity to dedifferentiate back into stem-like cells, making subclones with sustained or regained stemness features to highly promising targets in cancer therapy (reviewed in (Kreso and Dick 2014; van Neerven et al. 2016)). Despite their plasticity, the initial origin of CSCs is widely discussed in the field. While the origin of CSCs has been suggested by some researchers to be in mutant stem cells or progenitor cells, others have speculated that CSCs derive from fully differentiated cells through reprogramming. Today both theories have been proven, as for instance CSCs of the intestine were shown to derive from intestinal stem cells (Barker et al. 2009) as well as tumor formation has been reported to be induced by dedifferentiation of mature cells (Schwitalla et al. 2013).

Hence, based on the current knowledge, CSCs are defined as drivers of intratumoral heterogeneity, tumor growth and recurrence resting on their plastic stem-like properties including self-renewal, asymmetric division and multi-lineage differentiation (Batlle and Clevers 2017; Clevers 2011). Moreover, CSCs and metastasis have been found to be tightly connected as CSCs were shown to harbor the ability to reinitiate tumor growth in different tissues, probably by remodeling the process of epithelial to mesenchymal transition (EMT) (Mani et al. 2008). Another reported feature of CSCs is the ability to remain hidden from the immune system until their reactivation leads to tumor relapse or metastasis (reviewed in (Sultan et al. 2017)). Beside their properties for immune evasion, stemness of cancer cells was reported to be associated with chemoresistance, as quiescent CSC-populations were shown to sustain tumor growth after chemotherapy (Martins-Neves et al. 2016). Further, it was depicted that chemotherapy induces the upregulation of CSC-markers highlighting the plasticity of CSCs (Chen et al. 2012; Lu et al. 2017). This decreased sensitivity to conventional therapies is thought to rely on several mechanisms like increased drug efflux pump activity (Loebinger et al. 2008), increased levels of detoxification enzymes such as aldehyde dehydrogenases (Sládek et al. 2002), enriched activation of deoxyribonucleic acid (DNA) damage response (Bao et al. 2006) and quiescence (Liu et al. 2009). Further, deregulations of the cell metabolism as well as metabolic plasticity were associated with CSCs providing survival advantages and leading to cancer progression (reviewed in (Vander Heiden and DeBerardinis 2017; Ito and Suda 2014)). Lastly, not only genetic aberrations but also epigenetic events including the loss of DNA methylation or loose chromatin structures were indicated to regulate several CSC characteristics such as stemness, dedifferentiation, genetic reprogramming or chemoresistance (reviewed in (Feinberg et al. 2016)).

Collectively, CSCs were proven to harbor an enormous variety of mechanisms responsible for their maintenance and therapeutic failures. Thus, increasing research is being conducted to target CSCs by impairing factors or signaling pathways necessary for their sustainment. Nevertheless, the heterogeneity of these dynamic cell populations, as well as similarities with non-pathogenic (stem) cells complicate the development of novel therapeutics. Facing this challenge this thesis presents the establishment of novel primary CSC-like populations as *in vitro* models for the identification of CSC-specific signaling pathways and markers as basis for the design of novel cancer therapies to minimize CSC-mediated relapse rates.

2.2. Cancer stem-like cells as cellular models for the optimization of cancer therapies

2.2.1. Isolation of two novel primary human colorectal carcinoma-derived cancer stem-like cell populations

Colorectal cancer (CRC) is the third most common cancer worldwide and second most common cause of cancer-related mortality, with 1.9 million new cases and approximately 935000 deaths estimated in 2020 as reported by the Global Cancer Observatory (Sung et al. 2021). CRC comprises the development of malignancies in the colon (72%) and the rectum (28%), with 90% of all CRCs being an adenocarcinoma (AC) originated from epithelial mucosa cells (Fleming et al. 2012). Contrary, neuroendocrine carcinomas are a relatively rare and poorly understood subtype of CRC, comprised of poorly-differentiated neoplasms derived from endocrine or epithelial cells of the nervous system (Kim et al. 2018; Lee and Sung 2021). Next to their rarity of less than 1% of all CRCs (Shafqat et al. 2015; Bernick et al. 2004), neuroendocrine carcinomas are more aggressive in comparison to typical CRCs (Sorbye et al. 2014) with almost all patients having metastasis at the time of diagnosis (Fields et al. 2019). Most preclinical models for the investigation of CRCs are based on stable cell lines, but are mainly derived from metastases and scarce especially for colorectal neuroendocrine carcinomas (Takahashi et al. 2000; Pfragner et al. 2009; Krieg et al. 2014; Dizdar et al. 2018; Yanagihara et al. 2018). Even though some of these *in vitro* models originated from primary native tumor tissue (Takahashi et al. 2000; Pfragner et al. 2009; Gock et al. 2018), they still lack cancer stem cell characteristics. Importantly, CSC profiles were identified as independent prognostic markers correlating with low survival and metastasis in CRC patients (Sousa E Melo et al. 2011; Todaro et al. 2014; Horst et al. 2008),

underpinning the importance of CSCs in colorectal tumorigenesis. In line with other solid tumors, CSCs were also identified in colorectal carcinomas revealing the capacity to induce tumors in mice that resembled the original malignancy (Ricci-Vitiani et al. 2007; O'Brien et al. 2007). Moreover, colorectal CSCs (CCSC) were shown to be enriched by chemotherapy in xenotransplanted mice (Dylla et al. 2008). Next to the role of CCSC in therapy resistance, stemness in CRC cells was further linked to colonization, invasion and metastasis (Ma et al. 2019). However, metastases comprising cells positive for the CCSC-marker leucine-rich repeat-containing G protein-coupled receptor 5 (LGR5) could be even formed by LGR5-negative cells, highlighting their enormous plasticity (Fumagalli et al. 2020). Therefore, cellular models of CCSCs are highly important for further exploration of CSC biology and for the development of novel therapeutics to overcome CSC-driven carcinogenesis.

As basis for further research on CSC-driven carcinogenesis in CRC, this thesis presents two novel *in vitro* models of CCSCs established from primary human CRC tissue. The first cell population, named BKZ-2, was obtained from a rare rectal neuroendocrine carcinoma, and the second, termed BKZ-3, was isolated from a typical colorectal AC. Both populations were established by mechanical and enzymatic disintegration of the obtained tissue sample with subsequent cultivation within CSC-medium composed of Dulbecco´s Modified Eagle´s Medium/Ham´s-F12 supplemented with epidermal growth factor (EGF), fibroblast growth factor 2 (FGF-2) and B27 (Figure 1) accordingly to previously described protocols (Cammareri et al. 2008; Ricci-Vitiani et al. 2007).

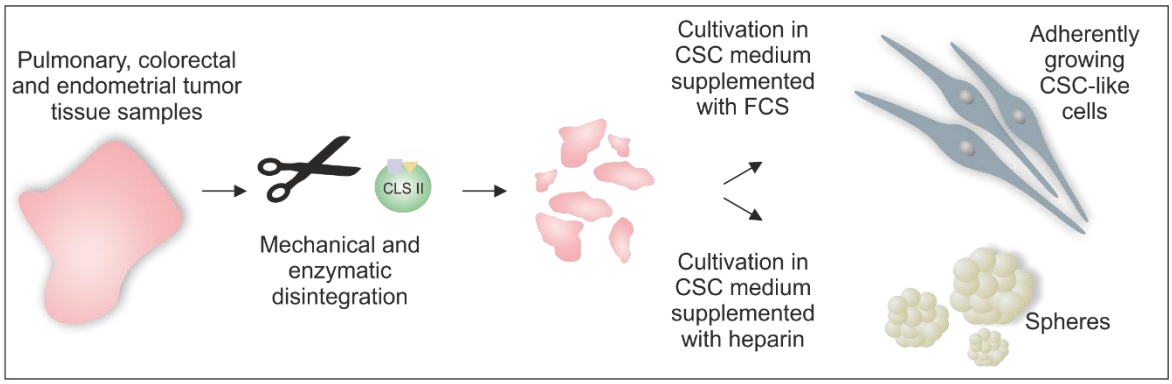

Figure 1: Schematic overview of the isolation procedure of primary human cancer stem cell (CSC)-like cells. CSC-like cell populations were isolated by mechanical and enzymatic disintegration of respective tumor tissue samples using collagenase type II (CLSII). Tumor material was then cultured either in CSC-medium supplemented with fetal calf serum (FCS) for adherent CSC-like cells, or with heparin for spherically grown CSC-like cells.

Cultivation in CSC-medium with additional 10% fetal calf serum (FCS) led to an adherently growing cell culture for both populations (Figure 2 A, E) (Schulte am Esch et al. 2020), while enrichment of CSCs was achieved via serial trypsin treatment as described by Morata-

Tarifa and coworkers (Morata-Tarifa et al. 2016) and the group around Walia (Walia and Elble 2010). Further, addition of 4 µg/ml heparin to the CSC-medium in the absence of FCS led to the formation of spheres (Figure 2 B, F) (Schulte am Esch et al. 2020). This is probably based on the capacity of heparin to stabilize, phosphorylate and activate the FGF receptor, leading to higher proliferation rates of various (stem) cell types (Spivak-Kroizman et al. 1994; Furue et al. 2008; Caldwell et al. 2004). Sphere formation capacity initially confirmed the successful isolation of CCSCs, as the *in vitro* propagation of spheres was demonstrated to be strongly associated with stemness in colorectal carcinoma derived cells (Ishiguro et al. 2017; Ohata et al. 2012). Furthermore, sphere formation was shown to be biologically reliable as the *in vitro* assay demonstrated uniformly results corresponding with murine *in vivo* xenograft models (Krieg et al. 2014; Wang et al. 2019). Notably, BKZ-2 and BKZ-3 revealed a higher number of formed spheres in comparison to established colon carcinoma cell lines HT-29 and HCT-116, further underlining the enrichment of a stem-like phenotype (Schulte am Esch et al. 2020).

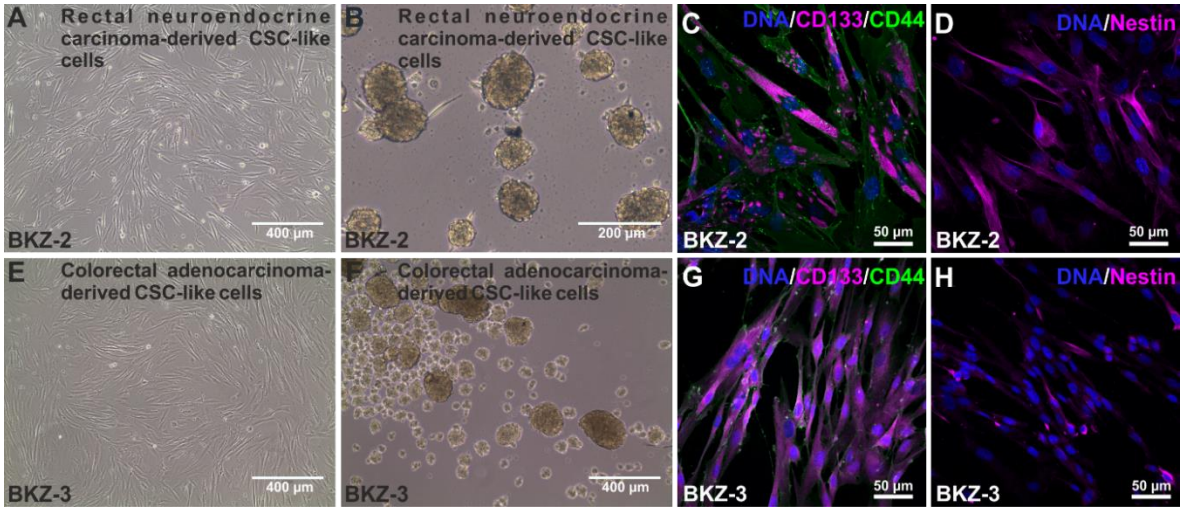

Figure 2: Successful isolation of one rectal neuroendocrine carcinoma-, and one colorectal adenocarcinoma-derived CSC-like population. Both, neuroendocrine-derived BKZ-2 and adenocarcinoma-derived BKZ-3 populations grew as **(A/E)** adherent culture as well as **(B/F)** sphere culture under serum free conditions and the supplementation with heparin. Immunocytochemical staining of CSC-markers CD133, CD44 and Nestin revealed expression in **(C/D)** BKZ-2 and **(G/H)** BKZ-3. Modified from (Schulte am Esch et al. 2020)

Next to the sphere formation capacity, the expression of several markers was shown to be characteristic for CSCs. Particularly, CCSCs were firstly isolated based on the expression of the cell surface glycoprotein Prominin-1 (CD133) (Ricci-Vitiani et al. 2007). In later studies, the pool of marker proteins defining CCSCs was extended to include LGR5, CD44-antigen (CD44), Aldehyde dehydrogenase 1 (ALDH1), Epithelial cell adhesion molecule (EPCAM) and Nestin, among others (Leng et al. 2018; Ricci-Vitiani et al. 2007; Dalerba et al. 2007; Dylla et al. 2008; Huang et al. 2009; Neradil and Veselska 2015), all involved in the

maintenance of CSC characteristics. Nevertheless, co-expression of multiple markers was shown to be more reliable for the identification of CCSCs compared to the use of only one marker protein, as it correlated more significantly with tumorigenicity and disease-free survival of CRC patients (Leng et al. 2018; Galizia et al. 2012; Haraguchi et al. 2008) (reviewed in (Abbasian et al. 2019)). Accordingly, immunocytochemical analysis of BKZ-2 and BKZ-3 revealed the co-expression of CSC-markers CD133 and CD44 as well as the expression of Nestin in the present work (Figure 2 C-D, G-H) (Schulte am Esch et al. 2020). CD133 and CD44 expression was further observed to be significantly elevated in BKZ-2 and BKZ-3 in comparison to established colon carcinoma cell lines HT-29 and HCT-116 (Schulte am Esch et al. 2020), substantiating their stem-like phenotype. Likewise, quantification of the messenger ribonucleic acid (mRNA) levels of several CSC-markers including *CD133*, *CD44*, and *EPCAM* depicted higher expression in BKZ-2 and BKZ-3 in comparison to human dermal fibroblasts (Schulte am Esch et al. 2020). Both cellular models further revealed subpopulations with high activity of the CSC-marker ALDH (Huang et al. 2009), making the two novel CSC-like populations promising cellular models to investigate CCSC biology (Schulte am Esch et al. 2020).

2.2.2. Establishment of human primary lung cancer stem-like cell populations

Similar to colorectal cancer stem cells, lung cancer-derived CSCs are of enormous clinical interest and human *in vitro* models are extremely important to gather more insights into the biology of these important drivers of lung cancer. Lung cancer in general is the leading cause of cancer-related deaths worldwide and can be classified into small cell lung cancer and non-small cell lung cancer (NSCLC) (Ferlay et al. 2021; Sung et al. 2021; Bray et al. 2018). With 80-85% of all lung cancer cases NSCLC represents the most common type and can be divided into adenocarcinomas (40%), squamous cell carcinomas (SCC, 25–30%), and large cell carcinomas (5–10%) (Ruiz-Ceja and Chirino 2017). In accordance with reports referring to other cancer types, there is growing evidence for CSCs being responsible for tumor growth, therapy resistance, recurrence as well as metastasis in lung cancer (Eramo et al. 2008; Tan et al. 2014; Bertolini et al. 2009)(reviewed in (Prabavathy et al. 2018)).

As model systems for lung CSCs (LCSC), this thesis presents seven novel primary human LCSC-like populations derived from three different lung cancer entities. The first one, named BKZ-1, was successfully isolated from a typical carcinoid of the lung, which represents a low-grade variant of neuroendocrine lung tumors (Windmöller et al. 2019).

These are comparatively rare with only 5% of all newly diagnosed pulmonary malignancies (Travis 2015) and treatment options are relatively unprogressive (reviewed in (Iyoda et al. 2020)), making this model even more important for potential future improvements of therapeutic strategies. Additional LCSC-like populations were derived from NSCLC specimens, including three ACs and three SCCs. SCC-derived LCSC-like populations were named BKZ-4, BKZ-5 and BKZ-6, while AC-derived populations were termed as BKZ-7, BKZ-8 and BKZ-9 (Windmöller et al. 2021a). All LCSC-like populations were isolated by mechanical and enzymatic disintegration of the tumor tissue and enriched for CSCs by using chemically defined media and serial trypsinization as described for the CCSC-like populations BKZ-2 and BKZ-3 (see chapter 2.2.1) (Figure 1). Established LCSC-like populations all grew as adherent cell culture and were able to form spheres as exemplarily shown for BKZ-1, BKZ-4 and BKZ-7 (Figure 3 A-B, E-F, I-J) (Windmöller et al. 2021a; Windmöller et al. 2019).

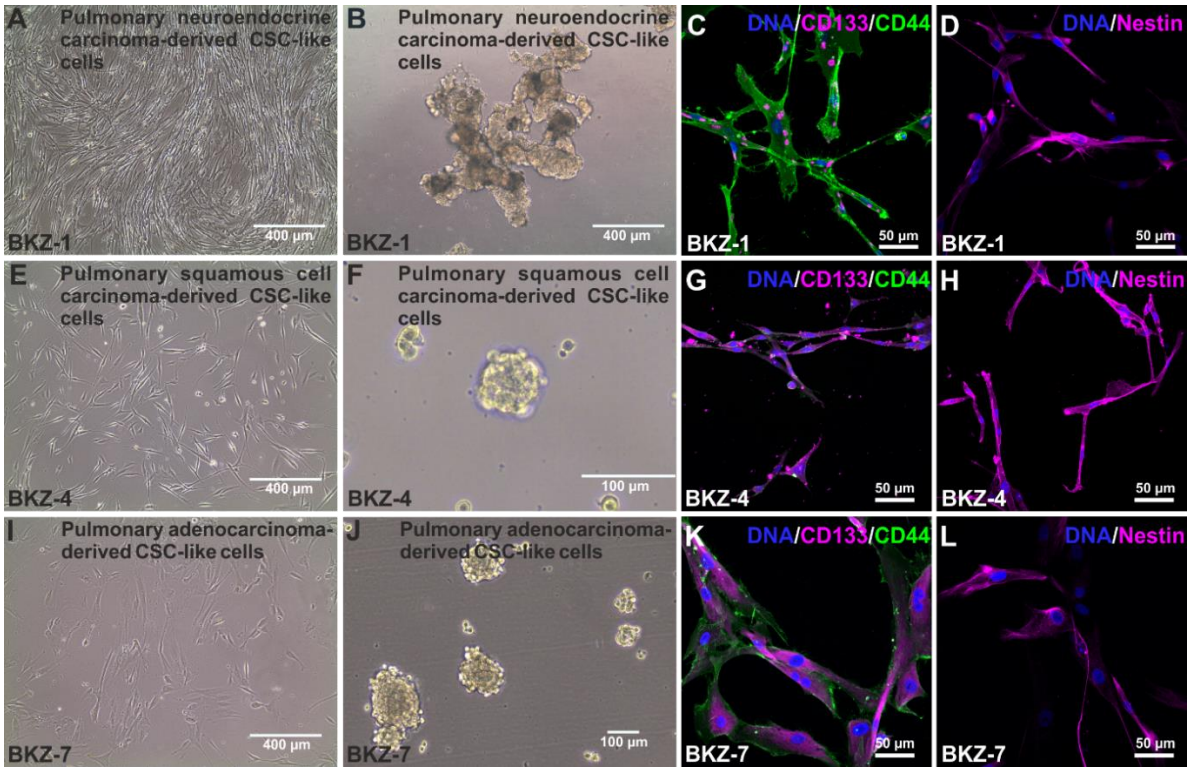

Figure 3: Establishment of seven pulmonary cancer stem cell (CSC)-like cell populations. In particular, one **(A/B)** pulmonary neuroendocrine carcinoma-, three **(E/F)** squamous cell carcinoma- and three **(I/J)** adenocarcinoma-derived CSC-like population were successfully isolated. All seven CSC-like populations expressed CSC-markers CD133, CD44 and Nestin, as shown for **(C/D)** BKZ-1, for **(G/H)** BKZ-4 and **(K/L)** BKZ-7, which served as representative populations for their respective group. Modified from (Windmöller et al. 2021a; Windmöller et al. 2019)

Next to the formation of spheres (Sun et al. 2015), the expression of several markers such as CD133 (Tirino et al. 2009; Eramo et al. 2008), CD44 (Leung et al. 2010), and Nestin (Liu et al. 2017; Narita et al. 2014) was reported to define LCSCs. Especially the expression of

CD133 and CD44 was linked to higher abilities for self-renewal, tumor initiation and resistance to chemotherapy in lung cancer cells (Chen et al. 2008; Huang et al. 2017; Leung et al. 2010; Satar et al. 2018; Liu et al. 2013). Accordingly, immunocytochemical analysis of the established LCSC-like populations revealed the expression of CD133, CD44 and Nestin on protein level, representatively shown for BKZ-1, BKZ-4 and BKZ-7 as exemplary populations of each parental lung tumor type (Figure 3 C-D, G-H, K-L) (Windmöller et al. 2019; Windmöller et al. 2021a). In contrast, the well-established lung adenocarcinoma cell line LXF-289 displayed no expression of CD133 and Nestin and lower expression of CD44 compared to NSCLC-derived LCSC-like cells, confirming the CSC-phenotype of the novel populations identified in this thesis (Windmöller et al. 2021a). Hence, the here presented LCSC-like cell populations can be used as excellent models to study LCSCs.

2.2.3. Isolation of three novel primary human endometrial cancer stem-like cells

Next to the establishment of several colorectal and pulmonary CSC-like populations, this thesis additionally demonstrates the successful isolation of three CSC-like populations derived from endometrial carcinomas (EC), which represent the most common type of gynecological malignancies and account for about 3% of worldwide mortality among women (Bray et al. 2018). High expression of CSC-markers like CD133 was shown to be correlated with worse overall survival in endometrial cancer as well as higher tumorigenicity, invasiveness and chemoresistance in EC-derived cells (Nakamura et al. 2010; Nakamura et al. 2014; Ding et al. 2017). Accordingly, enhanced tumorigenicity of CD133-positive endometrial CSCs (ECSC) was demonstrated by Rutella and coworkers, who additionally depicted an upregulation of the CSC-marker CD44 in these cells (Rutella et al. 2009). The ECSC-like populations described within this thesis were isolated from type I endometrial cancer, which accounts for 70-80% of all ECs and is typically less aggressive and estrogen-related in comparison to type II EC (Di Cristofano and Ellenson 2007). ECSC-like populations, named BKZ-10, BKZ-11 and BKZ-12 ((Windmöller et al. 2021b), under review), were established as described for CCSC-like (Schulte am Esch et al. 2020) and LCSC-like populations (Windmöller et al. 2019; Windmöller et al. 2021a) (see chapter 2.2.1, Figure 1). This cultivation procedure led to adherently as well as spherically growing cultures for all three populations, as representatively depicted for BKZ-10 (Figure 4 A-B). The ability of ECSCs to form spheres was shown to correlate with increased self-renewal and chemoresistance as well as tumorigenicity in xenograft studies (Kong et al. 2017; Rutella

et al. 2009), affirming a CSC-phenotype of the isolated ECSC-like cells. CD44 expression was associated with stemness in isolated ECSC-like populations (Kong et al. 2017; Kiyohara et al. 2017) as well as with infiltrating patterns and proliferation in EC (Park et al. 2019). Further, knockdown of the CSC-marker Nestin decreased invasiveness, cell growth, and colony formation of EC cell lines (Bokhari et al. 2016), which stands in line with the fact that expression of Nestin was demonstrated in highly tumorigenic CD133-positive ECSCs (Sun et al. 2017). Thus, the expression of the well-established ECSC-markers CD133, CD44 and Nestin confirmed a CSC-phenotype of BKZ-10, BKZ-11 and BKZ-12, as exemplarily shown in immunocytochemical stainings for BKZ-10 (Figure 4 C-D) ((Windmöller et al. 2021b), under review).

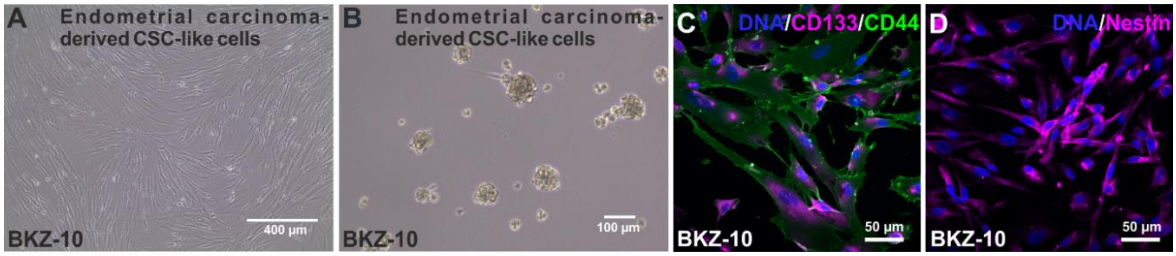

Figure 4: Successful propagation of three endometrial carcinoma-derived cancer stem cell (CSC)-like cell populations. All endometrial carcinoma-derived CSC-like populations, could be gown as **(A)** adherent cell culture and **(B)** sphere culture as well as every populations expressed CSC-markers **(C)** CD133, CD44 and **(D)** Nestin on protein level, as exemplarily shown for BKZ-10. Modified from ((Windmöller et al. 2021b) ,under review)

Notably, additional flow cytometric analysis of CD44 expression revealed over 99% positive cells for all three ECSC-like populations and up to 11% ALDH-high expressing cells ((Windmöller et al. 2021b), under review). This is consistent with observations by Liu and coworkers, who indicated plasticity of breast CSCs balancing between $CD24^{-}/CD44^{+}$-mesenchymal-like and ALDH-high epithelial-like stem cell populations (Liu et al. 2014). Thus, the here established primary ECSC-like populations appear to have a more mesenchymal-like-stem cell-phenotype. Conclusively, BKZ-10, BKZ-11 and BKZ-12 are highly promising *in vitro* models for the investigation of ECSC-driven carcinogenesis.

2.2.4. Synaptophysin as a new cancer stem-like cell marker

To verify the neuroendocrine origin of the firstly isolated CSC-like population BKZ-1 (see chapter 2.2.2), the expression of the well-established and prominent neuroendocrine marker Synaptophysin was investigated (Wiedenmann et al. 1986). Synaptophysin itself is an integral membrane protein of synaptic vesicles and ubiquitously expressed in presynaptic structures of neurons of the whole nervous system (Wiedenmann and Franke 1985; Navone

et al. 1986). There it plays an important role in sustaining presynaptic performance by maintaining vesicular proteins, like Synaptobrevin-II (Kokotos et al. 2019). As expected, the pulmonary neuroendocrine carcinoma-derived CSC-like cell population BKZ-1 expressed high amounts of Synaptophysin protein, but with predominantly nuclear instead of the common cytoplasmic localization (Figure 5 A) (Windmöller et al. 2019). Assuming nuclear localization of Synaptophysin as a general stem cell characteristic, non-pathogenic human stem cell populations revealed nuclear Synaptophysin as well. Nevertheless, nuclear Synaptophysin expression was significantly elevated in LCSC-like population BKZ-1 in comparison to human neural crest stem cells and mesenchymal stem cells, suggesting Synaptophysin as novel CSC-marker (Windmöller et al. 2019).

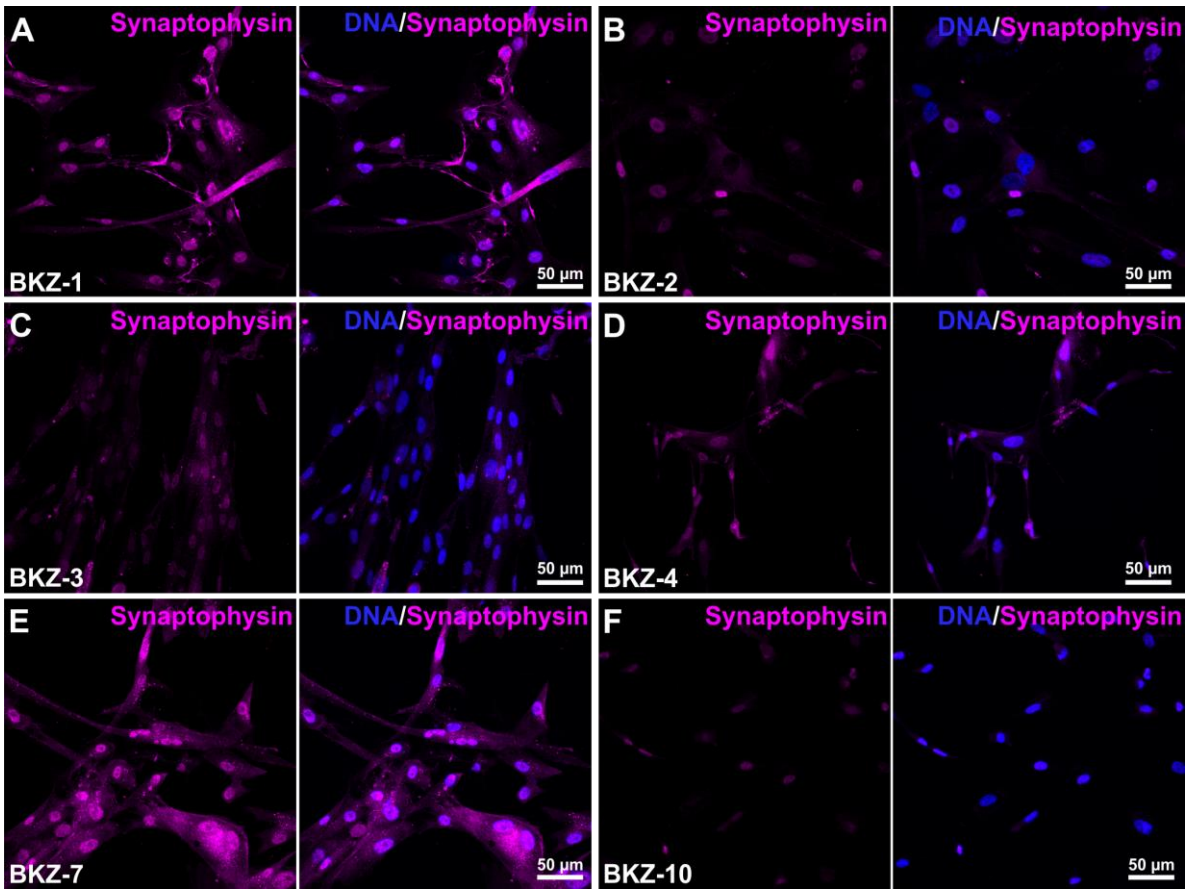

Figure 5: Synaptophysin as a putative cancer stem cell (CSC) marker. Isolated CSC-like populations all express nuclear Synaptophysin independent of their tissue origin. Immunocytochemistry of **(A)** pulmonary neuroendocrine carcinoma-derived BKZ-1, **(B)** rectal neuroendocrine carcinoma-derived BKZ-2, **(C)** colorectal adenocarcinoma-derived BKZ-3 and representative **(D)** pulmonary squamous cell carcinoma-derived BKZ-4, **(E)** pulmonary adenocarcinoma-derived BKZ-7 and **(F)** endometrial carcinoma-derived BKZ-10 depicted predominantly nuclear Synaptophysin expression. **A** modified from (Windmöller et al. 2019), **B-C** modified from (Schulte am Esch et al. 2020), **D** modified from (Flottmann 2020; Windmöller et al. 2021a), unpublished data, **E** (Windmöller et al. 2021a), unpublished data, **F** modified from ((Windmöller et al. 2021b), under review)

Accordingly, Synaptophysin was described as an unfavorable factor for patients suffering from squamous cell carcinomas and adenocarcinomas of the lung, as carcinomas with

presence of Synaptophysin had higher frequency of recurrence and lower survival rates (González-Aragoneses et al. 2007). Consistently, patients suffering from colorectal carcinomas with low levels of Synaptophysin depicted a better overall survival compared to those with high-level Synaptophysin (Tudoraşcu et al. 2017). Similar findings were reported for prostate cancer, where metastatic tumor samples of castration-resistant prostate cancer depicted significantly more Synaptophysin expression than specimens received from prostatectomies (Sainio et al. 2018). Accordingly, carcinosarcomas of the female genital tract with Synaptophysin expression were shown to have a tendency for worse prognosis (George et al. 1991). Synaptophysin expression was further shown to be enriched in endometriosis (Wang et al. 2010), which was reported to be associated with ovarian cancer and assumed to be connected to endometrial, cervical and breast cancer (Kalaitzopoulos et al. 2020). Similarly to BKZ-1, the colorectal neuroendocrine carcinoma-derived CSC-like population BKZ-2 expressed nuclear Synaptophysin as expected for a cell population with neuroendocrine origin (Figure 5 B) (Windmöller et al. 2019; Schulte am Esch et al. 2020). Notably, the non-neuroendocrine colorectal adenocarcinoma-derived BKZ-3 population also revealed nuclear Synaptophysin protein expression but in lower amount in comparison to BKZ-2, substantiating the possible role of nuclear Synaptophysin as CSC-marker (Figure 5 C) (Schulte am Esch et al. 2020). In this line, all further isolated CSC-like populations identified within this thesis showed nuclear Synaptophysin protein despite their neuroendocrine or non-neuroendocrine origin as well as regardless of tumor type (Figure 5 D-F) (Flottmann 2020) ((Windmöller et al. 2021b), under review) ((Windmöller et al. 2021a), unpublished data). Thus, the present observation strongly suggest Synaptophysin as novel CSC-marker for populations derived from colorectal, pulmonary and endometrial carcinogenic tissue. Despite the role of Synaptophysin in neuroendocrine differentiation and the association of this process with worse prognosis in different cancer types, the functional cause for the nuclear expression of this protein in cancer cells and particularly CSCs remains unclear. From a developmental prospective, Synaptophysin was correlated with synaptogenesis during the formation of the central nervous system, which was shown to be regulated by epigenetic modulations. These included a transition from a hypermethylation to a hypomethylation state of CpG sites within the Synaptophysin gene, leading to an increase in hippocampal expression of Synaptophysin in postnatal mice (Aizawa and Yamamuro 2020). There are many examples for epigenetic deregulations in CSCs too, promoting tumorigenesis and metastasis by alterations of key transcriptomic programs and signaling pathways (reviewed in (Feinberg et al. 2016; Toh et al. 2017)). Hence,

Synaptophysin expression in CSCs probably may be modulated on epigenetic level. Nevertheless, the exact mechanism and the role of Synaptophysin expression in CSCs still remains elusive and needs to be clarified in future studies.

2.3. MYC- and NF-κB-signaling in maintaining the survival of cancer stem-like cells

2.3.1. The role of MYC in cancer stem-like cells

The MYC family of basic helix-loop-helix transcription factors, consisting of MYC, NMYC and LMYC, is known to be crucial for the control of transcriptional networks regulating cell growth, cell cycle, cell division, cell metabolism, differentiation and apoptosis (reviewed in (Eilers and Eisenman 2008; Meyer and Penn 2008)). All three MYC proteins comprise a N-terminal region containing the transactivation domain, a central region involved in nuclear localization and stability as well as a C-terminal region participating in DNA binding and the interaction with the MYC-associated factor X (MAX) (reviewed in (Conacci-Sorrell et al. 2014)). This dimerization with MAX is obligated for MYC (Blackwood and Eisenman 1991) to regulate gene transcription and chromatin remodeling of more than hundred target genes (Zeller et al. 2006; Fernandez et al. 2003) (reviewed in (Conacci-Sorrell et al. 2014)). During developmental processes the expression of MYC family genes is tightly regulated ensuring high expression in proliferative stem and progenitor cells but low expression in maturated cells (reviewed in (DePinho et al. 1991)). However, based on the important role in modulating cell proliferation and growth, MYC proto-oncogenes are frequently subjects to genetic alterations in various cancer types (Schaub et al. 2018) facilitating tumorigenesis by uncoupling *MYC* expression from its regulatory factors leading to high MYC protein levels (reviewed in (Dang 2012)). Such a deregulation of MYC was not only shown to be associated with tumor growth and progression of several cancer types, but was also linked to the maintenance of CSCs (Kim et al. 2010; Galardi et al. 2016).

Particularly, MYC was reported to be consistently overexpressed in CCSCs, contributing to self-renewal and pluripotency as well as chemoresistance (reviewed in (Elbadawy et al. 2019)) (Gao et al. 2020; Sun et al. 2020; Zhang et al. 2019). Zhang and coworkers reported a high level of MYC protein in CD133-positive CSCs isolated from the well-established colorectal carcinoma cell line HT-29. In line with this, knockdown of MYC led to reduced tumor sphere formation, invasion and tumorigenicity of this subpopulation, emphasizing a

role of MYC in CCSC maintenance (Zhang et al. 2019). This co-expression of CSC-marker CD133 and MYC protein was also shown in the CCSC-like populations BKZ-2 and BKZ-3 identified in the present work, with MYC probably being transcriptionally active, as it was localized in the nucleus (Figure 6 C-D; Figure 2 C, G). Moreover, BKZ-2 and BKZ-3 revealed cytosolic NMYC protein expression and *NMYC* copy number gain, while *MYC* copy number was unaltered (Figure 6 A-B, E-F) (Schulte am Esch et al. 2020).

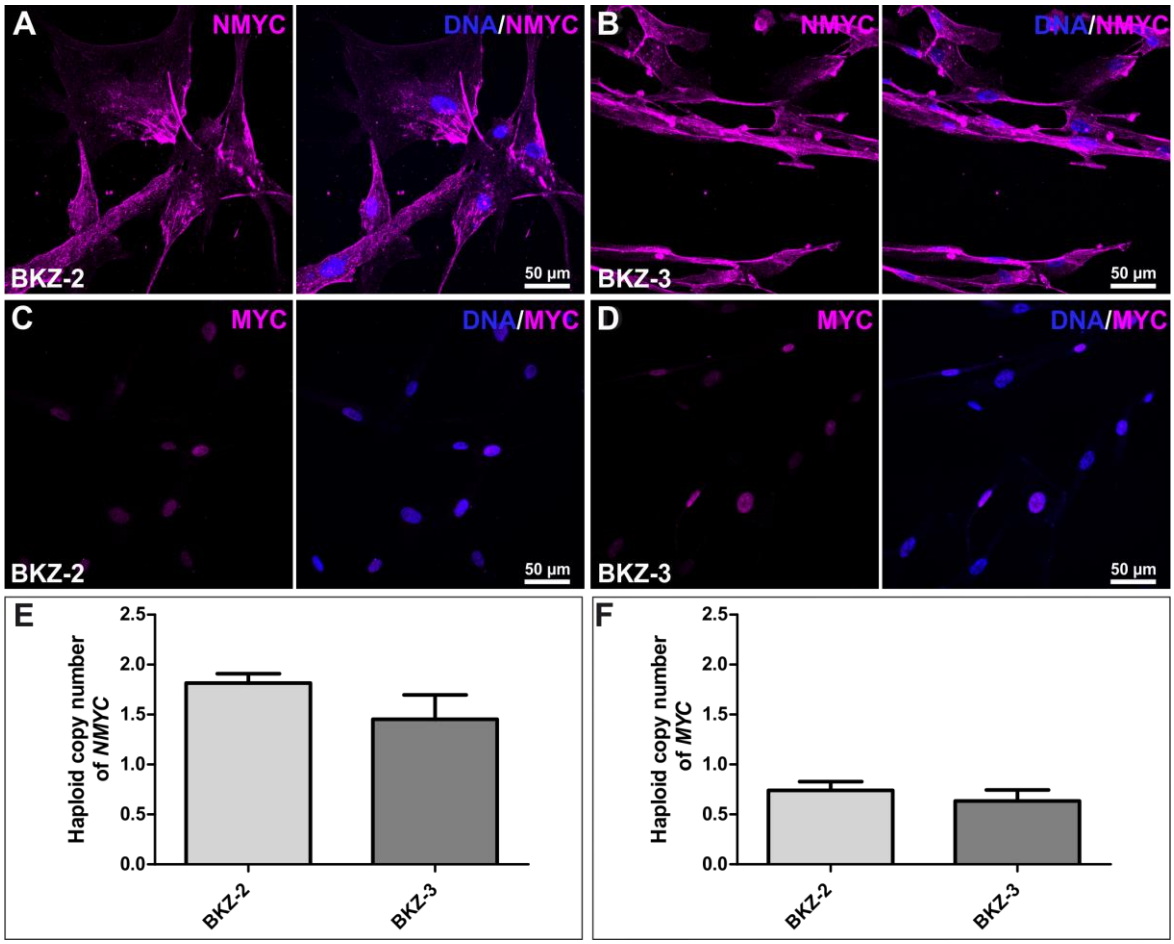

Figure 6: Rectal neuroendocrine carcinoma-derived BKZ-2 and colorectal adenocarcinoma-derived BKZ-3 highly express proto-oncogene NMYC and MYC. Immunocytochemical staining revealed high level of cytosolic **(A-B)** NMYC as well as nuclear expression for **(C-D)** MYC in BKZ-2 and BKZ-3. Further analysis of the haploid copy number of both proto-oncogenes depicted a two-fold increase of the haploid copy number of **(E)** NMYC, but a normal haploid copy number for **(F)** MYC for both cell populations, respectively. Modified from (Schulte am Esch et al. 2020)

Such a change in the copy number of MYC family members was shown to be an independent factor for poor prognosis in CRC patients (Lee et al. 2015). Likewise, NMYC overexpression was linked to highly proliferative, invasive prostate cancer with neuroendocrine features (Dardenne et al. 2016). Accordingly, high level of NMYC expression of BKZ-2 may be correlated with its neuroendocrine origin. Regarding ACs, NMYC was shown to drive the transformation of human prostate epithelial cells to prostate AC and ultimately neuroendocrine prostate cancer (Lee et al. 2016; Berger et al. 2019).

Hence, BKZ-3 may present a lineage plastic AC-derived CCSC-like population that probably harbors the potential to gain neuroendocrine features.

Consistent with the role of MYC in colorectal cancer, MYC family members were shown to be amplified in up to 33% of all lung ACs (Schaub et al. 2018), representing a poor prognostic marker (Iwakawa et al. 2011). Accordingly, MYC gain determined by fluorescence *in situ* hybridization was reported as a poor prognostic marker for the survival of lung AC patients (Seo et al. 2014). Moreover, MYC was shown to regulate the cell cycle transition and growth in NSCLC cells (Liu et al. 2021). Immunocytochemical analysis of the expression of MYC family members in the here identified NSCLC-derived CSC-like populations depicted expression of MYC protein localized in the nucleus as well as NMYC in the cytosol for each population, as exemplarily shown for BKZ-4 as SCC-derived LCSC-like cells and BKZ-7 as AC-derived LCSC-like cells (Figure 7 A-D) (Windmöller et al. 2021a). Regarding LCSCs, MYC expression was described to be associated with CSC characteristics, as suppression led to reduced viability, self-renewal, and invasiveness of LCSC-like cells derived from various lung cancer lines including A549, H460 and H292 (Tao et al. 2020; Bhummaphan et al. 2019). Thus, expression of MYC in the six primary NSCLC-derived CSC-like populations substantiates their CSC-phenotype and emphasizes a role of MYC in stemness of primary CSCs. This assumption could be further affirmed by elevated expression levels of MYC and NMYC protein in nearly all NSCLC-derived LCSC-like populations (except for BKZ-4 for MYC) in comparison to the well-established lung adenocarcinoma cell line LXF-289 (Figure 7 E-F) (Windmöller et al. 2021a). Western blot analysis of BKZ-populations also depicted an additional signal within the NMYC blot (Figure 7 E), suggesting the existence of further NMYC isoforms in LCSC-like cells in comparison to LXF-289 (Windmöller et al. 2021a). However, the presence and functional role of this potential new isoform needs to be clarified in future studies.

Similar to colorectal and lung cancer, MYC family members were also shown to play a role in the prognosis of endometrial cancer, while not only the presence or absence of MYC was reported as a prognostic factor but also its cellular location, as nuclear expression was correlated with worse survival of endometrial cancer patients (Geisler et al. 2004). Accordingly, nuclear MYC expression was also detected in the three ECSC-like populations BKZ-10, BKZ-11 and BKZ-12 (Figure 8 A-C) ((Windmöller et al. 2021b), under review), suggesting that ECSC-like cells revealing nuclear MYC expression play a role in EC progression.

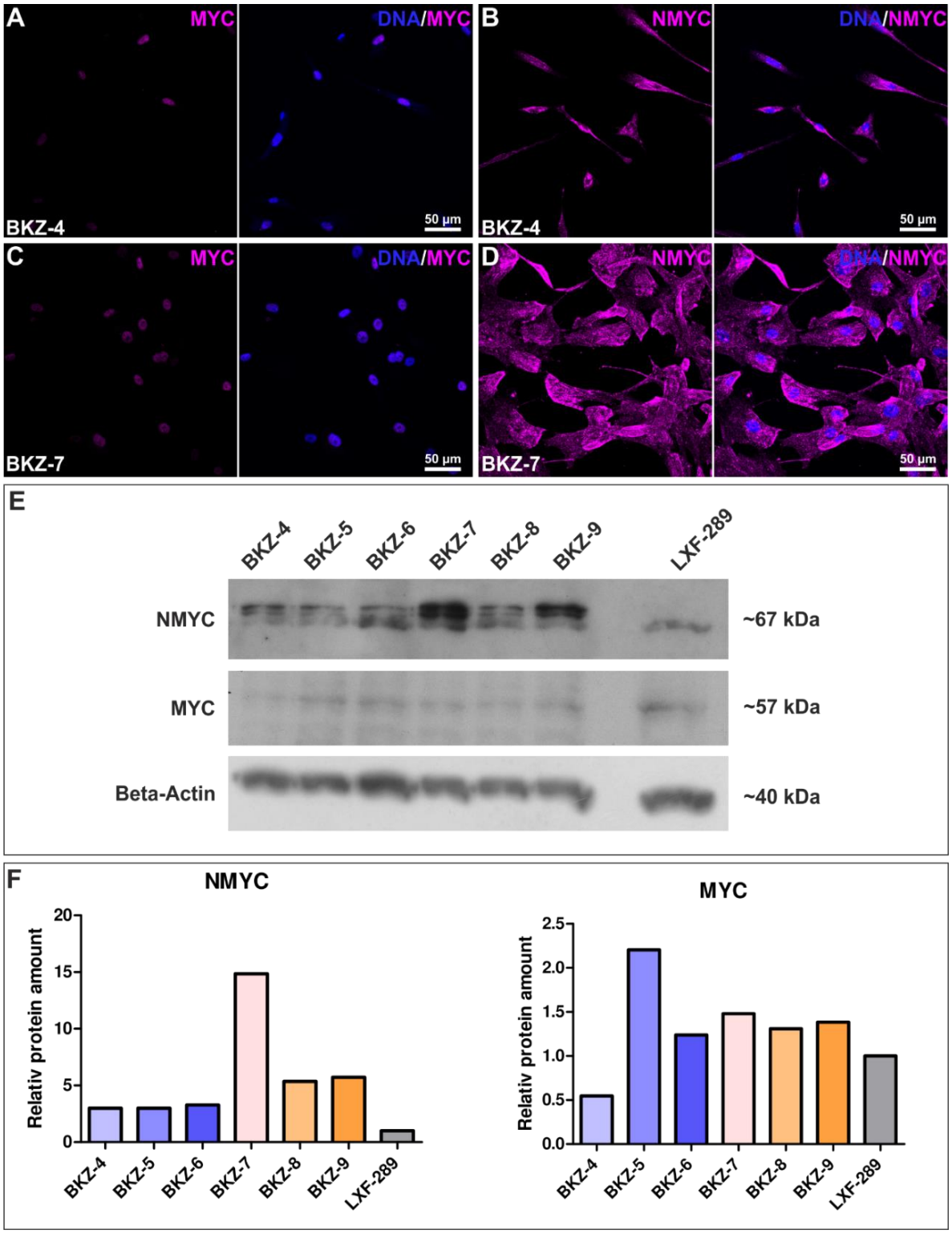

Figure 7: Non-small cell lung cancer (NSCLC)-derived cancer stem cell (CSC)-like cell populations show higher level of MYC and NMYC proto-oncogenes in comparison to adenocarcinoma-derived cell line LXF-289. Immunocytochemistry revealed nuclear MYC expression in all three squamous cell carcinoma-derived CSC-like cells, as exemplarily shown for **(A)** BKZ-4 and in all three adenocarcinoma-derived CSC-like cells, as representative demonstrated for **(C)** BKZ-7. Proto-oncogene NMYC was predominantly cytosolic expressed in all six NSCLC-derived CSC-like populations, as here exemplarily presented for **(B)** BKZ-4 and **(D)** BKZ-7. **(E)** Western blot analysis of NMYC and MYC protein verified expression within all six NSCLC-derived CSC-like populations. **(F)** Quantification depicted higher NMYC and MYC levels in all NSCLC-derived CSC-like populations in comparison to the well-established adenocarcinoma cell line LXF-289, except for BKZ-4 for MYC. Modified from (Windmöller et al. 2021a)

A study by Liu and colleagues further demonstrated the modulation of EMT-mediated invasiveness as well as drug resistance of EC cell lines via the regulation of MYC by the pluripotency-associated transcription factor SALL4 (Liu et al. 2015; Yang et al. 2010). Consistently, increased expression of MYC was reported in a CD133-positive subpopulation isolated from an endometrioid adenocarcinoma (Ding et al. 2017) and was associated with tumor growth in EC (Qiu et al. 2016). Thus, the protein expression of the proto-oncogenes MYC and NMYC in the here established ECSC-like populations strongly substantiates the CSC-phenotype of these novel *in vitro* models as MYC is strongly associated with CSC-characteristics. Nevertheless, especially MYC seems to be transcriptionally active as it was solely localized within the nucleus. Contrary, NMYC was predominantly cytosolically localized, suggesting a more dominant role of MYC in ECSC biology (Figure 8 A-F) ((Windmöller et al. 2021b), under review).

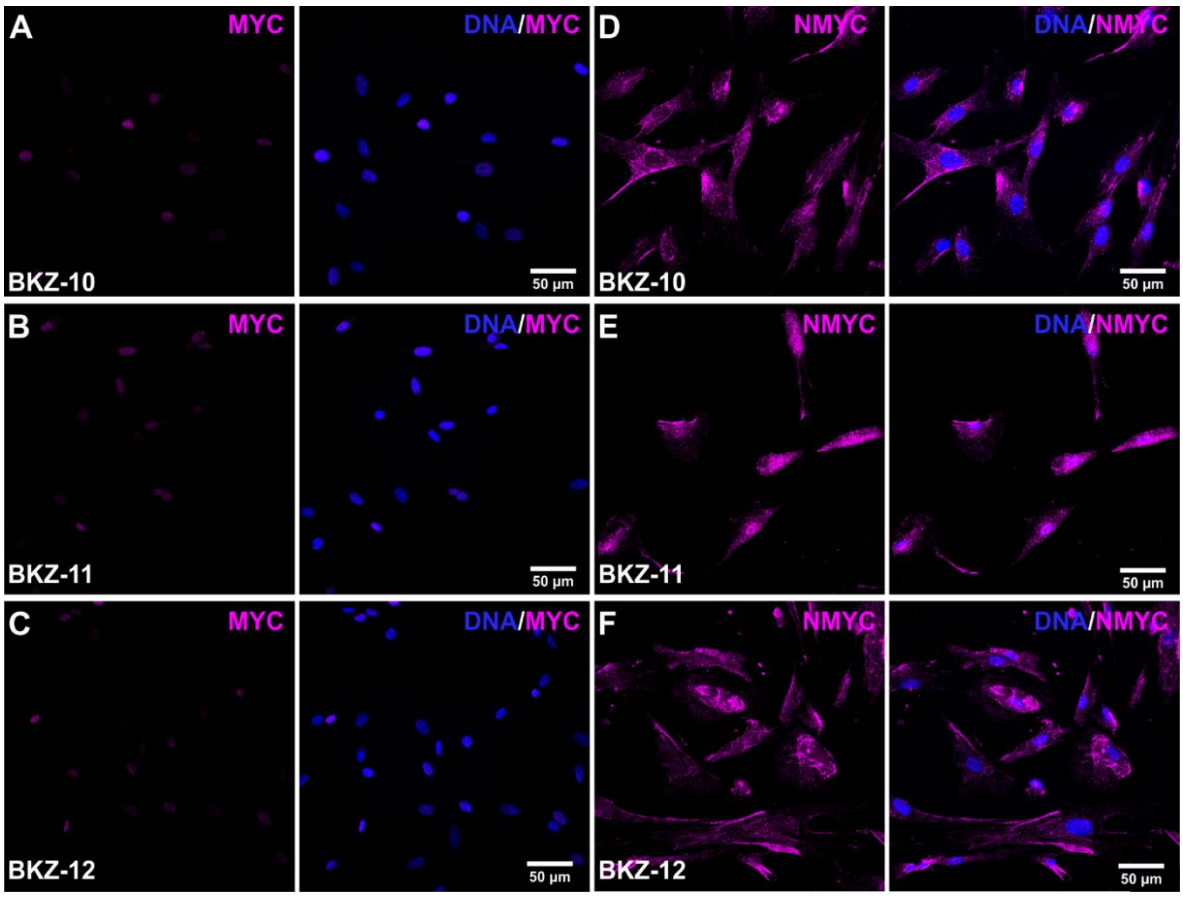

Figure 8: Endometrial carcinoma-derived cancer stem cell (CSC)-like cells express proto-oncogenes MYC and NMYC. **(A)** BKZ-10, **(B)** BKZ-11 and **(C)** BKZ-12 all revealed nuclear MYC expression. **(D-F)** Further, all three CSC-like populations depicted high cytosolic NMYC expression, with BKZ-11 even revealing nuclear NMYC. Modified from ((Windmöller et al. 2021b), under review)

Conclusively, the present work demonstrates the presence of MYC and NMYC proteins in all BKZ-populations, independent of their carcinogenic origin. Particularly, the expression of MYC may be of importance for sustaining the CSC-phenotype as it was contained in the

nucleus, suggesting transcriptional activity. The consistent expression of MYC and NMYC in the 12 BKZ-populations, including colorectal-, pulmonary- and endometrial-derived CSC-like cells and its tremendous role in carcinogenesis strongly suggests the MYC family as a highly promising target in the development of novel CSC-targeting therapies.

2.3.2. Targeting MYC significantly reduces cancer stem-like cell survival

In relation to the fundamental role of MYC in cancer formation, maintenance and progression as well as its tight correlation to CSC characteristics, MYC has been studied as a potential target in cancer therapies for decades. However, the development of MYC-affecting drugs is challenging due to the lack of catalytic activity or a hydrophobic pocket, making the use of enzyme inhibitors or low molecular weight compounds unfeasible. In addition, its nuclear localization as a transcription factor prohibits the use of big molecules like monoclonal antibodies. With regard to these challenges, no clinical approved therapy based on targeting MYC has been established so far, although eminent research focusing on different strategies such as targeting MYC transcription, translation, DNA binding or dimerization with its partner MAX has been conducted (reviewed in (Whitfield et al. 2017; Wolf and Eilers 2020)). One small molecule inhibiting the protein-protein interaction of MYC with its obligate partner MAX is KJ-Pyr-9, which was identified by screening a Kröhnke pyridine library and depicted effective blocking of MYC-dependent human cancer cell xenografts *in vivo* (Hart et al. 2014; Fujimori et al. 2003). Furthermore, only cytostatic and no cytocidal effects were demonstrated with doses of even 10mg/kg *in vivo* and KJ-Pyr-9 was shown to strongly inhibit not only the oncogenic activity of MYC but also of NMYC (Hart et al. 2014). Of note, recent efforts in drug development led to new derivates with similar activity but higher solubility and better stability (Jacob et al. 2018).

In the present work, MYC family members MYC and NMYC were shown to be highly expressed in all here established CSC-like populations, suggesting a role in maintaining CSCs characteristics and survival (see chapter 2.3.1) (Schulte am Esch et al. 2020; Windmöller et al. 2021a) ((Windmöller et al. 2021b) ,under review). Accordingly, the application of KJ-Pyr-9 on CCSC-like populations BKZ-2 and BKZ-3 led to a significant decrease of cellular survival with increasing concentrations of KJ-Pyr-9 over 20 µM respectively (Figure 9 A) (Schulte am Esch et al. 2020).

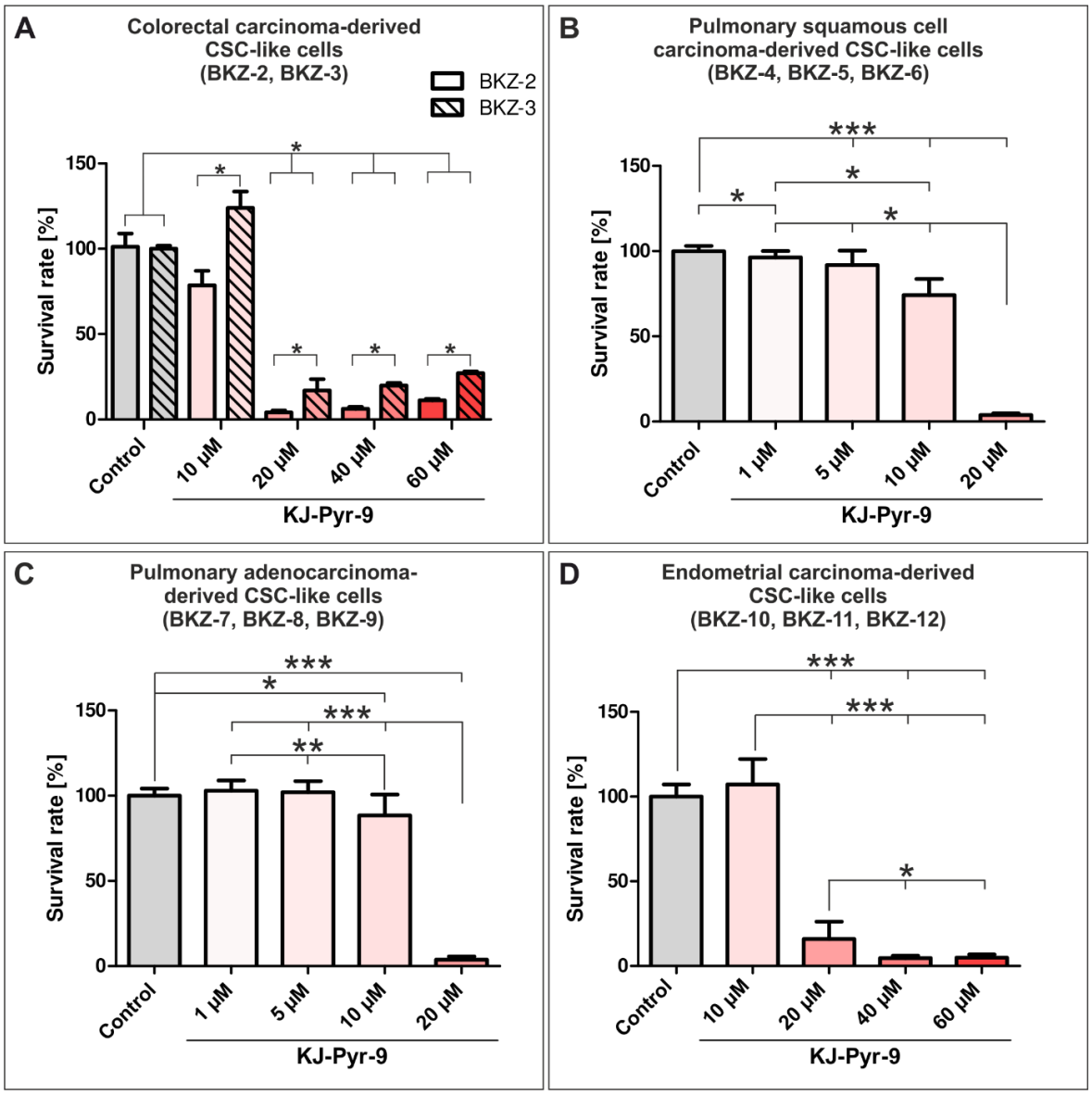

Figure 9: Inhibition of the protein-protein interaction of MYC and NMYC with the Myc-associated factor X significantly impairs survival of colorectal, pulmonary and endometrial-derived cancer stem cell (CSC)-like cells. Quantification of the normalized survival rates of the **(A)** rectal neuroendocrine carcinoma- and the colorectal adenocarcinoma-derived CSC-like populations BKZ-2 and BKZ-3 depicted significantly decreased survival rates after exposure to values greater than 20 µM of the MYC/NMYC inhibitor KJ-Pyr-9 in comparison to the control. Further comparisons between the two cell lines revealed a significant higher impairment of survival of BKZ-2 in comparison to BKZ-3 for all inhibitor concentrations. **(B)** Evaluation of the influence of KJ-Pyr-9 on the three pulmonary squamous cell carcinoma-derived CSC-like cell populations showed a significantly reduced survival after treatment with KJ-Pyr-9, with values higher than 5 µM. **(C)** Quantification of the impact of KJ-Pyr-9 on pulmonary adenocarcinoma-derived CSC-like cell populations revealed a significantly reduced survival upon KJ-Pyr-9 values higher than 10 µM. **(D)** Lastly, inhibition of MYC/NMYC-signaling using values greater than 20 µM KJ-Pyr-9 led to a significant reduction in cell survival of endometrial carcinoma-derived CSC-like cells. Non-parametric Mann-Whitney-test (A-B, D, $p \leq 0.05$). n = 3. Unpaired t-test (C, $p \leq 0.05$). n = 3, * $p \leq 0.05$, ** $p \leq 0.01$, *** $p \leq 0.001$. Mean ± SEM (standard error of the mean). **A** modified from (Schulte am Esch et al. 2020), **B-C** modified from (Windmöller et al. 2021a), **D** modified from ((Windmöller et al. 2021b), under review)

In line with their CSC-phenotype, BKZ-2 and BKZ-3 revealed a significantly higher survival rate in comparison to the two colon carcinoma cell lines HT-29 and HCT-116 after KJ-Pyr-9-treatment with 40 µM and 60 µM (Schulte am Esch et al. 2020). Nevertheless,

discrepancies in survival rates between both cell populations were detected too, as BKZ-3 was less sensitive when compared to BKZ-2, suggesting a more MYC-independent growth of BKZ-3 (Figure 9 A). Moreover, KJ-Pyr-9-mediated survival decrease was shown to correlate with induced apoptosis as demonstrated by rising levels of cleaved caspase 3-positive cells by the application of KJ-Pyr-9 (Schulte am Esch et al. 2020). Thus, MYC probably plays a role in sustaining CCSC-like cell survival by preventing apoptosis, which stands in line with studies by Zhang (Zhang et al. 2019) and Vadde (Vadde et al. 2015) reporting MYC to be involved in CCSC proliferation as well as in the inhibition of apoptosis. The role of MYC-mediated stemness in proliferation was also detected in cancer cells derived from the lung (Tao et al. 2020) and the endometrium (Liu et al. 2015). In accordance with these studies and the high expression of MYC and NMYC observed in this work, application of KJ-Pyr-9 significantly decreased survival of the here identified CSC-like populations isolated from NSCLC specimens as well as from EC tissues (Figure 9 B-D) (Windmöller et al. 2021a) ((Windmöller et al. 2021b), under review). Even though all populations depicted significant reductions in cell survival after the application of KJ-Pyr-9 concentrations greater than 20 µM, sensitivity for lower doses differed between the CSC-like populations. Particularly, the rectal neuroendocrine-derived population BKZ-2 and the groups of SCC- and AC-derived LCSC-like cell populations were more sensitive to KJ-Pyr-9-mediated MYC inhibition. Application of 10 µM KJ-Pyr-9 only reduced cell survival of these BKZ-populations, but did not affected survival rates of BKZ-3 and ECSC-like populations (Figure 9). Nevertheless, doses of 20 µM KJ-Pyr-9 significantly reduced survival of all CSC-like populations to rates ranging between 3.79% for AC-derived LCSC-like populations and 16.89% for the colorectal carcinoma-derived BKZ-3 population (Figure 9) (Schulte am Esch et al. 2020; Windmöller et al. 2021a) ((Windmöller et al. 2021b), under review). Additional calculations of the half maximal inhibitory concentrations (IC_{50}) for the NSCLC-derived populations revealed IC_{50} values between 10.33 and 11.57 µM KJ-Pyr-9 for the here-established LCSC-like cells (Windmöller et al. 2021a). Accordingly, recombinant MYC–MAX–DNA interaction was described to be inhibited with an IC_{50} of approximately 10 and 30 µM (Hart et al. 2014; Choi et al. 2017). However, KJ-Pyr-9 was reported to have no effect on the interaction of MYC with MAX in an SPR assay up to 10 µM, with no explanation for this inconsistency provided by the authors (Castell et al. 2018).

To gain further insights into the molecular mechanism of KJ-Pyr-9-mediated MYC inhibition, mRNA levels of several MYC target genes were analyzed in two representative

LCSC-like populations. Here, application of 20 µM KJ-Pyr-9 for 24 h led to a significant decrease of cyclin D1 (*CCND1*) as exemplarily shown for SCC- and AC-derived LCSC-like cells BKZ-6 and BKZ-8 (Figure 10) (Windmöller et al. 2021a). Notably, this regulatory mechanisms was only observable in the CSC-like populations and not in the well-established lung adenocarcinoma cell line LXF-289 (Figure 10) (Windmöller et al. 2021a). In accordance with that, Zhou and coworkers and Chen and colleagues also reported a link between MYC-dependent cell cycle regulation and growth as well as apoptosis in NSCLC cell lines (Chen et al. 2019; Zhou et al. 2017). Further, downregulation of MYC and CCND1 was associated with the inhibition of prostate cancer stem cell growth as well as downregulation of CSC-markers (Zhu et al. 2020), suggesting a role of *CCND1* in the KJ-Pyr-9-mediated survival decrease of the here presented CSC-like populations. Moreover, our department recently published high expression of ribosomal biosynthesis-related genes in several MYC expressing CSC-like populations, including the here presented ECSC-like and pulmonary AC-derived LCSC-like populations (Witte et al. 2021) (see also chapter 2.4.1).

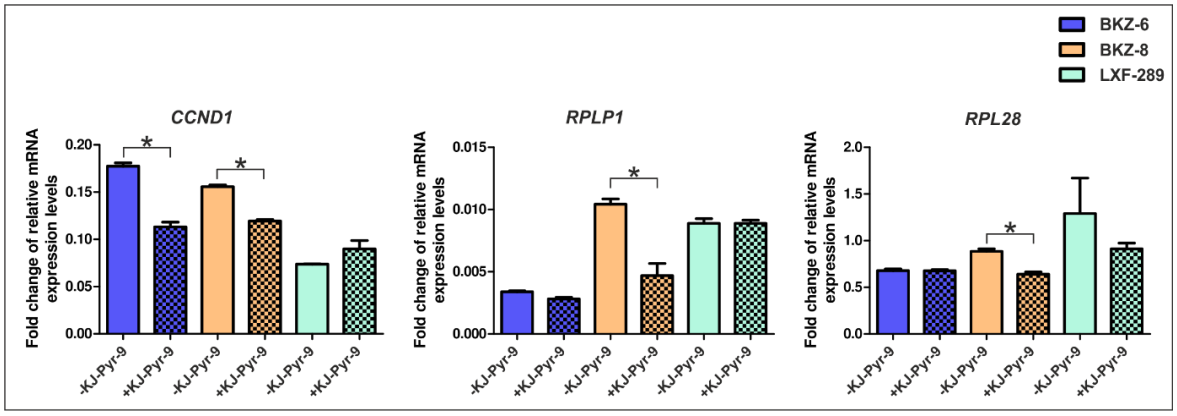

Figure 10: MYC-regulated target genes in pulmonary carcinoma-derived cancer stem cell (CSC)-like cells. Quantitative polymerase chain reaction of the MYC target genes cyclin D1 (*CCND1*), ribosomal protein lateral stalk subunit P1 (*RPLP1*) and ribosomal protein L28 (*RPL28*) showed significantly reduced *CCND1* after the application of 20 µM KJ-Pyr-9 for BKZ-6 and BKZ-8. These served as representative populations for the three squamous cell carcinoma- and three adenocarcinoma-derived CSC-like cells. In addition, BKZ-8 exhibited significant reductions of *RPLP1* and *RPL28* expression, while in BKZ-6 both mRNA levels remained unchanged. Expression levels of *CCND1*, *RPLP1* and *RPL28* of the well-established lung adenocarcinoma cell line LXF-289 were not influenced by KJ-Pyr-9-mediated MYC inhibition. Non-parametric Mann–Whitney-test ($p \leq 0.05$). n = 3, * $p \leq 0.05$. Mean ± SEM (standard error of the mean). Modified from (Windmöller et al. 2021a)

Accordingly, there is growing evidence that MYC plays a crucial role in the regulation of ribosomal biogenesis (reviewed in (Destefanis et al. 2020)). This could also be shown in this work for the AC-derived LCSC-like population BKZ-8, depicting significant reductions in the expression of ribosomal protein lateral stalk subunit P1 (*RPLP1*) and ribosomal protein L28 (*RPL28*), both involved in ribosomal biosynthesis. However, SCC-derived BKZ-6 and cell line LXF-289 did not reveal a significant downregulation of these genes, suggesting cell

population or tumor type specific differences (Figure 10) (Windmöller et al. 2021a). Besides the influence of KJ-Pyr-9-mediated MYC inhibition on cell cycle and ribosomal biogenesis of CSC-like cells, targeting MYC was reported to enhance chemotherapeutic efficacy of cisplatin in NSCLC cells (Li et al. 2017). Moreover, an interplay between MYC and NMYC was associated with radioresistance and CSC-like properties in neuroblastoma cells (Le Grand et al. 2020). Equivalently, Rihawi and colleagues reported restoring of sensitivity to ALK-inhibitors in NSCLC cell lines by the inhibition of MYC. Further, the authors showed increased expression of the immune checkpoint inhibitory molecule programmed death-ligand 1 (PD-L1) upon MYC overexpression (Rihawi et al. 2019). These findings suggest a role of MYC in the mediation of the immune system evasion, which is one major hallmark of CSCs (reviewed in (Marinkovic and Marinkovic 2021)). In this line, over 93% of MYC-expressing ECSC-like cells were positive for PD-L1 and PD-L2 (Figure 8) ((Windmöller et al. 2021b), under review). Thus, inhibition of MYC via KJ-Pyr-9 not only impairs cell cycle and partly ribosomal biogenesis while inducing apoptosis, but may also re-sensitizes CSC-like cells for chemotherapeutics and patients immune response. Still, results of this thesis suggests a complex mechanism involved in the regulation of MYC-signaling as variations in target gene expressions between different CSC-like populations were observable. These findings highlight the need for large-scale target gene analysis to fully understand the whole pathway for each specific CSC-like population. Conclusively, the present thesis demonstrates inhibition of MYC using KJ-Pyr-9 as a promising approach for targeting CSC-like cells from various origins. However, the underlying molecular mechanisms need to be further clarified and eminent *in vivo* studies will be necessary to enable the use of MYC inhibitors in clinical settings.

2.3.3. NF-κB-signaling in cancer stem-like cells

Similar to MYC, the transcription factor nuclear factor kappa-light-chain-enhancer of activated B-cells (NF-κB) plays an essential role in controlling a large number of biological processes including inflammation, apoptosis, differentiation, immune responses and proliferation (reviewed in (Perkins 2007)). Generally, the NF-κB family comprises the five subunits p50, p52, RelA (p65), c-Rel and RelB, which all contain a conserved REL homology domain involved in the formation of homo- and heterodimers and DNA binding. Subunits RelA, RelB and c-Rel additionally harbor a C-terminal transactivation domain, which enables them to activate target gene expression (reviewed in (Oeckinghaus and Ghosh

2009)). In its inactive form, NF-κB dimers are constrained in the cytoplasm by interacting with inhibitor of nuclear factor kappa B (IκB) proteins that mask the nuclear translocation signal (Kearns et al. 2006). Activation of the canonical NF-κB-pathway through signals including cytokines like Tumor Necrosis Factor α (TNF-α), lipopolysaccharides or growth factors (reviewed in (Hayden and Ghosh 2014, 2012)) facilitates the phosphorylation of the IκB kinase (IKK) complex, leading to the phosphorylation, ubiquitination and subsequent degradation of IκB. This in turn enables the translocation of NF-κB p50/RelA into the nucleus (reviewed in (Oeckinghaus and Ghosh 2009)). The non-canonical NF-κB-pathway relies on proteasomal processing of p100 to p52, mediated by the activation of IKK via NF-κB-inducing kinase, allowing the translocation of p52/RelB dimers into the nucleus (Senftleben et al. 2001). There arrived, dimers are binding to selective kB sites enabling the activation of more than 150 specific target genes, while p50/RelA is the most abundant heterodimer (May and Ghosh 1998).

Based on its diversity of regulatory functions, deregulations of the NF-κB-pathway were shown to be tightly associated with various aspects of carcinogenesis and the progression of cancer (reviewed in (Xia et al. 2018; Taniguchi and Karin 2018)). Furthermore, NF-κB-signaling was shown to be involved in the regulation of CSCs of various tumorigenic origins, participating in maintenance, proliferation, metastasis, avoidance of apoptosis, angiogenesis and stemness (reviewed in (Vazquez-Santillan et al. 2015; Kaltschmidt et al. 2019)). Even though there are a lot of reports for constitutive NF-κB-activation in various cancers (reviewed in (Dolcet et al. 2005)), the here established CSC-like populations did not reveal nuclear expression of NF-κB subunits. Nevertheless, all BKZ-populations including pulmonary and rectal neuroendocrine-derived (Figure 11 A-B) (Windmöller et al. 2019; Hanewinkel 2019)((Schulte am Esch et al. 2020), unpublished data), pulmonary and colorectal AC-derived (Figure 11 C, E) (Windmöller et al. 2021a; Hanewinkel 2019) ((Schulte am Esch et al. 2020), unpublished data), pulmonary SCC-derived (Figure 11 D) (Windmöller et al. 2021a) and EC-derived CSC-like populations (data not shown) depicted cytosolic RelA expression. Accordingly, Zakaria and coworkers revealed an involvement of the NF-κB-pathway in the regulation of LCSCs from NSCLC (Zakaria et al. 2015). High NF-κB expression was further reported to be associated with shorter overall survival of NSCLC patients (Gu et al. 2018). This correlation of NF-κB-signaling with stemness and tumorigenesis was also shown for colorectal cancer cells (Zhao et al. 2020) and gynecological cancer cells (Chefetz et al. 2013), suggesting a role of NF-κB RelA in the maintenance of CSC characteristics of the 12 novel BKZ-populations.

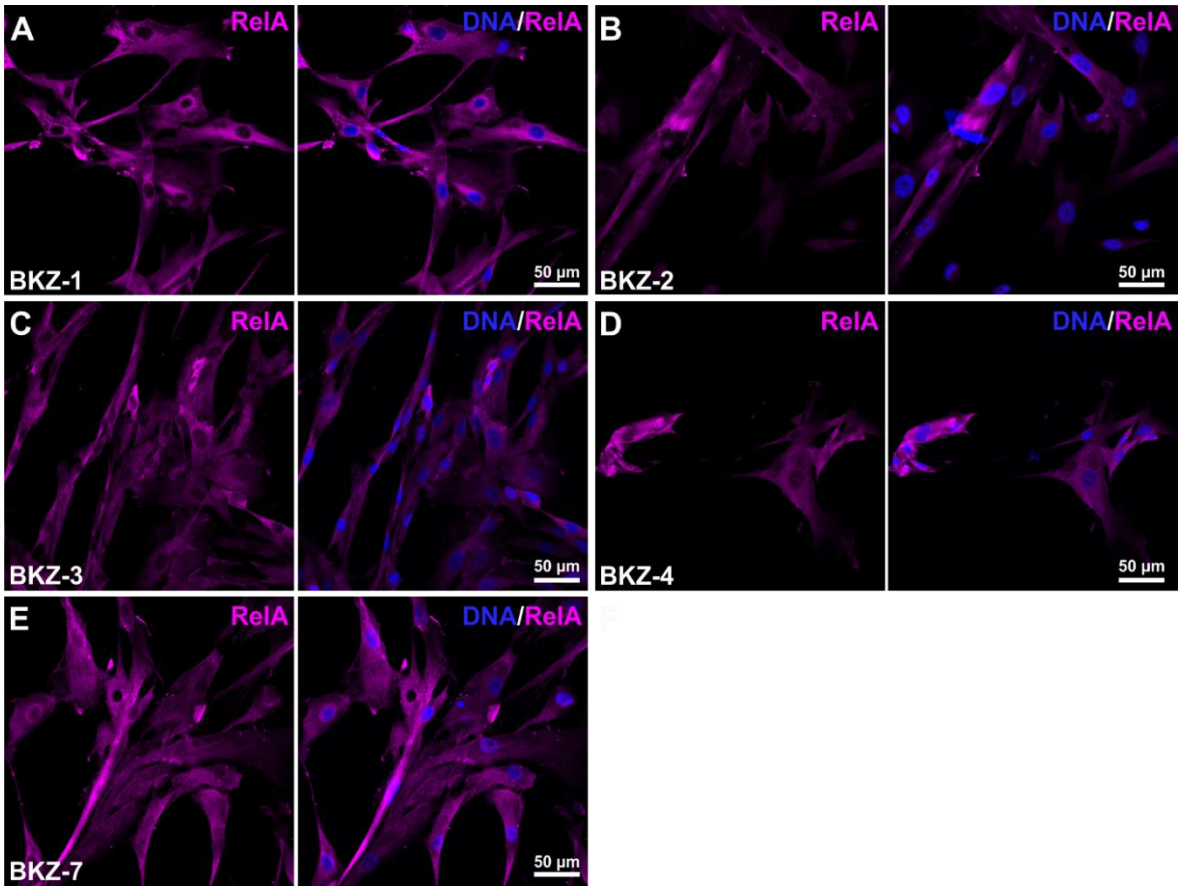

Figure 11: Established colorectal and pulmonary-derived cancer stem cell (CSC)-like cells all express NF-κB RelA. Immunocytochemistry of the different CSC-like cell populations revealed RelA protein expression for all, as depicted for **(A)** pulmonary neuroendocrine carcinoma-derived BKZ-1, **(B)** rectal neuroendocrine carcinoma-derived BKZ-2, **(C)** colorectal adenocarcinoma-derived BKZ-3, representative pulmonary **(D)** squamous cell carcinoma-derived BKZ-4 and **(E)** adenocarcinoma-derived BKZ-7. **A** modified from (Windmöller et al. 2019), **D-E** modified from (Windmöller et al. 2021a), **B-C** modified from (Hanewinkel 2019), ((Schulte am Esch et al. 2020), unpublished data).

Even though NF-κB RelA was only located in the cytosol, stimulation with the NF-κB activating cytokine TNF-α (Werner et al. 2008) led to nuclear translocation and thus to the activation of RelA in a time dependent manner. This result was observable in the colorectal AC-derived CSC-like population BKZ-3 (Figure 12 A-B, G) (Hanewinkel 2019) ((Schulte am Esch et al. 2020), unpublished data), the SCC- and AC-derived LCSC-like populations (Figure 12 C-F, H-I) (Windmöller et al. 2021a) as well as in the ECSC-like populations (data not shown). The pro-inflammatory cytokine TNF-α was already reported to be expressed in various tumors, elevating NF-κB activity and thus favoring tumorigenesis (reviewed in (Taniguchi and Karin 2018; Sethi et al. 2008)). For instance, TNF-α-mediated NF-κB-signaling was described to protect NSCLC cells from cell death (Gong et al. 2018) and promote CSC maintenance of breast cancer and leukemia (Kagoya et al. 2014; Liu et al. 2020). Contrary to the concept of pro-tumor inflammation in cancer (Taniguchi and Karin 2018) and the reported reduction of lung cancer mortality by anti-inflammatory therapies

(Ridker et al. 2017), analysis of the influence of TNF-α-mediated NF-κB-signaling in the six NSCLC-derived LCSC-like cell populations revealed no elevated cell survival (Figure 14 A-B) (Windmöller et al. 2021a). TNF-α expression was also shown to be involved in necroptosis of NSCLC cells (Yu et al. 2019) and in chemo sensitization of colon cancer cells (Walther et al. 2015).

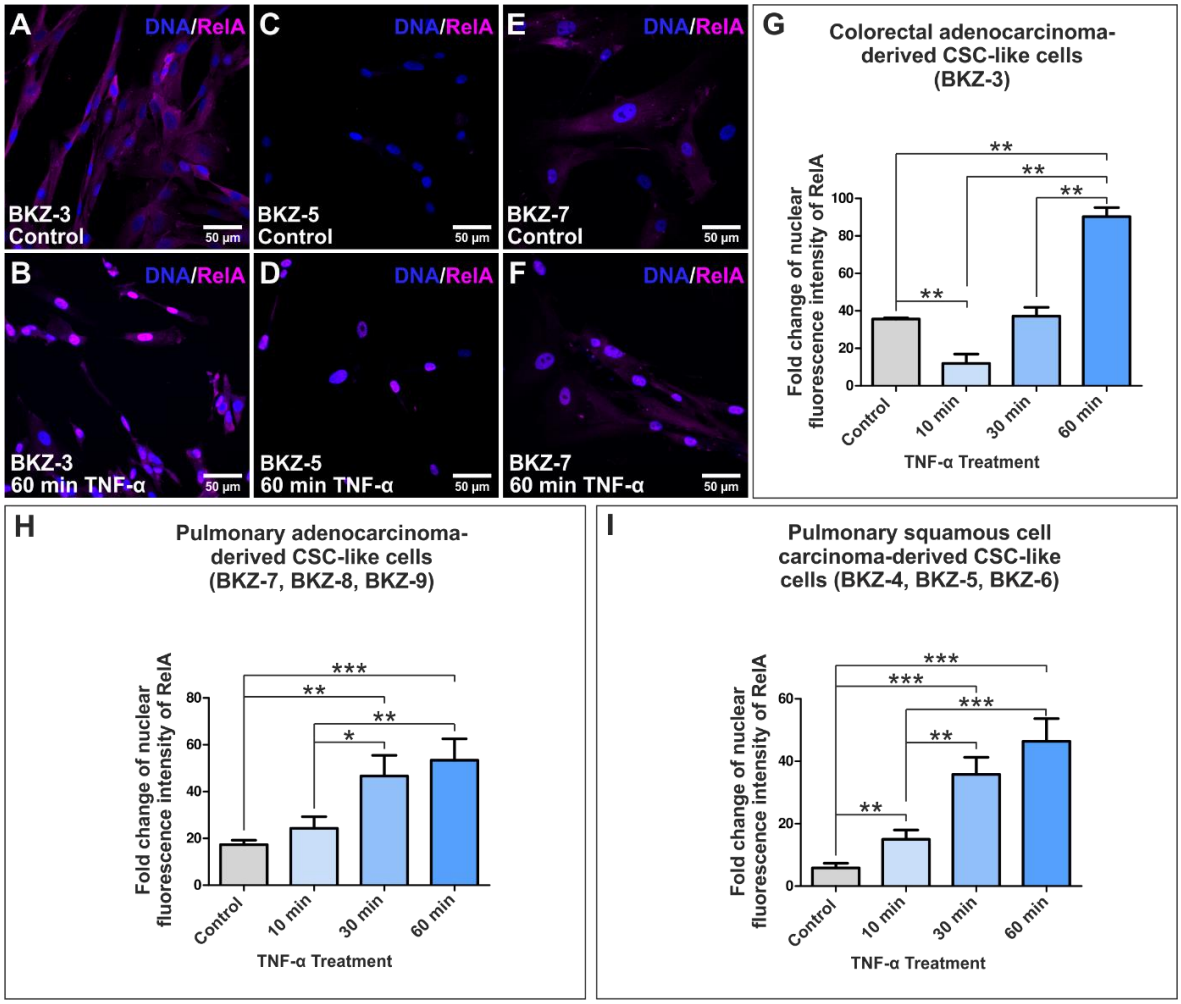

Figure 12: Tumor necrosis factor α (TNF-α) stimulation of colorectal and pulmonary-derived cancer stem cell (CSC)-like cells activates NF-κB subunit RelA. Exemplary pictures of immunocytochemical staining for RelA of untreated **(A)** colorectal adenocarcinoma (AC)-derived BKZ-3, **(C)** pulmonary squamous cell carcinoma (SCC)-derived BKZ-5 and **(E)** pulmonary AC-derived BKZ-7. TNF-α stimulation for 60 min led to nuclear translocation of RelA, as exemplarily shown for **(B)** BKZ-3 **(D)** BKZ-5 and **(F)** BKZ-7. **(G)** Quantification of fold change of nuclear fluorescence intensity of RelA demonstrated a significant increase after 60 min of TNF-α application for colorectal AC-derived BKZ-3 cells. **(H)** Evaluation of merged immunocytochemical assays for SCC-derived CSC-like populations BKZ-4, BKZ-5, and BKZ-6 depicted a statistically significant increase of the fold change of nuclear fluorescence intensity after stimulation with TNF-α for all three time points in comparison to the control. **(I)** Further, TNF-α treatment induced RelA translocation within pulmonary AC-derived CSC-like cells BKZ-7, BKZ-8, and BKZ-9 with statistical significance. Non-parametric Mann–Whitney-test (G, $p \leq 0.05$). n = 3. Unpaired t-test (H-I, $p \leq 0.05$). n = 3, * $p \leq 0.05$, ** $p \leq 0.01$, *** $p \leq 0.001$. Mean ± SEM (standard error of the mean). **C-F, H-I** modified from (Windmöller et al. 2021a), **A-B, G** modified from (Hanewinkel 2019), ((Schulte am Esch et al. 2020), unpublished data).

Accordingly, SCC-derived LCSC-like cells exhibited a significant reduction in cell survival, while AC-derived LCSC-like cell survival remain unchanged upon TNF-α treatment (Figure

14 A-B), suggesting different roles for TNF-α/NF-κB-mediated signaling in SCC- and AC-derived LCSC-like cells (Windmöller et al. 2021a). Still, all six LCSC-like cells expressed cytosolic RelA, suggesting an important role in the established BKZ-populations. Likewise, a meta-analysis conducted by Wu and coworkers revealed an association of NF-κB expression with worse survival in most solid tumors irrespective of its localization (Wu et al. 2015). Moreover, a recent study conducted by our department revealed an enrichment of the gene ontology (GO)-term "NF-κB binding" for the here established ECSC-like and AC-derived LCSC-like populations as well as for six CSC-like populations derived from glioblastoma multiforme and ACs of the prostate (Witte et al. 2021) (see also chapter 2.4.1). Thus, the expression of NF-κB RelA probably plays an essential role in sustaining CSC biology of the here established primary CSC-like populations. Notably, there is evidence for NF-κB playing a crucial role in mediating EMT-driven metastasis, which is one of the major hallmarks of CSCs and will be discussed in the following section.

2.3.4. Association of NF-κB with the process of epithelial to mesenchymal transition in cancer stem-like cells

As discussed in chapter 2.3.3, NF-κB is strongly associated with various processes in the development and maintenance of cancer and especially CSCs. Its involvement in CSC-driven metastasis and invasiveness is strongly associated with its role in the regulation of the process of EMT (reviewed in (Min et al. 2008)), where epithelial cells undergo morphological and biochemical changes, resulting in a mesenchymal phenotype with increased migratory and invasive properties (reviewed in (Kalluri and Weinberg 2009)). Key transcription factors regulating this process include SNAIL, SLUG and TWIST, which repress the epithelial phenotype and are either directly or indirectly regulated by NF-κB (reviewed in (Min et al. 2008)). For instance, in breast cancer cells NF-κB RelA was shown to act as direct transcriptional regulator of SLUG and TWIST (Pires et al. 2017). Moreover, NF-κB RelA-SLUG-mediated EMT was associated with the induction of a stem-like phenotype in breast cancer cells (Storci et al. 2010). Accordingly, NF-κB RelA was shown to induce EMT in CRC cells via upregulation of SNAIL, leading to increased expressions of CCSC-markers (El-Ashmawy et al. 2019). This link was also reported by Zou and coworkers, who demonstrated that radioresistant NSCLC cells depict higher activity of NF-κB-signaling and an elevated EMT- and CSC-phenotype in comparison to non-radioresistant cells (Zou et al. 2020). The interplay between NF-κB-, EMT- and CSC-characteristics could

be also found in the here established BKZ-populations, as the two CCSC-like populations BKZ-2 and BKZ-3 (Figure 13 A-B) (Schulte am Esch et al. 2020) as well as the six NSCLC-derived LCSC-like populations (Figure 13 C-D) (Windmöller et al. 2021a) revealed nuclear SLUG protein. Moreover, ECSC-like cells depicted nuclear SLUG protein, as exemplarily shown for BKZ-10 (Figure 13 E) ((Windmöller et al. 2021b), under review).

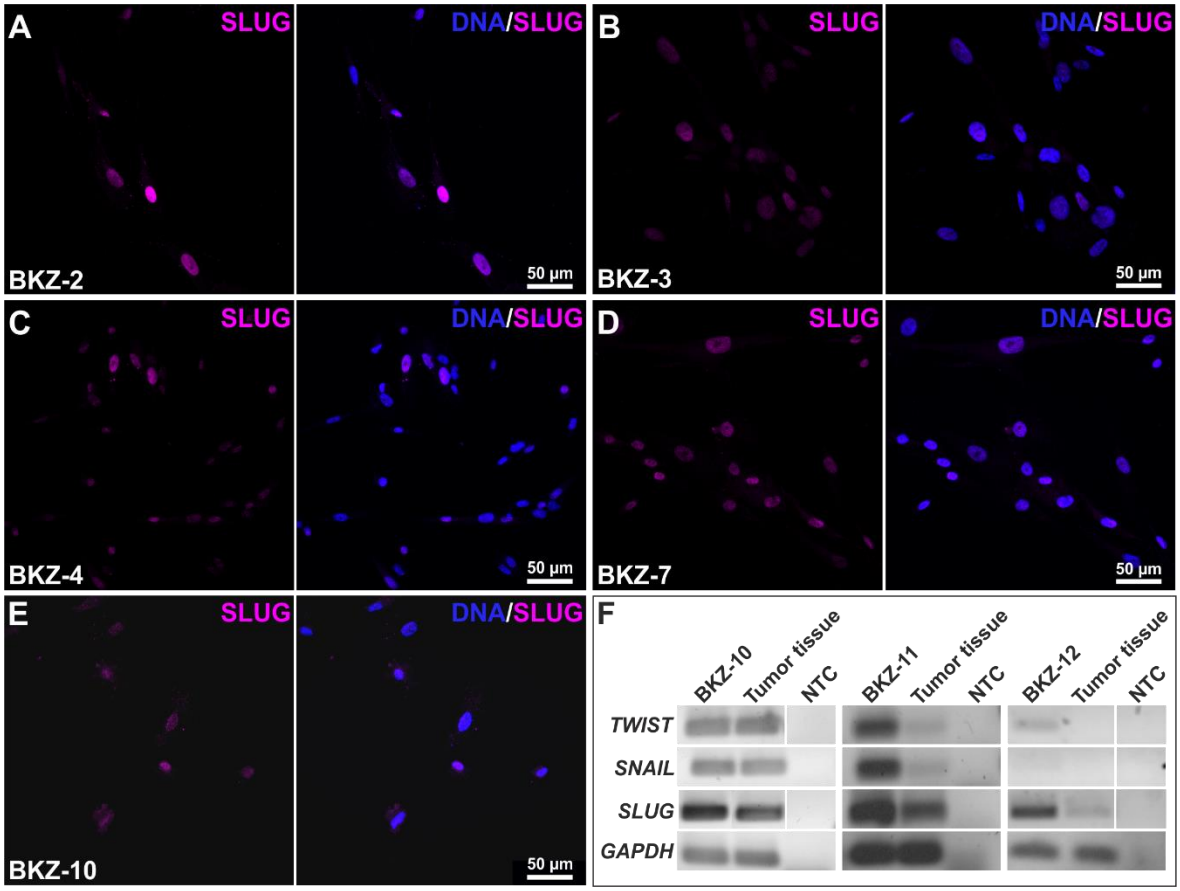

Figure 13: Cancer stem cell (CSC)-like populations all express nuclear Slug protein. **(A)** Rectal neuroendocrine carcinoma-derived CSC-like BKZ-2 cells and **(B)** colorectal adenocarcinoma-derived CSC-like BKZ-3 cells both reveal nuclear Slug expression. Further, **(C)** BKZ-4 and **(D)** BKZ-7 as representative populations for pulmonary squamous cell carcinoma-derived and pulmonary adenocarcinoma-derived CSC-like cells expressed nuclear Slug. **(E)** Lastly, all endometrial carcinoma-derived CSC-like populations BKZ-10, BKZ-11 and BKZ-12 revealed nuclear Slug, as exemplarily shown for BKZ-10. **(F)** Transcriptional profiling of the three populations and their respective parental tumor tissue for *TWIST*, *SNAIL* and *SLUG*, three key transcription factors of the process of epithelial-mesenchymal transition, depicted enriched expression in the isolated CSC-like populations in comparison to the tumor of origin. Nevertheless, expressions differed between the three populations, as BKZ-12 did not expressed SNAIL and only slightly TWIST. **A, B** modified from (Schulte am Esch et al. 2020), **E** modified from ((Windmöller et al. 2021b), under review), **C-D, F** unpublished data.

Notably, ECSC-like cells revealed elevated mRNA-levels of *TWIST*, *SLUG* and *SNAIL* in comparison to their parental tumor tissues (Figure 13 F) ((Windmöller et al. 2021b), under review, unpublished data), substantiating the correlation between stemness and the expression of NF-κB and EMT transcription factors. Correspondingly, elevated TNF-α levels in EC were described as an increased risk factor for the disease (Dossus et al. 2011),

which possibly may be due to a NF-κB-mediated enrichment of an EMT- and CSC-phenotype. Even tough SNAIL, SLUG and TWIST were all reported to play a pivotal role in maintaining an EMT-phenotype, SLUG seemed to be the most important one in the here isolated CSC-like populations, as it was the most prominently expressed transcription factor on mRNA-level in ECSC-like cells (Figure 13 F) and in almost all other BKZ-populations (data not shown). Thus, next to a vaccination against TWIST to overcome EMT-driven metastasis (Kwilas et al. 2015), a vaccine targeting SLUG may harbor a great potential to not only impair an EMT-phenotype in cancer cells but also stemness of CSCs. Next to EMT markers, targeting NF-κB-signaling in CSCs remains as a promising therapeutic strategy, which will be addressed in the following chapter.

2.3.5. Inhibition of NF-κB as therapeutic option to target lung cancer stem-like cells

Based on its crucial role in several CSC-associated processes, NF-κB represents a promising drug target to impair CSC-driven tumorigenesis and metastasis (reviewed in (Vazquez-Santillan et al. 2015)). Particularly, CD44-positive breast CSCs were shown to be significantly reduced as well as sphere formation was inhibited by the impairment of NF-κB-signaling pathway (Chung and Vadgama 2015; Kastrati et al. 2017). Furthermore, a novel quinone derivate was reported to reduce tumor growth and metastases of breast cancer cells *in vitro* and *in vivo* by downregulating NF-κB (Yang et al. 2019). This was also shown for pancreatic CSCs, where the inhibition of NF-κB RelA led to the disruption of stem-like properties and invasiveness (Sun et al. 2013). In hepatocellular carcinoma cell lines NF-κB-SNAIL-signaling was described to be involved in the EMT process and the preservation of CSC-like characteristics, which could be inhibited by blocking NF-κB (Yang et al. 2016). In this line, a pro inflammatory-induced EMT- and CSC-phenotype in a cervical carcinoma cell line could be disturbed by inhibiting the NF-κB-TWIST axis (Dong et al. 2019). Accordingly, investigation of the cell survival of the here isolated NSCLC-derived populations after inhibition of NF-κB-signaling utilizing dexamethasone and pyrrolidinedithiocarbamate (PDTC) depicted significantly reduced survival rates in comparison to the control (Figure 14) (Windmöller et al. 2021a). PDTC-treatment in SCC-derived LCSC-like cells impaired survival more significantly in comparison to dexamethasone, which was not observable in AC-derived LCSC-like cells. Further, no synergistic effect on the decrease of survival was visible after application of dexamethasone and PDTC simultaneously (Figure 14) (Windmöller et al. 2021a).

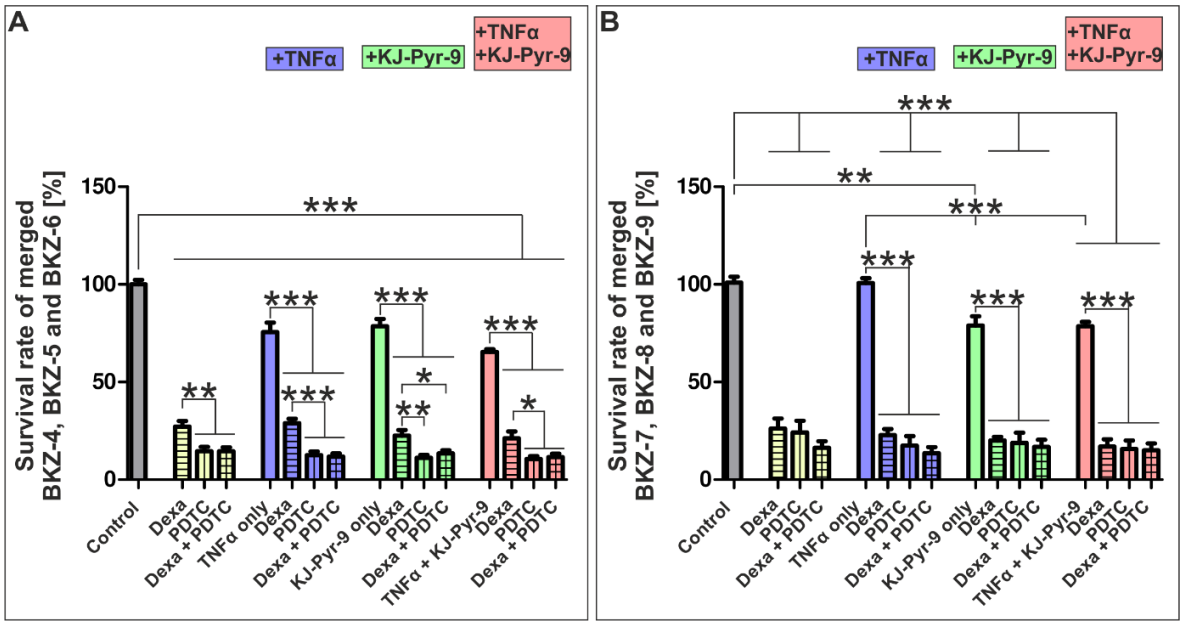

Figure 14: Inhibition of NF-κB-signaling significantly affects survival of non-small cell lung cancer-derived cancer stem cell (CSC)-like cells. To analyze the influence of NF-κB-signaling inhibition and possible synergistic effects of MYC and NF-κB co-inhibition, cells were treated with dexamethasone (Dexa; 300 µM), pyrrolidinedithiocarbamate (PDTC; 100 µM), TNF-α (Tumor necrosis factor α; 10 ng/mL), and KJ-Pyr-9 (10 µM) with subsequent analysis of cellular viability. **(A)** Quantification of normalized survival rates of squamous cell carcinoma (SCC)-derived CSC-like cells revealed a significantly impaired survival upon all treatment combinations but did not show any synergistically effect of the different reagents. Nevertheless, PDTC deceased cell survival more effective than dexamethasone. **(B)** Evaluation of the normalized cellular viability of adenocarcinoma (AC)-derived cells also revealed no synergistically effect of inhibition of MYC and NF-κB-signaling. However, TNF-α alone did not influence cell survival of AC-derived cells in contrast to SCC-derived ones. Further, the survival-decreasing effect of dexamethasone and PDTC did not differ significantly. Unpaired t-test ($p \leq 0.05$). n = 3, * $p \leq 0.05$, ** $p \leq 0.01$, *** $p \leq 0.001$. Mean ± SEM (standard error of the mean). Modified from (Windmöller et al. 2021a)

Even though it was shown that dexamethasone not only interferes with NF-κB-activation but also reduces TNF-α production (Crinelli et al. 2000; Chang et al. 1997), usage of TNF-α with dexamethasone and/or PDTC together did not influenced the impairment of cellular survival (Figure 14 A-B) (Windmöller et al. 2021a). Next to NF-κB inhibition, dexamethasone was shown to regulate the AKT/ERK-signaling in NSCLC cells leading to the inhibition of EMT (Zhang et al. 2020) as well as it was indicated to reduce stemness maintenance and self-renewal in hepatocellular carcinoma stem cells (Jiang et al. 2020). Accordingly, PDTC was shown to inhibit NF-κB-mediated EMT and CSC-marker expression in the bladder of mice (Geng et al. 2021) and was reported to reduce NF-κB-mediated angiogenesis of CCSCs (Chung et al. 2021). These findings are in accordance with the here revealed survival decreasing effects of dexamethasone and PDTC on NSCLC-derived LCSC-like cells that also exhibit an EMT- and stem-like phenotype. Moreover, PDTC was shown to suppress MYC expression thus leading to cytotoxic effects in small cell lung cancer cells (Tahata et al. 2014), emphasizing a role of PDTC in MYC modulation in NSCLC cells, too. This stands in line with evidences for the regulation of MYC through NF-

κB, as RelA was shown to bind to the promoter of MYC in breast cancer cells (Yuan et al. 2016) and c-Rel was exhibited to control MYC expression in leukemia cells (Li et al. 2020). Nevertheless, Page and colleagues reported that only nuclear expression of the NF-κB-signaling pathway member IKKα enhanced MYC activation, while cytoplasmic IKKα results in EGFR- and NF-κB-pathway over-activation (Page et al. 2019). Further, Ischenko and coworkers generated gene expression modules for MYC and NF-κB using human cancer gene sets and depicted that up- and downregulated genes in the MYC and NF-κB module were distinct from each other, suggesting the control of different aspects of tumorigenesis via MYC and NF-κB (Ischenko et al. 2017). Hence, no synergistic impairment of NSCLC-derived LCSC-like cell survival could be observed after co-treatments of 10 µM of the MYC inhibitor KJ-Pyr-9 with the NF-κB inhibitors dexamethasone and/or PDTC (Figure 14 A-B) (Windmöller et al. 2021a). As there is evidence for possible regulations of NF-κB on MYC expression in several cancer cell lines and BKZ-populations express NF-κB as well as MYC (see chapters 2.3.1 and 2.3.3), co-inhibition of NF-κB- and MYC-signaling could be of particular interest for the treatment of the here established CCSC-like cells and ECSC-like cells, which remains to be investigated in future studies. Of note, direct inhibition of MYC/NMYC with 20 µM KJ-Pyr-9 proved to be more effective than 100 µM PDTC or 300 µM dexamethasone treatment in both SCC- and AC-derived LCSC-like cells (Figure 9 B-C, Figure 14 A-B) (Windmöller et al. 2021a), suggesting MYC inhibition as more effective for NSCLC-derived LCSC-like cells. In addition, application of TNF-α, KJ-Pyr-9, dexamethasone and PDTC in parallel did not influence LCSC-like cell survival synergistically when compared to the respective control (Figure 14 A-B) (Windmöller et al. 2021a).

In summary, these results strongly suggest that NF-κB is a promising target for the impairment of LCSC-like cells, which is in accordance with Zakaria and coworkers, who reported induced apoptosis and the prevention of EMT for LCSCs after the inhibition of NF-κB (Zakaria et al. 2018). Nonetheless, targeting MYC seems to be promising as well, as even low amounts of KJ-Pyr-9 impaired LCSC-like cell survival with high effectiveness. From a clinical perspective, MYC targeting drugs still have to be approved, while dexamethasone (Kostaras et al. 2014) and the PDTC derivative zinc diethyldithiocarbamate (reviewed in (Ekinci et al. 2019)) are already in clinical use making them more rapidly applicable for NSCLC patients.

2.4. Role of ribosomes and mitochondria in cancer stem-like cells

2.4.1. Alterations of mitochondrial and ribosomal function in cancer stem-like cells

Besides the tremendous role of transcriptional deregulations in CSC biology including MYC- and NF-κB-signaling pathways, alterations in mitochondrial and ribosomal functions were also reported to promote acquisition and maintenance of CSCs of various carcinogenic tissues (reviewed in (Skoda et al. 2019; Bastide and David 2018)). In the present thesis, in depth analysis of the global transcriptome levels of the here established LCSC-like populations BKZ-7, BKZ-8 and BKZ-9 (there termed LCSC_a, LCSC_b, LCSC_c) and ECSC-like populations BKZ-10, BKZ-11 and BKZ-12 (there named ECSC_a, ECSC_b and ECSC_c) as well as three CSC-like populations each derived from glioblastoma and ACs of the prostate provided further indications for deregulations of mitochondrial and ribosomal function in CSCs of various origins (Witte et al. 2021). In this study, nanopore sequencing was used to analyze full length cDNA of the respective cells in order to identify conserved mechanisms in CSC-like populations isolated from different tissues. After bioinformatic processing of sequencing datasets, principal component analysis was conducted revealing three dominant clusters upon the 12 CSC-like populations. While the three CSC-like populations derived from glioblastoma and AC of the prostate clustered independently, ECSC-like and LCSC-like populations grouped more coherently in one cluster each, suggesting a more consistent gene expression within this CSC-like populations. Nevertheless, variances between the different BKZ-populations within the respective clusters could be seen, too (Figure 15 A) (Witte et al. 2021). Next to the general clustering of the 12 CSC-like populations, expression of the CSC-marker *CD44* was detected for every investigated BKZ-population, which is in accordance with the observed high protein amounts of CD44 within the BKZ-populations (Figure 2 C,G; Figure 3 C,G,K; Figure 4 C) (see chapter 2.2.). Further, all ECSC-like and LCSC-like populations depicted an expression of *MYC*, except for BKZ-12 (Figure 15 B) (Witte et al. 2021), which probably may be due to CSC plasticity or an eventually insufficient read depth of nanopore sequencing. Nevertheless, expression of *CD44* and *MYC* further confirmed the CSC-phenotype of the here established CSC-like populations on transcriptional level.

Sequencing datasets of this thesis were further used to create a hierarchical clustered heatmap of the 200 top expressed genes within the 12 CSC-like populations (Witte et al. 2021). Two extracts of the 200 top expressed genes especially comprised genes involved in

ribosome biosynthesis including various genes encoding for components of the 60S and the 40S subunit, but also mitochondria-associated genes e.g. cytochrome c oxidase subunit 7C (*COX7C*). However, expression levels of ribosome-associated genes differed between the CSC-like populations, being most highly expressed in BKZ-10, BKZ-12 and one of the CSC-like population derived from glioblastoma (Figure 16 A) (Witte et al. 2021), underlining differences in the expression profiles of CSC-like populations even from the same tumorigenic origin.

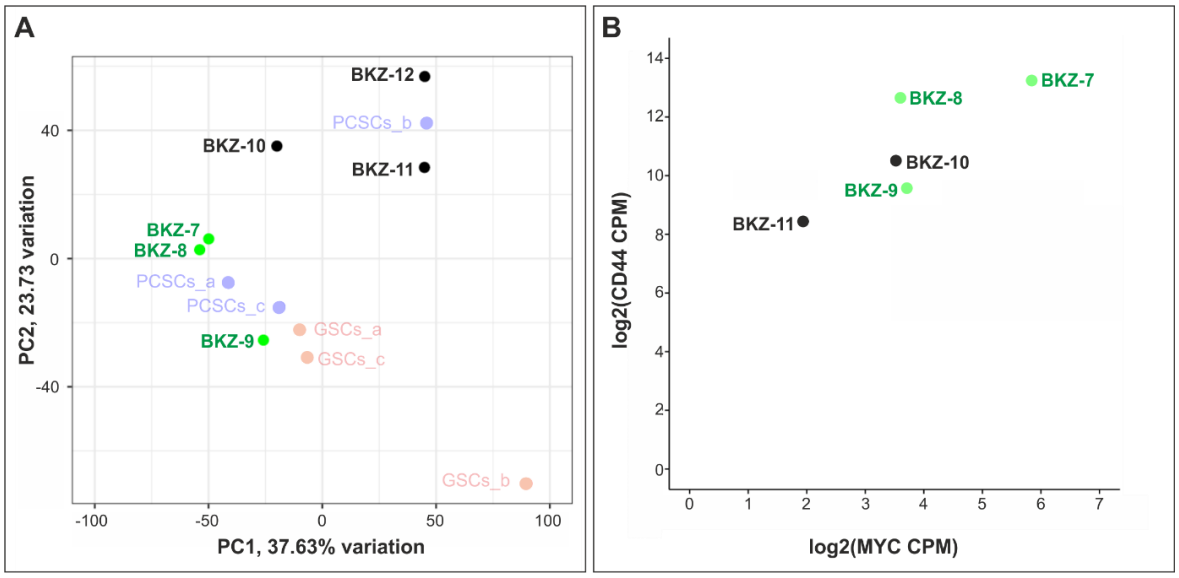

Figure 15: Correlation analysis of gene expression profiles from several primary human cancer stem cell (CSC)-like cells with different tumorigenic origin. **(A)** Principal component analysis depicted two predominant clusters of CSC-like cells, with no correlation to the parental tumor types. Nevertheless, endometrial carcinoma-derived CSC-like populations BKZ-10, BKZ-11 and BKZ-12 all clustered together with one of the three prostate CSC-like cell (PCSC) populations. Within the second cluster the three pulmonary adenocarcinoma-derived CSC-like populations BKZ-7, BKZ-8 and BKZ-9, the two remaining PCSCs as well as glioblastoma stem cell-like cells a (GSCs_a) and GSCs_c are comprised. GSCs_b clustered independently. **(B)** Correlated expression of CSC-marker CD44 with the expression of MYC. For each analysis, biological replicates depicted the mean of merged technical triplicates. Nanopore sequencing depicted expression of CD44 and MYC for all investigated pulmonary adenocarcinoma- as well as endometrial carcinoma-derived CSC-like populations, except for BKZ-12, where only CD44 expression was detectable. Modified from (Witte et al. 2021)

Nevertheless, the five top enriched KEGG pathways within all CSC-like populations included the gene pathway “Ribosome”, which was the most significantly enriched one, and “Oxidative phosphorylation”, further emphasizing an eminent role of ribosomes and mitochondria in the here established CSC-like populations independent of tumorigenic origin (Figure 16 B) (Witte et al. 2021). Further, GO-term enrichment analysis substantiated the enhancement of various ribosome- and mitochondria-associated terms as well as it depicted a 3.4-fold enrichment for the GO-term “NF-κB binding” (Witte et al. 2021), which is in accordance with the observed important role of NF-κB in the established CSC-like BKZ-populations (see chapter 2.3.3 - 2.3.5). According to the enrichment of ribosome- and

mitochondria-associated genes within the here established CSC-like populations, increased mitochondrial biogenesis as well as ribosomal biogenesis were shown to be consistent with the induction of a stem-like phenotype of breast cancer cells (Peiris-Pagès et al. 2019).

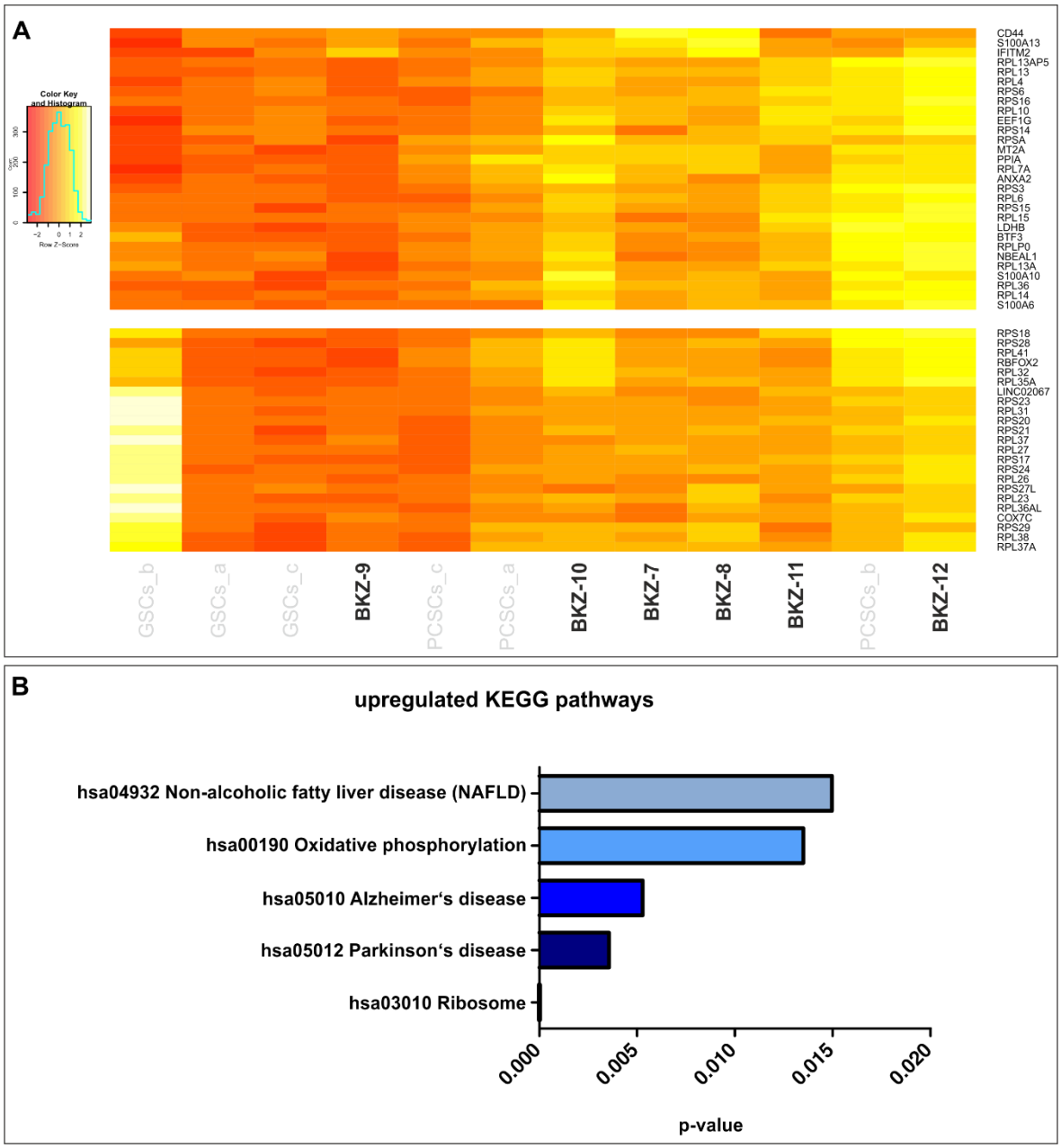

Figure 16: Mitochondrial and ribosomal genes expression is enriched in cancer stem cell (CSC)-like cell populations. **(A)** Extracts of the hierarchically clustered heatmap of the 200 top expressed genes within the 12 CSC-like cell populations depicted upregulated expressions of various ribosomal and mitochondrial biosynthesis associated genes. **(B)** Further, top five upregulated KEGG pathways ($p \leq 0.05$) included "oxidative phosphorylation (hsa00190)" and "ribosome (hsa03010)", when analyzing all 12 CSC-like cell populations. Modified from (Witte et al. 2021)

Accordingly, a study by Lamb and coworkers reported that CSC survival is dependent on mitochondrial biogenesis. Here the usage of mitochondria-targeting drugs significantly reduced the survival of CSCs of various origins including breast, ovarian, prostate,

pancreatic, lung, melanoma and glioblastoma, emphasizing a crucial role of enhanced mitochondrial function within these cells (Lamb et al. 2015). Moreover, it was reported that ribosomal RNA processing and the 60S ribosome biogenesis is involved in KRAS-driven lung cancer cell proliferation (Wang et al. 2021) as well as genes associated with ribosome biogenesis and translation are reported to be enriched in prostate CSCs in comparison to non-CSCs (Binal et al. 2020). As already discussed above MYC plays a crucial role in the regulation of ribosomal biogenesis and in maintaining the CSC state (reviewed in (Destefanis et al. 2020)) (Galardi et al. 2016) (see chapter 2.3.2). Accordingly, enriched expression of ribosome-associated genes and pathways in the here established CSC-like populations may be based on the expression of MYC, which was detected on protein and mRNA level in all established BKZ-populations (Figure 6, 7, 8, 15). This link could be already confirmed for AC-derived LCSC-like population BKZ-8, where KJ-Pyr-9-mediated MYC inhibition decreased *RPLP1* and *RPL28* mRNA expression. Nevertheless, a relation between MYC-signaling and the expression of ribosome-associated gene expression could not be detected for SCC-derived LCSC-like population BKZ-6 so far (Figure 10) (see chapter 2.3.2) (Windmöller et al. 2021a). Next to its involvement in the regulation of ribosomal biogenesis, MYC also takes part in modulating the metabolic phenotype of cancer cells, as it was shown to maintain mitochondrial respiration of chemo resistant breast CSCs (Lee et al. 2017). Equivalently, in leukemia cells NF-κB c-Rel was shown to increase mitochondrial respiration via the upregulation of MYC (Li et al. 2020). Further, NMYC-amplified cancer cells were reported to significantly promote mitochondrial respiration (reviewed in (Yoshida 2020)), indicating a role of MYC family proteins in the regulation of mitochondrial biogenesis. Hence, global transcriptional analysis of the here established LCSC-like and ECSC-like populations not only substantiated their molecular CSC-profile, but also strongly suggests an important function of ribosomes and mitochondria in CSC biology possibly regulated by members of the MYC family.

2.4.2. Metformin-mediated targeting of mitochondria impairs endometrial carcinoma-derived cancer stem-like cell survival

Increased mitochondrial biogenesis is associated with stemness of various cancer cells (reviewed in (Skoda et al. 2019)) (see chapter 2.4.1). This increase is strongly related with the upturn of the process of oxidative phosphorylation (OXPHOS), where mitochondrial adenosine triphosphate is generated by the consumption of oxygen (reviewed in (Porporato

et al. 2018)). Thus, contrary to the concept of Otto Warburg (Warburg 1925), not all cancer cells rely on aerobic glycolysis, as CSCs show a high metabolic plasticity allowing them to switch preferably to an OXPHOS-phenotype (reviewed in (Desbats et al. 2020)) (Sancho et al. 2015). Correspondingly, Wei and colleagues depicted enhanced mitochondrial function in liver CSCs maintaining their stemness, whereas non-CSCs revealed aerobic glycolysis (Wei et al. 2019). Similar results were also reported for breast cancer cell lines, as cells with high mitochondrial mass exhibited a stem-like phenotype and chemoresistance (Farnie et al. 2015), suggesting the inhibition of OXPHOS as a promising anti-CSC therapy. Likewise, targeting mitochondrial metabolism was reported to eradicate CSCs, impairing only pathogenic but no healthy cells (Francesco et al. 2019). More recently, clinical evidence has provided that mitochondria-enriched CSCs play an eminent role in breast cancer metastasis. The authors also revealed inhibition of tumor cell metastases by utilizing mitochondrial inhibitors without observing cytotoxic side effects (Ózsvári et al. 2020). One well-investigated standard type 2 diabetes medication and the most frequently administered drug treating metabolic syndromes is metformin (reviewed in (Bailey 2017)). Mechanistically, metformin decreases OXPHOS by directly diminishing mitochondrial function, thus altering the redox status of mitochondria and increasing glycolysis as compensatory mechanism (Andrzejewski et al. 2014). This mitochondria targeting action of metformin was depicted to inhibit EMT (Zhang et al. 2015) as well as CSC gene expression (Bao et al. 2012) leading to apoptosis of e.g. pancreatic CSCs (Sancho et al. 2015). Furthermore, a meta-analysis by Tang and coworkers showed that the usage of metformin was linked to a 13% reduced risk for EC in patients suffering from diabetes as well as it improved survival of EC patients in general (Tang et al. 2017). As metformin was reported to impair the survival of ECSCs enriched from well-established EC cell lines (Kitson et al. 2019b), the survival improving benefit of metformin may rely on its action on CSCs. Accordingly, results of this thesis showed that the usage of metformin significantly decreased survival rates of the three established primary ECSC-like populations. Notably, observed survival decreasing effects of metformin were dose dependent with only 15.65% survival left after the application of 20 mM metformin (Figure 17 A) ((Windmöller et al. 2021b), under review). Moreover, calculation of IC_{50} exhibited coherent values for each of the ECSC-like population with values ranging from 5.99 mM to 6.79 mM metformin ((Windmöller et al. 2021b), under review), which are in accordance with IC_{50} values reported for metformin-treated ECSCs enriched from well-established cell lines (Kitson et al. 2019b). Additionally, application of 10 and 20 mM metformin decreased mitochondrial membrane potential of ECSC-like cells

significantly in comparison to the control (Figure 17 B) ((Windmöller et al. 2021b), under review), suggesting the survival decreasing effect of metformin to be caused by acting on mitochondrial function. Hence, these results suggest metformin as a promising drug targeting ECSC-like cells by interfering with mitochondrial respiration. Even though a multicenter study investigating metformin administration prior to surgery of endometrioid endometrial cancer did not report impaired tumor proliferation (Kitson et al. 2019a), a pilot study revealed that doxycycline, which is an antibiotic targeting mitochondria administered 14 days before surgery reduced breast CSCs between 17.65 and 66.67% in the resected tumors (Scatena et al. 2018).

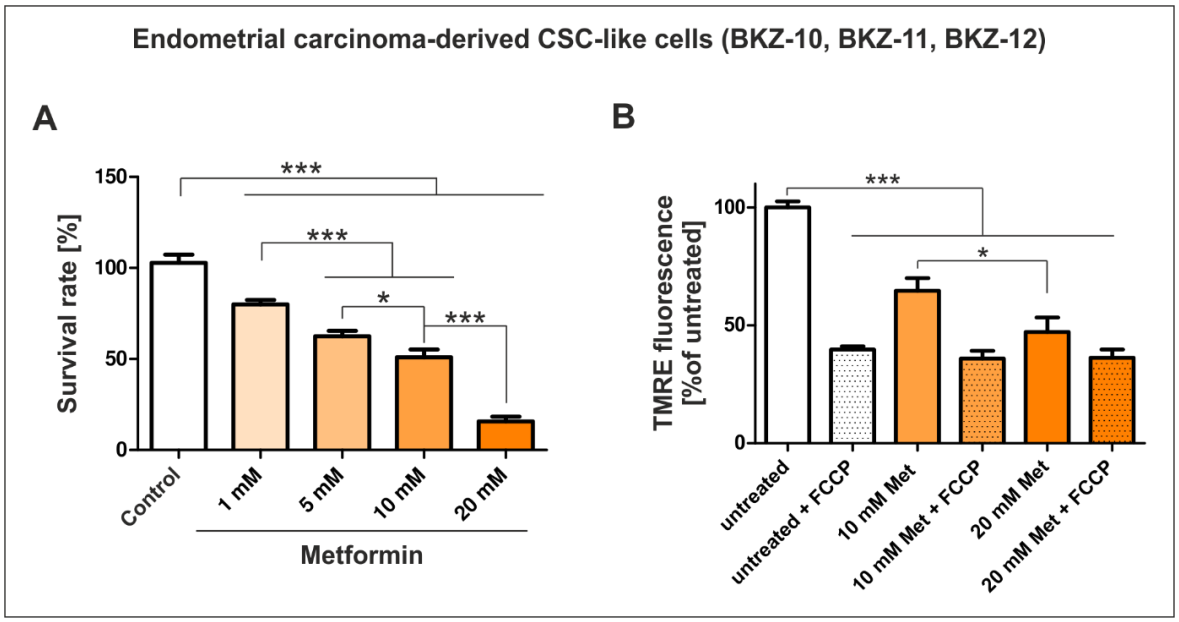

Figure 17: Treatment with metformin significantly impairs survival of endometrial carcinoma-derived cancer stem cell (CSC)-like cell populations. **(A)** Quantification of the influence of metformin on endometrial carcinoma-derived BKZ-10, BKZ-11 and BKZ-12 depicted a significantly decreased survival in a dose-dependent manner. **(B)** Mitochondrial membrane potential of endometrial carcinoma-derived CSC-like (ECSC) populations was measured using tetramethylrhodamine ethyl ester (TMRE), with the mitochondrial oxidative phosphorylation uncoupler carbonyl cyanide 4-(trifluoromethoxy) phenylhydrazone (FCCP) serving as technical control. Usage of 10 and 20 mM metformin significantly reduced the mitochondrial membrane potential of ECSCs in comparison to untreated cells. Unpaired t-test ($p \leq 0.05$). n = 3, * $p \leq 0.05$, *** $p \leq 0.001$. Mean ± SEM (standard error of the mean). Modified from ((Windmöller et al. 2021b), under review)

Further, a phase II clinical trial investigated the impact of metformin on CSC-amounts and clinical outcomes in non-diabetic patients suffering from epithelial ovarian cancer and showed promising results. In particular, metformin-treated tumors harbored 2.4-fold less ALDH/CD133-positive CSCs and patients revealed better overall survival (Brown et al. 2020). Thus, metformin application alone may not affect tumor proliferation of ECs, but probably impairs ECSC amounts, suggesting a reduced tumor recurrence and therapy resistance in the metformin-treated EC patients, which was not analyzed in the study of Kitson (Kitson et al. 2019a). Nevertheless, further clinical studies are needed to substantiate

the metformin-mediated reduction in ECSC-survival observed in this thesis and the survival-enhancing benefit in EC patients *in vivo*.

3 Summary and Outlook

In summary, this thesis demonstrates the successful establishment of 12 novel primary cancer stem-like populations derived from colorectal, pulmonary and endometrial carcinogenic tissue and their use as excellent *in vitro* models for molecular research and drug development targeting CSCs (Figure 18). Expression of several CSC-markers including CD133, CD44, and Nestin as well as the capacity for forming spheres confirmed a CSC-phenotype of the isolated populations (see chapter 2.2.1, 2.2.2 and 2.2.3). Moreover, nuclear Synaptophysin protein was identified as a potential novel CSC-marker, as it was expressed in all BKZ-populations (see chapter 2.2.4). Additionally, BKZ-populations revealed an EMT-phenotype based on their nuclear SLUG expression (see chapter 2.3.4).

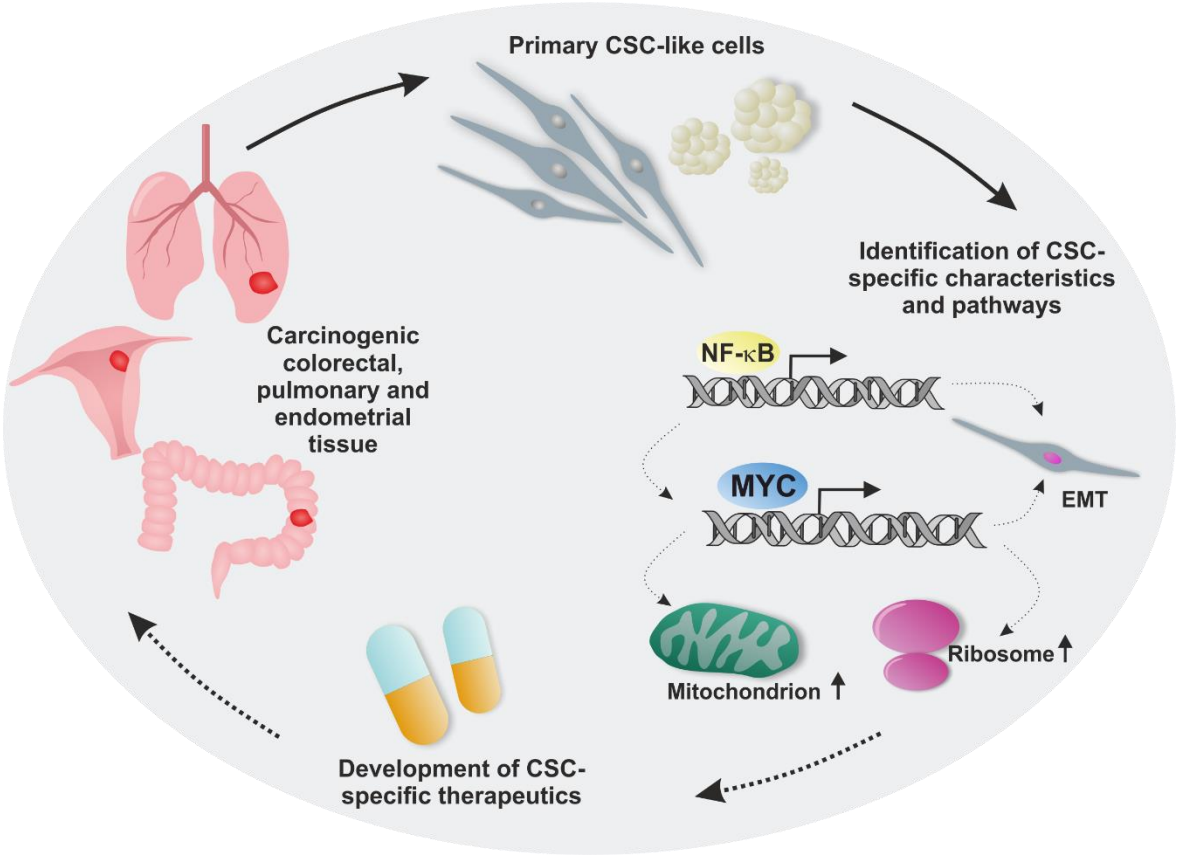

Figure 18: Schematic overview of potential applications of primary novel cancer stem cell (CSC)-like populations in the development of CSC-specific therapies. Nuclear factor kappa-light-chain-enhancer of activated B-cells (NF-κB), epithelial to mesenchymal transition (EMT).

Regarding transcriptional signaling, especially members of the MYC and NF-κB family were shown to be expressed in all CSC-like populations (see chapter 2.3.1 and 2.3.3), emphasizing a crucial role of both pathways in CSC-biology. Accordingly, inhibition of NF-κB-signaling in LCSC-like populations exhibited promising survival decreasing effects, suggesting pro-inflammatory inhibitors as an encouraging therapy option for NSCLC (see

chapter 2.3.5). Nevertheless, inhibition of MYC-signaling was shown to be more effective in interfering with LCSC survival compared to the inhibition of NF-κB-signaling and was also depicted to be a promising therapeutic target in CSC-like populations derived from colorectal and endometrial carcinogenic tissue (see chapter 2.3.2). RNA-sequencing of six of the 12 BKZ-populations depicted increased ribosomal and mitochondrial biogenesis in ECSC-like and AC-derived LCSC-like populations (see chapter 2.4.1), while the inhibition of mitochondrial function by the application of metformin impaired ECSC survival significantly (see chapter 2.4.2). Based on evidences for the involvement of MYC not only in maintaining CSC proliferation and stemness but also regulating mitochondrial and ribosomal biogenesis as well as EMT, targeting MYC would be extremely favorable to decrease CSC associated metastasis and mitochondrial respiration. In this regard, future research directions may focus on the regulatory networks driven by MYC to validate its role in mitochondrial and ribosomal biogenesis as well as its relation to NF-κB and EMT in the here established primary CSC-like populations. Next to the underlying molecular mechanisms involved in the MYC-regulated maintenance of CSCs, future work may include *in vivo* investigations confirming the survival decreasing effect of MYC inhibition on CSC-driven tumorigenesis.

In summary, the findings presented in this thesis strongly emphasize the involvement of MYC and NF-κB in the maintenance of CSC-like populations derived from pulmonary, colorectal and endometrial tumorigenic tissue and characterize the established populations as promising cellular models for future research on CSC-behavior and the generation of novel CSC-specific therapeutics.

4 References

Abbasian, Mahdi; Mousavi, Elham; Arab-Bafrani, Zahra; Sahebkar, Amirhossein (2019): The most reliable surface marker for the identification of colorectal cancer stem-like cells: A systematic review and meta-analysis. In *Journal of cellular physiology* 234 (6), pp. 8192–8202. DOI: 10.1002/jcp.27619.

Aizawa, Shu; Yamamuro, Yutaka (2020): Possible involvement of DNA methylation in hippocampal synaptophysin gene expression during postnatal development of mice. In *Neurochemistry international* 132, p. 104587. DOI: 10.1016/j.neuint.2019.104587.

Al-Hajj, Muhammad; Wicha, Max S.; Benito-Hernandez, Adalberto; Morrison, Sean J.; Clarke, Michael F. (2003): Prospective identification of tumorigenic breast cancer cells. In *Proceedings of the National Academy of Sciences of the United States of America* 100 (7), pp. 3983–3988. DOI: 10.1073/pnas.0530291100.

Andrzejewski, Sylvia; Gravel, Simon-Pierre; Pollak, Michael; St-Pierre, Julie (2014): Metformin directly acts on mitochondria to alter cellular bioenergetics. In *Cancer & metabolism* 2, p. 12. DOI: 10.1186/2049-3002-2-12.

Bailey, Clifford J. (2017): Metformin: historical overview. In *Diabetologia* 60 (9), pp. 1566–1576. DOI: 10.1007/s00125-017-4318-z.

Bao, Bin; Wang, Zhiwei; Ali, Shadan; Ahmad, Aamir; Azmi, Asfar S.; Sarkar, Sanila H. et al. (2012): Metformin inhibits cell proliferation, migration and invasion by attenuating CSC function mediated by deregulating miRNAs in pancreatic cancer cells. In *Cancer prevention research (Philadelphia, Pa.)* 5 (3), pp. 355–364. DOI: 10.1158/1940-6207.CAPR-11-0299.

Bao, Shideng; Wu, Qiulian; McLendon, Roger E.; Hao, Yueling; Shi, Qing; Hjelmeland, Anita B. et al. (2006): Glioma stem cells promote radioresistance by preferential activation of the DNA damage response. In *Nature* 444 (7120), pp. 756–760. DOI: 10.1038/nature05236.

Barker, Nick; Ridgway, Rachel A.; van Es, Johan H.; van de Wetering, Marc; Begthel, Harry; van den Born, Maaike et al. (2009): Crypt stem cells as the cells-of-origin of intestinal cancer. In *Nature* 457 (7229), pp. 608–611. DOI: 10.1038/nature07602.

Bastide, Amandine; David, Alexandre (2018): The ribosome, (slow) beating heart of cancer (stem) cell. In *Oncogenesis* 7 (4), p. 34. DOI: 10.1038/s41389-018-0044-8.

Batlle, Eduard; Clevers, Hans (2017): Cancer stem cells revisited. In *Nature medicine* 23 (10), pp. 1124–1134. DOI: 10.1038/nm.4409.

Berger, Adeline; Brady, Nicholas J.; Bareja, Rohan; Robinson, Brian; Conteduca, Vincenza; Augello, Michael A. et al. (2019): N-Myc-mediated epigenetic reprogramming drives lineage plasticity in advanced prostate cancer. In *The Journal of clinical investigation* 129 (9), pp. 3924–3940. DOI: 10.1172/JCI127961.

Bernick, P. E.; Klimstra, D. S.; Shia, J.; Minsky, B.; Saltz, L.; Shi, W. et al. (2004): Neuroendocrine carcinomas of the colon and rectum. In *Diseases of the colon and rectum* 47 (2), pp. 163–169. DOI: 10.1007/s10350-003-0038-1.

Bertolini, Giulia; Roz, Luca; Perego, Paola; Tortoreto, Monica; Fontanella, Enrico; Gatti, Laura et al. (2009): Highly tumorigenic lung cancer CD133+ cells display stem-like features and are spared by cisplatin treatment. In *Proceedings of the National Academy of Sciences of the United States of America* 106 (38), pp. 16281–16286. DOI: 10.1073/pnas.0905653106.

Bhummaphan, Narumol; Petpiroon, Nalinrat; Prakhongcheep, Ornjira; Sritularak, Boonchoo; Chanvorachote, Pithi (2019): Lusianthridin targeting of lung cancer stem cells via Src-STAT3 suppression. In *Phytomedicine : international journal of phytotherapy and phytopharmacology* 62, p. 152932. DOI: 10.1016/j.phymed.2019.152932.

Binal, Z.; Açıkgöz, E.; Kızılay, F.; Öktem, G.; Altay, B. (2020): Cross-talk between ribosome biogenesis, translation, and mTOR in CD133+ 4/CD44+ prostate cancer stem cells. In *Clinical & translational oncology : official publication of the Federation of Spanish Oncology Societies and of the National Cancer Institute of Mexico* 22 (7), pp. 1040–1048. DOI: 10.1007/s12094-019-02229-1.

Blackwood, E. M.; Eisenman, R. N. (1991): Max: a helix-loop-helix zipper protein that forms a sequence-specific DNA-binding complex with Myc. In *Science (New York, N.Y.)* 251 (4998), pp. 1211–1217. DOI: 10.1126/science.2006410.

Bokhari, Amber A.; Baker, Tabari M.; Dorjbal, Batsukh; Waheed, Sana; Zahn, Christopher M.; Hamilton, Chad A. et al. (2016): Nestin suppression attenuates invasive potential of endometrial cancer cells by downregulating TGF-β signaling pathway. In *Oncotarget* 7 (43), pp. 69733–69748. DOI: 10.18632/oncotarget.11947.

Bonnet, D.; Dick, J. E. (1997): Human acute myeloid leukemia is organized as a hierarchy that originates from a primitive hematopoietic cell. In *Nature medicine* 3 (7), pp. 730–737. DOI: 10.1038/nm0797-730.

Bray, Freddie; Ferlay, Jacques; Soerjomataram, Isabelle; Siegel, Rebecca L.; Torre, Lindsey A.; Jemal, Ahmedin (2018): Global cancer statistics 2018: GLOBOCAN estimates of incidence and mortality worldwide for 36 cancers in 185 countries. In *CA: a cancer journal for clinicians* 68 (6), pp. 394–424. DOI: 10.3322/caac.21492.

Brown, Jason R.; Chan, Daniel K.; Shank, Jessica J.; Griffith, Kent A.; Fan, Huihui; Szulawski, Robert et al. (2020): Phase II clinical trial of metformin as a cancer stem cell-targeting agent in ovarian cancer. In *JCI insight* 5 (11). DOI: 10.1172/jci.insight.133247.

Caldwell, Maeve A.; Garcion, Emmanuel; terBorg, Melanie G.; He, Xiaoling; Svendsen, Clive N. (2004): Heparin stabilizes FGF-2 and modulates striatal precursor cell behavior in response to EGF. In *Experimental neurology* 188 (2), pp. 408–420. DOI: 10.1016/j.expneurol.2004.05.007.

Cammareri, Patrizia; Lombardo, Ylenia; Francipane, Maria Giovanna; Bonventre, Sebastino; Todaro, Matilde; Stassi, Giorgio (2008): Isolation and Culture of Colon Cancer Stem Cells. In : Stem Cell Culture, vol. 86: Elsevier (Methods in Cell Biology), pp. 311–324.

Chang, C. K.; Llanes, S.; Schumer, W. (1997): Effect of dexamethasone on NF-kB activation, tumor necrosis factor formation, and glucose dyshomeostasis in septic rats. In *The Journal of surgical research* 72 (2), pp. 141–145. DOI: 10.1006/jsre.1997.5173.

Chefetz, Ilana; Alvero, Ayesha B.; Holmberg, Jennie C.; Lebowitz, Noah; Craveiro, Vinicius; Yang-Hartwich, Yang et al. (2013): TLR2 enhances ovarian cancer stem cell self-renewal and promotes tumor repair and recurrence. In *Cell cycle (Georgetown, Tex.)* 12 (3), pp. 511–521. DOI: 10.4161/cc.23406.

Chen, Jian; Li, Yanjiao; Yu, Tzong-Shiue; McKay, Renée M.; Burns, Dennis K.; Kernie, Steven G.; Parada, Luis F. (2012): A restricted cell population propagates glioblastoma growth after chemotherapy. In *Nature* 488 (7412), pp. 522–526. DOI: 10.1038/nature11287.

Chen, Shengjie; Gu, Tianyi; Lu, Ziwen; Qiu, Lipeng; Xiao, Guoliang; Zhu, Xiaozhong et al. (2019): Roles of MYC-targeting long non-coding RNA MINCR in cell cycle regulation and apoptosis in non-small cell lung Cancer. In *Respiratory research* 20 (1), p. 202. DOI: 10.1186/s12931-019-1174-z.

Chen, Yu-Chih; Hsu, Han-Shui; Chen, Yi-Wei; Tsai, Tung-Hu; How, Chorng-Kuang; Wang, Chien-Ying et al. (2008): Oct-4 expression maintained cancer stem-like properties in lung cancer-derived CD133-positive cells. In *PloS one* 3 (7), e2637. DOI: 10.1371/journal.pone.0002637.

Choi, Seung H.; Mahankali, Madhupriya; Lee, Sang Jun; Hull, Mitchell; Petrassi, H. Michael; Chatterjee, Arnab K. et al. (2017): Targeted Disruption of Myc-Max Oncoprotein Complex by a Small Molecule. In *ACS chemical biology* 12 (11), pp. 2715–2719. DOI: 10.1021/acschembio.7b00799.

Chung, Seyung S.; Vadgama, Jaydutt V. (2015): Curcumin and epigallocatechin gallate inhibit the cancer stem cell phenotype via down-regulation of STAT3-NFκB signaling. In *Anticancer research* 35 (1), pp. 39–46.

Chung, Shin-Yi; Chao, Ta-Chung; Su, Yeu (2021): The Stemness-High Human Colorectal Cancer Cells Promote Angiogenesis by Producing Higher Amounts of Angiogenic Cytokines via Activation of the Egfr/Akt/Nf-κB Pathway. In *International journal of molecular sciences* 22 (3). DOI: 10.3390/ijms22031355.

Clevers, Hans (2011): The cancer stem cell: premises, promises and challenges. In *Nature medicine* 17 (3), pp. 313–319. DOI: 10.1038/nm.2304.

Conacci-Sorrell, Maralice; McFerrin, Lisa; Eisenman, Robert N. (2014): An overview of MYC and its interactome. In *Cold Spring Harbor perspectives in medicine* 4 (1), a014357. DOI: 10.1101/cshperspect.a014357.

Cooper, Melinda (2009): Regenerative Pathologies: Stem Cells, Teratomas and Theories of Cancer. In *Medicine Studies* 1 (1), pp. 55–66. DOI: 10.1007/s12376-008-0002-4.

Crinelli, R.; Antonelli, A.; Bianchi, M.; Gentilini, L.; Scaramucci, S.; Magnani, M. (2000): Selective inhibition of NF-kB activation and TNF-alpha production in macrophages by red blood cell-mediated delivery of dexamethasone. In *Blood cells, molecules & diseases* 26 (3), pp. 211–222. DOI: 10.1006/bcmd.2000.0298.

Dalerba, Piero; Dylla, Scott J.; Park, In-Kyung; Liu, Rui; Wang, Xinhao; Cho, Robert W. et al. (2007): Phenotypic characterization of human colorectal cancer stem cells. In *Proceedings of the National Academy of Sciences of the United States of America* 104 (24), pp. 10158–10163. DOI: 10.1073/pnas.0703478104.

Dang, Chi V. (2012): MYC on the path to cancer. In *Cell* 149 (1), pp. 22–35. DOI: 10.1016/j.cell.2012.03.003.

Dardenne, Etienne; Beltran, Himisha; Benelli, Matteo; Gayvert, Kaitlyn; Berger, Adeline; Puca, Loredana et al. (2016): N-Myc Induces an EZH2-Mediated Transcriptional Program Driving Neuroendocrine Prostate Cancer. In *Cancer cell* 30 (4), pp. 563–577. DOI: 10.1016/j.ccell.2016.09.005.

DePinho, Ronald A.; Schreiber-Agus, Nicole; Alt, Frederick W. (1991): myc Family Oncogenes in the Development of Normal and Neoplastic Cells. In, vol. 57: Elsevier (Advances in Cancer Research), pp. 1–46.

Desbats, Maria Andrea; Giacomini, Isabella; Prayer-Galetti, Tommaso; Montopoli, Monica (2020): Metabolic Plasticity in Chemotherapy Resistance. In *Frontiers in oncology* 10, p. 281. DOI: 10.3389/fonc.2020.00281.

Destefanis, Francesca; Manara, Valeria; Bellosta, Paola (2020): Myc as a Regulator of Ribosome Biogenesis and Cell Competition: A Link to Cancer. In *International journal of molecular sciences* 21 (11). DOI: 10.3390/ijms21114037.

Di Cristofano, Antonio; Ellenson, Lora Hedrick (2007): Endometrial carcinoma. In *Annual review of pathology* 2, pp. 57–85. DOI: 10.1146/annurev.pathol.2.010506.091905.

Ding, Dah-Ching; Liu, Hwan-Wun; Chang, Yu-Hsun; Chu, Tang-Yuan (2017): Expression of CD133 in endometrial cancer cells and its implications. In *Journal of Cancer* 8 (11), pp. 2142–2153. DOI: 10.7150/jca.18869.

Dizdar, Levent; Drusenheimer, Jasmin; Werner, Thomas A.; Möhlendick, Birte; Schütte, Sina C.; Esposito, Irene et al. (2018): Establishment and Characterization of a Novel Cell Line Derived from a Small Cell Neuroendocrine Carcinoma of the Anal Canal. In *Neuroendocrinology* 107 (3), pp. 246–256. DOI: 10.1159/000492222.

Dolcet, Xavier; Llobet, David; Pallares, Judit; Matias-Guiu, Xavier (2005): NF-kB in development and progression of human cancer. In *Virchows Archiv : an international journal of pathology* 446 (5), pp. 475–482. DOI: 10.1007/s00428-005-1264-9.

Dong, Weilei; Chen, A.; Chao, Xiaocheng; Li, Xiang; Cui, YingHong; Xu, Chang et al. (2019): Chrysin Inhibits Proinflammatory Factor-Induced EMT Phenotype and Cancer Stem Cell-Like Features in HeLa Cells by Blocking the NF-κB/Twist Axis. In *Cellular physiology and biochemistry : international journal of experimental cellular physiology, biochemistry, and pharmacology* 52 (5), pp. 1236–1250. DOI: 10.33594/000000084.

Dossus, Laure; Becker, Susen; Rinaldi, Sabina; Lukanova, Annekatrin; Tjønneland, Anne; Olsen, Anja et al. (2011): Tumor necrosis factor (TNF)-α, soluble TNF receptors and endometrial cancer risk: the EPIC study. In *International journal of cancer* 129 (8), pp. 2032–2037. DOI: 10.1002/ijc.25840.

Dylla, Scott J.; Beviglia, Lucia; Park, In-Kyung; Chartier, Cecile; Raval, Janak; Ngan, Lucy et al. (2008): Correction: Colorectal Cancer Stem Cells Are Enriched in Xenogeneic Tumors Following Chemotherapy. In *PloS one* 3 (8). DOI: 10.1371/annotation/2aa6a20a-e63c-49b6-aeea-aae62435617f.

Eilers, Martin; Eisenman, Robert N. (2008): Myc's broad reach. In *Genes & development* 22 (20), pp. 2755–2766. DOI: 10.1101/gad.1712408.

Ekinci, Elmira; Rohondia, Sagar; Khan, Raheel; Dou, Qingping P. (2019): Repurposing Disulfiram as An Anti-Cancer Agent: Updated Review on Literature and Patents. In *Recent patents on anti-cancer drug discovery* 14 (2), pp. 113–132. DOI: 10.2174/1574892814666190514104035.

El-Ashmawy, Nahla E.; El-Zamarany, Enas A.; Khedr, Eman G.; Abo-Saif, Mariam A. (2019): Activation of EMT in colorectal cancer by MTDH/NF-κB p65 pathway. In *Molecular and cellular biochemistry* 457 (1-2), pp. 83–91. DOI: 10.1007/s11010-019-03514-x.

Elbadawy, Mohamed; Usui, Tatsuya; Yamawaki, Hideyuki; Sasaki, Kazuaki (2019): Emerging Roles of C-Myc in Cancer Stem Cell-Related Signaling and Resistance to Cancer Chemotherapy: A Potential Therapeutic Target Against Colorectal Cancer. In *International journal of molecular sciences* 20 (9). DOI: 10.3390/ijms20092340.

Eramo, A.; Lotti, F.; Sette, G.; Pilozzi, E.; Biffoni, M.; Di Virgilio, A. et al. (2008): Identification and expansion of the tumorigenic lung cancer stem cell population. In *Cell death and differentiation* 15 (3), pp. 504–514. DOI: 10.1038/sj.cdd.4402283.

Farnie, Gillian; Sotgia, Federica; Lisanti, Michael P. (2015): High mitochondrial mass identifies a sub-population of stem-like cancer cells that are chemo-resistant. In *Oncotarget* 6 (31), pp. 30472–30486. DOI: 10.18632/oncotarget.5401.

Feinberg, Andrew P.; Koldobskiy, Michael A.; Göndör, Anita (2016): Epigenetic modulators, modifiers and mediators in cancer aetiology and progression. In *Nature reviews. Genetics* 17 (5), pp. 284–299. DOI: 10.1038/nrg.2016.13.

Ferlay, Jacques; Colombet, Murielle; Soerjomataram, Isabelle; Parkin, Donald M.; Piñeros, Marion; Znaor, Ariana; Bray, Freddie (2021): Cancer statistics for the year 2020: An overview. In *International journal of cancer*. DOI: 10.1002/ijc.33588.

Fernandez, Paula C.; Frank, Scott R.; Wang, Luquan; Schroeder, Marianne; Liu, Suxing; Greene, Jonathan et al. (2003): Genomic targets of the human c-Myc protein. In *Genes & development* 17 (9), pp. 1115–1129. DOI: 10.1101/gad.1067003.

Fields, Adam C.; Lu, Pamela; Vierra, Benjamin M.; Hu, Frances; Irani, Jennifer; Bleday, Ronald et al. (2019): Survival in Patients with High-Grade Colorectal Neuroendocrine Carcinomas: The Role of Surgery and Chemotherapy. In *Annals of surgical oncology* 26 (4), pp. 1127–1133. DOI: 10.1245/s10434-019-07203-3.

Fleming, Matthew; Ravula, Sreelakshmi; Tatishchev, Sergei F.; Wang, Hanlin L. (2012): Colorectal carcinoma: Pathologic aspects. In *Journal of gastrointestinal oncology* 3 (3), pp. 153–173. DOI: 10.3978/j.issn.2078-6891.2012.030.

Flottmann, Clara (2020): Characterization and treatment of squamous cell carcinoma and adenocarcinoma derived lung cancer stem cells using ICC. Bachelor thesis.

Francesco, Ernestina Marianna de; Ózsvári, Béla; Sotgia, Federica; Lisanti, Michael P. (2019): Dodecyl-TPP Targets Mitochondria and Potently Eradicates Cancer Stem Cells (CSCs): Synergy With FDA-Approved Drugs and Natural Compounds (Vitamin C and Berberine). In *Frontiers in oncology* 9, p. 615. DOI: 10.3389/fonc.2019.00615.

Fujimori, Taketoshi; Wirsching, Peter; Janda, Kim D. (2003): Preparation of a Kröhnke Pyridine Combinatorial Library Suitable for Solution-Phase Biological Screening. In *J. Comb. Chem.* 5 (5), pp. 625–631. DOI: 10.1021/cc0300208.

Fumagalli, Arianna; Oost, Koen C.; Kester, Lennart; Morgner, Jessica; Bornes, Laura; Bruens, Lotte et al. (2020): Plasticity of Lgr5-Negative Cancer Cells Drives Metastasis in Colorectal Cancer. In *Cell stem cell* 26 (4), 569-578.e7. DOI: 10.1016/j.stem.2020.02.008.

Furue, Miho K.; Na, Jie; Jackson, Jamie P.; Okamoto, Tetsuji; Jones, Mark; Baker, Duncan et al. (2008): Heparin promotes the growth of human embryonic stem cells in a defined serum-free medium. In *Proceedings of the National Academy of Sciences of the United States of America* 105 (36), pp. 13409–13414. DOI: 10.1073/pnas.0806136105.

Galardi, Silvia; Savino, Mauro; Scagnoli, Fiorella; Pellegatta, Serena; Pisati, Federica; Zambelli, Federico et al. (2016): Resetting cancer stem cell regulatory nodes upon MYC inhibition. In *EMBO Reports* 17 (12), pp. 1872–1889. DOI: 10.15252/embr.201541489.

Galizia, Gennaro; Gemei, Marica; Del Vecchio, Luigi; Zamboli, Anna; Di Noto, Rosa; Mirabelli, Peppino et al. (2012): Combined CD133/CD44 expression as a prognostic indicator of disease-free survival in patients with colorectal cancer. In *Archives of surgery (Chicago, Ill. : 1960)* 147 (1), pp. 18–24. DOI: 10.1001/archsurg.2011.795.

Gao, Qingzu; Zhou, Rui; Meng, Yuan; Duan, Rongfei; Wu, Ling; Li, Rui et al. (2020): Long noncoding RNA CMPK2 promotes colorectal cancer progression by activating the FUBP3-c-Myc axis. In *Oncogene* 39 (19), pp. 3926–3938. DOI: 10.1038/s41388-020-1266-8.

Geisler, J. P.; Geisler, H. E.; Manahan, K. J.; Miller, G. A.; Wiemann, M. C.; Zhou, Z.; Crabtree, W. (2004): Nuclear and cytoplasmic c-myc staining in endometrial carcinoma and their relationship to survival. In *Int J Gynecol Cancer* 14 (1), pp. 133–137. DOI: 10.1136/ijgc-00009577-200401000-00018.

Geng, Hao; Guo, Wenhao; Feng, Lei; Xie, Dongdong; Bi, Liangkuan; Wang, Yi et al. (2021): Diallyl trisulfide inhibited tobacco smoke-mediated bladder EMT and cancer stem cell marker expression via the NF-κB pathway in vivo. In *The Journal of international medical research* 49 (3), 300060521992900. DOI: 10.1177/0300060521992900.

George, E.; Manivel, J. C.; Dehner, L. P.; Wick, M. R. (1991): Malignant mixed müllerian tumors: an immunohistochemical study of 47 cases, with histogenetic considerations and clinical correlation. In *Human pathology* 22 (3), pp. 215–223. DOI: 10.1016/0046-8177(91)90153-g.

Gerlinger, Marco; Rowan, Andrew J.; Horswell, Stuart; Math, M.; Larkin, James; Endesfelder, David et al. (2012): Intratumor heterogeneity and branched evolution revealed by multiregion sequencing. In *The New England journal of medicine* 366 (10), pp. 883–892. DOI: 10.1056/NEJMoa1113205.

Gock, Michael; Mullins, Christina S.; Harnack, Christine; Prall, Friedrich; Ramer, Robert; Göder, Anja et al. (2018): Establishment, functional and genetic characterization of a colon derived large cell neuroendocrine carcinoma cell line. In *World journal of gastroenterology* 24 (33), pp. 3749–3759. DOI: 10.3748/wjg.v24.i33.3749.

Gong, Ke; Guo, Gao; Gerber, David E.; Gao, Boning; Peyton, Michael; Huang, Chun et al. (2018): TNF-driven adaptive response mediates resistance to EGFR inhibition in lung

cancer. In *The Journal of clinical investigation* 128 (6), pp. 2500–2518. DOI: 10.1172/JCI96148.

González-Aragoneses, Federico; Moreno-Mata, Nicolás; Cebollero-Presmanes, María; García-Yuste, Mariano; Cañizares-Carretero, Miguel Angel; Molins-López-Rodó, Laureano et al. (2007): Prognostic significance of synaptophysin in stage I of squamous carcinoma and adenocarcinoma of the lung. In *Cancer* 110 (8), pp. 1776–1781. DOI: 10.1002/cncr.22985.

Gu, Lijun; Wang, Zhiyan; Zuo, Jing; Li, Hongmei; Zha, Lin (2018): Prognostic significance of NF-κB expression in non-small cell lung cancer: A meta-analysis. In *PloS one* 13 (5), e0198223. DOI: 10.1371/journal.pone.0198223.

Hanahan, D.; Weinberg, R. A. (2000): The hallmarks of cancer. In *Cell* 100 (1), pp. 57–70. DOI: 10.1016/s0092-8674(00)81683-9.

Hanahan, Douglas; Weinberg, Robert A. (2011): Hallmarks of cancer: the next generation. In *Cell* 144 (5), pp. 646–674. DOI: 10.1016/j.cell.2011.02.013.

Hanewinkel, Johannes (2019): Isolation and characterization of two novel cancer stem cell lines from human colorectal cancer. Master thesis.

Haraguchi, Naotsugu; Ohkuma, Masahisa; Sakashita, Hiroyuki; Matsuzaki, Shinji; Tanaka, Fumiaki; Mimori, Koshi et al. (2008): CD133+CD44+ population efficiently enriches colon cancer initiating cells. In *Annals of surgical oncology* 15 (10), pp. 2927–2933. DOI: 10.1245/s10434-008-0074-0.

Harding, Michael C.; Sloan, Chantel D.; Merrill, Ray M.; Harding, Tiffany M.; Thacker, Brian J.; Thacker, Evan L. (2018): Transitions From Heart Disease to Cancer as the Leading Cause of Death in US States, 1999-2016. In *Preventing chronic disease* 15, E158. DOI: 10.5888/pcd15.180151.

Hart, Jonathan R.; Garner, Amanda L.; Yu, Jing; Ito, Yoshihiro; Sun, Minghao; Ueno, Lynn et al. (2014): Inhibitor of MYC identified in a Kröhnke pyridine library. In *Proceedings of the National Academy of Sciences of the United States of America* 111 (34), pp. 12556–12561. DOI: 10.1073/pnas.1319488111.

Hayden, Matthew S.; Ghosh, Sankar (2012): NF-κB, the first quarter-century: remarkable progress and outstanding questions. In *Genes & development* 26 (3), pp. 203–234. DOI: 10.1101/gad.183434.111.

Hayden, Matthew S.; Ghosh, Sankar (2014): Regulation of NF-κB by TNF family cytokines. In *Seminars in immunology* 26 (3), pp. 253–266. DOI: 10.1016/j.smim.2014.05.004.

Horst, D.; Kriegl, L.; Engel, J.; Kirchner, T.; Jung, A. (2008): CD133 expression is an independent prognostic marker for low survival in colorectal cancer. In *British journal of cancer* 99 (8), pp. 1285–1289. DOI: 10.1038/sj.bjc.6604664.

Huang, Emina H.; Hynes, Mark J.; Zhang, Tao; Ginestier, Christophe; Dontu, Gabriela; Appelman, Henry et al. (2009): Aldehyde dehydrogenase 1 is a marker for normal and malignant human colonic stem cells (SC) and tracks SC overpopulation during colon tumorigenesis. In *Cancer research* 69 (8), pp. 3382–3389. DOI: 10.1158/0008-5472.CAN-08-4418.

Huang, Xiaolong; Huang, Jingsong; Leng, Dewen; Yang, Shuo; Yao, Qi; Sun, Jin; Hu, Jun (2017): Gefitinib-loaded DSPE-PEG2000 nanomicelles with CD133 aptamers target lung cancer stem cells. In *World journal of surgical oncology* 15 (1), p. 167. DOI: 10.1186/s12957-017-1230-4.

Ischenko, Irene; Zhi, Jizu; Hayman, Michael J.; Petrenko, Oleksi (2017): KRAS-dependent suppression of MYC enhances the sensitivity of cancer cells to cytotoxic agents. In *Oncotarget* 8 (11), pp. 17995–18009. DOI: 10.18632/oncotarget.14929.

Ishiguro, Tatsuya; Ohata, Hirokazu; Sato, Ai; Yamawaki, Kaoru; Enomoto, Takayuki; Okamoto, Koji (2017): Tumor-derived spheroids: Relevance to cancer stem cells and clinical applications. In *Cancer science* 108 (3), pp. 283–289. DOI: 10.1111/cas.13155.

Ito, Keisuke; Suda, Toshio (2014): Metabolic requirements for the maintenance of self-renewing stem cells. In *Nature reviews. Molecular cell biology* 15 (4), pp. 243–256. DOI: 10.1038/nrm3772.

Iwakawa, Reika; Kohno, Takashi; Kato, Motohiro; Shiraishi, Kouya; Tsuta, Koji; Noguchi, Masayuki et al. (2011): MYC amplification as a prognostic marker of early-stage lung adenocarcinoma identified by whole genome copy number analysis. In *Clinical cancer research : an official journal of the American Association for Cancer Research* 17 (6), pp. 1481–1489. DOI: 10.1158/1078-0432.ccr-10-2484.

Iyoda, Akira; Azuma, Yoko; Sano, Atsushi (2020): Neuroendocrine tumors of the lung: clinicopathological and molecular features. In *Surgery today* 50 (12), pp. 1578–1584. DOI: 10.1007/s00595-020-01988-7.

Jacob, Nicholas T.; Miranda, Pedro O.; Shirey, Ryan J.; Gautam, Ritika; Zhou, Bin; Orbe Izquierdo, M. Elena de et al. (2018): Synthetic molecules for disruption of the MYC protein-protein interface. In *Bioorganic & medicinal chemistry* 26 (14), pp. 4234–4239. DOI: 10.1016/j.bmc.2018.07.019.

Jiang, Zhongmin; Zhang, Chunyan; Liu, Xiaozhi; Ma, Xiaofang; Bian, Xiyun; Xiao, Xiaolin et al. (2020): Dexamethasone inhibits stemness maintenance and enhances chemosensitivity of hepatocellular carcinoma stem cells by inducing deSUMOylation of HIF- 1α and Oct4. In *International journal of oncology* 57 (3), pp. 780–790. DOI: 10.3892/ijo.2020.5097.

Kagoya, Yuki; Yoshimi, Akihide; Kataoka, Keisuke; Nakagawa, Masahiro; Kumano, Keiki; Arai, Shunya et al. (2014): Positive feedback between NF-κB and TNF-α promotes leukemia-initiating cell capacity. In *The Journal of clinical investigation* 124 (2), pp. 528–542. DOI: 10.1172/JCI68101.

Kalaitzopoulos, Dimitrios Rafail; Mitsopoulou, Angeliki; Iliopoulou, Sotiria Maria; Daniilidis, Angelos; Samartzis, Eleftherios P.; Economopoulos, Konstantinos P. (2020): Association between endometriosis and gynecological cancers: a critical review of the literature. In *Archives of gynecology and obstetrics* 301 (2), pp. 355–367. DOI: 10.1007/s00404-020-05445-1.

Kalluri, Raghu; Weinberg, Robert A. (2009): The basics of epithelial-mesenchymal transition. In *The Journal of clinical investigation* 119 (6), pp. 1420–1428. DOI: 10.1172/JCI39104.

Kaltschmidt, Christian; Banz-Jansen, Constanze; Benhidjeb, Tahar; Beshay, Morris; Förster, Christine; Greiner, Johannes et al. (2019): A Role for NF-κB in Organ Specific Cancer and Cancer Stem Cells. In *Cancers* 11 (5). DOI: 10.3390/cancers11050655.

Kastrati, Irida; Delgado-Rivera, Loruhama; Georgieva, Gergana; Thatcher, Gregory R. J.; Frasor, Jonna (2017): Synthesis and Characterization of an Aspirin-fumarate Prodrug that Inhibits NFκB Activity and Breast Cancer Stem Cells. In *Journal of visualized experiments : JoVE* (119). DOI: 10.3791/54798.

Kearns, Jeffrey D.; Basak, Soumen; Werner, Shannon L.; Huang, Christine S.; Hoffmann, Alexander (2006): IkappaBepsilon provides negative feedback to control NF-kappaB oscillations, signaling dynamics, and inflammatory gene expression. In *The Journal of cell biology* 173 (5), pp. 659–664. DOI: 10.1083/jcb.200510155.

Kim, Jang Jin; Park, Sung Su; Lee, Taek-Gu; Lee, Ho-Chang; Lee, Sang-Jeon (2018): Large Cell Neuroendocrine Carcinoma of the Colon With Carcinomatosis Peritonei. In *Annals of coloproctology* 34 (4), pp. 222–225. DOI: 10.3393/ac.2018.02.27.

Kim, Jonghwan; Woo, Andrew J.; Chu, Jianlin; Snow, Jonathan W.; Fujiwara, Yuko; Kim, Chul Geun et al. (2010): A Myc rather than core pluripotency module accounts for the shared signatures of embryonic stem and cancer cells. In *Cell* 143 (2), pp. 313–324. DOI: 10.1016/j.cell.2010.09.010.

Kitson, Sarah J.; Maskell, Zoe; Sivalingam, Vanitha N.; Allen, Jennifer L.; Ali, Saad; Burns, Sean et al. (2019a): PRE-surgical Metformin In Uterine Malignancy (PREMIUM): a Multi-Center, Randomized Double-Blind, Placebo-Controlled Phase III Trial. In *Clinical cancer research : an official journal of the American Association for Cancer Research* 25 (8), pp. 2424–2432. DOI: 10.1158/1078-0432.CCR-18-3339.

Kitson, Sarah J.; Rosser, Matthew; Fischer, Deborah P.; Marshall, Kay M.; Clarke, Robert B.; Crosbie, Emma J. (2019b): Targeting Endometrial Cancer Stem Cell Activity with Metformin Is Inhibited by Patient-Derived Adipocyte-Secreted Factors. In *Cancers* 11 (5). DOI: 10.3390/cancers11050653.

Kiyohara, M. H.; Dillard, C.; Tsui, J.; Kim, S. R.; Lu, J.; Sachdev, D. et al. (2017): EMP2 is a novel therapeutic target for endometrial cancer stem cells. In *Oncogene* 36 (42), pp. 5793–5807. DOI: 10.1038/onc.2017.142.

Kokotos, Alexandros C.; Harper, Callista B.; Marland, Jamie R. K.; Smillie, Karen J.; Cousin, Michael A.; Gordon, Sarah L. (2019): Synaptophysin sustains presynaptic performance by preserving vesicular synaptobrevin-II levels. In *Journal of neurochemistry* 151 (1), pp. 28–37. DOI: 10.1111/jnc.14797.

Kong, Fan-Fei; Da Li; Yang, Hui; Ma, Jian; Pan, Xin; Liu, Hong-Xiang et al. (2017): Preliminary identification of endometrial cancer stem cells in vitro and in vivo. In *Biochemical and biophysical research communications* 490 (2), pp. 506–513. DOI: 10.1016/j.bbrc.2017.06.070.

Kostaras, X.; Cusano, F.; Kline, G. A.; Roa, W.; Easaw, J. (2014): Use of dexamethasone in patients with high-grade glioma: a clinical practice guideline. In *Current oncology (Toronto, Ont.)* 21 (3), e493-503. DOI: 10.3747/co.21.1769.

Kreso, Antonija; Dick, John E. (2014): Evolution of the cancer stem cell model. In *Cell stem cell* 14 (3), pp. 275–291. DOI: 10.1016/j.stem.2014.02.006.

Krieg, Andreas; Mersch, Sabrina; Boeck, Inga; Dizdar, Levent; Weihe, Eberhard; Hilal, Zena et al. (2014): New model for gastroenteropancreatic large-cell neuroendocrine carcinoma: establishment of two clinically relevant cell lines. In *PloS one* 9 (2), e88713. DOI: 10.1371/journal.pone.0088713.

Kwilas, Anna R.; Ardiani, Andressa; Dirmeier, Ulrike; Wottawah, Cornelia; Schlom, Jeffery; Hodge, James W. (2015): A poxviral-based cancer vaccine the transcription factor twist inhibits primary tumor growth and metastases in a model of metastatic breast cancer and improves survival in a spontaneous prostate cancer model. In *Oncotarget* 6 (29), pp. 28194–28210. DOI: 10.18632/oncotarget.4442.

Lamb, Rebecca; Ozsvari, Bela; Lisanti, Camilla L.; Tanowitz, Herbert B.; Howell, Anthony; Martinez-Outschoorn, Ubaldo E. et al. (2015): Antibiotics that target mitochondria effectively eradicate cancer stem cells, across multiple tumor types: treating cancer like an infectious disease. In *Oncotarget* 6 (7), pp. 4569–4584. DOI: 10.18632/oncotarget.3174.

Lapidot, T.; Sirard, C.; Vormoor, J.; Murdoch, B.; Hoang, T.; Caceres-Cortes, J. et al. (1994): A cell initiating human acute myeloid leukaemia after transplantation into SCID mice. In *Nature* 367 (6464), pp. 645–648. DOI: 10.1038/367645a0.

Le Grand, Marion; Mukha, Anna; Püschel, Jakob; Valli, Emanuele; Kamili, Alvin; Vittorio, Orazio et al. (2020): Interplay between MycN and c-Myc regulates radioresistance and cancer stem cell phenotype in neuroblastoma upon glutamine deprivation. In *Theranostics* 10 (14), pp. 6411–6429. DOI: 10.7150/thno.42602.

Lee, John K.; Phillips, John W.; Smith, Bryan A.; Park, Jung Wook; Stoyanova, Tanya; McCaffrey, Erin F. et al. (2016): N-Myc Drives Neuroendocrine Prostate Cancer Initiated from Human Prostate Epithelial Cells. In *Cancer cell* 29 (4), pp. 536–547. DOI: 10.1016/j.ccell.2016.03.001.

Lee, Kyu Sang; Kwak, Yoonjin; Nam, Kyung Han; Kim, Duck-Woo; Kang, Sung-Bum; Choe, Gheeyoung et al. (2015): c-MYC Copy-Number Gain Is an Independent Prognostic Factor in Patients with Colorectal Cancer. In *PloS one* 10 (10), e0139727. DOI: 10.1371/journal.pone.0139727.

Lee, Kyung-Min; Giltnane, Jennifer M.; Balko, Justin M.; Schwarz, Luis J.; Guerrero-Zotano, Angel L.; Hutchinson, Katherine E. et al. (2017): MYC and MCL1 Cooperatively Promote Chemotherapy-Resistant Breast Cancer Stem Cells via Regulation of Mitochondrial Oxidative Phosphorylation. In *Cell metabolism* 26 (4), 633-647.e7. DOI: 10.1016/j.cmet.2017.09.009.

Lee, Sun Mi; Sung, Chang Ohk (2021): Comprehensive analysis of mutational and clinicopathologic characteristics of poorly differentiated colorectal neuroendocrine carcinomas. In *Scientific reports* 11 (1), p. 6203. DOI: 10.1038/s41598-021-85593-9.

Leng, Zhengwei; Xia, Qinghua; Chen, Jinhuang; Li, Yong; Xu, Jiqian; Zhao, Ende et al. (2018): Lgr5+CD44+EpCAM+ Strictly Defines Cancer Stem Cells in Human Colorectal Cancer. In *Cellular physiology and biochemistry : international journal of experimental cellular physiology, biochemistry, and pharmacology* 46 (2), pp. 860–872. DOI: 10.1159/000488743.

Leung, Elaine Lai-Han; Fiscus, Ronald R.; Tung, James W.; Tin, Vicky Pui-Chi; Cheng, Lik Cheung; Sihoe, Alan Dart-Loon et al. (2010): Non-small cell lung cancer cells expressing

CD44 are enriched for stem cell-like properties. In *PloS one* 5 (11), e14062. DOI: 10.1371/journal.pone.0014062.

Li, Qian-Qian; Xie, You-Ke; Wu, Yue; Li, Lin-Lin; Liu, Ying; Miao, Xiao-Bo et al. (2017): Sulforaphane inhibits cancer stem-like cell properties and cisplatin resistance through miR-214-mediated downregulation of c-MYC in non-small cell lung cancer. In *Oncotarget* 8 (7), pp. 12067–12080. DOI: 10.18632/oncotarget.14512.

Li, Xinyuan; Luo, George; Li, Ting; Sun, Honghong; Wang, Wei; Eiler, Emily et al. (2020): The c-Rel-c-Myc axis controls metabolism and proliferation of human T leukemia cells. In *Molecular immunology* 125, pp. 115–122. DOI: 10.1016/j.molimm.2020.06.029.

Liu, Fang; Zhang, Yuan; Lu, Ming; Wang, Cong; Li, Qingbao; Gao, Yongsheng et al. (2017): Nestin servers as a promising prognostic biomarker in non-small cell lung cancer. In *American journal of translational research* 9 (3), pp. 1392–1401.

Liu, Jiahao; Wen, Yinghao; Liu, Zhen; Liu, Shu; Xu, Ping; Xu, Yan et al. (2021): VPS33B modulates c-Myc/p53/miR-192-3p to target CCNB1 suppressing the growth of non-small cell lung cancer. In *Molecular therapy. Nucleic acids* 23, pp. 324–335. DOI: 10.1016/j.omtn.2020.11.010.

Liu, Jing; Xiao, Zhijie; Wong, Sunny Kit-Man; Tin, Vicky Pui-Chi; Ho, Ka-Yan; Wang, Junwen et al. (2013): Lung cancer tumorigenicity and drug resistance are maintained through ALDH(hi)CD44(hi) tumor initiating cells. In *Oncotarget* 4 (10), pp. 1698–1711. DOI: 10.18632/oncotarget.1246.

Liu, Lei; Zhang, Jing; Yang, Xiaoming; Fang, Chi; Xu, Huali; Xi, Xiaowei (2015): SALL4 as an Epithelial-Mesenchymal Transition and Drug Resistance Inducer through the Regulation of c-Myc in Endometrial Cancer. In *PloS one* 10 (9), e0138515. DOI: 10.1371/journal.pone.0138515.

Liu, Qinghai; Nguyen, David H.; Dong, Qinghua; Shitaku, Peter; Chung, Kenneth; Liu, On Ying et al. (2009): Molecular properties of CD133+ glioblastoma stem cells derived from treatment-refractory recurrent brain tumors. In *Journal of neuro-oncology* 94 (1), pp. 1–19. DOI: 10.1007/s11060-009-9919-z.

Liu, Suling; Cong, Yang; Wang, Dong; Sun, Yu; Deng, Lu; Liu, Yajing et al. (2014): Breast cancer stem cells transition between epithelial and mesenchymal states reflective of their normal counterparts. In *Stem cell reports* 2 (1), pp. 78–91. DOI: 10.1016/j.stemcr.2013.11.009.

Liu, Wenjing; Lu, Xiaoqing; Shi, Peiguo; Yang, Guangxi; Zhou, Zhongmei; Li, Wei et al. (2020): TNF-α increases breast cancer stem-like cells through up-regulating TAZ expression via the non-canonical NF-κB pathway. In *Scientific reports* 10 (1), p. 1804. DOI: 10.1038/s41598-020-58642-y.

Loebinger, M. R.; Giangreco, A.; Groot, K. R.; Prichard, L.; Allen, K.; Simpson, C. et al. (2008): Squamous cell cancers contain a side population of stem-like cells that are made chemosensitive by ABC transporter blockade. In *British journal of cancer* 98 (2), pp. 380–387. DOI: 10.1038/sj.bjc.6604185.

Lu, Haiquan; Chen, Ivan; Shimoda, Larissa A.; Park, Youngrok; Zhang, Chuanzhao; Tran, Linh et al. (2017): Chemotherapy-Induced Ca2+ Release Stimulates Breast Cancer Stem Cell Enrichment. In *Cell reports* 18 (8), pp. 1946–1957. DOI: 10.1016/j.celrep.2017.02.001.

Ma, Lixin; Dong, Lihua; Chang, Pengyu (2019): CD44v6 engages in colorectal cancer progression. In *Cell death & disease* 10 (1), p. 30. DOI: 10.1038/s41419-018-1265-7.

Mani, Sendurai A.; Guo, Wenjun; Liao, Mai-Jing; Eaton, Elinor Ng; Ayyanan, Ayyakkannu; Zhou, Alicia Y. et al. (2008): The epithelial-mesenchymal transition generates cells with properties of stem cells. In *Cell* 133 (4), pp. 704–715. DOI: 10.1016/j.cell.2008.03.027.

Marinkovic, Dragan; Marinkovic, Tatjana (2021): The new role for an old guy: MYC as an immunoplayer. In *Journal of cellular physiology* 236 (5), pp. 3234–3243. DOI: 10.1002/jcp.30123.

Markham, Merry Jennifer; Wachter, Kerri; Agarwal, Neeraj; Bertagnolli, Monica M.; Chang, Susan Marina; Dale, William et al. (2020): Clinical Cancer Advances 2020: Annual Report on Progress Against Cancer From the American Society of Clinical Oncology. In *Journal of clinical oncology : official journal of the American Society of Clinical Oncology* 38 (10), p. 1081. DOI: 10.1200/JCO.19.03141.

Martins-Neves, Sara R.; Paiva-Oliveira, Daniela I.; Wijers-Koster, Pauline M.; Abrunhosa, Antero J.; Fontes-Ribeiro, Carlos; Bovée, Judith V. M. G. et al. (2016): Chemotherapy induces stemness in osteosarcoma cells through activation of Wnt/β-catenin signaling. In *Cancer letters* 370 (2), pp. 286–295. DOI: 10.1016/j.canlet.2015.11.013.

May, M. J.; Ghosh, S. (1998): Signal transduction through NF-kappa B. In *Immunology today* 19 (2), pp. 80–88. DOI: 10.1016/s0167-5699(97)01197-3.

Meyer, Natalie; Penn, Linda Z. (2008): Reflecting on 25 years with MYC. In *Nature reviews. Cancer* 8 (12), pp. 976–990. DOI: 10.1038/nrc2231.

Min, Chengyin; Eddy, Sean F.; Sherr, David H.; Sonenshein, Gail E. (2008): NF-kappaB and epithelial to mesenchymal transition of cancer. In *Journal of cellular biochemistry* 104 (3), pp. 733–744. DOI: 10.1002/jcb.21695.

Morata-Tarifa, Cynthia; Jiménez, Gema; García, María A.; Entrena, José M.; Griñán-Lisón, Carmen; Aguilera, Margarita et al. (2016): Low adherent cancer cell subpopulations are enriched in tumorigenic and metastatic epithelial-to-mesenchymal transition-induced cancer stem-like cells. In *Scientific reports* 6, p. 18772. DOI: 10.1038/srep18772.

Nakamura, Mitsuhiro; Kyo, Satoru; Zhang, Bo; Zhang, Xiuzhi; Mizumoto, Yasunari; Takakura, Masahiro et al. (2010): Prognostic impact of CD133 expression as a tumor-initiating cell marker in endometrial cancer. In *Human pathology* 41 (11), pp. 1516–1529. DOI: 10.1016/j.humpath.2010.05.006.

Nakamura, Mitsuhiro; Zhang, Xiuzhi; Mizumoto, Yasunari; Maida, Yoshiko; Bono, Yukiko; Takakura, Masahiro; Kyo, Satoru (2014): Molecular characterization of CD133+ cancer stem-like cells in endometrial cancer. In *International journal of oncology* 44 (3), pp. 669–677. DOI: 10.3892/ijo.2013.2230.

Narita, Kosuke; Matsuda, Yoko; Seike, Masahiro; Naito, Zenya; Gemma, Akihiko; Ishiwata, Toshiyuki (2014): Nestin regulates proliferation, migration, invasion and stemness of lung adenocarcinoma. In *International journal of oncology* 44 (4), pp. 1118–1130. DOI: 10.3892/ijo.2014.2278.

Navone, F.; Jahn, R.; Di Gioia, G.; Stukenbrok, H.; Greengard, P.; Camilli, P. de (1986): Protein p38: an integral membrane protein specific for small vesicles of neurons and

neuroendocrine cells. In *The Journal of cell biology* 103 (6 Pt 1), pp. 2511–2527. DOI: 10.1083/jcb.103.6.2511.

Neradil, Jakub; Veselska, Renata (2015): Nestin as a marker of cancer stem cells. In *Cancer science* 106 (7), pp. 803–811. DOI: 10.1111/cas.12691.

Nowell, P. C. (1976): The clonal evolution of tumor cell populations. In *Science (New York, N.Y.)* 194 (4260), pp. 23–28. DOI: 10.1126/science.959840.

O'Brien, Catherine A.; Pollett, Aaron; Gallinger, Steven; Dick, John E. (2007): A human colon cancer cell capable of initiating tumour growth in immunodeficient mice. In *Nature* 445 (7123), pp. 106–110. DOI: 10.1038/nature05372.

Oeckinghaus, Andrea; Ghosh, Sankar (2009): The NF-kappaB family of transcription factors and its regulation. In *Cold Spring Harbor perspectives in biology* 1 (4), a000034. DOI: 10.1101/cshperspect.a000034.

Ohata, Hirokazu; Ishiguro, Tatsuya; Aihara, Yuki; Sato, Ai; Sakai, Hiroaki; Sekine, Shigeki et al. (2012): Induction of the stem-like cell regulator CD44 by Rho kinase inhibition contributes to the maintenance of colon cancer-initiating cells. In *Cancer research* 72 (19), pp. 5101–5110. DOI: 10.1158/0008-5472.CAN-11-3812.

Ózsvári, Béla; Sotgia, Federica; Lisanti, Michael P. (2020): First-in-class candidate therapeutics that target mitochondria and effectively prevent cancer cell metastasis: mitoriboscins and TPP compounds. In *Aging* 12 (11), pp. 10162–10179. DOI: 10.18632/aging.103336.

Page, Angustias; Ortega, Alba; Alameda, Josefa P.; Navarro, Manuel; Paramio, Jesús M.; Saiz-Pardo, Melchor et al. (2019): IKKα Promotes the Progression and Metastasis of Non-Small Cell Lung Cancer Independently of its Subcellular Localization. In *Computational and structural biotechnology journal* 17, pp. 251–262. DOI: 10.1016/j.csbj.2019.02.003.

Pardal, Ricardo; Clarke, Michael F.; Morrison, Sean J. (2003): Applying the principles of stem-cell biology to cancer. In *Nature reviews. Cancer* 3 (12), pp. 895–902. DOI: 10.1038/nrc1232.

Park, Ji Y.; Hong, Daegy; Park, Ji Young (2019): Association between Morphological Patterns of Myometrial Invasion and Cancer Stem Cell Markers in Endometrial Endometrioid Carcinoma. In *Pathology oncology research : POR* 25 (1), pp. 123–130. DOI: 10.1007/s12253-017-0320-5.

Peiris-Pagès, Maria; Ozsvári, Béla; Sotgia, Federica; Lisanti, Michael P. (2019): Mitochondrial and ribosomal biogenesis are new hallmarks of stemness, oncometabolism and biomass accumulation in cancer: Mito-stemness and ribo-stemness features. In *Aging* 11 (14), pp. 4801–4835. DOI: 10.18632/aging.102054.

Perkins, Neil D. (2007): Integrating cell-signalling pathways with NF-kappaB and IKK function. In *Nature reviews. Molecular cell biology* 8 (1), pp. 49–62. DOI: 10.1038/nrm2083.

Pfragner, Roswitha; Behmel, Annemarie; Höger, Harald; Beham, Alfred; Ingolic, Elisabeth; Stelzer, Ingeborg et al. (2009): Establishment and characterization of three novel cell lines - P-STS, L-STS, H-STS - derived from a human metastatic midgut carcinoid. In *Anticancer research* 29 (6), pp. 1951–1961.

Pires, Bruno R. B.; Mencalha, Andre L.; Ferreira, Gerson M.; Souza, Waldemir F. de; Morgado-Díaz, José A.; Maia, Amanda M. et al. (2017): NF-kappaB Is Involved in the Regulation of EMT Genes in Breast Cancer Cells. In *PloS one* 12 (1), e0169622. DOI: 10.1371/journal.pone.0169622.

Porporato, Paolo Ettore; Filigheddu, Nicoletta; Pedro, José Manuel Bravo-San; Kroemer, Guido; Galluzzi, Lorenzo (2018): Mitochondrial metabolism and cancer. In *Cell research* 28 (3), pp. 265–280. DOI: 10.1038/cr.2017.155.

Prabavathy, D.; Swarnalatha, Y.; Ramadoss, Niveditha (2018): Lung cancer stem cells-origin, characteristics and therapy. In *Stem cell investigation* 5, p. 6. DOI: 10.21037/sci.2018.02.01.

Qiu, Haifeng; Li, Jing; Clark, Leslie H.; Jackson, Amanda L.; Zhang, Lu; Guo, Hui et al. (2016): JQ1 suppresses tumor growth via PTEN/PI3K/AKT pathway in endometrial cancer. In *Oncotarget* 7 (41), pp. 66809–66821. DOI: 10.18632/oncotarget.11631.

Reya, T.; Morrison, S. J.; Clarke, M. F.; Weissman, I. L. (2001): Stem cells, cancer, and cancer stem cells. In *Nature* 414 (6859), pp. 105–111. DOI: 10.1038/35102167.

Ricci-Vitiani, Lucia; Lombardi, Dario G.; Pilozzi, Emanuela; Biffoni, Mauro; Todaro, Matilde; Peschle, Cesare; Maria, Ruggero de (2007): Identification and expansion of human colon-cancer-initiating cells. In *Nature* 445 (7123), pp. 111–115. DOI: 10.1038/nature05384.

Ridker, Paul M.; MacFadyen, Jean G.; Thuren, Tom; Everett, Brendan M.; Libby, Peter; Glynn, Robert J. (2017): Effect of interleukin-1β inhibition with canakinumab on incident lung cancer in patients with atherosclerosis: exploratory results from a randomised, double-blind, placebo-controlled trial. In *Lancet (London, England)* 390 (10105), pp. 1833–1842. DOI: 10.1016/S0140-6736(17)32247-X.

Rihawi, Karim; Alfieri, Roberta; Fiorentino, Michelangelo; Fontana, Francesca; Capizzi, Elisa; Cavazzoni, Andrea et al. (2019): MYC Amplification as a Potential Mechanism of Primary Resistance to Crizotinib in ALK-Rearranged Non-Small Cell Lung Cancer: A Brief Report. In *Translational oncology* 12 (1), pp. 116–121. DOI: 10.1016/j.tranon.2018.09.013.

Ruiz-Ceja, Karla A.; Chirino, Yolanda I. (2017): Current FDA-approved treatments for non-small cell lung cancer and potential biomarkers for its detection. In *Biomedicine & pharmacotherapy = Biomedecine & pharmacotherapie* 90, pp. 24–37. DOI: 10.1016/j.biopha.2017.03.018.

Rutella, Sergio; Bonanno, Giuseppina; Procoli, Annabella; Mariotti, Andrea; Corallo, Maria; Prisco, Maria Grazia et al. (2009): Cells with characteristics of cancer stem/progenitor cells express the CD133 antigen in human endometrial tumors. In *Clinical cancer research : an official journal of the American Association for Cancer Research* 15 (13), pp. 4299–4311. DOI: 10.1158/1078-0432.CCR-08-1883.

Sainio, Miika; Visakorpi, Tapio; Tolonen, Teemu; Ilvesaro, Joanna; Bova, G. Steven (2018): Expression of neuroendocrine differentiation markers in lethal metastatic castration-resistant prostate cancer. In *Pathology, research and practice* 214 (6), pp. 848–856. DOI: 10.1016/j.prp.2018.04.015.

Sancho, Patricia; Burgos-Ramos, Emma; Tavera, Alejandra; Bou Kheir, Tony; Jagust, Petra; Schoenhals, Matthieu et al. (2015): MYC/PGC-1α Balance Determines the Metabolic

Phenotype and Plasticity of Pancreatic Cancer Stem Cells. In *Cell metabolism* 22 (4), pp. 590–605. DOI: 10.1016/j.cmet.2015.08.015.

Satar, Nazilah Abdul; Fakiruddin, Kamal Shaik; Lim, Moon Nian; Mok, Pooi Ling; Zakaria, Norashikin; Fakharuzi, Noor Atiqah et al. (2018): Novel triple- positive markers identified in human non- small cell lung cancer cell line with chemotherapy-resistant and putative cancer stem cell characteristics. In *Oncology reports* 40 (2), pp. 669–681. DOI: 10.3892/or.2018.6461.

Sawyers, Charles (2004): Targeted cancer therapy. In *Nature* 432 (7015), pp. 294–297. DOI: 10.1038/nature03095.

Scatena, Cristian; Roncella, Manuela; Di Paolo, Antonello; Aretini, Paolo; Menicagli, Michele; Fanelli, Giovanni et al. (2018): Doxycycline, an Inhibitor of Mitochondrial Biogenesis, Effectively Reduces Cancer Stem Cells (CSCs) in Early Breast Cancer Patients: A Clinical Pilot Study. In *Frontiers in oncology* 8, p. 452. DOI: 10.3389/fonc.2018.00452.

Schaub, Franz X.; Dhankani, Varsha; Berger, Ashton C.; Trivedi, Mihir; Richardson, Anne B.; Shaw, Reid et al. (2018): Pan-cancer Alterations of the MYC Oncogene and Its Proximal Network across the Cancer Genome Atlas. In *Cell systems* 6 (3), 282-300.e2. DOI: 10.1016/j.cels.2018.03.003.

Schulte am Esch, Jan; Windmöller, Beatrice Ariane; Hanewinkel, Johannes; Storm, Jonathan; Förster, Christine; Wilkens, Ludwig et al. (2020): Isolation and Characterization of Two Novel Colorectal Cancer Cell Lines, Containing a Subpopulation with Potential Stem-Like Properties: Treatment Options by MYC/NMYC Inhibition. In *Cancers* 12 (9). DOI: 10.3390/cancers12092582.

Schwitalla, Sarah; Fingerle, Alexander A.; Cammareri, Patrizia; Nebelsiek, Tim; Göktuna, Serkan I.; Ziegler, Paul K. et al. (2013): Intestinal tumorigenesis initiated by dedifferentiation and acquisition of stem-cell-like properties. In *Cell* 152 (1-2), pp. 25–38. DOI: 10.1016/j.cell.2012.12.012.

Senftleben, U.; Cao, Y.; Xiao, G.; Greten, F. R.; Krähn, G.; Bonizzi, G. et al. (2001): Activation by IKKalpha of a second, evolutionary conserved, NF-kappa B signaling pathway. In *Science (New York, N.Y.)* 293 (5534), pp. 1495–1499. DOI: 10.1126/science.1062677.

Seo, A. N.; Yang, J. M.; Kim, H.; Jheon, S.; Kim, K.; Lee, C. T. et al. (2014): Clinicopathologic and prognostic significance of c-MYC copy number gain in lung adenocarcinomas. In *British journal of cancer* 110 (11), pp. 2688–2699. DOI: 10.1038/bjc.2014.218.

Sethi, Gautam; Sung, Bokyung; Aggarwal, Bharat B. (2008): TNF: a master switch for inflammation to cancer. In *Frontiers in bioscience : a journal and virtual library* 13, pp. 5094–5107. DOI: 10.2741/3066.

Shafqat, Hammad; Ali, Shihab; Salhab, Mohammed; Olszewski, Adam J. (2015): Survival of patients with neuroendocrine carcinoma of the colon and rectum: a population-based analysis. In *Diseases of the colon and rectum* 58 (3), pp. 294–303. DOI: 10.1097/DCR.0000000000000298.

Sigerist, H. E. (1932): The Historical Development of the Pathology and Therapy of Cancer. In *Bulletin of the New York Academy of Medicine* 8 (11), pp. 642–653.

Skoda, Jan; Borankova, Karolina; Jansson, Patric J.; Huang, Michael L-H; Veselska, Renata; Des Richardson, R. (2019): Pharmacological targeting of mitochondria in cancer stem cells: An ancient organelle at the crossroad of novel anti-cancer therapies. In *Pharmacological research* 139, pp. 298–313. DOI: 10.1016/j.phrs.2018.11.020.

Sládek, Norman E.; Kollander, Rahn; Sreerama, Lakshmaiah; Kiang, David T. (2002): Cellular levels of aldehyde dehydrogenases (ALDH1A1 and ALDH3A1) as predictors of therapeutic responses to cyclophosphamide-based chemotherapy of breast cancer: a retrospective study. Rational individualization of oxazaphosphorine-based cancer chemotherapeutic regimens. In *Cancer chemotherapy and pharmacology* 49 (4), pp. 309–321. DOI: 10.1007/s00280-001-0412-4.

Sorbye, Halfdan; Strosberg, Jonathan; Baudin, Eric; Klimstra, David S.; Yao, James C. (2014): Gastroenteropancreatic high-grade neuroendocrine carcinoma. In *Cancer* 120 (18), pp. 2814–2823. DOI: 10.1002/cncr.28721.

Sousa E Melo, Felipe de; Colak, Selcuk; Buikhuisen, Joyce; Koster, Jan; Cameron, Kate; Jong, Joan H. de et al. (2011): Methylation of cancer-stem-cell-associated Wnt target genes predicts poor prognosis in colorectal cancer patients. In *Cell stem cell* 9 (5), pp. 476–485. DOI: 10.1016/j.stem.2011.10.008.

Spivak-Kroizman, T.; Lemmon, M. A.; Dikic, I.; Ladbury, J. E.; Pinchasi, D.; Huang, J. et al. (1994): Heparin-induced oligomerization of FGF molecules is responsible for FGF receptor dimerization, activation, and cell proliferation. In *Cell* 79 (6), pp. 1015–1024. DOI: 10.1016/0092-8674(94)90032-9.

Storci, Gianluca; Sansone, Pasquale; Mari, Sara; D'Uva, Gabriele; Tavolari, Simona; Guarnieri, Tiziana et al. (2010): TNFalpha up-regulates SLUG via the NF-kappaB/HIF1alpha axis, which imparts breast cancer cells with a stem cell-like phenotype. In *Journal of cellular physiology* 225 (3), pp. 682–691. DOI: 10.1002/jcp.22264.

Sultan, Mohammad; Coyle, Krysta Mila; Vidovic, Dejan; Thomas, Margaret Lois; Gujar, Shashi; Marcato, Paola (2017): Hide-and-seek: the interplay between cancer stem cells and the immune system. In *Carcinogenesis* 38 (2), pp. 107–118. DOI: 10.1093/carcin/bgw115.

Sun, Feng-Feng; Hu, Yong-He; Xiong, Lv-Ping; Tu, Xiao-Yun; Zhao, Ji-Hua; Chen, Sheng-Song et al. (2015): Enhanced expression of stem cell markers and drug resistance in sphere-forming non-small cell lung cancer cells. In *International Journal of Clinical and Experimental Pathology* 8 (6), pp. 6287–6300.

Sun, Lei; Mathews, Lesley A.; Cabarcas, Stephanie M.; Zhang, Xiaohu; Yang, Acong; Zhang, Ying et al. (2013): Epigenetic regulation of SOX9 by the NF-κB signaling pathway in pancreatic cancer stem cells. In *Stem cells (Dayton, Ohio)* 31 (8), pp. 1454–1466. DOI: 10.1002/stem.1394.

Sun, Wu; Li, Jialu; Zhou, Likun; Han, Jiayi; Liu, Rui; Zhang, Haiyang et al. (2020): The c-Myc/miR-27b-3p/ATG10 regulatory axis regulates chemoresistance in colorectal cancer. In *Theranostics* 10 (5), pp. 1981–1996. DOI: 10.7150/thno.37621.

Sun, Yi; Yoshida, Toshiko; Okabe, Motonori; Zhou, Kaixuan; Wang, Fang; Soko, Chika et al. (2017): Isolation of Stem-Like Cancer Cells in Primary Endometrial Cancer Using Cell Surface Markers CD133 and CXCR4. In *Translational oncology* 10 (6), pp. 976–987. DOI: 10.1016/j.tranon.2017.07.007.

Sung, Hyuna; Ferlay, Jacques; Siegel, Rebecca L.; Laversanne, Mathieu; Soerjomataram, Isabelle; Jemal, Ahmedin; Bray, Freddie (2021): Global Cancer Statistics 2020: GLOBOCAN Estimates of Incidence and Mortality Worldwide for 36 Cancers in 185 Countries. In *CA: a cancer journal for clinicians* 71 (3), pp. 209–249. DOI: 10.3322/caac.21660.

Tahata, Shinichi; Yuan, Bo; Kikuchi, Hidetomo; Takagi, Norio; Hirano, Toshihiko; Toyoda, Hiroo (2014): Cytotoxic effects of pyrrolidine dithiocarbamate in small-cell lung cancer cells, alone and in combination with cisplatin. In *International journal of oncology* 45 (4), pp. 1749–1759. DOI: 10.3892/ijo.2014.2564.

Takahashi, Y.; Onda, M.; Tanaka, N.; Seya, T. (2000): Establishment and characterization of two new rectal neuroendocrine cell carcinoma cell lines. In *Digestion* 62 (4), pp. 262–270. DOI: 10.1159/000007825.

Tan, Yaoxi; Chen, Bo; Xu, Wei; Zhao, Weihong; Wu, Jianqing (2014): Clinicopathological significance of CD133 in lung cancer: A meta-analysis. In *Molecular and clinical oncology* 2 (1), pp. 111–115. DOI: 10.3892/mco.2013.195.

Tang, Yun-Liang; Zhu, Ling-Yan; Li, Yu; Yu, Jiao; Wang, Jiao; Zeng, Xiang-Xia et al. (2017): Metformin Use Is Associated with Reduced Incidence and Improved Survival of Endometrial Cancer: A Meta-Analysis. In *BioMed research international* 2017, p. 5905384. DOI: 10.1155/2017/5905384.

Taniguchi, Koji; Karin, Michael (2018): NF-κB, inflammation, immunity and cancer: coming of age. In *Nature reviews. Immunology* 18 (5), pp. 309–324. DOI: 10.1038/nri.2017.142.

Tao, Xiaomei; Yin, Yefeng; Lian, Dongbo; Gu, Hongyan; Chen, Wen; Yang, Lu et al. (2020): Puerarin 6″-O-xyloside suppresses growth, self-renewal and invasion of lung cancer stem-like cells derived from A549 cells via regulating Akt/c-Myc signalling. In *Clinical and experimental pharmacology & physiology* 47 (7), pp. 1311–1319. DOI: 10.1111/1440-1681.13294.

Tirino, Virginia; Camerlingo, Rosa; Franco, Renato; Malanga, Donatella; La Rocca, Antonello; Viglietto, Giuseppe et al. (2009): The role of CD133 in the identification and characterisation of tumour-initiating cells in non-small-cell lung cancer. In *European journal of cardio-thoracic surgery : official journal of the European Association for Cardio-thoracic Surgery* 36 (3), pp. 446–453. DOI: 10.1016/j.ejcts.2009.03.063.

Todaro, Matilde; Gaggianesi, Miriam; Catalano, Veronica; Benfante, Antonina; Iovino, Flora; Biffoni, Mauro et al. (2014): CD44v6 is a marker of constitutive and reprogrammed cancer stem cells driving colon cancer metastasis. In *Cell stem cell* 14 (3), pp. 342–356. DOI: 10.1016/j.stem.2014.01.009.

Toh, Tan Boon; Lim, Jhin Jieh; Chow, Edward Kai-Hua (2017): Epigenetics in cancer stem cells. In *Molecular cancer* 16 (1), p. 29. DOI: 10.1186/s12943-017-0596-9.

Travis, William D. (Ed.) (2015): WHO classification of tumours of lung, pleura, thymus and heart. … reflects the views of a working group that convened for a consensus and editorial meeting at the International Agency for Research on Cancer, Lyon, April 24 - 26, 2014. Weltgesundheitsorganisation; International Agency for Research on Cancer; Consensus and editorial meeting at the Agency for Research on Cancer (IARC). 4. ed. Lyon: International

Agency for Research on Cancer (World Health Organization Classification of tumours, 7 (der 4. ed.)).

Tudoraşcu, Diana Rodica; Pirici, Daniel; Târtea, Elena Anca; Mustafa, Edme Roxana; Florescu, Cristina; Vere, Cristin Constantin et al. (2017): Synaptophysin expression as prognostic factor for survival in colorectal carcinomas. In *Romanian journal of morphology and embryology = Revue roumaine de morphologie et embryologie* 58 (4), pp. 1409–1415.

Vadde, Ramakrishna; Radhakrishnan, Sridhar; Reddivari, Lavanya; Vanamala, Jairam K. P. (2015): Triphala Extract Suppresses Proliferation and Induces Apoptosis in Human Colon Cancer Stem Cells via Suppressing c-Myc/Cyclin D1 and Elevation of Bax/Bcl-2 Ratio. In *BioMed research international* 2015, p. 649263. DOI: 10.1155/2015/649263.

van Neerven, Sanne M.; Tieken, Mathijs; Vermeulen, Louis; Bijlsma, Maarten F. (2016): Bidirectional interconversion of stem and non-stem cancer cell populations: A reassessment of theoretical models for tumor heterogeneity. In *Molecular & cellular oncology* 3 (2), e1098791. DOI: 10.1080/23723556.2015.1098791.

Vander Heiden, Matthew G.; DeBerardinis, Ralph J. (2017): Understanding the Intersections between Metabolism and Cancer Biology. In *Cell* 168 (4), pp. 657–669. DOI: 10.1016/j.cell.2016.12.039.

Vazquez-Santillan, K.; Melendez-Zajgla, J.; Jimenez-Hernandez, L.; Martínez-Ruiz, G.; Maldonado, V. (2015): NF-κB signaling in cancer stem cells: a promising therapeutic target? In *Cellular oncology (Dordrecht)* 38 (5), pp. 327–339. DOI: 10.1007/s13402-015-0236-6.

Vitale, Ilio; Shema, Efrat; Loi, Sherene; Galluzzi, Lorenzo (2021): Intratumoral heterogeneity in cancer progression and response to immunotherapy. In *Nature medicine* 27 (2), pp. 212–224. DOI: 10.1038/s41591-021-01233-9.

Vogelstein, Bert; Papadopoulos, Nickolas; Velculescu, Victor E.; Zhou, Shibin; Diaz, Luis A.; Kinzler, Kenneth W. (2013): Cancer genome landscapes. In *Science (New York, N.Y.)* 339 (6127), pp. 1546–1558. DOI: 10.1126/science.1235122.

Walia, Vijay; Elble, Randolph C. (2010): Enrichment for breast cancer cells with stem/progenitor properties by differential adhesion. In *Stem cells and development* 19 (8), pp. 1175–1182. DOI: 10.1089/scd.2009.0430.

Walther, Wolfgang; Kobelt, Dennis; Bauer, Lisa; Aumann, Jutta; Stein, Ulrike (2015): Chemosensitization by diverging modulation by short-term and long-term TNF-α action on ABCB1 expression and NF-κB signaling in colon cancer. In *International journal of oncology* 47 (6), pp. 2276–2285. DOI: 10.3892/ijo.2015.3189.

Wang, Guoyun; Tokushige, Natsuko; Russell, Peter; Dubinovsky, Sylvia; Markham, Robert; Fraser, Ian S. (2010): Neuroendocrine cells in eutopic endometrium of women with endometriosis. In *Human reproduction (Oxford, England)* 25 (2), pp. 387–391. DOI: 10.1093/humrep/dep379.

Wang, Xiaowen; Zhang, Hong; Sapio, Russell; Yang, Jun; Wong, Justin; Zhang, Xin et al. (2021): SOD1 regulates ribosome biogenesis in KRAS mutant non-small cell lung cancer. In *Nature communications* 12 (1), p. 2259. DOI: 10.1038/s41467-021-22480-x.

Wang, Yuanyuan; Zhou, Ling; Qing, Qing; Li, Yingfei; Li, Lixuan; Dong, Xiaoying; Xiao, Bing (2019): Gene expression profile of cancer stem- like cells in the SW480 colon

adenocarcinoma cell line. In *Oncology reports* 42 (1), pp. 386–398. DOI: 10.3892/or.2019.7146.

Warburg, Otto (1925): über den Stoffwechsel der Carcinomzelle. In *Klin Wochenschr* 4 (12), pp. 534–536. DOI: 10.1007/BF01726151.

Wei, Zhihao; Jia, Jiankun; Heng, Gang; Xu, Huailong; Shan, Juanjuan; Wang, Guiqin et al. (2019): Sirtuin-1/Mitochondrial Ribosomal Protein S5 Axis Enhances the Metabolic Flexibility of Liver Cancer Stem Cells. In *Hepatology (Baltimore, Md.)* 70 (4), pp. 1197–1213. DOI: 10.1002/hep.30622.

Werner, Shannon L.; Kearns, Jeffrey D.; Zadorozhnaya, Victoria; Lynch, Candace; O'Dea, Ellen; Boldin, Mark P. et al. (2008): Encoding NF-kappaB temporal control in response to TNF: distinct roles for the negative regulators IkappaBalpha and A20. In *Genes & development* 22 (15), pp. 2093–2101. DOI: 10.1101/gad.1680708.

West, Howard; McCleod, Michael; Hussein, Maen; Morabito, Alessandro; Rittmeyer, Achim; Conter, Henry J. et al. (2019): Atezolizumab in combination with carboplatin plus nab-paclitaxel chemotherapy compared with chemotherapy alone as first-line treatment for metastatic non-squamous non-small-cell lung cancer (IMpower130): a multicentre, randomised, open-label, phase 3 trial. In *The Lancet Oncology* 20 (7), pp. 924–937. DOI: 10.1016/S1470-2045(19)30167-6.

Whitfield, Jonathan R.; Beaulieu, Marie-Eve; Soucek, Laura (2017): Strategies to Inhibit Myc and Their Clinical Applicability. In *Frontiers in cell and developmental biology* 5, p. 10. DOI: 10.3389/fcell.2017.00010.

Wiedenmann, B.; Franke, W. W. (1985): Identification and localization of synaptophysin, an integral membrane glycoprotein of Mr 38,000 characteristic of presynaptic vesicles. In *Cell* 41 (3), pp. 1017–1028. DOI: 10.1016/s0092-8674(85)80082-9.

Wiedenmann, B.; Franke, W. W.; Kuhn, C.; Moll, R.; Gould, V. E. (1986): Synaptophysin: a marker protein for neuroendocrine cells and neoplasms. In *Proceedings of the National Academy of Sciences of the United States of America* 83 (10), pp. 3500–3504. DOI: 10.1073/pnas.83.10.3500.

Windmöller, Beatrice A.; Beshay, Morris; Helweg, Laureen P.; Flottmann, Clara; Beermann, Miriam; Förster, Christine et al. (2021a): Novel Primary Human Cancer Stem-Like Cell Populations from Non-Small Cell Lung Cancer: Inhibition of Cell Survival by Targeting NF-κB and MYC Signaling. In *Cells* 10 (5), p. 1024. DOI: 10.3390/cells10051024.

Windmöller, Beatrice A.; Helweg, Laureen P.; Burghardt, Leonie; Storm, Jonathan; Förster, Christine; Wilkens, Ludwig et al. (2021b): Diminishment of novel endometrial carcinoma-derived stem-like cells by targeting mitochondrial bioenergetics and MYC. Under review at *Gynecologic Oncology*.

Windmöller, Beatrice Ariane; Greiner, Johannes F. W.; Förster, Christine; Wilkens, Ludwig; Mertzlufft, Fritz; Am Schulte Esch, Jan et al. (2019): A typical carcinoid of the lung - a case report with pathological correlation and propagation of the cancer stem cell line BKZ1 with synaptophysin expression. In *Medicine* 98 (49), e18174. DOI: 10.1097/MD.0000000000018174.

Witte, Kaya E.; Hertel, Oliver; Windmöller, Beatrice A.; Helweg, Laureen P.; Höving, Anna L.; Knabbe, Cornelius et al. (2021): Nanopore Sequencing Reveals Global Transcriptome Signatures of Mitochondrial and Ribosomal Gene Expressions in Various Human Cancer Stem-like Cell Populations. In *Cancers* 13 (5). DOI: 10.3390/cancers13051136.

Wolf, Elmar; Eilers, Martin (2020): Targeting MYC Proteins for Tumor Therapy. In *Annu. Rev. Cancer Biol.* 4 (1), pp. 61–75. DOI: 10.1146/annurev-cancerbio-030518-055826.

Wu, Dang; Wu, Pin; Zhao, Lufeng; Huang, Lijian; Zhang, Zhigang; Zhao, Shuai; Huang, Jian (2015): NF-κB Expression and Outcomes in Solid Tumors: A Systematic Review and Meta-Analysis. In *Medicine* 94 (40), e1687. DOI: 10.1097/MD.0000000000001687.

Xia, Longzheng; Tan, Shiming; Zhou, Yujuan; Lin, Jingguan; Wang, Heran; Oyang, Linda et al. (2018): Role of the NFκB-signaling pathway in cancer. In *OncoTargets and therapy* 11, pp. 2063–2073. DOI: 10.2147/OTT.S161109.

Yanagihara, Kazuyoshi; Kubo, Takanori; Mihara, Keichiro; Kuwata, Takeshi; Ochiai, Atsushi; Seyama, Toshio; Yokozaki, Hiroshi (2018): Establishment of a novel cell line from a rare human duodenal poorly differentiated neuroendocrine carcinoma. In *Oncotarget* 9 (92), pp. 36503–36514. DOI: 10.18632/oncotarget.26367.

Yang, Hsin-Ling; Thiyagarajan, Varadharajan; Shen, Pei-Chun; Mathew, Dony Chacko; Lin, Kai-Yuan; Liao, Jiunn-Wang; Hseu, You-Cheng (2019): Anti-EMT properties of CoQ0 attributed to PI3K/AKT/NFKB/MMP-9 signaling pathway through ROS-mediated apoptosis. In *Journal of experimental & clinical cancer research : CR* 38 (1), p. 186. DOI: 10.1186/s13046-019-1196-x.

Yang, Jianchang; Gao, Chong; Chai, Li; Ma, Yupo (2010): A novel SALL4/OCT4 transcriptional feedback network for pluripotency of embryonic stem cells. In *PloS one* 5 (5), e10766. DOI: 10.1371/journal.pone.0010766.

Yang, Xiaojun; Ye, Jing; Yan, Han; Tang, Zhaoyang; Shen, Jian; Zhang, Jianping; Yang, Lihua (2016): MiR-491 attenuates cancer stem cells-like properties of hepatocellular carcinoma by inhibition of GIT-1/NF-κB-mediated EMT. In *Tumour biology : the journal of the International Society for Oncodevelopmental Biology and Medicine* 37 (1), pp. 201–209. DOI: 10.1007/s13277-015-3687-5.

Yoshida, Go J. (2020): Beyond the Warburg Effect: N-Myc Contributes to Metabolic Reprogramming in Cancer Cells. In *Frontiers in oncology* 10, p. 791. DOI: 10.3389/fonc.2020.00791.

Yu, Wan-Nien; Lai, Ying-Ju; Ma, Jui-Wen; Ho, Chi-Tang; Hung, Shan-Wei; Chen, Yu-Hsin et al. (2019): Citronellol Induces Necroptosis of Human Lung Cancer Cells via TNF-α Pathway and Reactive Oxygen Species Accumulation. In *In vivo (Athens, Greece)* 33 (4), pp. 1193–1201. DOI: 10.21873/invivo.11590.

Yuan, Yi; Anbalagan, Durkeshwari; Lee, Lay Hoon; Samy, Ramar Perumal; Shanmugam, Muthu K.; Kumar, Alan Prem et al. (2016): ANXA1 inhibits miRNA-196a in a negative feedback loop through NF-kB and c-Myc to reduce breast cancer proliferation. In *Oncotarget* 7 (19), pp. 27007–27020. DOI: 10.18632/oncotarget.8875.

Zakaria, Norashikin; Mohd Yusoff, Narazah; Zakaria, Zubaidah; Widera, Darius; Yahaya, Badrul Hisham (2018): Inhibition of NF-κB Signaling Reduces the Stemness Characteristics

of Lung Cancer Stem Cells. In *Frontiers in oncology* 8, p. 166. DOI: 10.3389/fonc.2018.00166.

Zakaria, Norashikin; Yusoff, Narazah Mohd; Zakaria, Zubaidah; Lim, Moon Nian; Baharuddin, Puteri J. Noor; Fakiruddin, Kamal Shaik; Yahaya, Badrul (2015): Human non-small cell lung cancer expresses putative cancer stem cell markers and exhibits the transcriptomic profile of multipotent cells. In *BMC cancer* 15, p. 84. DOI: 10.1186/s12885-015-1086-3.

Zeller, Karen I.; Zhao, XiaoDong; Lee, Charlie W. H.; Chiu, Kuo Ping; Yao, Fei; Yustein, Jason T. et al. (2006): Global mapping of c-Myc binding sites and target gene networks in human B cells. In *Proceedings of the National Academy of Sciences of the United States of America* 103 (47), pp. 17834–17839. DOI: 10.1073/pnas.0604129103.

Zhang, Daye; Zhang, Yongxiang; Cai, Zeyuan; Tu, Ying; Hu, Zhansong (2020): Dexamethasone and lenvatinib inhibit migration and invasion of non-small cell lung cancer by regulating EKR/AKT and VEGF signal pathways. In *Experimental and therapeutic medicine* 19 (1), pp. 762–770. DOI: 10.3892/etm.2019.8225.

Zhang, Huan-Le; Wang, Ping; Lu, Miao-Zhen; Zhang, San-Dian; Zheng, Lu (2019): c-Myc maintains the self-renewal and chemoresistance properties of colon cancer stem cells. In *Oncology letters* 17 (5), pp. 4487–4493. DOI: 10.3892/ol.2019.10081.

Zhang, Rongrong; Zhang, Ping; Wang, Hong; Hou, Dongming; Li, Wentao; Xiao, Guishan; Li, Chenwei (2015): Inhibitory effects of metformin at low concentration on epithelial-mesenchymal transition of CD44(+)CD117(+) ovarian cancer stem cells. In *Stem cell research & therapy* 6, p. 262. DOI: 10.1186/s13287-015-0249-0.

Zhang, Xiu-Wei; Ma, Yu-Xiang; Sun, Yang; Cao, Yu-Bo; Li, Qin; Xu, Chong-An (2017): Gemcitabine in Combination with a Second Cytotoxic Agent in the First-Line Treatment of Locally Advanced or Metastatic Pancreatic Cancer: a Systematic Review and Meta-Analysis. In *Targeted oncology* 12 (3), pp. 309–321. DOI: 10.1007/s11523-017-0486-5.

Zhao, Xiaopeng; Ma, Lu; Dai, Lu; Di Zuo; Li, Xin; Zhu, Hongli; Xu, Fang (2020): TNF- α promotes the malignant transformation of intestinal stem cells through the NF- κB and Wnt/β- catenin signaling pathways. In *Oncology reports* 44 (2), pp. 577–588. DOI: 10.3892/or.2020.7631.

Zhou, Li; Wu, Feifei; Jin, Wangdong; Yan, Bo; Chen, Xin; He, Yingfei et al. (2017): Theabrownin Inhibits Cell Cycle Progression and Tumor Growth of Lung Carcinoma through c-myc-Related Mechanism. In *Frontiers in pharmacology* 8, p. 75. DOI: 10.3389/fphar.2017.00075.

Zhu, Mingming; Yu, Xi; Zheng, Zongmei; Huang, Jiaming; Yang, Xuepan; Shi, Hongfei (2020): Capsaicin suppressed activity of prostate cancer stem cells by inhibition of Wnt/β-catenin pathway. In *Phytotherapy research : PTR* 34 (4), pp. 817–824. DOI: 10.1002/ptr.6563.

Zou, Kun; Li, Zongjuan; Zhang, Yang; Mu, Lin; Chen, Miao; Wang, Ruonan et al. (2020): β-Elemene enhances radiosensitivity in non-small-cell lung cancer by inhibiting epithelial-mesenchymal transition and cancer stem cell traits via Prx-1/NF-kB/iNOS signaling pathway. In *Aging* 13 (2), pp. 2575–2592. DOI: 10.18632/aging.202291.

5 Acknowledgement

At first, I would like to thank my supervisors Prof. Dr. Christian Kaltschmidt and Prof. Dr. Fritz Mertzlufft for giving me the opportunity to work on such a highly relevant topic as well as for their guidance and support through the three years of work. Further, I also thank Prof. Dr. Barbara Kaltschmidt for invaluably constructive discussions and friendly advice during the project. My special thank goes to Dr. Johannes Greiner, who supported, encouraged and helped me a lot with his supervision and proofreading of this thesis.

I also extend my thanks to all the members of the Forschungsverbund BioMedizin Bielefeld/OWL FBMB e. V. and other collaboration partners. Special thanks goes to Prof. Dr. Jan Schulte am Esch, Dr. Morris Beshay, Prof. Dr. Constanze Banz-Jansen and Dr. Christine Förster for close and fruitful cooperations that immensely contributed to the success of this work.

Additionally, I would like to thank all the current and former members of the Department of Cell Biology for a pleasant working atmosphere and helpfulness. Especially, I thank Kaya Witte, Laureen Helweg, Angela Kralemann-Köhler and Elke Redecker for the support and teamwork in the lab.

I thank all the co-authors of the publications of which this thesis is composed of, namely: Christian Kaltschmidt, Fritz Mertzlufft, Barbara Kaltschmidt, Jan Schulte Am Esch, Morris Beshay, Constanze Banz-Jansen, Johannes F. W. Greiner, Christine Förster, Ludwig Wilkens, Johannes Hanewinkel, Jonathan Storm, Martin Krüger, Kaya E. Witte, Oliver Hertel, Laureen P. Helweg, Anna L. Höving, Cornelius Knabbe, Tobias Busche, Jörn Kalinowski, Thomas Noll, Jesco Pfitzenmaier, Matthias Simon, Clara Flottmann, Miriam Beermann and Leonie Burghardt.

Finally, I would like to thank my family and friends, who supported and encouraged me throughout all the time. Especially, I deeply thank Johannes for his patience and caring support. I love you.

6 Declaration

I hereby declare that I am the sole author of the dissertation

„Targeting of MYC- and NF-κB-signaling in primary human cancer stem-like cells“

and did not use any material or sources other than the ones I have named. Passages that use wording (or words of that effect), tables or pictures of other sources have always been duly acknowledged with a reference to the original material. This dissertation or similar versions have not been previously submitted for a degree.

Bielefeld, 14.07.2021 _____

Beatrice Ariane Windmöller

7 Selected Publications

Original Research Article

“A typical carcinoid of the lung - a case report with pathological correlation and propagation of the cancer stem cell line BKZ1 with synaptophysin expression”

Beatrice A. Windmöller, Johannes F. W. Greiner, Christine Förster, Ludwig Wilkens, Fritz Mertzlufft, Jan Schulte Am Esch, Barbara Kaltschmidt, Christian Kaltschmidt, Morris Beshay

Medicine (Baltimore). 2019 Dec; 98(49): e18174.

Clinical Case Report

Medicine®

OPEN

A typical carcinoid of the lung – a case report with pathological correlation and propagation of the cancer stem cell line BKZ1 with synaptophysin expression

Beatrice Ariane Windmöller, MSc[a,g,*], Johannes F.W. Greiner, PhD[a,g], Christine Förster, MD[b,g], Ludwig Wilkens, MD[b,g], Fritz Mertzlufft, MD[c,g], Jan Schulte am Esch, MD[d,g], Barbara Kaltschmidt, PhD[a,e,g], Christian Kaltschmidt, PhD[a,g], Morris Beshay, MD[f,g]

Abstract

Rationale: Neuroendocrine tumors (NETs) of the lung account for 5% of all cases of lung cancer, which itself is the leading cause of cancer-related death worldwide. In accordance to its rarity, only few cell lines of NETs exist, which even often lack key characteristics of the primary tumor, making it difficult to study underlying molecular mechanisms.

Patient concerns: The patient reported in this case is a 71-year old woman, which never smoked but suffered under dry cough.

diagnoses: Chest CT-scan showed a paracardiac nodule of the lingula with 2 × 1.8 cm in diameter.

Interventions: The detected paracardiac nodule of the lingula was anatomically resected using video assisted thoracic surgery.

Outcomes: Histopathological diagnostic of the removed tissue identified the tumor as a well-differentiated typical carcinoid (TC), which represents one of the four subgroups of pulmonary NETs. Next to the successful treatment of the patient, we were able to propagate cancer stem cells (CSCs) out of the resected tumor tissue. To the best of our knowledge, we firstly isolated CSCs of a typical carcinoid, which were positive for the prominent CSC markers CD44, CD133 and nestin, confirming their stem cell properties. Additionally, CSCs, further referred as BKZ1, expressed the neuroendocrine marker synaptophysin, verifying their neuroendocrine origin. However, nuclear synaptophysin protein was also present in other stem cell populations, suggesting a role as general stem cell marker.

Lesson: In line with the importance of CSCs in cancer treatment and the lack of CSC-models for neuroendocrine neoplasms, the here described BKZ1 cancer stem cell line of a typical carcinoid represents a promising new model to study pulmonary carcinoids and particular NETs.

Abbreviations: AC = atypical carcinoid, bFGF/FGF-2 = basic fibroblast growth factor, BKZ1 = Bethel-Kaltschmidt Zelllinie 1, CSCs = cancer stem cells, CT = computed tomography, EGF = epidermal growth factor, GGT = gamma-glutamyl-transferase, LCNEC = large cell neuroendocrine carcinoma, LRP16 = leukemia related protein 16, NETs = neuroendocrine tumors, NF-κB = nuclear factor kappa-light-chain-enhancer of activated B-cells, PBS = phosphate buffered saline, PNECs = pulmonary neuroendocrine cells, SCLC = small cell lung carcinoma, TC = typical carcinoid, VATS = video assisted thoracic surgery, WHO = World Health Organization.

Keywords: cancer stem cell, nestin, neuroendocrine tumors, synaptophysin, typical carcinoids

Editor: N/A.

CK and MB contributed equally to this work.

All experiments involved patient's informed consent and were ethically approved by the ethics commission of the University of Münster, Germany and the General Medical Council at Münster, Germany (approval reference number 2017–522-f-S). Patient has provided informed consent for publication of the case.The study was funded by the University of Bielefeld and the Research Association of Biomedicine Bielefeld (Forschungsverbund BioMedizin Bielefeld; FBMB)."

The authors report no conflicts of interest.

[a] Department of Cell Biology, University of Bielefeld, Universitätsstrasse 25, Bielefeld, [b] Institute of Pathology, KRH Hospital Nordstadt, Haltenhoffstrasse 41, Hannover, [c] Protestant Hospital of Bethel Foundation, Maraweg 21, [d] Department of General and Visceral Surgery, Protestant Hospital of Bethel Foundation, Schildescher Strasse 99, [e] Molecular Neurobiology, University of Bielefeld, Universitätsstrasse 25, [f] Department of General Thoracic Surgery, Protestant Hospital of Bethel Foundation, Burgsteig 13, [g] Forschungsverbund BioMedizin Bielefeld, FBMB, Maraweg 21, Bielefeld, Germany.

[*] Correspondence: Beatrice Ariane Windmöller, University of Bielefeld, Bielefeld, North Rhine-Westphalia, Germany (e-mail: beatrice.windmoeller@uni-bielefeld.de).

How to cite this article: Windmöller BA, Greiner JF, Förster C, Wilkens L, Mertzlufft F, Esch JS, Kaltschmidt B, Kaltschmidt C, Beshay M. A typical carcinoid of the lung – a case report with pathological correlation and propagation of the cancer stem cell line BKZ1 with synaptophysin expression. Medicine 2019;98:49(e18174).

Received: 1 July 2019 / Received in final form: 14 October 2019 / Accepted: 30 October 2019

http://dx.doi.org/10.1097/MD.0000000000018174

1. Introduction

Lung cancer is the leading cause of cancer-related death worldwide, with about 34,500 new cases of male and 19,300 new cases of female annually in Germany. The relative overall 5-year survival rate, is 15% in males and 20% in females.[1] Neuroendocrine tumors (NETs) of the lung are rare with only 5% of all newly diagnosed malignancies.[2,3] Although the lungs are the second most common site of origin for neuroendocrine tumors especially for typical carcinoid after the gastrointestinal tract,[4] it has been reported to develop even synchronously in both lungs.[5] In the lung, NETs derive from solitary pulmonary neuroendocrine cells (PNECs) or from aggregated PNEC clusters (neuroepithelial bodies),[6–8] which initially act as the stem cell niche.[9,10] PNECs gain various mutations during carcinogenesis, which are responsible for the dedifferentiation into high tumorigenic cancer stem cells (CSCs).[11] Based on the capacity for self-renewal and differentiation as well as their invasiveness and resistance to chemotherapy, CSCs are crucial mediators of metastasis, cancer relapse or immune system escape and are thus of enormous clinical interest.[12–14]

In the current World Health Organization (WHO) classification 2015 lung NETs are categorized into four histologic variants defined as well differentiated, low-grade typical carcinoid (TC), well-differentiated, intermediate-grade atypical carcinoid (AC), slightly differentiated, high-grade large cell neuroendocrine carcinoma (LCNEC) and slightly differentiated, high-grade small cell lung carcinoma (SCLC).[15,3]

The group of well-differentiated lung NETs comprise approximately 27% of all NETs[16] and develop in non or current light smokers.[17] Moreover, TCs and ACs are capable of lower mitotic rates, necrosis and genetic abnormalities in comparison to high-grade NETs.[18] Although well-differentiated NETs are not that aggressive, the incidence increased over the last 30 years about 6% annually,[19] with TCs being the more frequent form of well-differentiated NETs.[20] Here, we report a case of a typical carcinoid (TC) of the upper lobe of the left lung as well as the successful *in vitro* propagation and characterization of cancer stem cells out of the resected tumor tissue.

2. Case report

A 71-year old woman was admitted to the hospital in November 2018. The clinical examination showed no abnormalities. Biochemical parameters in blood showed normal values apart from slightly elevated gamma-glutamyl-transferase (GGT) (160 U/l, normal up to 40U/l). She never smoked and had no family history of lung or gastrointestinal cancers. She developed dry cough over the last 6 weeks, which was resistant to treat. Therefore a chest X-ray was done, which showed an irregular left border of the heart. A subsequent chest CT-scan showed a paracardiac nodule with 2×1.8 cm in diameter (Fig. 1), no mediastinal lymph nodes enlargement and no pleural effusions were detected.

A bronchoscopic examination with bronchial lavage was done. The lavage revealed acid proof rods, which were immediately tested for *M. tuberculosis* by quantiferon screening. Since the medical report was negative for tuberculosis, surgery was performed for histological diagnosis.

The exploration of the entire hemithorax left showed massive dorso-basal adhesions between the lower lobe and the thoracic wall, as well as the diaphragm. After adhesiolysis, the tumor within the lingual segment was exposed, biopsied and a histopathological frozen section examination was performed, which showed malignancy. The tumor was then anatomically resected using video assisted thoracic surgery (VATS) to remove both segments of the lingual. Complete mediastinal lymph node dissection was done. Histopathological analysis of the removed tissue indicated a neuroendocrine neoplasm, which was confirmed by immunohistochemistry. In particular, cancerous tissue was positive for synaptophysin (Fig. 2), chromogranin A as well as high and low molecular weight cytokeratins detected by the antibody combination of AE1/AE3. Based on the absence of the epithelial marker TTF1 as well as the neuroendocrine markers CDX2 and cytokeratin 20 of the gastrointestinal tract, LCNEC, SCLC or a metastasis of the gastrointestinal tract could be excluded. Neither an apparent necrosis within the tissue, nor pathologic lymph node structures were observed. Further analysis revealed only 1% to 2% Ki67-positive mitotic cells

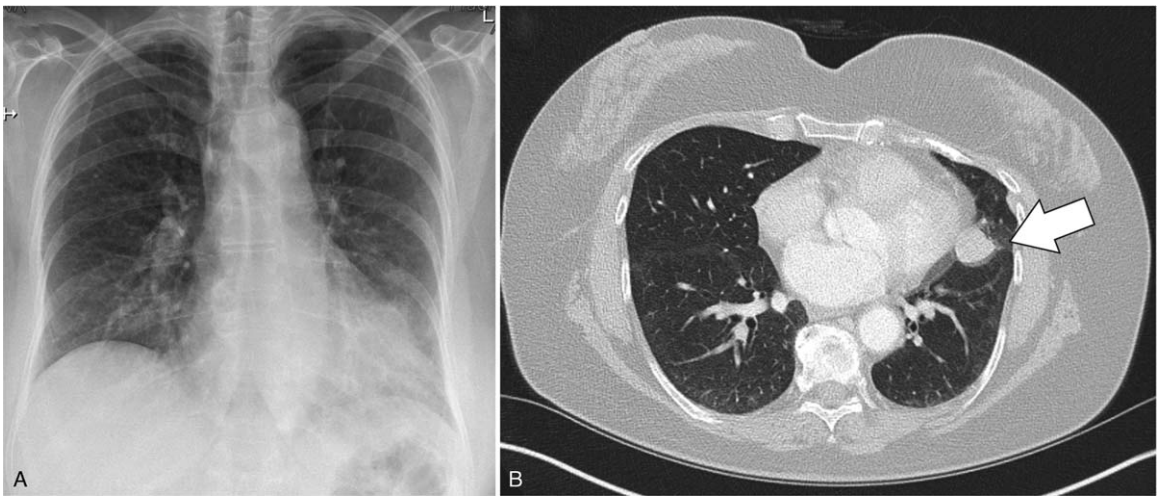

Figure 1. Radiological examination of the chest of the patient. (A) Radiograph of the chest revealed an uneven mass in the left lung. (B) Chest CT scan displayed a paracardiac tumor (arrow).

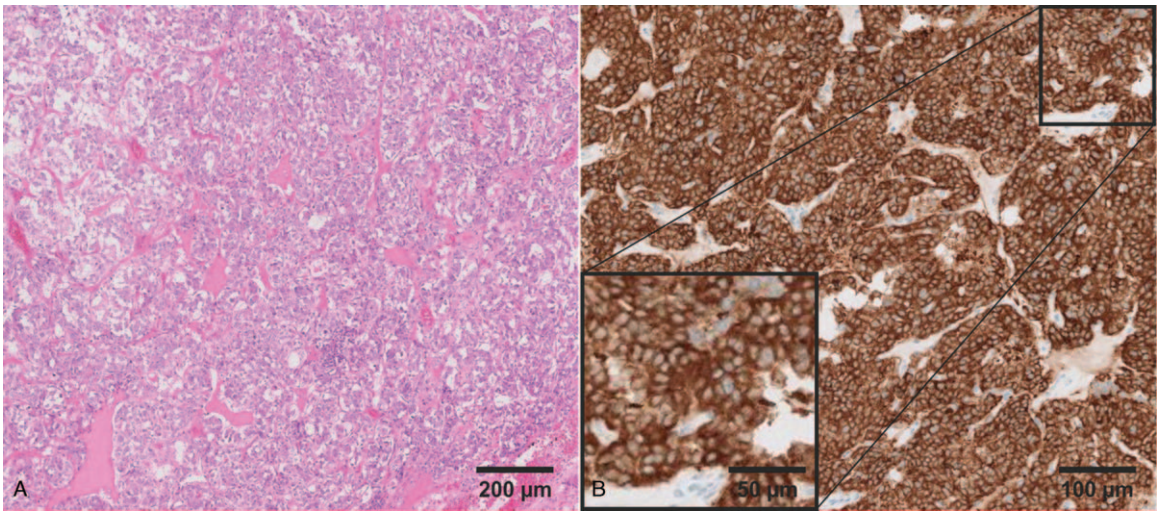

Figure 2. Histopathological analysis of the neuroendocrine tumor tissue. (A) Hematoxylin and eosin staining revealed a well differentiated neuroendocrine morphology, characteristic for typical carcinoids. (B) Moreover, tissue was positive for the neuroendocrine marker synaptophysin.

within the tumor, resulting in the final classification of a well-differentiated, low-grade typical carcinoid (TC) in stage IA. Therefore, no adjuvant therapy was suggested. The patient was discharged on the fifth day after surgery in a good general condition. 6 months follow up showed no abnormalities. The somatostatin receptor imaging with ^{68}G DOTATATE PET/CT-showed no abnormal findings.

Next to a histopathological analysis, a part of the resected typical carcinoid was used for the attempt to cultivate and characterize cancer stem cells. Informed consent according to local and international guidelines was signed and all further experimental procedures were ethically approved (Ethics committee Münster, Germany, 2017–522-f-S). For the isolation of the CSCs the specimen was washed twice with ice-cold phosphate buffered saline (PBS), mechanically disintegrated in 2 to 5 mm pieces followed by an enzymatically digestion with collagenase for 2 hours at 37°C. One half of the minced tissue was used to cultivate spheres in Dulbecco modified Eagle's medium/Ham's F-12 with addition of 200 mM L-Glutamin, epidermal growth factor (EGF; 20 ng/mL), basic fibroblast growth factor (bFGF/FGF-2; 40 ng/mL) and B27 supplement in low adhesion T25 tissue culture flasks (Fig. 3B). The other half of the tissue was used to grow adherent CSCs, where the cells were cultivated on gelatin coated culture dishes in the medium described above supplemented with 10% fetal calf serum (Fig. 3A).

After successful cultivation, cells were analyzed according to their expression profile of cancer stem cell and neuroendocrine specific markers, as well as their morphology. Immunocytochemical double staining of the lung cancer stem cell markers CD133 and CD44 confirmed the isolation of cancer stem cells (Fig. 3C). Additionally, cultivated cells were positive for the neuroendocrine marker synaptophysin underscoring the establishment of the relevant cancer stem cells. Synaptophysin was especially localized within the nucleus of the cells, although some cells also revealed synaptophysin within their cytoplasm (Fig. 3E). Next to the expression of synaptophysin in the isolated neuroendocrine cancer stem cells (Fig. 3E, 4C), we detected synaptophysin in neural crest-derived stem cells from the nasal cavity of a female donor[23,22] (Fig. 4A) and female adipose tissue-derived mesenchymal stem cells (Fig. 4B), suggesting a new role of synaptophysin as a stem cell marker. Quantification of the nuclear fluorescence intensity of synaptophysin within the different stem cells revealed a significant higher expression within the isolated BKZ1 cell line in comparison to non-pathogenic stem cells (Fig. 4D). Furthermore, cells expressed the primitive neuroectoderm and stem cell marker nestin, underlining the stem cell characteristics and suggesting a neural crest origin of the cultivated cells (Fig. 3D). Due to the strong association of NF-κB with chronic inflammation and different cancer types, TC-derived BKZ1 cells were analyzed according to their NF-κB expression. Immunocytochemical staining of the subunit RELA (p65) displayed a high perinuclear expression of the cultured cells (Fig. 3F).

3. Discussion

Neuroendocrine lung tumors can be divided into four histological groups, comprising typical carcinoid (TC), atypical carcinoid (AC), large cell neuroendocrine carcinoma (LCNEC) and small cell carcinoma (SCC).[15] Although the distinction between the different neuroendocrine lung tumor types is possible by a good histopathological analysis, the diagnosis of a neuroendocrine lung tumor at all is difficult.[18] Symptoms of lung NETs are often nonspecific or absent, leading to delays in diagnosis. Moreover, clinical data regarding lung NETs are rare, especially for carcinoids, making diagnosis and treatment difficult.[24] This problem is also described by a recently published global survey, which collected data on NETs from a patient's perspective, revealing that the diagnosis of lung NETs of 50% of the 222 patients lasts up to 2 years.[25] Moreover, the incidence of the carcinoids, especially TCs, increased over the last 30 years about 6% annually in contrast to the incidence of SCC.[19] Furthermore, they possess the earliest occurrence age on average within the group of NETs with 45 years.[18,26,27] Treatment of choice for localized TCs is the anatomical resection of the tumor,[18] with 5 to 10-year survival rates higher than 90%,[28] whereas the use of adjuvant therapy is usually not recommended for TCs due to rare involvement of the lymph nodes.[18] Even if TCs are known as

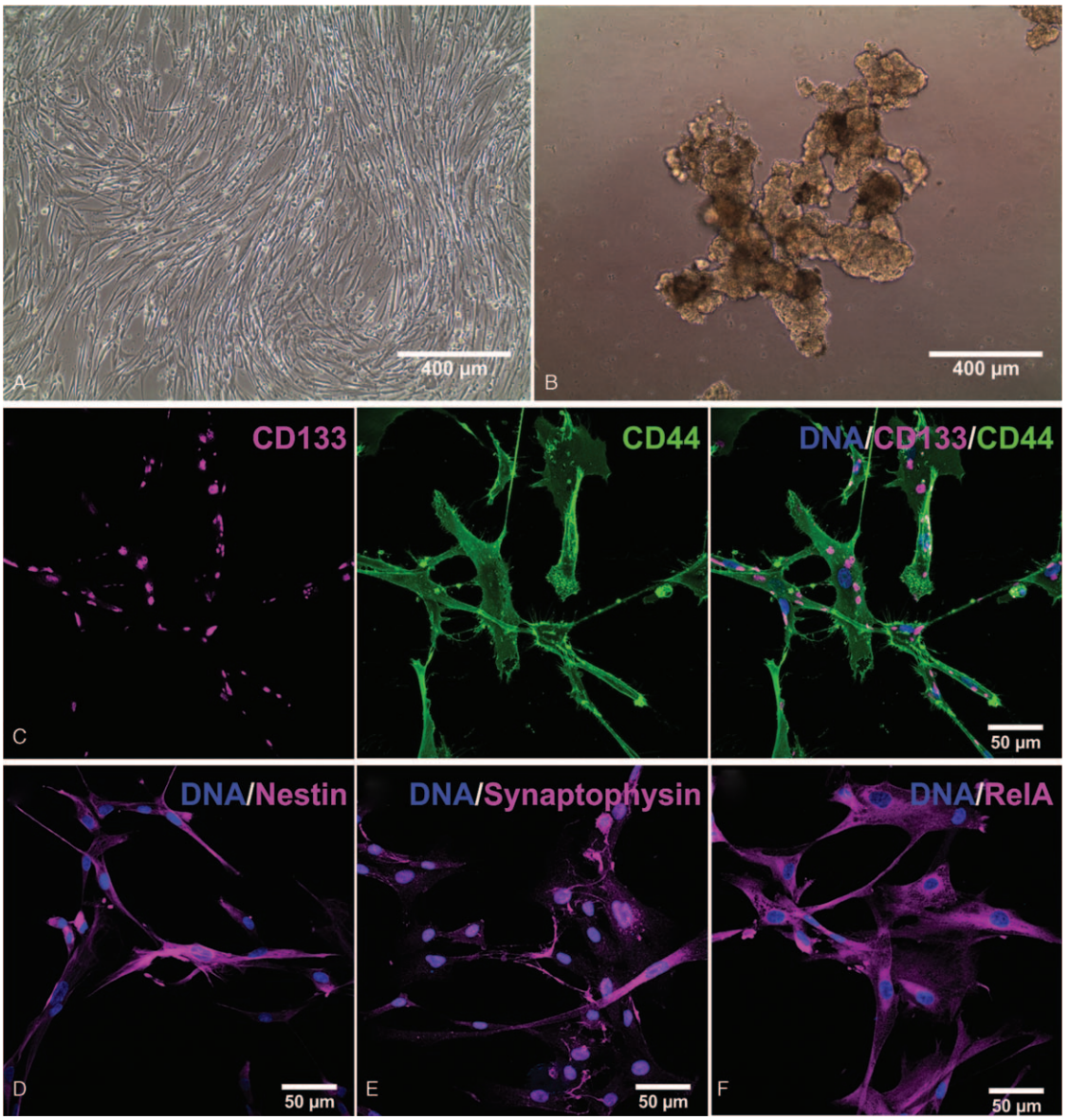

Figure 3. Successful isolation and characterization of cancer stem cells out of the tumor tissue of a typical carcinoid. (A) Cancer stem cells were grown as adherent culture within stem cell media supplemented with 10% fetal calve serum (FCS), (B) as well as sphere culture in a low attachment flask without FCS as supplement. (C) Immunocytochemical staining for the stem cell markers CD133 and CD44, revealed double positive cells, confirming the isolation of cancer stem cells. Additionally, cells were positive for the stem cell and primitive neuroectoderm marker (D) nestin, the neuroendocrine marker (E) synaptophysin, and the (F) NF-κB subunit p65.

low-grade NET, 5% to 20% of TCs metastasize, preferentially to the liver or bone.[29]

Based on the increased incidence, the difficult diagnosis, and the limited knowledge about the underlying molecular mechanisms of TCs, it is important to establish a good model for studying the biology of this tumor type. Currently there are only few TC cell lines available. Moreover, many of those cell lines failed to generate xenograft tumors, displaying the absence of cancer stem cells within the cell population.[30] We now present a successful isolation of cancer stem cells out of the tissue of this rare tumor type, which enables new opportunities to investigate the molecular mechanisms of resistance to conventional chemotherapeutics, biological molecules, targeted therapies and radiotherapy, which are known to be caused by cancer stem cells. Initial characterization of the isolated CSCs, revealed a high expression of the cancer stem cell marker CD44, which is known to mediate cancer cell survival, proliferation and motility, as well as the modulation of tumor microenvironment.[31,32] Moreover, it is known that CD44 expression is dominant within pulmonary carcinoids, decreasing from TC to AC to very low levels in LCNEC and SCLC,[33,34] which stands in line with the presented data. Moreover, isolated CSCs expressed the cell surface glycoprotein and CSC marker CD133, which is linked to poor prognosis in NSCLC.[35] Additionally, CD133 positive cells are known to have significantly higher abilities of self-renew, drug resistance and tumor initiation.[36] Although, concerning the expression of CD133 within typical carcinoid cell lines only less is known, which can be explained by the failure to isolate CSCs by

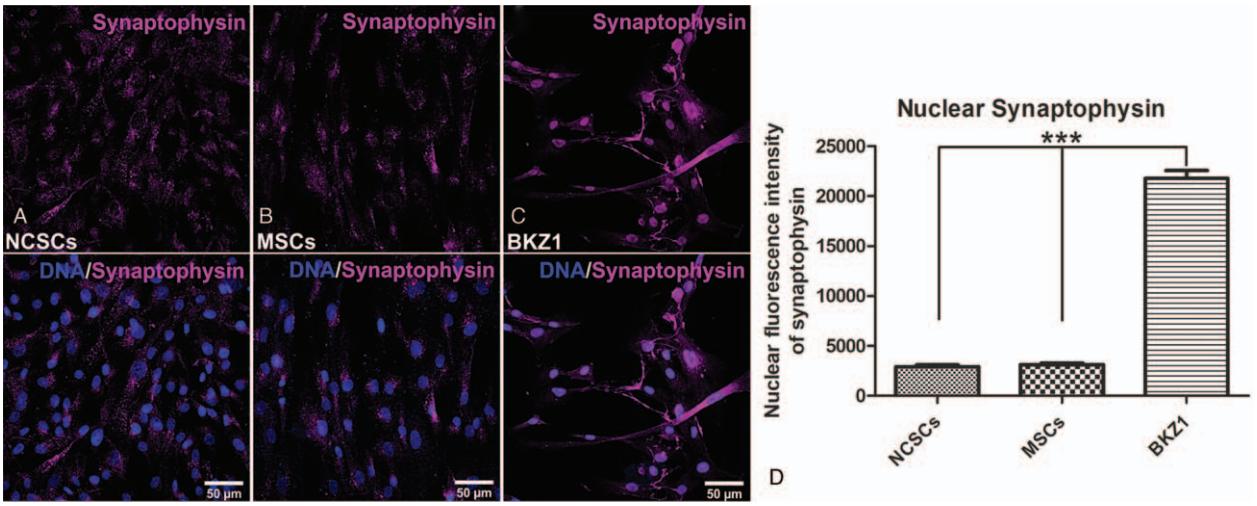

Figure 4. Nuclear synaptophysin expression of BKZ1 and different non-pathogenic stem cells. Immunocytochemical staining of synaptophysin in female donor-derived (A) human neural crest-derived stem cells (NCSCs),[21,22] (B) adipose tissue-derived mesenchymal stem cells (MSCs) isolated according to Solemani and Nadri[23] and (C) the here described neuroendocrine lung cancer stem cells (CSCs). (D) Quantification of the nuclear fluorescence intensity of synaptophysin within the different stem cell populations. Means ± SD was analyzed by one way ANOVA test (Kruskal-Wallis statistic). $P < .05$ was considered as statistically significant. Analysis of data was done by using GraphPad Prism 5.00 software (San Diego, CA).

other groups, Sakai et al. showed that 18% of well-differentiated pancreatic neuroendocrine tumors are CD133 positive.[37] Due to the identification of nestin as CSC marker in NSCLC,[38] its protein expression was investigated and highly detected within the here presented isolated CSCs. Furthermore, nestin is known as primitive neuroectoderm[39] and neural stem cell[40] marker, which suggests a possible correlation between pulmonary typical carcinoids and the neural fate. Within a retrospective evaluation of 88 patients with neuroendocrine lung tumors using immunhistochemistry, nestin was detected in 17% of specimens, being a negative prognostic factor and significantly higher expressed in LCNEC in comparison to carcinoids.[41] This suggests that the CSC amount increases from TC to AC and LCNEC to SCC, indicated by a higher expression of nestin, leading to a decrease in the survival rate of the patient. Moreover, isolated CSCs showed a high amount of synaptophysin protein, underlying their neuroendocrine origin.[42] Assuming nuclear localization of synaptophysin as a general stem cell characteristic, we demonstrated the appearance of nuclear synaptophysin protein also in non-pathogenic human stem cell populations like NCSCs and MSCs. However, the nuclear expression of synaptophysin of the CSCs was significantly higher in comparison to the other stem cells, which may be due to their cancerous origin.[43] Next to stemness related proteins, the isolated CSCs expressed the NF-κB subunit RelA. NF-κB is involved in multiple steps in carcinogenesis and in cancer cell's resistance to chemo- and radio-therapy. Moreover, tumor samples obtain from lung cancer patients revealed high levels of NF-κB activation, which was significantly associated with poor prognosis and tumor stage.[44,45] This is in accordance with a meta-analysis concerning the prognostic significance of NF-κB expression in NSCLC, where Gu et al. showed that high NF-κB expression is positively associated with poor survival outcome of NSCLC patients, suggesting a tumor promotive function of NF-κB. Additionally, they presented a positive correlation of NF-κB with tumor stage and lymph node metastasis.[46] Concerning the particular effect of RelA, Chen et al. could show its influence on the sensitivity of NSCLC to paclitaxel, which was increased by the knockout of NF-κB p65.[47] Furthermore, Khan et al. linked the anti-cancer efficacy of curcumin, to its HIF-1α and RelA decreasing activity in lung cancer cells.[48] Regarding neuroendocrine lung tumors NF-κB is known to play a crucial role regulating tumor cell proliferation and resistance to apoptosis.[49,50] Furthermore, Shao et al. displayed that 55.6% of neuroendocrine tumors were positive for the leukemia related protein 16 (LRP16), which is an important estrogen-responsive gene and a crucial regulator for NF-κB activation, suggesting a proliferative effect due to the activation of NF-κB pathway.[51]

In conclusion, cancer stem cells were for the first time to our knowledge successfully isolated out of a typical carcinoid of the lung, representing a promising model to study the underlying molecular mechanism and possible treatment strategies for this rare tumor type.

Acknowledgments

The excellent technical assistance of Angela Kralemann-Köhler, Claudia Rose and Ulrike Hormel is gratefully acknowledged.

Author contributions

Conceptualization: Barbara Kaltschmidt, Christian Kaltschmidt, Morris Beshay.
Data curation: Beatrice Ariane Windmöller, Barbara Kaltschmidt, Christian Kaltschmidt, Morris Beshay.
Formal analysis: Beatrice Ariane Windmöller, Morris Beshay.
Investigation: Beatrice Ariane Windmöller, Johannes F. W. Greiner, Christine Förster, Ludwig Wilkens, Fritz Mertzlufft, Jan Schulte am Esch, Barbara Kaltschmidt, Christian Kaltschmidt, Morris Beshay.
Writing – original draft: Beatrice Ariane Windmöller, Johannes F. W. Greiner.
Beatrice Ariane Windmöller orcid: 0000-0002-5918-9384.

References

[1] Robert Koch Institute. Report on cancer events in Germany 2016 (Robert Koch Institut. Bericht zum Krebsgeschehen in Deutschland 2016) (page 32-35). [access date May 10, 2019]

[2] Taal BG, Visser O. Epidemiology of neuroendocrine tumours. Neuroendocrinology 2004;80(Suppl 1):3–7.

[3] Travis W D., ed. WHO classification of tumours of lung, pleura, thymus and heart: . . . reflects the views of a working group that convened for a consensus and editorial meeting at the International Agency for Research on Cancer, Lyon, April 24–26, 2014. 4th ed. Lyon: International Agency for Research on Cancer; 2015. World Health Organization Classification of tumors; 7 (der 4th ed.).

[4] Modlin IM, Lye KD, Kidd M. A 5-decade analysis of 13,715 carcinoid tumors. Cancer 2003;97:934–59.

[5] Beshay M, Roth T, Stein R, et al. Synchronous bilateral typical pulmonary carcinoid tumors. Eur J Cardiothorac Surg 2003;23:251–3.

[6] Ito T, Nogawa H, Udaka N, et al. Development of pulmonary neuroendocrine cells of fetal hamster in explant culture. Lab Invest 1997;77:449–57.

[7] Lauweryns JM, van Lommel AT, Dom RJ. Innervation of rabbit intrapulmonary neuroepithelial bodies. Quantitative and qualitative ultrastructural study after vagotomy. J Neurol Sci 1985;67:81–92.

[8] Derks JL, Leblay N, Lantuejoul S, et al. New insights into the molecular characteristics of pulmonary carcinoids and large cell neuroendocrine carcinomas,;1; and the impact on their clinical management. J Thorac Oncol 2018;13:752–66.

[9] Cutz E, Yeger H, Pan J. Pulmonary neuroendocrine cell system in pediatric lung disease-recent advances. Pediatr Dev Pathol 2007;10: 419–35.

[10] van Lommel A, Bollé T, Fannes W, et al. The pulmonary neuroendocrine system: the past decade. Arch Histol Cytol 1999;62:1–6.

[11] Pardal R, Clarke MF, Morrison SJ. Applying the principles of stem-cell biology to cancer. Nat Rev Cancer 2003;3:895–902.

[12] Koren E, Fuchs Y. The bad seed: Cancer stem cells in tumor development and resistance. Drug Resist Updat 2016;28:1–2.

[13] Nassar D, Blanpain C. Cancer stem cells: basic concepts and therapeutic implications. Annu Rev Pathol 2016;11:47–76.

[14] Maiuthed A, Chantarawong W, Chanvorachote P. Lung cancer stem cells and cancer stem cell-targeting natural compounds. Anticancer Res 2018;38:3797–809.

[15] Travis Wd, Brambilla E, Nicholson AG, et al. The 2015 World Health Organization classification of lung tumors: impact of genetic, clinical and radiologic advances since the 2004 classification. J Thorac Oncol 2015;10:1243–60.

[16] Yao JC, Hassan M, Phan A, et al. One hundred years after "carcinoid": epidemiology of and prognostic factors for neuroendocrine tumors in 35,825 cases in the United States. J Clin Oncol 2008;26:3063–72.

[17] Hassan MM, Phan A, Li D, et al. Risk factors associated with neuroendocrine tumors: A U.S.-based case-control study. Int J Cancer 2008;123:867–73.

[18] Caplin ME, Baudin E, Ferolla P, et al. Pulmonary neuroendocrine (carcinoid) tumors: European Neuroendocrine Tumor Society expert consensus and recommendations for best practice for typical and atypical pulmonary carcinoids. Ann Oncol 2015;26:1604–20.

[19] Gustafsson BI, Kidd M, Chan A, et al. Bronchopulmonary neuroendocrine tumors. Cancer 2008;113:5–21.

[20] Rekhtman N. Neuroendocrine tumors of the lung: an update. Arch Pathol Lab Med 2010;134:1628–38.

[21] Greiner JFW, Hauser S, Widera D, et al. Efficient animal-serum free 3D cultivation method for adult human neural crest-derived stem cell therapeutics. Eur Cell Mater 2011;22:403–19.

[22] Hauser S, Widera D, Qunneis F, et al. Isolation of novel multipotent neural crest-derived stem cells from adult human inferior turbinate. Stem Cells Dev 2012;21:742–56.

[23] Soleimani M, Nadri S. A protocol for isolation and culture of mesenchymal stem cells from mouse bone marrow. Nat Protoc 2009; 4:102–6.

[24] Hendifar AE, Marchevsky AM, Tuli R. Neuroendocrine tumors of the lung: current challenges and advances in the diagnosis and management of well-differentiated disease. J Thorac Oncol 2017;12:425–36.

[25] Singh S, Granberg D, Wolin E, et al. Patient-reported burden of a neuroendocrine tumor (NET) diagnosis: results from the first global survey of patients with NETs. J Glob Oncol 2017;3:43–53.

[26] Filosso PL, Rena O, Donati G, et al. Bronchial carcinoid tumors: surgical management and long-term outcome. J Thorac Cardiovasc Surg 2002; 123:303–9.

[27] Zuetenhorst JM, Taal BG. Metastatic carcinoid tumors: a clinical review. Oncologist 2005;10:123–31.

[28] Detterbeck FC. Management of carcinoid tumors. Ann Thorac Surg 2010;89:998–1005.

[29] Chong CR, Wirth LJ, Nishino M, et al. Chemotherapy for locally advanced and metastatic pulmonary carcinoid tumors. Lung Cancer 2014;86:241–6.

[30] Asiedu MK, Thomas CF, Tomaszek SC, et al. Generation and sequencing of pulmonary carcinoid tumor cell lines. J Thorac Oncol 2014;9:1763–71.

[31] Prochazka L, Tesarik R, Turanek J. Regulation of alternative splicing of CD44 in cancer. Cell Signal 2014;26:2234–9.

[32] Yan Y, Zuo X, Wei D. Concise review: emerging role of CD44 in cancer stem cells: a promising biomarker and therapeutic target. Stem Cells Transl Med 2015;4:1033–43.

[33] Coppola D, Clarke M, Landreneau R, et al. Bcl-2, p53, CD44, and CD44v6 isoform expression in neuroendocrine tumors of the lung. Mod Pathol 1996;9:484–90.

[34] Papaxoinis G, Nonaka D, O'Brien C, et al. Prognostic significance of CD44 and orthopedia homeobox protein (OTP) expression in pulmonary carcinoid tumours. Endocr Pathol 2017;28:60–70.

[35] Mizugaki H, Sakakibara-Konishi J, Kikuchi J, et al. CD133 expression: a potential prognostic marker for non-small cell lung cancers. Int J Clin Oncol 2014;19:254–9.

[36] Chen YC, Hsu HS, Chen YW, et al. Oct-4 expression maintained cancer stem-like properties in lung cancer-derived CD133-positive cells. PLoS One 2008;3:e2637.

[37] Sakai Y, Hong S-M, An S, et al. CD133 expression in well-differentiated pancreatic neuroendocrine tumors: a potential predictor of progressive clinical courses. Hum Pathol 2017;61:148–57.

[38] Janikova M, Skarda J, Dziechciarkova M, et al. Identification of CD133 +/nestin+ putative cancer stem cells in non-small cell lung cancer. Biomed Pap Med Fac Univ Palacky Olomouc Czech Repub 2010;154:321–6.

[39] Reubinoff BE, Pera MF, Fong CY, et al. Embryonic stem cell lines from human blastocysts: somatic differentiation in vitro. Nat Biotechnol 2000;18:399–404.

[40] Reynolds BA, Weiss S. Generation of neurons and astrocytes from isolated cells of the adult mammalian central nervous system. Science 1992;255:1707–10.

[41] Brominska B, Gabryel P, Jarmołowska-Jurczyszyn D, et al. Clinical significance of nestin and its association with survival in neuroendocrine lung tumours. Pol J Pathol 2017;68:291–6.

[42] Wiedenmann B, Franke WW, Kuhn C, et al. Synaptophysin: a marker protein for neuroendocrine cells and neoplasms. Proc Natl Acad Sci U S A 1986;83:3500–4.

[43] Kasprzak A, Zabel M, Biczysko W. Selected markers (chromogranin A, neuron-specific enolase, synaptophysin, protein gene product 9.5) in diagnosis and prognosis of neuroendocrine pulmonary tumours. Pol J Pathol 2007;58:23–33.

[44] Karin M, Greten FR. NF-kappaB: linking inflammation and immunity to cancer development and progression. Nat Rev Immunol 2005;5:749–59.

[45] Jin X, Wang Z, Qiu L, et al. Potential biomarkers involving IKK/RelA signal in early stage non-small cell lung cancer. Cancer Sci 2008;99:582–9.

[46] Gu L, Wang Z, Zuo J, et al. Prognostic significance of NF- κB expression in non-small cell lung cancer: A meta-analysis. PLoS One 2018;13: e0198223.

[47] Chen X, Sun X, Guan J, et al. Rsf-1 influences the sensitivity of non-small cell lung cancer to paclitaxel by regulating NF- κB pathway and its downstream proteins. Cell Physiol Biochem 2017;44:2322–36.

[48] Khan MN, Haggag YA, Lane ME, et al. Polymeric nano-encapsulation of curcumin enhances its anti-cancer activity in breast (MDA-MB231) and Lung (A549) cancer cells through reduction in expression of HIF- 1α and Nuclear p65 (Rel A). Curr Drug Deliv 2018;15:286–95.

[49] Li YD, Liu YP, Cao DM, et al. Induction of small G protein RhoB by non-genotoxic stress inhibits apoptosis and activates NF-(B. J Cell Physiol 2011;226:729–38.

[50] Li Z, Guo Y, Jiang H, et al. Differential regulation of MMPs by E2F1, Sp1 and NF-kappa B controls the small cell lung cancer invasive phenotype. BMC Cancer 2014;14:276.

[51] Shao Y, Li X, Lu Y, et al. Aberrant LRP16 protein expression in primary neuroendocrine lung tumors. Int J Clin Exp Pathol 2015;8:6560–5.

Original Research Article

“Isolation and Characterization of Two Novel Colorectal Cancer Cell Lines, Containing a Subpopulation with Potential Stem-Like Properties: Treatment Options by MYC/NMYC Inhibition”

Jan Schulte Am Esch*, **Beatrice A. Windmöller***, Johannes Hanewinkel, Jonathan Storm, Christine Förster, Ludwig Wilkens, Martin Krüger, Barbara Kaltschmidt, Christian Kaltschmidt

(*: equal contribution)

Cancers (Basel). 2020 Sep; 12(9): 2582.

cancers

MDPI

Article

Isolation and Characterization of Two Novel Colorectal Cancer Cell Lines, Containing a Subpopulation with Potential Stem-Like Properties: Treatment Options by MYC/NMYC Inhibition

Jan Schulte am Esch [1,2,†], Beatrice Ariane Windmöller [2,3,*,†], Johannes Hanewinkel [3], Jonathan Storm [2,3], Christine Förster [2,4], Ludwig Wilkens [2,4], Martin Krüger [2,5], Barbara Kaltschmidt [2,3,6,‡] and Christian Kaltschmidt [2,3,‡]

1 Department of General and Visceral Surgery, Protestant Hospital of Bethel Foundation, 33611 Bielefeld, Germany; Jan.SchulteamEsch@evkb.de
2 Forschungsverbund BioMedizin Bielefeld (FBMB), 33611 Bielefeld, Germany; jonathan.storm@uni-bielefeld.de (J.S.); christine.foerster@krh.eu (C.F.); ludwig.wilkens@krh.eu (L.W.); Martin.Krueger@evkb.de (M.K.); barbara.kaltschmidt@uni-bielefeld.de (B.K.); C.Kaltschmidt@uni-bielefeld.de (C.K.)
3 Department of Cell Biology, University of Bielefeld, 33611 Bielefeld, Germany; johannes-hanewinkel@hotmail.de
4 Institute of Pathology, KRH Hospital Nordstadt, affiliated with the Protestant Hospital of Bethel Foundation, 30167 Hannover, Germany
5 Department of Internal Medicine and Gastroenterology, Protestant Hospital of Bethel Foundation, 33611 Bielefeld, Germany
6 Molecular Neurobiology, University of Bielefeld, 33615 Bielefeld, Germany
* Correspondence: beatrice.windmoeller@uni-bielefeld.de; Tel.: +49-0521-106-5629
† These authors contributed equally as Co-First authors.
‡ These authors contributed equally as Co-Last authors.

Received: 14 August 2020; Accepted: 8 September 2020; Published: 10 September 2020

Simple Summary: The aim of this study was to gain a better understanding of cancer stem cells, which are a small subpopulation of tumor cells with high plasticity driving tumor growth and metastasis. Here we isolated two novel colorectal cancer cell lines originating from a rectal neuroendocrine carcinoma and a colorectal adenocarcinoma, depicting stem-like properties. These in vitro models offer the possibility to evaluate pathophysiological mechanisms in order to develop tailored therapeutic strategies for distinct colorectal malignancies. Investigations revealed gene copy number gain of the N-myc proto-oncogene for both. Accordingly, inhibition of the protein–protein interaction of myc and N-myc proto-oncogenes with the myc-associated factor X utilizing small molecule KJ-Pyr-9, exhibited a significant reduction in survival of both cell lines by the induction of apoptosis. Consequently, the blockage of these interactions may serve as a possible treatment strategy for colorectal cancer cell lines with gene copy number gain of the N-myc proto-oncogene.

Abstract: Cancer stem cells (CSC) are crucial mediators of cancer relapse. Here, we isolated two primary human colorectal cancer cell lines derived from a rectal neuroendocrine carcinoma (BKZ-2) and a colorectal adenocarcinoma (BKZ-3), both containing subpopulations with potential stem-like properties. Protein expression of CSC-markers prominin-1 and CD44 antigen was significantly higher for BKZ-2 and BKZ-3 in comparison to well-established colon carcinoma cell lines. High sphere-formation capacity further confirmed the existence of a subpopulation with potential stem-like phenotype. Epithelial–mesenchymal transition markers as well as immune checkpoint ligands were expressed more pronounced in BKZ-2. Both cell populations demonstrated N-myc proto-oncogene (*NMYC*) copy number gain. Myc proto-oncogene (MYC)/NMYC activity inhibitor

all-trans retinoic acid (ATRA) significantly reduced the number of tumor spheres for both and the volume of BKZ-2 spheres. In contrast, the sphere volume of ATRA-treated BKZ-3 was increased, and only BKZ-2 cell proliferation was reduced in monolayer culture. Treatment with KJ-Pyr-9, a specific inhibitor of MYC/NMYC-myc-associated factor X interaction, decreased survival by the induction of apoptosis of both. In summary, here, we present the novel colorectal cancer cell lines BKZ-2 and BKZ-3 as promising cellular in vitro models for colorectal carcinomas and identify the MYC/NMYC molecular pathway involved in CSC-induced carcinogenesis with relevant therapeutic potential.

Keywords: colorectal cancer stem cells; NMYC; MYC; ATRA; EMT; KJ-Pyr-9; rectal neuroendocrine carcinoma; colorectal adenocarcinoma

1. Introduction

Colorectal cancer (CRC) is the third most common cancer worldwide and second most common cause of cancer-related mortality, with 1.8 million new cases and approximately 861,000 deaths in 2018 as reported by the World Health Organization (WHO) GLOBOCON database [1]. CRC comprises the development of malignancies in the colon (72%) and the rectum (28%) and is the most common malignancy in the gastrointestinal tract [2], with 90% of all CRCs being an adenocarcinoma (AC) originating from epithelial mucosa cells [3]. A comparatively rare and poorly understood subtype of CRC is the neuroendocrine carcinoma (NEC), representing a subgroup of neuroendocrine neoplasms comprised of poorly-differentiated neoplasms originating from epithelial cells of the endocrine or nervous system [4]. According to the WHO classification of 2010, colorectal gastro-entero-pancreatic neuroendocrine-carcinoma (GEP-NEC) is a rare and aggressive variant of neuroendocrine tumors (NET) as well as CRC with more than one third having metastatic disease at the time of diagnosis [5,6].

To evaluate pathophysiological mechanisms and therapeutic strategies for CRCs, preclinical models were developed based on stable cell lines. However, latter are scarce especially for GEP-NECs and were mainly established from metastatic spread [7–11]. Although some established cellular model lines were derived from primary native tumor tissue [7,8,12], such cell lines still lack cancer stem cell characteristics. Cancer stem cells (CSC) are a small subpopulation of tumor cells of high plasticity driving tumor growth, repopulation after injury, and metastasis in a broad range of solid tumors including CRC [13,14]. Next to mediating invasiveness and resistance to chemotherapy, CSC also use immune system escape and are thus crucial mediators of cancer relapse. Next to in vitro propagation as spheres [14–17], cancer stem cell markers like prominin-1 (CD133) and CD44 antigen (CD44) are frequently used to identify cancer stem cells in CRC [3,6]. Important regulators of cancer stem cell characteristics particularly include the members of the MYC transcription factor family, consisting of L-, N-, and CMYC. In colorectal cancer stem cells (CCSC) the myc proto-oncogene protein (MYC) was reported to be consistently overexpressed, contributing to self-renewal and pluripotency as well as drug resistance [18–20]. Moreover, the overexpression of N-myc proto-oncogene protein (NMYC) was detected for different tumor types, most notably for cancers of neural and neuroendocrine origin [21], making the MYC-family a highly promising therapeutic target.

Next to the influence of the MYC-family to the tumor development, recent studies showed a direct influence of MYC on the formation of metastasis by colon cancer cells in vivo [22]. Here, the authors reported that the drug Astaxanthin increases the expression of micro ribonucleic acid (miRNA)-29a-3p and miRNA-200a by the transcriptional repression of *MYC*. This repression leads to the abrogation of their downstream target genes matrix metallopeptidase 2 and zinc finger E-box binding homeobox 1 (*ZEB1*), and consequently to the suppression of epithelial–mesenchymal transition (EMT) and metastasis [22]. The process of EMT, during which epithelial cells acquire fibroblast-like properties and show reduced intercellular adhesion and increased motility, allows the tumor cells to metastasize and establish secondary tumors at distant sites [23,24]. Additionally, Xu and coworkers discovered that cells

undergoing EMT acquire stem cell-like characteristics, thus providing a further link between EMT and stem cell pathways, making EMT to a possible therapeutic target, too [25]. Differentiation therapy using retinoic acids, especially all-trans retinoic acid (ATRA), showed clinical potential for different cancer types, including breast cancer [26], neuroblastoma [27], glioblastoma [28], and CRC [29]. However, ATRA is only clinically used for the treatment of acute promyelocytic leukemia [30]. In CRC cell lines treatment with ATRA led to decreased proliferation, sphere formation and aldehyde dehydrogenase (ALDH) + CSC-population size by inducing neuroendocrine differentiation [29]. Moreover, Shi and colleagues found evidence that ATRA reverses EMT in chemotherapy resistant CRC cell lines [31]. Furthermore, a study with *NMYC*-amplified neuroblastoma cells could show that a combined treatment of ATRA and a peptide derived from tenascin-C induced differentiation and led to a decrease of NMYC protein [27], highlighting the involvement of ATRA in NMYC signaling.

In the present study, we established the first primary rectal GEP-NEC cell line named BKZ-2, as well as a primary colonic AC cell line named BKZ-3 enriched for a subset of cells with markers of stemness and EMT as a pre-clinical model system. Beyond the validation of these cell lines having a subpopulation of cells with potential stem-like properties, we detected in each a genetic amplification of the oncogene *NMYC*. Although MYC/NMYC inhibition using KJ-Pyr-9 led to a significant decrease of survival of both cell lines, KJ-Pyr-9-treated BKZ-3 cells revealed a higher survival rate than BKZ-2. Additionally, we show that ATRA-treatment of BKZ-2 cells decreased sphere volume as well as total cell mass and seems to induce differentiation, as well as it decreased proliferation of BKZ-2 in monolayer. In contrast, ATRA-treatment of BKZ-3 led to an increase in sphere volume with no alteration in total cell mass or proliferation in monolayer. Next to our findings that targeting NMYC could have therapeutic activity in CRC patients, the establishment of those primary cell lines also highlights the differences in CCSC. Moreover, the isolation of BKZ-2 and BKZ-3 offers the possibility to evaluate further pathophysiological mechanisms systematically in order to develop tailored therapeutic strategies for distinct colorectal malignancies.

2. Results

2.1. Tumor Characterization

An endoscopically retrieved bioptic sample of the primary tumor of patient 1 (Figure 1A–D) revealed the pathological diagnosis of a rectal NET with G3 differentiation and 25% proliferation marker protein Ki-67 (KI67) expression (Figure 2H). It was 100% positive for epithelial marker pan-cytokeratin (panCK), 40% positive for special AT-rich sequence-binding protein 2 (SATB2), 10% positive for neural cell adhesion molecule (CD56) and 100% positive for Synaptophysin (Figure 2A–D) characterizing the colorectal tumor as large cell GEP-NEC according to the WHO-classification of 2010. It was tested negative for cytokeratin 20 (CK20), cytokeratin 7 (CK7) and homeobox protein CDX-2 (CDX2) (Figure 2E–G). Next to the immunopathological analysis of the tissue, we performed an immunohistochemical staining for the proto-oncogenes MYC and NMYC, which were both positive (Figure 2I–L). Analysis of the expression of the immune checkpoint ligand programed death ligand 1 (PDL1) was done according to international standards by calculating combined positive score (CPS) and tumor proportion score (TPS), as described in the material and methods section (Formulas (3) and (4)). Quantification revealed 2% of PDL1 positive non-necrotic tumor cells. Analysis of the percentage of PDL1 positive vital (non-necrotic) tumor cells, lymphocytes and macrophages were done by calculating CPS and revealed a score of 2. Quantification of PDL1 positive lymphocytes, macrophages, dendritic cells and granulocytes per tumor area displayed an immune cell score (IC) of 1 (Figure 2M, Formula (5)). There was no micro-satellite-instability nor positivity for human epidermal growth factor receptor (EGFR) 2. Kirsten rat sarcoma 2 viral oncogene homolog/neuroblastoma rat sarcoma viral oncogene homolog evaluation revealed a wild type.

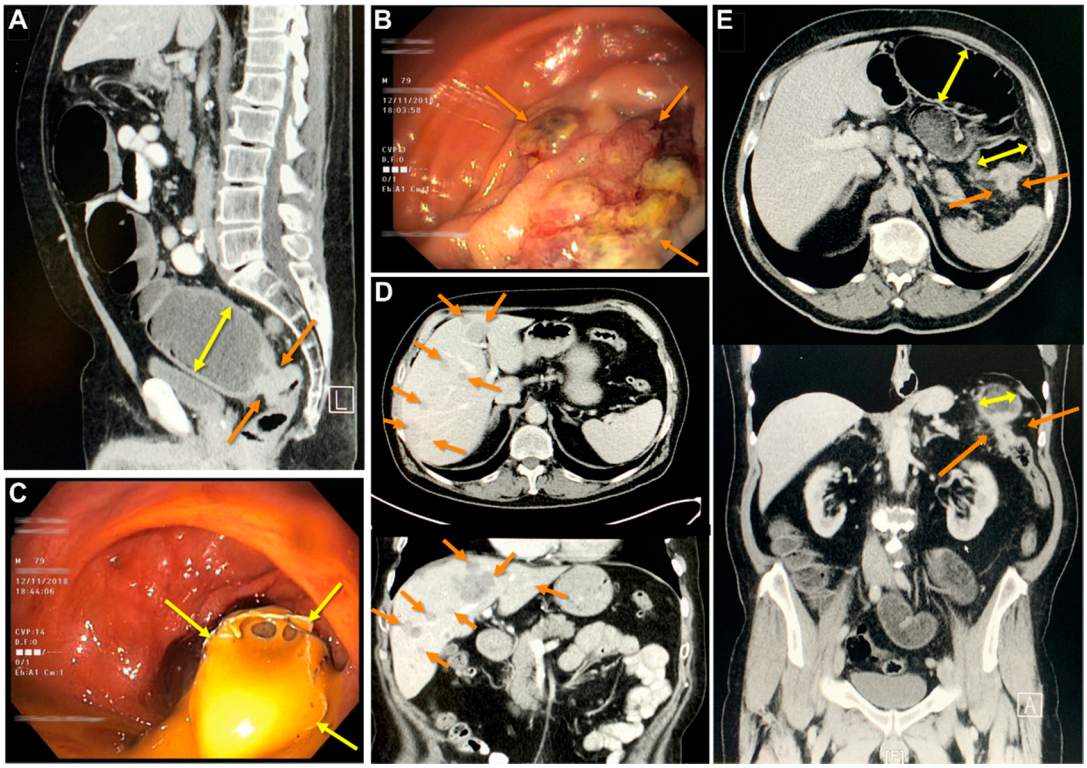

Figure 1. Clinical imaging derived from the two donors of the colorectal cancer cell lines. Patient BKZ-2: (**A**) Computerized tomography (CT)-scan with demonstration of a rectal stenotic mass (orange arrows) with pre-stenotic obstructed bowel (yellow double arrow). Endoscopic appearance of carcinoma BKZ-2 (**B**) with intestinal discharge following (**C**) endoscopic bowel stenting of the neoplastic stenosis. (**D**) Staging CT-scan visualizing hepatic metastases (orange arrows). Patient BKZ-3: (**E**) CT-scan indicating the neoplastic mass of the left colon (orange arrows) with pre-stenotic obstructed bowel (yellow double arrows).

Histopathological examination of a bioptic sample retrieved from the primary tumor of patient 2 (Figure 1E) revealed the diagnosis of a colorectal AC. Carcinoma tissue was 100% positive for SATB2, 95% positive for CK20 and positive for KI67 with 50% being highly positive and 25% expressing moderate levels of KI67 (Figure 2P–R). Analysis of the expression of PDL1 revealed 0% of PDL1 positive vital tumor cells. However, CPS was 3 for the adenocarcinoma tissue and IC was 1 (Figure 2S). Further, it was tested negative for CK7 and Synaptophysin, characterizing the tumor as a colorectal AC (Figure 2N,O). Analysis of the two oncogenes MYC and NMYC revealed positivity of the tissue for both (Figure 2T–W).

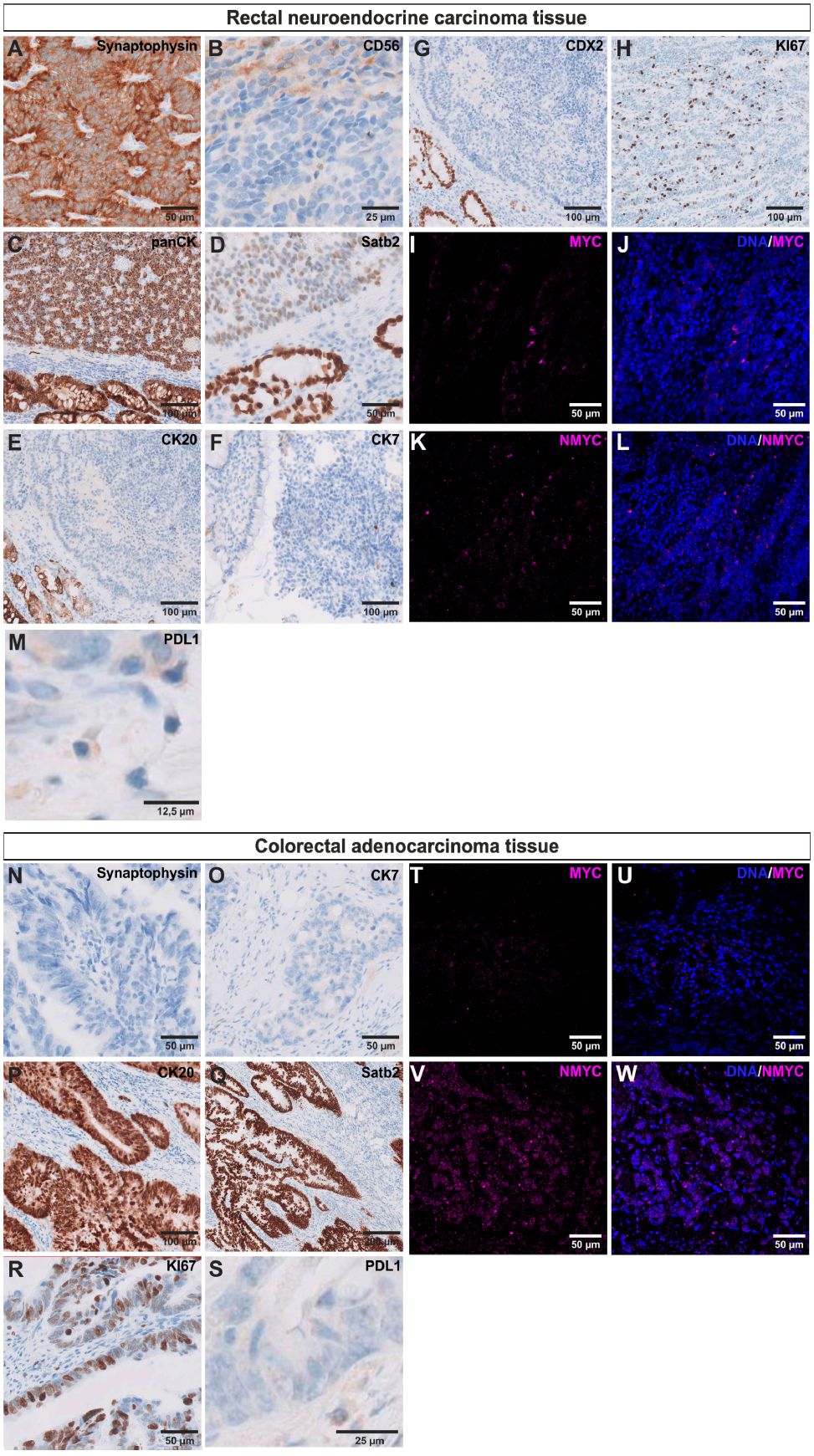

Figure 2. Immunohistochemical characterization of the primary rectal large cell neuroendocrine carcinoma (NEC) and the colorectal adenocarcinoma (AC). NEC tissue was tested positive for (**A**) Synaptophysin,

(**B**) neural cell adhesion molecule (CD56), (**C**) epithelial marker pan-cytokeratin (panCK) and (**D**) special AT-rich sequence-binding protein 2 (SATB2), but was negative for (**E**) cytokeratin 20 (CK20) and (**F**) cytokeratin 7 (CK7). Moreover, immunohistological staining for (**G**) the intestinal differentiation marker homeobox protein CDX2 was negative. (**H**) Staining for the proliferation marker protein Ki-67 (KI67) revealed 25% positive cells. Further immunohistochemical stainings of the NEC tissue displayed positivity for the (**I**/**J**) myc proto-oncogene protein (MYC) and (**K**/**L**) N-myc proto-oncogene protein (NMYC). (**M**) Immunohistochemical staining for programed death ligand 1 (PDL1) revealed only slight expression with 2% of vital tumor cells being positive. AC tissue was tested negative for neuroendocrine marker (**N**) Synaptophysin and (**O**) CK7, but was positive for (**P**) CK20 and (**Q**) SATB2. AC revealed (**R**) 50% KI67 highly positive cells and 25% cells with moderate KI67 expression. (**S**) Immunohistochemical characterization of PDL1 expression displayed 0% positive vital tumor cells, but revealed positivity for both (**T**/**U**) MYC and (**V**/**W**) NMYC in the AC tissue.

2.2. BKZ-2 and BKZ-3 Demonstrate Characteristics of Stemness and EMT–Relation to Immune Response Involved Targets

We established colorectal cancer cell lines BKZ-2 and BKZ-3 derived from primarily resected native tumor tissue (Figure 3A–C) by mechanical and enzymatic disintegration of the tissue sample. Subsequent cultivation within Dulbecco's Modified Eagle's Medium/Ham's -F12 supplemented with epidermal growth factor (EGF), fibroblast growth factor 2 (FGF-2), B27 and 10% fetal calf serum (FCS) led to an adherently growing cell culture for both tumor tissue samples (Figure 3D,E). Initial culture conditions were designed to obtain subpopulation of CSC from native tumor tissue. Analysis of serine/threonine-protein kinase B-raf (*BRAF*) gene mutations displayed wild type alleles of *BRAF* for exon 11 and 15 for both parental tumor tissue and isolated BKZ-2 and BKZ-3 cells. To confirm the stem-like nature of BKZ-2 and BKZ-3, we tested the sphere formation capacity of both cell populations. Both BKZ-2 and BKZ-3 formed spheres under serum-free conditions and supplementation with heparin (Figure 3F,H). Quantification of the averaged sphere diameter of BKZ-2 and BKZ-3 revealed a significant difference of the sphere-formation capacity for all three different heparin concentrations and time points in comparison to the control. Moreover, the increase in sphere diameter of BKZ-2 was significant with a peak value of 61.9 µm (±0.35) in the approach with 4 µg/mL heparin after 7 days of culture. However, the increase in sphere diameter of BKZ-3 cells was not significant, although there was also a tendency to form larger spheres over time with the highest value of sphere diameter of 61.9 µm (±3.95) after the addition of 4 µg/mL heparin and cultivation for one week (Figure 3G,I). Quantification of the population doubling time of BKZ-2 and BKZ-3 in comparison to the established colon adenocarcinoma cell line HT-29 and colon carcinoma cell line HCT-116, revealed a significantly higher ($p \leq 0.01$) population doubling time for BKZ-2 with 40.12 h (±1.56) in comparison to BKZ-3 with 21.88 h (±1.19). Furthermore, HT-29 displayed a population doubling time of 21.87 h (±0.12) and HCT-116 of 18.14 h (±0.051), which were significantly lower than the newly described cell line BKZ-2. In addition, BKZ-3 and HT-29 both displayed a significantly higher population doubling time in comparison to HCT-116 (Figure 4A, Formulas (1) and (2)). Comparison of sphere formation capacity of BKZ-2, BKZ-3, HT-29 and HCT-116, revealed a significantly higher ($p \leq 0.001$) volume of spheres formed by HT-29 and HCT-116 when compared to BKZ-2 and BKZ-3. Moreover, HT-29 spheres displayed a significantly ($p \leq 0.001$) higher volume in comparison to HCT-116 (Figure 4B–F, Formula (6)). Further quantification concerning the number of spheres in relation to the count of seeded cells, showed more than double amount of sphere formation rates for BKZ-2 and BKZ-3 ($p \leq 0.05$) in comparison to HT-29 and HCT-116 (Figure 4G).

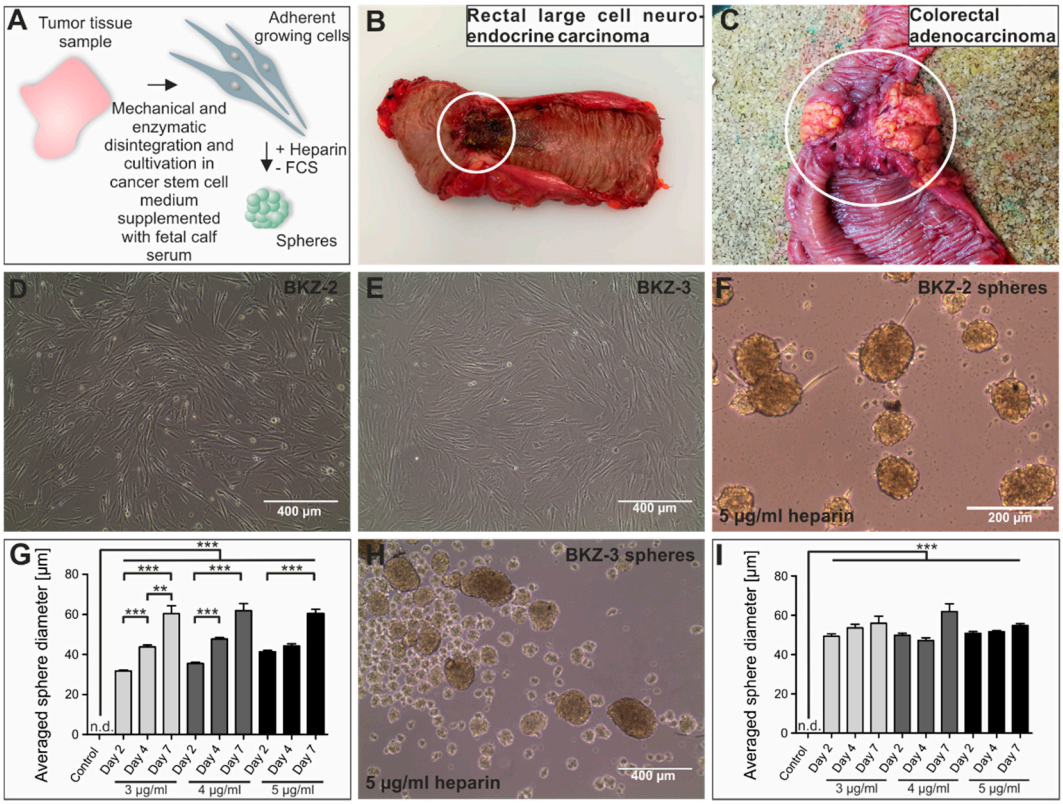

Figure 3. Successful isolation of the rectal large cell neuroendocrine carcinoma (NEC)-derived cancer cell line BKZ-2 and the colorectal adenocarcinoma (AC)-derived cancer cell line BKZ-3. (**A**) For the isolation of those cell lines that contain a subpopulation of cells with potential stem-like properties a tissue sample of either the (**B**) rectal large cell NEC or the (**C**) colorectal AC was obtained, mechanically and enzymatically disintegrated, and cultivated in CSC medium supplemented with fetal calf serum (FCS), leading to (**D**/**E**) adherent growing cells. (**F**/**H**) Cultivation of the cells with the addition of heparin and in the absence of FCS led to the formation of spheres, further validating stem-like properties of BKZ-2 and BKZ-3. (**G**/**I**) Quantification of the averaged sphere diameter showed a significant increase after the addition of heparin in comparison to the control for BKZ-2 and BKZ-3, regardless of the tested heparin concentrations. Moreover, BKZ-2 showed a continuous growth of the spheres over a time-period of one week. Non-parametric Kruskal-Wallis test ($p \leq 0.05$), followed by Dunn's Multiple Comparison post-hoc test. $n = 5$, *** $p \leq 0.001$, ** $p \leq 0.01$. Mean ± standard error of the mean (SEM). n.d. = not detectable.

In addition to the sphere formation capacity, BKZ-2 and BKZ-3 express the prominent CSC-markers CD133, CD44 and Nestin on protein level (Figure 5A–D and Figure S3). Immunocytochemical analysis of CD133, CD44 and Nestin expression of colon adenocarcinoma cell line HT-29 and colon carcinoma cell line HCT-116 only revealed slight expression of these CSC-markers (Figure 5E–H). Quantification of the percentage of CD133 high, medium and low cells showed significantly ($p \leq 0.01$) higher percentages of CD133 high cells for BKZ-3 cells in comparison to BKZ-2, HT-29 and HCT-116. Moreover, HT-29 and HCT-116 revealed significantly ($p \leq 0.01$) more CD133 low cells in comparison to BKZ-3. Even though BKZ-2 cells showed significantly more CD133 low cells in comparison to BKZ-3, HT-29 revealed significantly more CD133 low cells when compared to BKZ-2. Additionally, BKZ-2 revealed more CD133 medium cells when compared to HT-29 (Figure 5I). Quantification of CD44 expressing cells revealed no difference between BKZ-2 and BKZ-3 concerning the percentage of CD44 high cells. However, both cell lines showed significantly ($p \leq 0.01$) more CD44 high expressing cells in comparison to HT-29 and HCT-116 (Figure 5J). Thus, both HT-29 and HCT-116 revealed a tendency for higher percentages of CD133 and CD44 low expressing cells, as percentage of CD44 medium expressing

cells was significantly higher in BKZ-2 and BKZ-3, too (Figure 5I,J). Further flow cytometric analysis concerning the ALDH activity of BKZ-2 and BKZ-3 showed that 7.93% of BKZ-2 and 26.14% of BKZ-3 cells are ALDH high expressing cells (Figure 6), further showing that those cell lines contain a subpopulation of cells with potential stem-like characteristics.

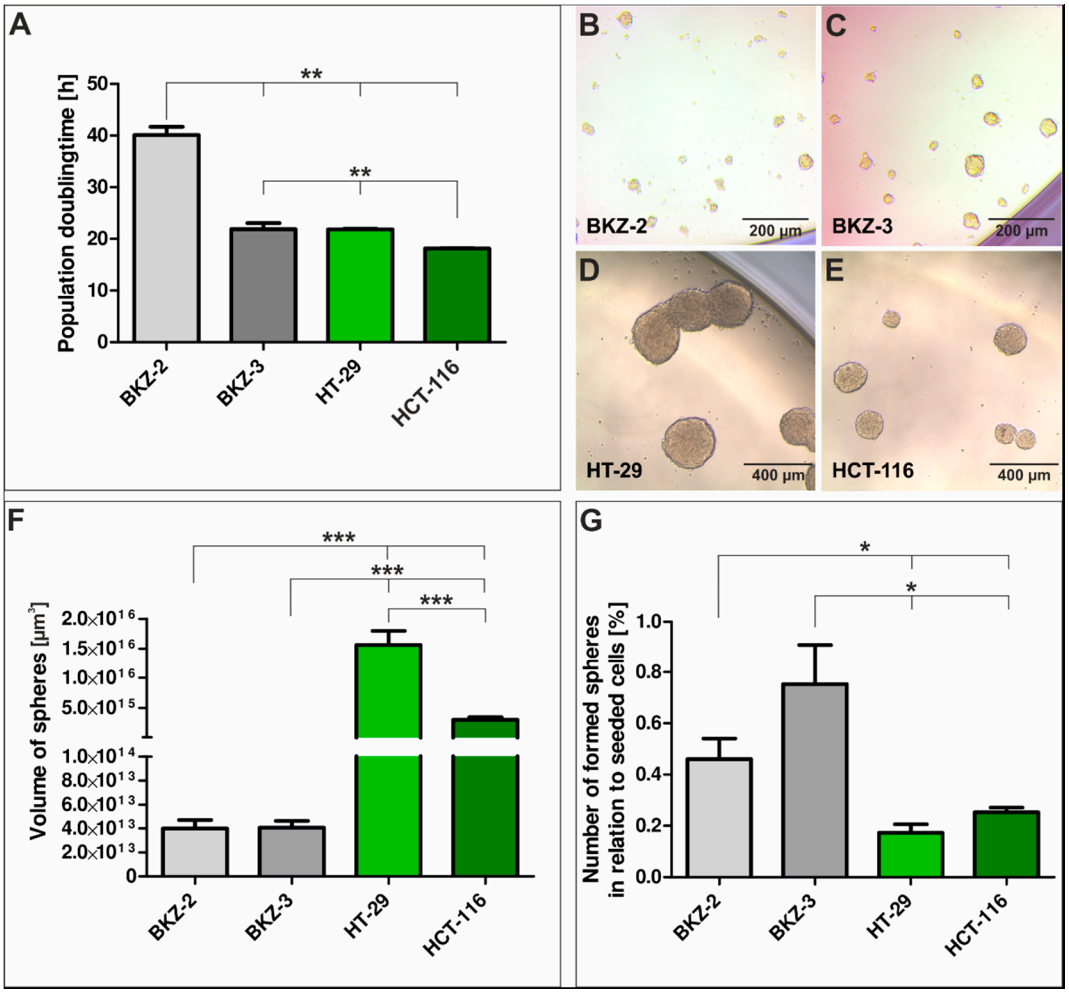

Figure 4. BKZ-2 and BKZ-3 reveal higher population doubling times and formed higher numbers of spheres in comparison to HT-29 and HCT-116. (**A**) Quantification of the population doubling times of the newly isolated colorectal cancer cell lines BKZ-2 and BKZ-3 as well as the common colon adenocarcinoma cell line HT-29 and colon carcinoma cell line HCT-116 revealed a significantly higher population doubling time for BKZ-2 in comparison to BKZ-3, HT-29 and HCT-116. Moreover, BKZ-3 and HT-29 displayed a significantly higher population doubling time when compared with HCT-116. (**B**–**E**) All cell populations formed spheres when 5000 cells per 200 µL cancer stem cell (CSC) medium containing 4 µg/mL heparin were cultured in low adhesion 96 well-plates. Quantification of the (**F**) volume of spheres formed by each cell line showed a significantly higher volume for HT-29 and HCT-116 when compared to BKZ-2 and BKZ-3. Moreover, sphere volume of HT-29 was significantly higher in comparison to HCT-116. Further quantification concerning (**G**) the number of formed spheres in relation to seeded cells revealed significantly less percent spheres for HT-29 and HCT-116 in comparison to BKZ-2 and BKZ-3. Non-parametric Mann-Whitney-test ($p \leq 0.05$). $n \leq 3$, *** $p \leq 0.001$, ** $p \leq 0.01$, * $p \leq 0.05$. Mean ± SEM (standard error of the mean).

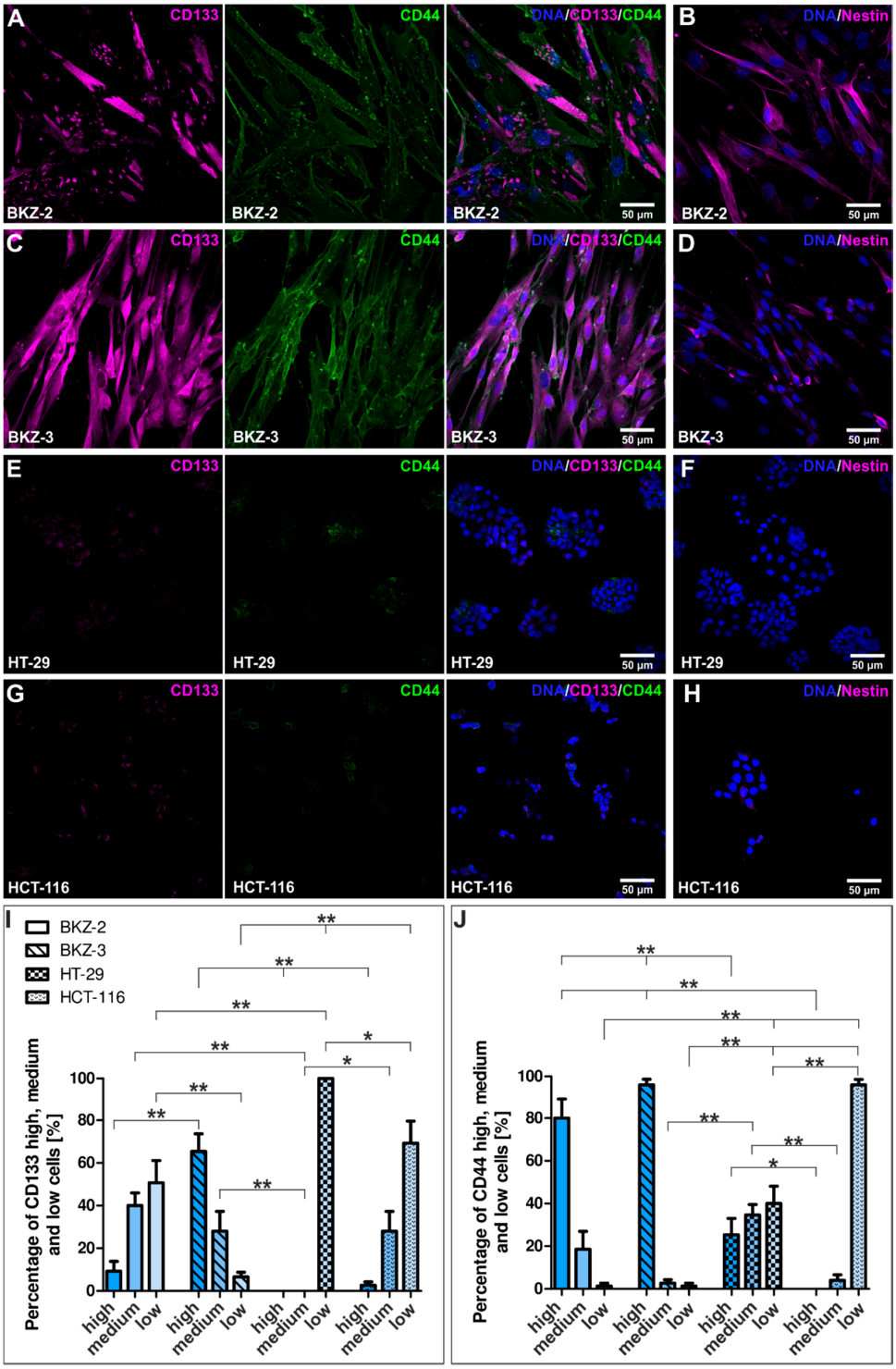

Figure 5. BKZ-2 and BKZ-3 express higher amounts of prominin-1 (CD133) and CD44 antigen (CD44) in comparison to HT-29 and HCT-116. Immunocytochemical analysis of BKZ-2 and BKZ-3 displayed high positivity for the cancer stem cell (CSC)-markers (**A**/**C**) CD133, CD44 and (**B**/**D**) Nestin, validating the isolation of two new cell lines that contain a subpopulation of cells with potential stem-like properties. Immunocytochemical analysis of the common colon carcinoma cell lines HT-29 and HCT-116 only displayed slight expression of the CSC-markers (**E**/**G**) CD133, CD44 and (**F**/**H**) Nestin. Quantification of the percentage of (**I**) CD133 high, medium and low cells revealed a significantly elevated amount of CD133 high BKZ-3 cells in comparison to BKZ-2, HT-29 and HCT-116. Moreover, the percentage of HT-29 and HCT-116 CD133 low cells was significantly higher when compared to BKZ-2 and BKZ-3.

Quantification of (**J**) CD44 high, medium and low cells displayed for both populations a significantly higher percentage of CD44 high cells in comparison to HT-29 and HCT-116. Non-parametric Kruskal-Wallis equality-of-populations rank test ($p \leq 0.05$) followed by Mann-Whitney test ($p \leq 0.05$). $n = 3$, ** $p \leq 0.01$, * $p \leq 0.05$, ns = not significant. Mean ± SEM (standard error of the mean).

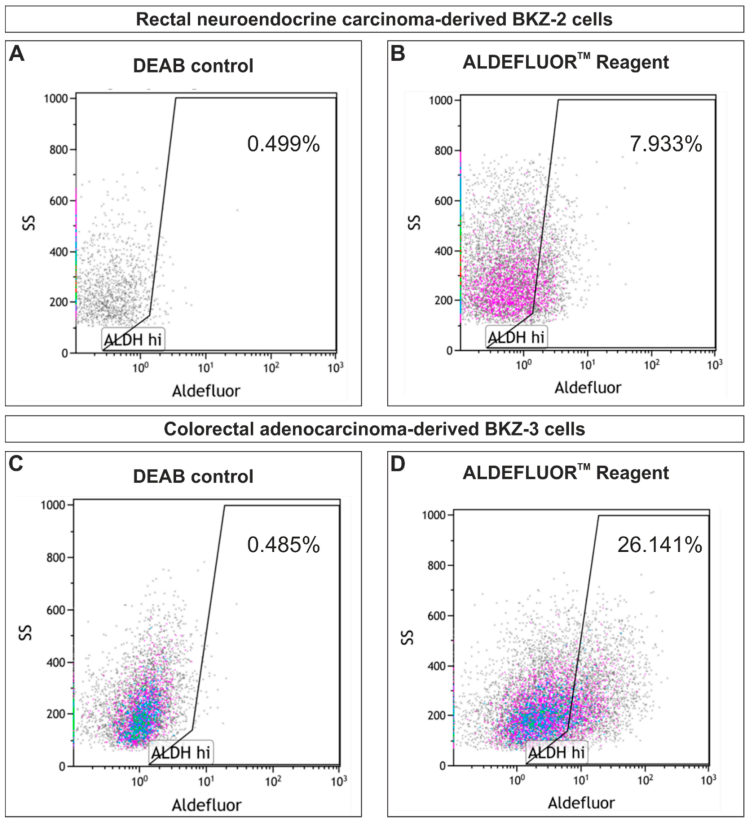

Figure 6. BKZ-2 and BKZ-3 both show aldehyde dehydrogenase (ALDH) activity. Flow-cytometric-analysis of ALDH activity of (**B**) BKZ-2 and (**D**) BKZ-3 revealed 7.993% ALDH high cells for BKZ-2 and 26.141% ALDH high cells for BKZ-3 in comparison to the appropriate (**A**/**C**) control with the specific ALDH inhibitor diethylaminobenzaldehyde (DEAB).

Further investigation concerning the transcriptional profile of BKZ-2 and BKZ-3 in comparison to human dermal fibroblasts (HDF) via quantitative polymerase chain reaction (qPCR) exhibited the expression of CSC-markers *CD133*, *CD44*, leucine rich repeat containing G protein-coupled receptor 5 (*LGR5*) and epithelial cell adhesion molecule (*EPCAM*) as well as the expression of SRY-box transcription factor 2 (*SOX2*) and octamer-binding transcription factor 4 (*OCT4*) in both BKZ-2 and BKZ-3. A statistical comparison of the transcription levels of BKZ-2, BKZ-3, and HDF revealed significant differences in the expression of *CD133* ($p \leq 0.05$), with BKZ-3 revealing higher levels in comparison to BKZ-2 and HDF and *CD44* ($p \leq 0.05$), with BKZ-2 showing higher expression level in comparison to BKZ-3 and HDF (Figure 7A,B). Even though, *LGR5* was significantly higher expressed in BKZ-2 when compared to BKZ-3 ($p \leq 0.05$), both BKZ-2 and BKZ-3 show significantly lower ($p \leq 0.05$) level in comparison to HDF (Figure 7C). Comparison of the endothelial and CSC-marker *EPCAM* revealed significantly higher ($p \leq 0.05$) expression for BKZ-3 in comparison to HDF, but no difference between BKZ-2 and BKZ-3 (Figure 7D). *SOX2* was significantly higher ($p \leq 0.05$) expressed in BKZ-2 and BKZ-3 in comparison to HDF, with significantly higher ($p \leq 0.05$) expression for BKZ-3 when compared to BKZ-2 (Figure 7E). The pluripotency marker *OCT4* did not show any statistical difference between the two cell lines, but was significantly higher expressed in HDF in comparison to BKZ-3 (Figure 7F). As phenotypic stemness often coincides with a pronounced ability to proliferate, to migrate and to invade in consequence of EMT, we tested for EMT-markers such as snail family transcriptional repressor

2 (*SLUG*), snail family transcriptional repressor 1 (*SNAIL*) and twist family bHLH transcription factor 1 (*TWIST*). Although the three key transcription factors of EMT were detectable in both cell lines, the expression levels of BKZ-2 were significantly higher than the expression of BKZ-3 for *TWIST* ($p \leq 0.05$) and especially for *SLUG* ($p \leq 0.05$). Moreover, *SNAIL* was expressed significantly higher in BKZ-2 and BKZ-3 in comparison to HDF (Figure 7G–I). Further, we tested for immune response checkpoint related ligands *PDL1* and programmed death ligand 2 (*PDL2*). Transcriptional analysis revealed an expression of both *PDL1* and *PDL2* in BKZ-2 and BKZ-3, with *PDL2* being higher expressed than *PDL1*. Quantification displayed a significantly higher expression of *PDL1* ($p \leq 0.05$) and *PDL2* ($p \leq 0.05$) for BKZ-2 in comparison to BKZ-3 and HDF (Figure 7J,K).

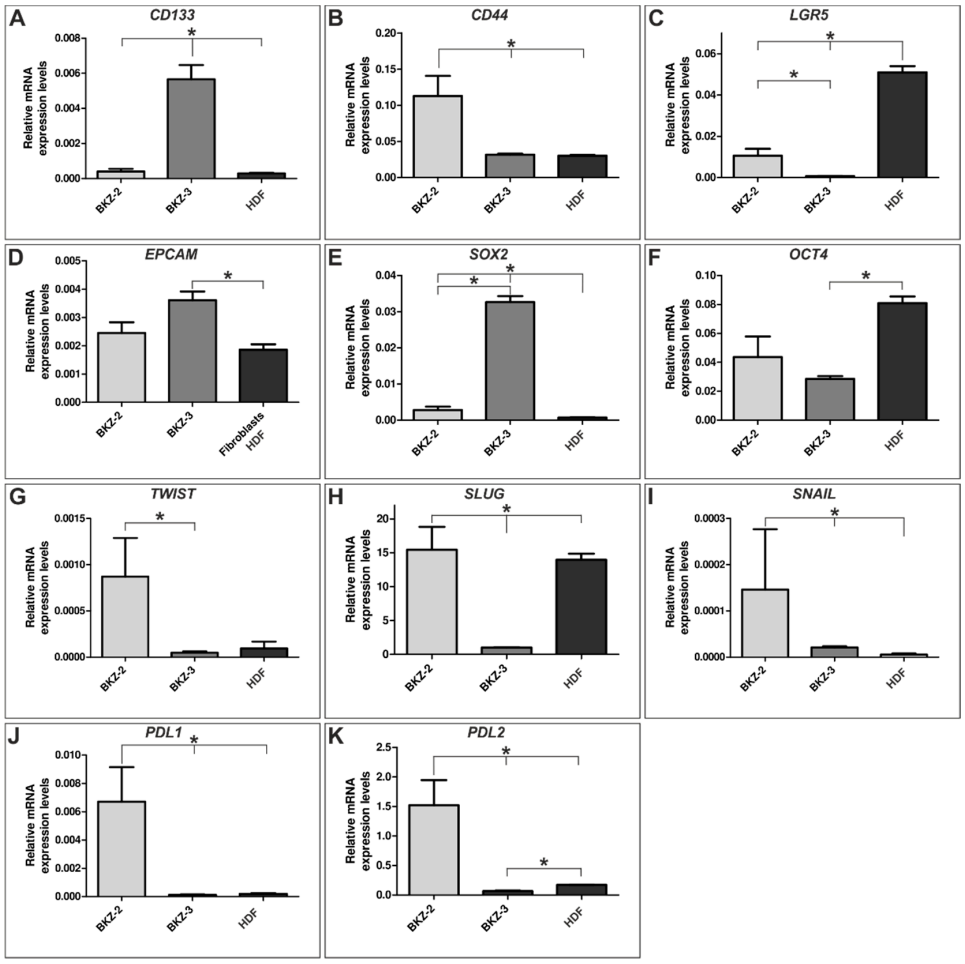

Figure 7. BKZ-2 and BKZ-3 show higher messenger ribonucleic acid (mRNA)-level of cancer stem cell (CSC)- and epithelial-mesenchymal-transition (EMT)-markers as well as immune checkpoint ligands in comparison to human dermal fibroblasts (HDF). Quantitative polymerase chain reaction revealed an expression of CSC-markers (**A**) prominin-1 (*CD133*), (**B**) CD44 antigen (*CD44*), (**C**) leucine rich repeat containing G protein-coupled receptor 5 *(LGR5*), (**D**) epithelial cell adhesion molecule (*EPCAM*), (**E**) SRY-box transcription factor 2 (*SOX2*) and (**F**) octamer-binding transcription factor 4 (*OCT4*) in both cell lines. Comparison of the two cell lines, demonstrated significant differences of the relative mRNA expression for *CD133*, *CD44*, *LGR5* and *SOX2*. Further analysis revealed an expression of the key transcription factors of the process of EMT (**G**) twist family bHLH transcription factor 1 (*TWIST*), (**H**) snail family transcriptional repressor 2 (*SLUG*) and (**I**) snail family transcriptional repressor 1 (*SNAIL*), with *TWIST* and *SLUG* being significantly different expressed in BKZ-2 and BKZ-3. Moreover, quantification displayed a significantly altered expression of the immune checkpoint ligands (**J**) programmed death ligand 1 (*PDL1*) and (**K**) programmed death ligand 2 (*PDL2*) in the two cell lines. Non-parametric Mann-Whitney-test ($p \leq 0.05$). $n = 3$, * $p \leq 0.05$. Mean ± SEM (standard error of the mean).

2.3. BKZ-2 and BKZ-3 Feature Neuroendocrine, Neural Crest and Neuronal Characteristics

In a next step, we tested whether BKZ-2 share both neuroendocrine as well as neuronal characteristics respectively as a cell line derived from a rectal carcinoma typed as a neuroendocrine carcinoma. Synaptophysin was expressed on protein level confirmed by immunocytochemistry as nuclear staining for BKZ-2 (Figure 8A). Moreover, BKZ-3 was also tested positive for Synaptophysin (Figure 8C). Quantification of the percentage of nuclear Synaptophysin positive cells revealed 90.27% (±2.73) for BKZ-2 and 92.92% (±6.45) for BKZ-3 (Figure 8E). Further quantification concerning Synaptophysin high and low nuclei displayed significantly more high nuclei ($p \leq 0.05$) for BKZ-2 in comparison to BKZ-3. However, both cell populations revealed significantly more Synaptophysin low ($p \leq 0.01$) nuclei in comparison to Synaptophysin high (Figure 8G).

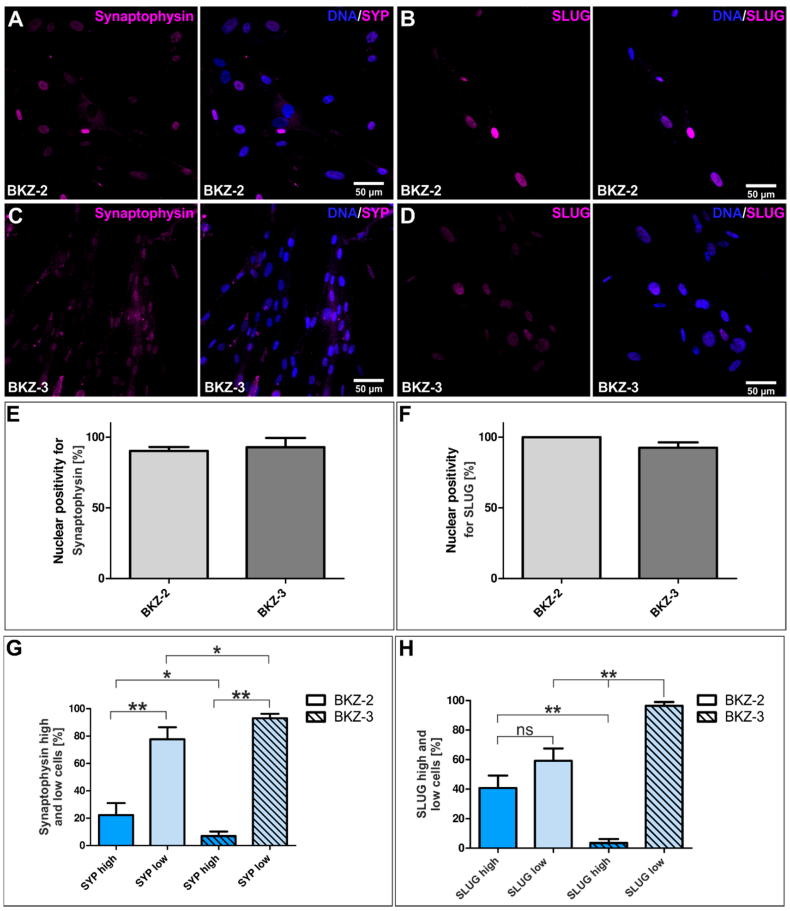

Figure 8. BKZ-2 cells reveal higher levels of Synaptophysin (SYP) and snail family transcriptional repressor 2 (SLUG) protein in comparison to BKZ-3 cells. Immunocytochemical stainings revealed the expression of neuroendocrine and cancer stem cell marker (**A/C**) Synaptophysin as well as the expression of (**B/D**) SLUG, one of the key transcription factors of the process of epithelial to mesenchymal transition in both populations. (**E**) Quantification of cells positive for nuclear Synaptophysin revealed a mean of 90.27% for BKZ-2 and 92.92% for BKZ-3. (**G**) Further classification in Synaptophysin high and low cells, showed a significantly higher amount of Synaptophysin low nuclei in comparison to Synaptophysin high nuclei for both BKZ-2 and BKZ-3. However, BKZ-2 revealed a significantly higher percentage of Synaptophysin high nuclei in comparison to BKZ-3. (**F**) Quantification of nuclear positivity for SLUG displayed 100% positive cells for BKZ-2 and a mean of 92.57% positive cells for BKZ-3. (**H**) Comparison of SLUG high and low cells displayed a significantly higher amount of SLUG high cells of BKZ-2 when compared to BKZ-3. Moreover, BKZ-3 cells in general showed a significantly higher percentage of SLUG low cells in comparison to the amount of SLUG high cells. Non-parametric Mann-Whitney-test ($p \leq 0.05$). $n = 3$, ** $p \leq 0.01$, * $p \leq 0.05$, ns = not significant. Mean ± SEM (standard error of the mean).

As neural crest characteristics are strongly related to the EMT process, we also investigated the expression of key transcription factor SLUG and neural crest and calcium binding protein S100 (S100) on protein level. Immunological staining displayed a strong expression of nuclear SLUG in both BKZ-2 and BKZ-3, representing an EMT-phenotype (Figure 8B,D). Quantification of the amount of nuclear SLUG positive cells displayed 100% positive BKZ-2 cells and 92.57 (±3.71) positive BKZ-3 cells (Figure 8F). Further quantification revealed significantly more ($p \leq 0.01$) SLUG high cells for BKZ-2 in comparison to BKZ-3. Additionally, BKZ-3 cells showed significantly more ($p \leq 0.01$) SLUG low cells when compared to the amount of SLUG low BKZ-2 cells and SLUG high BKZ-3 cells (Figure 8H). Moreover, S100 could be detected nuclear as well as cytoplasmatic in both cell lines (Figure S1A,E). Next, further traits of neuronal differentiation utilizing a comprehensive panel of neuronal markers were evaluated. Examined by immunocytochemistry, BKZ-2 and BKZ-3 were positive for cytosolic vesicular glutamate transporter 2 (vGLUT2), cytosolic dopamine and mainly nuclear tyrosine hydroxylase (TH), highlighting their neuronal characteristic. Moreover, the nuclear expression of TH indicates an undifferentiated phenotype, further suggesting stemness-like features of a subpopulation of BKZ-2 and BKZ-3 since TH was also detectable in the nuclei of BKZ-3 (Figure S1B–D,F–H). HDF were used as negative control for all immunocytochemical stainings (Figure S2A–J).

2.4. ATRA-Treatment Leads to a Contrary Switch in Growth Habits of BKZ-2 and BKZ-3

Next we investigated the influence of ATRA on BKZ-2 and BKZ-3 cells as ATRA was shown to decrease proliferation, sphere formation and CSC population size in CRC cell lines. For this, sphere-formation capacity of BKZ-2 and BKZ-3 was analyzed after treatment with different ATRA concentrations. After five days of culture, volume, and number of spheres of BKZ-2 were quantified, revealing a significant decrease of sphere volume ($p \leq 0.001$) after cultivation with 1, 5, or 10 µM ATRA (Figure 9E, Formula (6)). Furthermore, there was a non-significant trend of reduced number of spheres formed by BKZ-2 when co-incubated with ATRA regardless of used concentration (Figure 9F). Representative images of each treatment condition suggested the induction of a differentiation towards fibroblast-like morphology of BKZ-2 upon ATRA-treatment with cells becoming more adherent (Figure 9A–D).

A corresponding experiment was performed for BKZ-3, however unexpectedly results were opposed to those for BKZ-2. Quantification revealed no significant decrease as for BKZ-2, but a significant increase in sphere volume of BKZ-3 after 10 µM ATRA-treatment ($p \leq 0.001$) (Figure 9G–K). In contrast to the increase of sphere volume, number of spheres formed by BKZ-3 declined significantly when treated with 10 µM ATRA ($p \leq 0.05$) (Figure 9L), suggesting a switch in the growth behavior of BKZ-3 upon ATRA stimulation. A direct comparison of the volume of formed spheres by BKZ-2 and BKZ-3 revealed a statistically significant difference between the volumes of spheres induced by ATRA stimulation ($p \leq 0.05$). The sphere volume of BKZ-3 was significantly higher in comparison to BKZ-2 independent of ATRA concentration (Figure 10A). Additionally, calculation of the total cell mass of BKZ-2 and BKZ-3 by multiplying the mean of the volume with the mean of sphere number exhibited a significant decrease for BKZ-2 ($p \leq 0.05$), but no alteration in cell mass for BKZ-3 upon ATRA-treatment (Figure 10B). Thus, ATRA stimulation seems to lead to a switch in growth behavior of spheres in both cell lines, however BKZ-2 cells seem to switch to a more differentiated phenotype with less total cell mass and BKZ-3 cells generate bigger but fewer spheres without any significant change in total cell mass. Next to the analysis of the influence of ATRA on sphere formation of BKZ-2 and BKZ-3, its influence on monolayer cultures was investigated. For this, BKZ-2 and BKZ-3 cells as monolayers were treated for five days with different ATRA concentrations. Afterwards, the cell count was determined utilizing Orangu™ (Cell Guidance Systems, Cambridge, UK). Statistical analysis revealed a significant decrease ($p \leq 0.05$) in cell count for BKZ-2 cells after ATRA-treatment, but not for BKZ-3 (Supplementary Figure S4A,B). Further immunocytochemical stainings for cleaved caspase 3 protein after ATRA-treatment of BKZ-2 and BKZ-3 did not showed any positivity for this apoptosis marker, suggesting an influence of ATRA on cell proliferation only (Figure S4C–J). Finally, BKZ-2 and

BKZ-3 seem to behave differently in relation to ATRA, even though ATRA reduced the number of formed spheres for both cell populations.

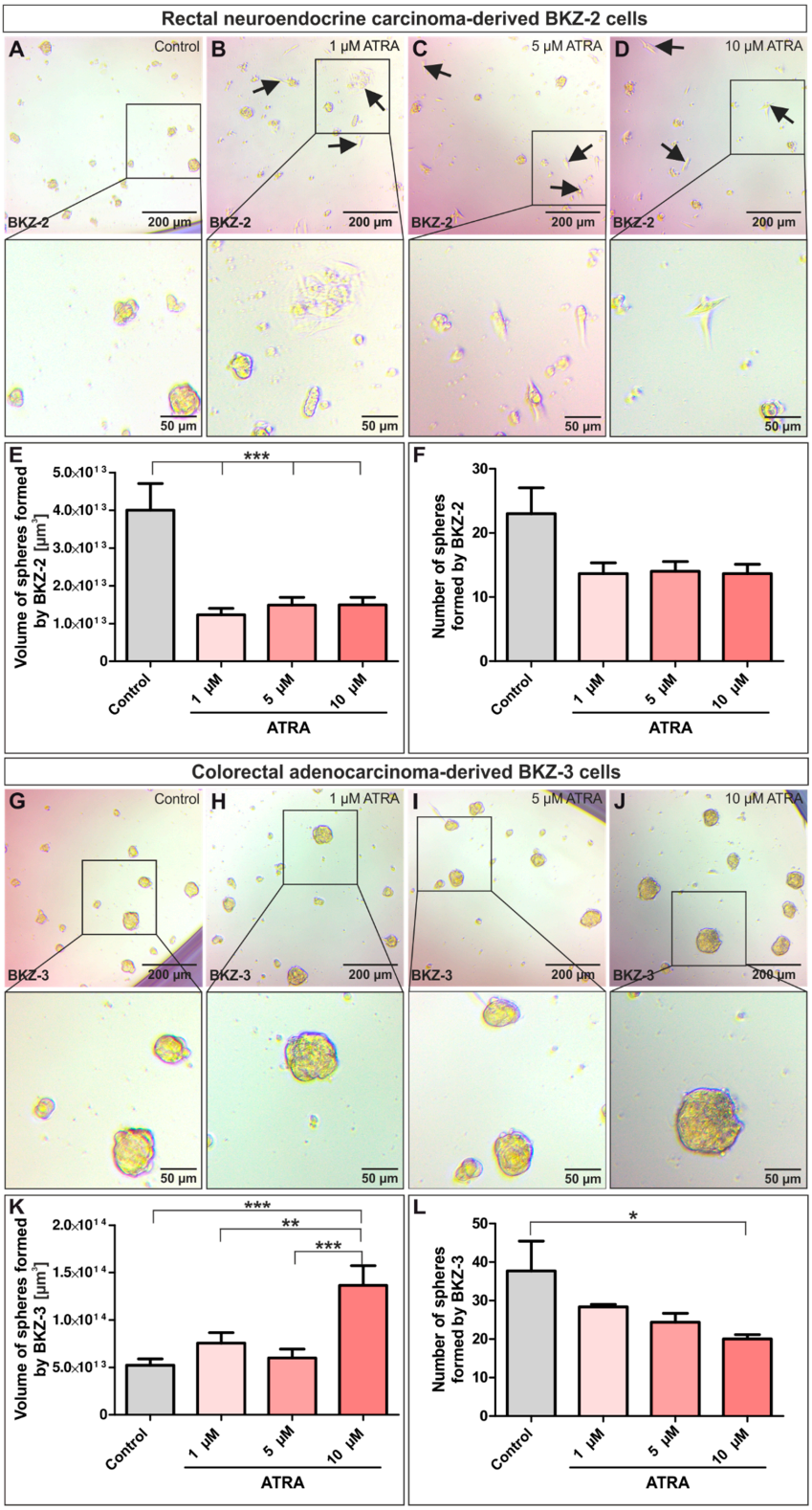

Figure 9. All-trans retinoic acid (ATRA) reduce number of BKZ-2 and BKZ-3 formed spheres respectively, but cause opposed effects concerning sphere volume of BKZ-2 and BKZ-3. Cells were cultured in an amount

of 5000 cells per 200 µL cancer stem cell (CSC) medium containing 4 µg/mL heparin in a low adhesion 96 well-plate. Medium was supplemented with (**A**/**G**) dimethylsulfoxide, (**B**/**H**) 1 µM ATRA, (**C**/**I**) 5 µM ATRA or (**D**/**J**) 10 µM ATRA. (**A**–**D**) Representative images already display a morphological change of BKZ-2 after the cultivation with 1 µM ATRA, indicated by the adherence of the cells (arrows). Quantification of the (**E**) volume of spheres formed by BKZ-2 cells showed a significant decrease after ATRA-treatment. Further quantification concerning (**F**) the number of spheres revealed a tendency for fewer spheres after ATRA-treatment for BKZ-2. (**G**–**J**) Representative images of BKZ-3 spheres and quantification of the (**K**) volume of spheres formed by BKZ-3 cells showed a significant increase subsequent to treatment with 10 µM ATRA. Further quantification concerning the (**L**) number of spheres revealed a significant decrease of the number of spheres after the treatment with 10 µM ATRA. Non-parametric Mann-Whitney-test ($p \leq 0.05$). $n = 3$, *** $p \leq 0.001$, ** $p \leq 0.01$, * $p \leq 0.05$. Mean ± SEM (standard error of the mean).

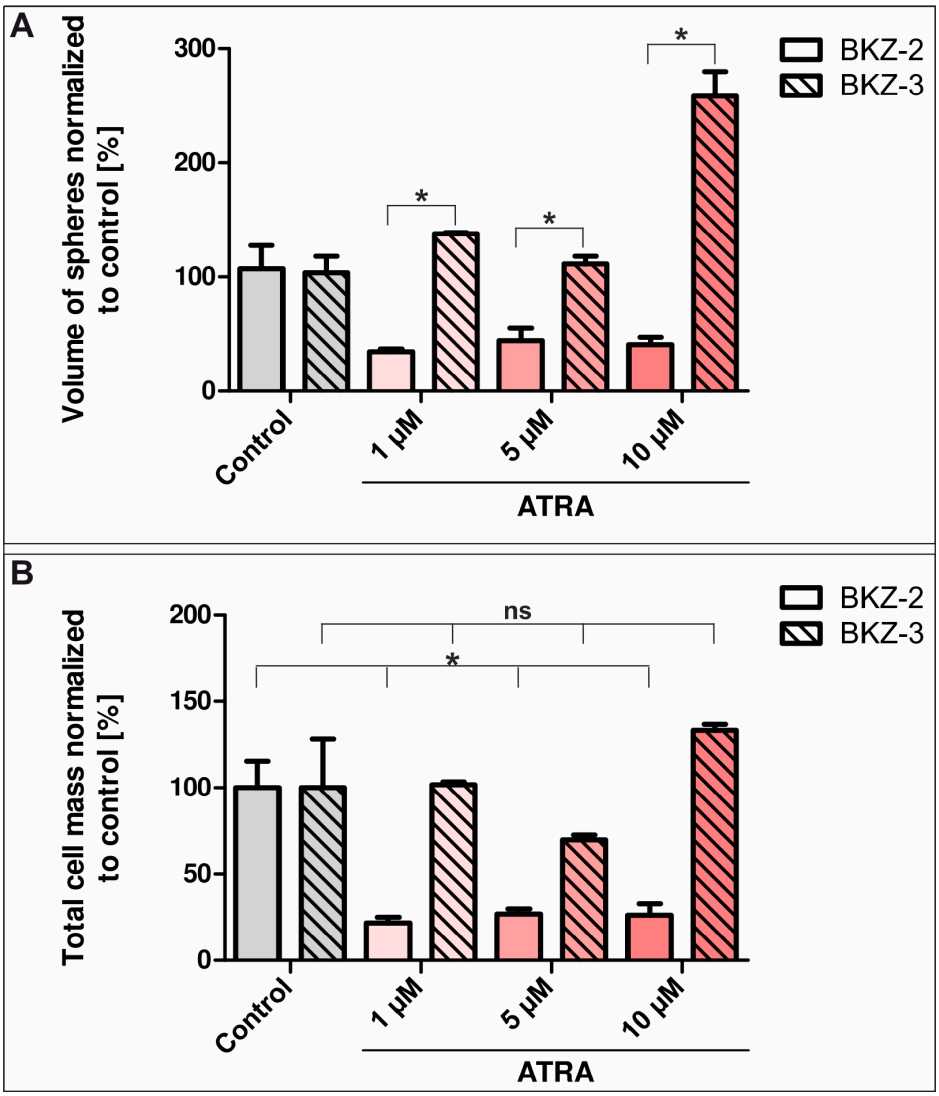

Figure 10. All-trans retinoic acid (ATRA)-treatment reduced total cell mass of BKZ-2 formed spheres, but does not have an effect on total cell mass of BKZ-3 formed spheres. Analysis of the quantification of the (**A**) volume of the spheres formed by the two colorectal cancer cell lines revealed a significant difference after ATRA-treatment. ATRA-treatment led to the formation of significant bigger spheres formed by BKZ-3 in comparison to BKZ-2. Further quantification of (**B**) the total cell mass revealed a significantly decreased cell mass for BKZ-2 upon ATRA stimulation, while the total cell mass of BKZ-3 was not altered. Non-parametric Mann-Whitney-test ($p \leq 0.05$). $n = 3$, * $p \leq 0.05$, ns = not significant. Mean ± SEM (standard error of the mean).

2.5. NMYC Copy Number Gain Sensitize BKZ-2 and BKZ-3 for MYC/NMYC Inhibitor Induced Apoptosis

MYC and NMYC were reported to play an important role for plasticity, proliferation and apoptosis in various entities of malignancies. To investigate a possible correlation of ATRA resistance and MYC/NMYC, we analyzed BKZ-2 and BKZ-3 regarding MYC/NMYC expression levels. First, we determined protein expression levels in BKZ-2 and BKZ-3 cells using immunocytochemistry, revealing the expression of NMYC and MYC in both. Although both oncogenes were expressed, NMYC was mainly detected cytosolic contrary to MYC, which was detected in the nuclei of BKZ-2 and BKZ-3 (Figure 11A–D).

Further, relative haploid normalized gain in gene copy numbers of *NMYC* and *MYC* was investigated for BKZ-2 and BKZ-3. Calculation of relative haploid copy number of *NMYC* displayed a 1.82 (±0.094)-fold amplification for BKZ-2 and a 1.45 (±0.24)-fold amplification for BKZ-3, indicating a duplication of the *NMYC* gene in both cell lines (Figure 11E). No amplification was detected for relative haploid gene copy number of *MYC*, as BKZ-2 represents a relative haploid copy number of 0.74 (±0.089) and BKZ-3 0.63 (±0.11) (Figure 11F). Thus, no differences in MYC and NMYC expression could be detected for BKZ-2 and BKZ-3, suggesting additional molecular pathways involved in ATRA mediated differentiation.

Previously, KJ-Pyr-9 as inhibitor of both MYC and NMYC showed proliferation inhibiting effects on various tumor cell lines. Accordingly, we investigated this small molecule concerning its effect on survival of BKZ-2 and BKZ-3 cells. After 120 h co-incubation with the inhibitor, survival rate of both cell lines revealed a significant decrease ($p \leq 0.05$) with increasing concentrations of KJ-Pyr-9 over 20 µM respectively. Moreover, discrepancies in the survival rates between both cell lines were detected, represented by significantly higher ($p \leq 0.05$) survival rates for BKZ-3 in comparison to BKZ-2 after treatment with KJ-Pyr-9 independent on inhibitor concentrations (Figure 11G). Normalized survival rate after stimulation with 10 µM KJ-Pyr-9 was 78.59% (±8.53) for BKZ-2 and 123.9% (±9.62) for BKZ-3 and with 20 µM KJ-Pyr-9 4.12% (±1.09) for BKZ-2 and 16.89% (±6.61) for BKZ-3. Cultivation with 40 µM KJ-Pyr-9 led to a survival rate of 6.19% (±1.14) for BKZ-2 and 19.85% (±1.42) for BKZ-3 and with 60 µM KJ-Pyr-9 to a survival of 11.18% (±0.92) for BKZ-2 and 27.11% (±0.97) for BKZ-3. This significantly higher survival rate of BKZ-3 in contrast to BKZ-2 possibly demonstrates a higher MYC/NMYC inhibitor tolerance of BKZ-3, suggesting a more MYC-independent growth behavior in comparison to BKZ-2. This result stands in line with the here presented inefficient differentiation of BKZ-3 using ATRA, which is also known to target MYC/NMYC activity. Comparison of survival rate of BKZ-2 and BKZ-3 with the two colon carcinoma cell lines HT-29 and HCT-116 after KJ-Pyr-9-treatment revealed a significantly higher ($p \leq 0.05$) survival of BKZ-2 and BKZ-3 subsequent to treatment with 40 µM and 60 µM (Figure 11H). Survival rates following the addition of 40 µM KJ-Pyr-9 were 6.19% (±1.14) for BKZ-2, 19.85% (±1.42) for BKZ-3, 2.83 (±0.12) for HT-29 and 1.78 (±0.27) and after 60 µM 11.18% (±0.92) for BKZ-2, 27.11% (±0.97) for BKZ-3, 3.18 (±0.16) for HT-29, and 1.93 (±0.14) for HCT-116. To address whether the reduction in survival is caused by regulation of proliferation or apoptosis BKZ-2 and BKZ-3 cells were treated with KJ-Pyr-9 as described before, followed by immunocytochemical staining for cleaved caspase 3 to determine the number of apoptotic cells (Figure 12A–J). Quantification of cleaved caspase 3 staining displayed a significantly higher ($p \leq 0.001$) amount of apoptotic BKZ-2 cells with 93.65 (±6.35) after 10 µM KJ-Pyr-9 in comparison to BKZ-3 with 4.32 (±2.78). In accordance with that, BKZ-3 displayed a trend for less cleaved caspase 3 positive cells after 20 µM of KJ-Pyr-9 with 91.89 (±4.62) in comparison to BKZ-2 with 100% apoptotic cells. However, BKZ-2 seem to be more sensitive for KJ-Pyr-9 induced apoptosis, BKZ-2 and BKZ-3 showed 100% cleaved caspase 3 positivity for KJ-Pyr-9-incubation with concentrations greater than 40 µM (Figure 12K).

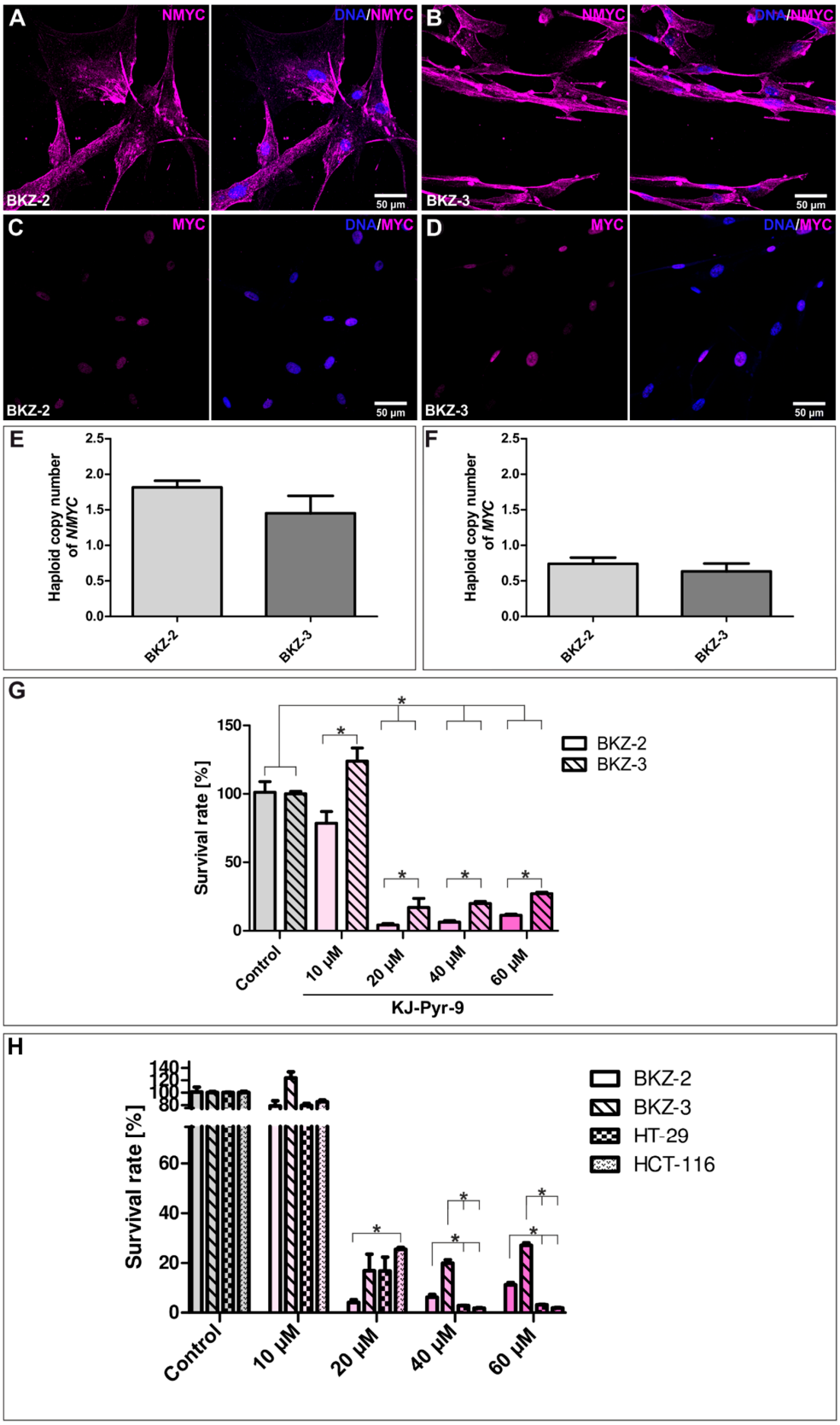

Figure 11. Inhibition of the myc proto-oncogene protein (MYC) and N-myc proto-oncogene protein (NMYC) significantly decreases the survival rate of BKZ-2 and BKZ-3 cells. Immunocytochemical staining

revealed a strong expression of the oncogene (**A**/**B**) NMYC, as well as a nuclear expression of the oncogene (**C**/**D**) MYC, in both BKZ-2 and BKZ-3 on protein level. Evaluation of the haploid copy number of the two oncogenes, demonstrated a two-fold increase of the haploid copy number of (**E**) *NMYC*, but a normal haploid copy number for (**F**) *MYC* within both cell lines. To investigate the influence of the MYC/NMYC inhibitor KJ-Pyr-9 on the proliferation, 3000 cells per 100 µL cancer stem cell medium were cultured in a 96 well for 120 h with the inhibitor or dimethylsulfoxide and 10% fetal calf serum. Afterwards, metabolism was measured using Orangu^{TM} (Cell Guidance Systems, Cambridge, UK) and cell count was determined by using a standard curve. (**G**) Normalized survival rate was quantified and significantly decreased after exposure to values greater than 20 µM of KJ-Pyr-9 in comparison to the control for BKZ-2 and BKZ-3. Further comparisons between the two cell lines displayed a significant decrease of the survival rate of BKZ-2 in comparison to BKZ-3 for all inhibitor concentrations. (**H**) Although comparison of survival rates after KJ-Pyr-9-treatment showed significantly higher survival of HCT-116 when compared to BKZ-2 after 20 µM K-Pyr-9, cell survival of BKZ-2 and BKZ-3 was significantly improved in comparison to HT-29 and HCT-116 after treatment with inhibitor concentrations over 40 µM. Non-parametric Mann-Whitney-test ($p \leq 0.05$). $n = 3$, * $p \leq 0.05$. Mean ± SEM (standard error of the mean).

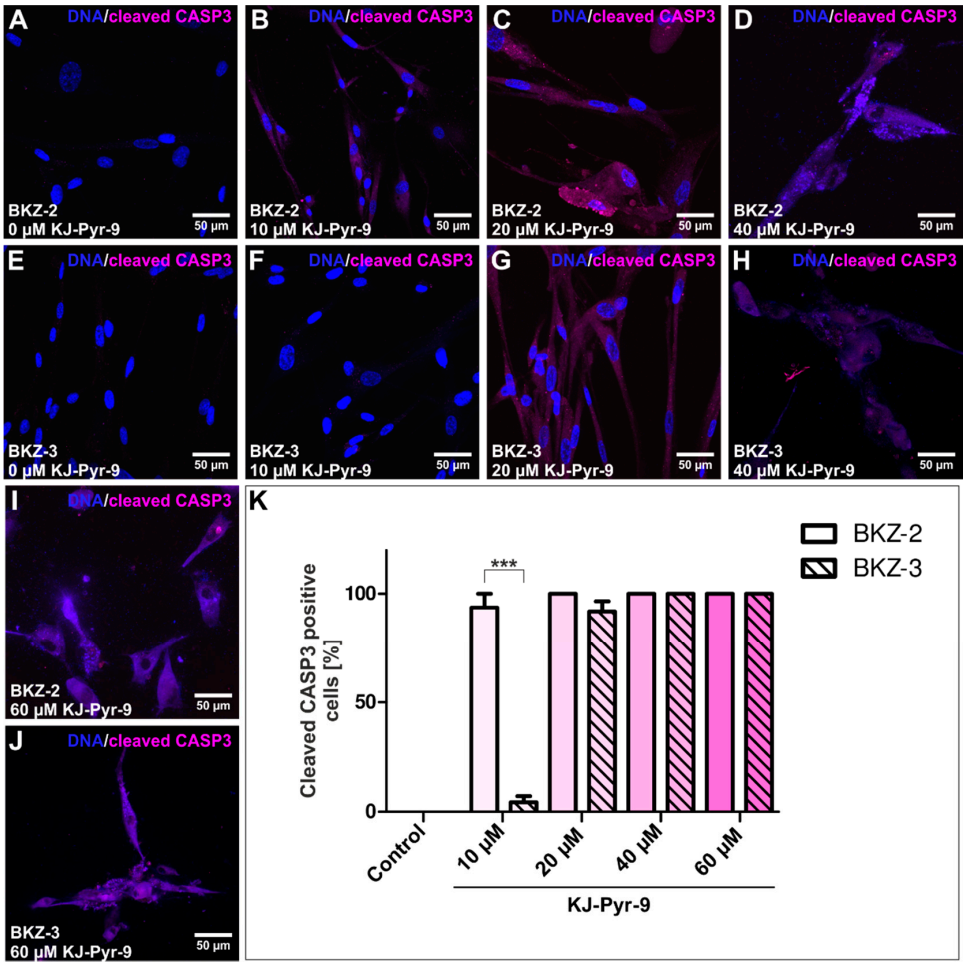

Figure 12. Myc proto-oncogene (MYC)/N-myc proto-oncogene (NMYC) inhibitor KJ-Pyr-9 induces apoptosis of BKZ-2 and BKZ-3. Representative images of immunocytochemical staining for cleaved caspase 3 (CASP3) after KJ-Pyr-9-treatment of (**A**–**E**) BKZ-2 and (**F**–**J**) BKZ-3. (**K**) Quantification of the percentage of cleaved CASP3 positive cells after the addition of 10 µM KJ-Pyr-9 revealed a significantly higher amount for BKZ-2 with about 94% in comparison to BKZ-3 with about 4%. However, concentrations higher than 40 µM lead to 100% cleaved CASP3 positive cells for BKZ-2 and BKZ-3. Student's *t*-test ($p \leq 0.05$). $n = 3$, *** $p \leq 0.001$. Mean ± SEM (standard error of the mean).

3. Discussion

In this study, we present the establishment of two primary human colorectal cancer cell lines that contain a subpopulation with potential stem-like properties. One very rare case of a GEP-NEC of the rectum is named BKZ-2 and one colorectal AC is referred to as BKZ-3. We characterized stemness-like properties by high CD133 and CD44 expression, relatively slow proliferation rates, and high number of formed spheres in the in vitro model systems, providing the basis for further exploration of patho-mechanisms in order to develop therapeutical strategies. As initial steps to that respect, we further tested for the impact and role of ATRA and the MYC/NMYC inhibitor KJ-Pyr-9 in these cells, as both are interfering with MYC/NMYC signaling in CCSC. However, some limitations of this study should be noted, as identification of the subpopulation with stem cell-like properties was only done by in vitro not in vivo experiments.

CCSC are defined with a group of cell surface markers such as CD44, CD133, EPCAM and LGR5 [32,33], which all were tested positive in BKZ-2 and BKZ-3 cells on transcriptional and/or on protein level. CD133 is a robust biomarker to identify primary CSC and can be proposed as a prognostic marker of CRC patients. Moreover, it is reported to be expressed in poorly-differentiated NECs and well-differentiated NETs of the digestive tract [34] and was demonstrated to be expressed in CCSC-lines [35]. It is the most well-known marker for the isolation and investigation of CSC in different types of cancer [36–38] and known to be responsible for radio- and chemotherapy-resistance in CCSC [39,40]. However, it seems to be more reliable to use CD133 in combination with other markers, such as CD44 as target biomarkers for the isolation of CCSC in both cell lines and primary tumor cell populations as done in our study [6]. CSC-marker CD44 is known to mediate cancer cell survival, proliferation, and motility, as well as the modulation of tumor microenvironment [36,41,42], indicating CD133 and CD44 as an excellent marker set to validate a CCSC-like-phenotype. Next to the protein expression of CD133 and CD44, class VI intermediate filament protein Nestin was shown to be expressed in both cell lines, further confirming potential stem-like properties of BKZ-2 and BKZ-3 as Nestin is commonly accepted to play a role in CSC-phenotypes, particularly regarding the capacity for self-renewal [43]. Additionally, in vitro tumorigenicity, as proven here for BKZ-2 and BKZ-3 utilizing sphere formation assays and the higher number of formed spheres of BKZ-2 and BKZ-3 in comparison to established colon carcinoma cell lines HT-29 and HCT-116, underline the existence of a subpopulation with potential stem-like characteristics [15]. Moreover, sphere formation seems to be biologically reliable as these in vitro testing modalities demonstrated uniformly results corresponding with murine in vivo xenograft models if tested with the same cancer cells including NEC-cell lines [9,44,45]. Further analysis of the proliferation and comparison of population doubling times of BKZ-2 and BKZ-3 with established colon carcinoma cell lines HT-29 and HCT-116, respectively, showed significantly higher population doubling times for BKZ-2 and BKZ-3. This may be due to the fact, that CSC have the ability to become more quiescent with slow proliferation rates to escape from chemotherapy. These slow-cycling cells are tumorigenic and more resistant to traditional chemotherapies than rapidly dividing cells [46,47]. Analysis of *BRAF* mutation status showed no mutation for codons 600, 464, 466, and 469 in both parental tumor tissue and cell populations. Concerning *BRAF* mutation in CRC a retrospective study showed that patients whose tumors had microsatellite stability with mutant *BRAF* demonstrated significantly reduced overall survival [48]. However, only 6–18% of CRC patients harbor a *BRAF* mutation [48–50].

Quantitative PCR analysis displayed *LGR5* expression in both BKZ-2 and BKZ-3 cells. Nevertheless, their expression levels were significantly lower in comparison to HDF. LGR5 is well-established as a marker of native intestinal stem cells [51] as well as CCSC [52] and plays an active role in pathogenesis of CRC [53]. Certainly, Fumagalli and colleagues observed most disseminated CRC cells in circulation to be LGR5 negative. Latter cells formed distant metastases in which CSC appeared LGR5 positive [54]. This plasticity of CCSC may explain the relatively low level of *LGR5*, as BKZ-2 and BKZ-3 also revealed an EMT-phenotype reflected by a high level of SLUG. Positivity in BKZ-2 and BKZ-3 cells for the 40 kDa single transmembrane protein *EPCAM* encoded by tumor-associated calcium signal transducer-1

gene [55] was relevant as epithelial adhesion molecule playing a role in carcinogenesis of epithelial cells by activating expression of proto-oncogenes *MYC* and *CYCLIN A/E* [56]. Further, it was demonstrated to correlate with the level of malignancy in foregut-NET of the pancreas [57]. It was also shown to be involved in regulation of intercellular adhesion-mediated signal transduction, cell migration, proliferation and differentiation [55]. Significantly higher expression of *SOX2* was observed in primary CRC tissues and metastatic tumor tissues compared to paratumoral tissues with 80% of the analyzed primary tumor samples [58]. Further, in a CRC-derived CSC-line (SW620) [59], SOX2 was associated with cell migration, invasion, colony formation and tumorigenesis as well as with spherogenicity and chemoresistance [58], representing SOX2 as a CSC-marker. Interestingly, a knock-down of SOX2 in SW620 cells induced a mesenchymal–epithelial transition process, reducing the migration and invasion capabilities of cells [60], and suggesting a link between EMT and stemness. *SOX2* as well as CSC-marker *OCT4* were expressed in BKZ-2 and BKZ-3. However, *OCT4* expression was also prominent in HDF, which is not unexpected as fibroblasts are able to express *OCT4* under different cell culture microenvironmental conditions [61]. Expression of *CD133*, *CD44*, *EPCAM*, *SOX2*, and *OCT4* substantiates that BKZ-2 and BKZ-3 include a subpopulation with potential stem-like properties. Moreover, differences in messenger RNA (mRNA) expression levels of *CD133*, *CD44*, *LGR5*, and *SOX2* between BKZ-2 and BKZ-3 possibly demonstrate a balance between different CSC-markers necessary for CSC maintenance.

Histopathological analysis of Synaptophysin as a neuroendocrine marker within the tumor tissue revealed expression only within NEC. However, immunocytochemically both, BKZ-2 and BKZ-3 were demonstrated to be positive for Synaptophysin. This finding emphasizes that Synaptophysin not only plays a role as neuroendocrine marker [62], but also as marker for stemness, as recently reported by us [63]. Quantification of Synaptophysin in nuclei revealed significantly more highly positive nuclei for BKZ-2 in comparison to BKZ-3, possibly reflecting the neuroendocrine origin or a potential more stem cell-like phenotype. Further investigation on neuronal and neural-crest related protein expressions displayed a strong expression of S100A1 for BKZ-2 and BKZ-3, which was shown to be negatively associated with the frequency of lymph node metastasis and level of dedifferentiation in ovarian cancer, enhancing the ovarian cancer cell proliferation and migration [64]. Further, S100A9 was shown to be required for the proliferation of CRC spheroids upon mammalian target of rapamycin complex 1 signaling [65], suggesting a role of S100 family in stemness of CRC cells. Moreover, the neuronal marker vGLUT2 [66], as well as the dopaminergic marker dopamine were detected in BKZ-2 and BKZ-3, highlighting the neuroendocrine origin of BKZ-2 and suggesting a neuronal differentiation potential for BKZ-3, too [67]. TH protein, which is a rate-limiting enzyme of dopamine synthesis [68], and thus a marker for dopaminergic neurons, was expressed predominantly nuclear, but also cytosolic in BKZ-2 cells. Moreover, it could be detected in the nuclei of BKZ-3 cells, possibly reflecting the multipotent phenotype of a subpopulation with potential stem cell-like characteristics, since mature neurons would express TH predominantly cytosolic.

There is increasing evidence that CSC lay the foundation for cancer invasiveness. A critical role of EMT and stemness for tumor plasticity and aggressiveness was discussed for NET variants of prostate cancer in more depth [69–71] and to some extent for pancreatic neoplasms [72]. Additionally, targeting cancer cells using ATRA-dependent differentiation therapy has been recently described for several solid cancer types including CRC [29] and has been clinically proven for acute promyelocytic leukemia. There are indications that ATRA suppresses proliferation, migration, CSC population size and sphere formation of cancer cell lines by reversing EMT. During EMT, the E-cadherin promoter is frequently repressed by specific transcriptional repressors, including *SNAIL*, *SLUG*, *ZEB1*, high mobility group AT-hook 2, and *TWIST*, making E-cadherin expression a valuable prognostic factor of CRC [73]. We even demonstrated for precursor lesions of CRC *SNAIL*-up- and e-cadherin-down-regulation, which was not found in normal colorectal tissue [74]. In this study, BKZ-2 expressed higher level of the EMT key transcription factors *TWIST*, *SLUG*, and *SNAIL* as well as SLUG on protein level in comparison to BKZ-3. Thus, BKZ-2 seem to harbor a more pronounced EMT-phenotype in comparison to BKZ-3. Cui and

coworkers demonstrated that ATRA induced differentiation by decreasing invasion, proliferation and migration of the murine hepatocellular carcinoma cell lines hepa1-6. Moreover, they showed impaired in vitro liver function upon the reversal of EMT [75]. Those results stand in line with the study of Modarai and colleagues, in which ATRA-treatment of human CRC lines decreased proliferation, sphere formation and ALDH + CSC population size by inducing neuroendocrine differentiation [29]. Within the presented study, this phenomenon was also shown for the neuroendocrine-derived cell line BKZ-2, revealing a decreased sphere volume and reduction in total cell mass, which is probably caused by decreased proliferation. Further, BKZ-2 cells seem to demonstrate a more differentiated phenotype after ATRA-treatment. However, analysis of the ATRA effect on apoptosis revealed no increase in apoptotic cells after ATRA-stimulation for BKZ-2 and BKZ-3. This suggests that ATRA suppresses proliferation in neuroendocrine-derived colorectal cancer cells with potential stem-like properties possibly by targeting an EMT-phenotype and inducing differentiation, as already shown for human CSC of head and neck squamous carcinoma [76], glioblastoma multiforme [77], and gastric cancer [78]. The AC-derived colorectal cancer cell line BKZ-3 exhibited lower mRNA levels of EMT transcription factors as well as SLUG high nuclei and behaved contrary subsequent to ATRA-treatment, as volume of spheres increased with no change in total cell mass. This possibly represents some sort of ATRA resistance for BKZ-3 cells, even if ATRA induced a shift in growth behavior for BKZ-3 cells. There is growing evidence that mechanisms inducing the degradation of retinoic acid receptor β [79] or cytoplasmic retinoid X receptor α play crucial roles in the ATRA resistance of colonic AC cell lines [80]. A similar downregulation of retinoic acid receptors could explain the opposed effect in BKZ-3 cells compared to BKZ-2, however the actual molecular pathway behind this still needs to be clarified. The CSC-marker ALDH [81] is a key enzyme in retinoid acid signaling and was shown to be targeted by ATRA in CRC cell lines [29]. Analysis of ALDH activity demonstrated a slightly higher proportion of BKZ-3 cells with high ALDH activity of about 26% in comparison to BKZ-2 with about 8% of highly active cells. However, Khorrami and coworkers have shown that HT-29-derived colonospheres with low ALDH activity demonstrate increased tumorigenic potential and stemness properties, reflecting the need for a set of CSC-marker and CSC plasticity. Even though it was presented that ATRA treatment decreased colony and sphere formation capacities only in an ALDH-high not in ALDH-low subpopulation of a human ovarian cancer cell line [82], the mechanism behind the higher sensitivity of BKZ-2 in comparison to BKZ-3 cannot be explained solely by ALDH activity.

There is evidence that differentiation therapy using ATRA involves MYC/NMYC regulation in cancer cells. This was shown by Farrell and coworkers, who validated that peptidyl-prolyl cis-trans isomerase Pin1 (PIN1) regulates MYC activity by acting on MYC degradation and activation [83]. ATRA acts as inhibitor of PIN1, reducing for example in vivo growth of triple-negative breast cancer xenografts by the degradation of PIN1 protein [84]. This stands in line with results concerning hepatocellular carcinoma xenografts using slow-release poly L-lactic acid microparticle containing ATRA [85]. Less sensitivity of BKZ-3 for ATRA-treatment was not reflected by differences in MYC-family member protein expressions but may be due to dysregulation in PIN1 signaling, leading to less inhibitory effects of ATRA on MYC activity. MYC-family proteins function as potent transcription factors that organize multiple cellular processes, including adhesion, proliferation, survival, and differentiation. Thus, MYC expression is frequently enhanced in cancer leading to elevated MYC RNA and protein expression [86,87]. Likewise, we demonstrated gene copy number gain for *NMYC* in both colorectal cancer cell lines that comprise a subpopulation of cells with potential stem-like properties. Gain of gene copy numbers of members of the *MYC*-family is reported to be an independent factor for poor prognosis in consecutive CRC patients and in the stage II–III subgroups [88]. Accordingly, neuroendocrine prostate cancer tumors, associated with aggressive disease and poor prognosis, are partly driven by aberrant expression of NMYC. NMYC overexpression and its subsequent deoxyribonucleic acid (DNA) binding induce epigenomic and transcriptomic reprogramming, resulting in a castration-resistant, promoting lineage-plasticity [21]. Further, NMYC overexpression was associated with highly proliferative, invasive prostate cancer with neuroendocrine features and was associated with an induction of EMT

genes and poor outcome [89]. In accordance to that, *NMYC* copy number gain of BKZ-2 and BKZ-3 correlated with the expression of EMT genes and stem-like characteristics. Moreover, *NMYC* copy number gain of BKZ-2 as a neuroendocrine-derived colorectal cancer cell population goes along with the known correlation of neuroendocrine neoplasms with NMYC derangement in prostate cancer. As NMYC was shown to drive transformation of human prostate epithelial cells to prostate AC and neuroendocrine prostate cancer [90], BKZ-3 may present a lineage plastic AC-derived colorectal cancer cell line with a subpopulation of cells with potential stem-like characteristics and the potential to gain neuroendocrine features. Even though a copy number gain was not detected for *MYC*, it was also expressed on protein level within BKZ-2 and BKZ-3 cells. Thus, probably playing a role in maintaining CCSC-like phenotype, too. It was demonstrated that MYC positively regulate check point inhibitor proteins leukocyte surface antigen CD47 and PDL1 via direct binding to their encoding gene promoters suppressing both the innate and the adaptive immune response while favoring tumor growth [91]. Further, immune checkpoint ligand PDL1 is upregulated in EMT-activated human breast cancer cells [92] and was shown to be more highly expressed in metastatic CRC than in primary CRC [93], suggesting its correlation with stem cell characteristics. Intriguingly, EMT and immune checkpoint proteins maybe related to each other as EGFR activation induces EMT and PDL1 expression in cancer. Moreover, MYC is required for EGFR-mediated PDL1 upregulation but not EMT [94]. Further, in vitro experiments on CRC-derived tumor cell lines provided evidence that PDL2 is involved in tumor cell invasion [95]. Giving these facts, the higher level of EMT genes, SLUG protein and immune checkpoint ligands of BKZ-2 are probably associated with each other and may reflect a more invasive and aggressive phenotype of the isolated neuroendocrine-derived colorectal cancer cell line BKZ-2 in comparison to BKZ-3 cells. Accordingly, the difference in PDL1 expression was also detected in parental tumor tissue of the two cell lines with 2% of PDL1 positive vital tumor cells shown in BKZ-2 originating tissue and 0% in BKZ-3, respectively. Further analysis on CPS displayed a value of 2% for parental tumor tissue of BKZ-2 and a CPS of 3 for tissue donating BKZ-3 cells. Thus, a slight correlation between higher PDL1 expression in tumor cells and less PDL1 positive immune cell infiltration may be assumed.

MYC/NMYC inhibition decreases the survival rates of both BKZ-2 and BKZ-3 cells. However, survival rate was significantly higher for BKZ-3 cells, further reflecting a protective mechanism against MYC/NMYC inhibitory molecules or rather a more MYC/NMYC independent growth of BKZ-3. Moreover, BKZ-2 and BKZ-3 seem to be more resistant to KJ-Pyr-9 in comparison to HT-29 and HCT-116, with BKZ-3 even revealing higher survival after 10 µM KJ-Pyr-9 treatment. This may be due to lower expression levels of the CSC-markers CD133 and CD44 in HT-29 and HCT-116, which stands in line with a study of Zhang and coworkers demonstrating a CD133 high expressing subpopulation of HT-29 cells paralleled by higher levels of MYC. Further, MYC silencing led to higher chemo sensitivity [18]. The KJ-Pyr-9 inhibitor used here as a small molecule antagonist of the protein–protein interaction of MYC and NMYC with myc-associated factor X (MAX) was reported to inhibit dimerization of these two molecules. Reduced survival rates were demonstrated subsequent to KJ-Pyr-9-treatment in vitro on various tumor cell lines with concentrations of 5 to 20 µM as well as in vivo in a human to mouse tumor xenograft model with a dosage of 10 mg/kg body weight [96], which was here presented for BKZ-2 and BKZ-3, too. Moreover, KJ-Pyr-9-treatment led to high percentages of apoptotic cells, revealing that its influence on survival is based on apoptosis. Interestingly, BKZ-2 cells showed significantly higher sensitivity in comparison to BKZ-3 when treated with 10 µM. Even though BKZ-3 was less sensitive for MYC/NMYC inhibition in comparison to BKZ-2, both colorectal cancer cell lines revealed significant reductions of survival rates due to induced apoptosis upon MYC/NMYC inhibition. Consequently, the usage of inhibitors of the protein–protein interaction of MYC and NMYC with MAX is a possible treatment strategy for both neuroendocrine- and AC-derived colorectal cancer cell lines that harbor a subpopulation with potential stem-like properties.

4. Materials and Methods

4.1. Patients Clinical Characterisation and Oncological Treatment

Patient 1 (donor of BKZ-2 cell line) was a 79-year-old Caucasian male when admitted to the emergency room of the Protestant Hospital of Bethel Foundation (Bielefeld, Germany) with abdominal pain and clinical signs of an obstructive ileus. Computerized tomography (CT)-scan revealed a malignant tumorous lesion of the upper third of the rectum with consecutive massive dilated upstream colon (Figure 1A). Flexible rectal endoscopy confirmed a luminal subtotally occluding neoplastic lesion (Figure 1B). Following the introduction of a self-expanding metallic endo-prosthetic stent, a passage was reestablished (Figure 1C). Staging revealed multiple synchronic hepatic metastases of all segments (Figure 1D). Patient 1 was scheduled for robotic deep rectal resection with primary, circular stapler performed descendo-rectostomy. Following national guidelines and the recommendation of the local oncological board, a systemic chemotherapy with carboplatin and Etoposid was initiated and further switched to cisplatin and Etoposid due to hepatic progress. Patient 2 (donor of BKZ-3 cell line) was a 64 year old Caucasian male when admitted to the emergency room of the Protestant Hospital of Bethel Foundation (Bielefeld, Germany) with signs of sub-total ileus, abdominal crampy pain and a history of recurring nausea and vomitus paralleled by weight loss of 15 kg in the last three months prior admission. The patient presented a bloated abdomen without peritonism and scarce peristaltic of the bowel. CT-scan revealed a mass of the splenic flexure of the left colon suspicious for malignancy with distension of the pre-stenotic bowel (Figure 1E). Staging revealed no evidence of extra colonic malignant lesions. The patient was urgently scheduled for an open left hemicolectomy with worsening signs of mechanical bowel obstruction.

Isolation of genomic DNA of parental tumor tissue for *BRAF* mutation analysis was performed using automatically DNA-extraction with Maxwell® RSC DNA FFPE Kit and the Maxwell® RSC instrument (Promega, Walldorf, Germany) according to the manufacturers guidelines in the Institute of Pathology KRH Hospital Nordstadt (Hannover, Germany). Sequencing of isolated genomic DNA of parental tissue and genomic DNA of isolated cell lines (as described below) was performed using DTCS Quick Start Kit (Beckman Coulter Life Sciences, Indianapolis, IN, USA) and GenomeLab GeXP™ Genetic Analysis System (Beckman Coulter Life Sciences) according to the manufacturers guidelines.

Informed consent according to local and international guidelines was signed by both patients. All further experimental procedures were ethically approved (Ethics committee Münster, Germany, 2017-522-f-S).

4.2. Colorectal Cancer Cell Line Establishment and Cell Culture

To obtain primary tumor material for cell culture, a cubic sample measuring 5 mm was collected from each tumor type. The sample was transferred to ice-cold Dulbecco's Phosphate Buffered Saline (PBS; Sigma Aldrich, Munich, Germany) supplemented with antibiotics penicillin/streptomycin (500 µg/mL; Sigma Aldrich), gentamicin (100 µg/mL; Ratiopharm, Ulm, Germany) and metronidazole (5 µg/mL; B.Braun, Melsungen, Germany), as well as the antimycotic amphotericin B (12.5 µg/mL; Sigma Aldrich) to control colic microbiom contamination. For the isolation of the cells, the specimen was washed ten times with ice-cold PBS, mechanically disintegrated in 2–5 mm pieces followed by enzymatical digestion with collagenase for 2 h at 37 °C as described previously [63]. One half of the minced tissue was used to cultivate spheres in Dulbecco's Modified Eagle's medium/Ham's F-12 (Sigma Aldrich) with the addition of 2 mM L-Glutamin (Sigma Aldrich), penicillin/streptomycin (100 µg/mL), gentamicin (20 µg/mL), metronidazole (1 µg/mL), amphotericin B (2.5 µg/mL), EGF (20 ng/mL; Miltenyi Biotec, Bergisch Gladbach, Germany), FGF-2 (40 ng/mL; Miltenyi Biotec) and B27 supplement (Gibco, Thermo Fisher Scientific, Bremen, Germany) in low adhesion T25 tissue culture flasks. The other half of the tissue was used to grow adherent cells, where the cells were cultivated on gelatin from bovine skin (type B; Sigma Aldrich) coated culture dishes in the medium described above supplemented with 10% FCS (Sigma Aldrich).

Colon adenocarcinoma cell line HT-29 (DSMZ-German Collection of Microorganisms and Cell Cultures, Braunschweig, Germany) and colon carcinoma cell line HCT-116 (DSMZ-German Collection of Microorganisms and Cell Cultures) were maintained in McCoy's 5A medium (Sigma Aldrich) with 10% FCS, 2 mM L-Glutamin, and penicillin/streptomycin (100 µg/mL). Adult HDF (Genlantis, San Diego, CA, USA) were a kind gift from Dr. Isabel Faust, Institute for Laboratory and Transfusion Medicine, Heart and Diabetes Centre NRW (Bad Oeynhausen, Germany) and were cultured in Dulbecco's Modified Eagle's Medium-high glucose (Sigma Aldrich) with 10% FCS, 2 mM L-Glutamin, and penicillin/streptomycin (100 µg/mL). All cells were cultured at 37 °C and 5% CO2 in a humidified incubator.

Population doubling times were determined using the Orangu^{TM} Cell Counting Solution and were performed at least six times per cell population according to the manufacturers guidelines. For this 1000, 2500, 5000, 7500, and 10,000 cells per 100 µL CSC medium containing 10% FCS were seeded in a 96 well and used as a standard curve. To calculate the population doubling time 3000 cells per 100 µL CSC medium containing 10% FCS were seeded in a 96 well and cultured for 72 h, followed by the measurement of cell viability and quantification of cell count using the appropriate standard curve. Growth rates and population doubling times were determined by the following equations:

$$growth\ rate = \frac{\ln(xt) - \ln(x0)}{t - t0} \quad (1)$$

$$population\ doubling\ time = \frac{\ln(2)}{growth\ rate} \quad (2)$$

4.3. Immunocytochemistry and Immunohistochemistry

For immunocytochemical cell staining, BKZ-2, BKZ-3, HT-29, HCT-116, and HDF were pre-cultured as an explant culture as described above. After harvesting, 1.5×10^4 cells per 500 µL CSC medium supplemented with 10% FCS were planted on top of etched cover slips. After 2–3 days of cultivation, cells were fixed with 4% phosphate-buffered paraformaldehyde (lab-made) for 15 min at room temperature (RT) followed by three washing steps with 1 × PBS. Cells were blocked and permeabilized using 0.02% Triton-X 100 (Sigma Aldrich) with 5% appropriate serum (Dianova, Hamburg, Germany) or 1% bovine serum albumin (Sigma-Aldrich) for 30 min at RT. Afterwards, cells were incubated with primary antibodies for 1 h at RT. Antibodies used were anti-CD44 (1:400; 156-3C11; Cell Signaling, Frankfurt am Main, Germany), anti-CD133 (1:100; NB120-16518; NovusBio, Bio-Techne, Wiesbaden-Nordenstadt, Germany), anti-Nestin (1:200; MAB5326; Millipore, Merck, Darmstadt, Germany), anti-Synaptophysin (1:250; MAB5258;Abcam, Berlin, Germany), anti-SLUG (1:100; C19G7; Cell Signaling), anti-S100 (1:400; Z 0311; DAKO, Agilent, Santa Clara, CA, USA), anti-Dopamine (1:100; AB1225; Millipore, Merck), anti-vGLUT2 (1:50; MAB5504; Millipore, Merck), anti-TH (1:50; H-196; Santa Cruz, Heidelberg, Germany), anti-Cleaved Caspase-3 (1:400; Asp175/5A1E; Cell Signaling), anti-MYC (10 µg/mL; Y69; Abcam) and anti-NMYC (2,5 µg/mL; NCM II 100; Abcam). Secondary fluorochrome-conjugated antibodies (1:300; goat anti-mouse Alexa 555, goat anti-rabbit Alexa 555, goat anti-mouse Alexa 488; Life Technologies, Thermo Fisher Scientific) were incubated for 1 h at RT in the dark. Nuclear counterstaining was performed with 4',6-diamidino-2-phenylindole (DAPI; 1 µg/mL; Sigma Aldrich) for 10 min at RT. Fluorescence imaging was performed using a confocal laser scanning microscope (LSM 780; Carl Zeiss, Jena, Germany) and analyzed using ZEN software from the same provider or Fiji ImageJ [97]. For the quantification of immunofluorescence stainings, at least five images per condition were analyzed. Percentages of SLUG and Synaptophysin high and low cells were quantified by the mean of the nuclear fluorescence intensity, with cells showing a nuclear mean fluorescence intensity over 15,000 clustered as SLUG and Synaptophysin high. CD133 and CD44 high, medium and low cells were determined by 10 randomly applied measurements for fluorescence intensity on at least five images per cell population. HDF were used as negative control and their background fluorescence was subtracted from each measurement. Cells were classified as CD133 high: ≥ 10,000, CD133 medium:

< 10,000 ≥ 5000 and CD133 low: < 5000 ≥ 0. For CD44 expression, cells were classified in CD44 high: ≥ 2000, CD44 medium: < 2000 ≥ 1000 and CD44 low: < 1000 ≥ 0.

All immunohistochemical stainings, except for the staining for MYC and NMYC, were performed in the Institute of Pathology of KRH Hospital Nordstadt (Hannover, Germany) using the automated immunohistochemistry and in situ hybridization platform Dako Omnis (DAKO, Agilent) according to the manufacturer's instructions. Antibodies used were: Anti-CD56 (123C3; DAKO, Agilent), anti-CK20 (K_s20.8; DAKO, Agilent), anti-Ki67 (MIB-1; DAKO, Agilent), anti-Synaptophysin (DAK-SYNAP; DAKO, Agilent), anti-CDX2 (DAK-CDX2; DAKO, Agilent), anti-panCK (AE1/AE3; DAKO, Agilent), anti-PDL1 (22C3; DAKO, Agilent), anti-CK7 (OV-TL 12/30; DAKO, Agilent) and anti-SATB2 (EP281; Cell Marque, Rocklin, CA, USA). For visualization the EnVision FLEX, High pH (DAKO, Agilent) visualization system was used according to the manufacturers guidelines. Each scoring pathologist had specific training for the specific antibody and particular indication for testing as appropriate. Analysis of the expression of the immune checkpoint ligand PDL1 was done according to international standards [98].

$$TPS = \frac{PDL1\ positive\ vital\ tumor\ cells}{PDL1\ positive + negative\ vital\ tumor\ cells} \quad (3)$$

$$CPS = \frac{PDL1\ positive\ vital\ tumor\ cells + lymphocytes + macrophages}{PDL1\ positive + negative\ vital\ tumor\ cells} * 100 \quad (4)$$

$$IC = \frac{PDL1\ positive\ lymphocytes + macrophages + dendritic\ cells + granulocytes}{tumor\ area} \quad (5)$$

IC is given as a score with the following values: 0 = 0–<1%, 1 = ≥1%–<5%, 2 = 5%–<10%, 3 = ≥10%. For immunocytochemical staining of MYC and NMYC paraffin-embedded sections were deparaffinized and rehydrated. For this, sections were washed two times for 10 min in xylol followed by 10 min 100% ethanol. Afterwards, sections were rehydrated by 5 min washes in 90% ethanol, followed by 80% ethanol and 70% ethanol. Epitope retrieval was performed by boiling the slides within 0.01 M citrate buffer, pH 6.0 (lab made) for 20 min. After cool down for at least 30 min at RT slides were washed two times with 0.02% Triton-X 100. Afterwards, slides were blocked and permeabilized using 0.02%Triton-X 100 with 10% appropriate serum (Dianova) and 1% bovine serum albumin for 2 h at RT. Anti-MYC (5 µg/mL; Y69; Abcam) and anti-NMYC (5 µg/mL; NCM II 100; Abcam) first antibodies were diluted in blocking solution and incubated over night at 4 °C. After three washing steps in PBS, secondary fluorochrome-conjugated antibodies (1:300; goat anti-mouse Alexa 555, goat anti-rabbit Alexa 555; Life Technologies, Thermo Fisher Scientific) were applied and incubated for 1 h at RT in the dark. Nuclear counterstaining was performed with DAPI (1 µg/mL) for 10 min at RT and fluorescence imaging was performed using a confocal laser scanning microscope (LSM 780; Carl Zeiss) and analyzed using Fiji ImageJ.

4.4. Sphere-Formation and ATRA-Treatments

To analyze the sphere-formation capacity of BKZ-2 and BKZ-3, cells were cultured in low adhesion culture plates in CSC medium without FCS with different concentrations of heparin. Cells were seeded in triplicates at 1×10^5 cells per 1000 µL CSC medium. Heparin (Sigma Aldrich) was added in concentrations of 3 µg/mL, 4 µg/mL, 5 µg/mL or 0 µg/mL as a control. Cells were cultured for seven days in a humidified cell incubator at 37 °C and 5% CO_2. The size of the spheres was quantified for each treatment condition at day 2, day 4, and day 7 after initial cell seeding. Therefore, five randomized images of each well were taken, and every sphere was measured in length and width using Fiji ImageJ. Then, the diameter of each sphere as mean of length and width was calculated. For the comparison of sphere formation capacity of BKZ-2, BKZ-3 with HT-29 and HCT-116 and for sphere-formation under the treatment of different concentrations of ATRA (Sigma Aldrich), cells were seeded at 5000 cells per 200 µL CSC medium containing 4 µg/ml heparin in a low adhesion 96 well-plate and cultured for five days. For the treatment, medium was supplemented with 1 µM ATRA, 5 µM ATRA, 10 µM ATRA or

dimethylsulfoxide (DMSO) as a control in triplicates for each treatment condition. For quantification, two representative images of each well were taken and every sphere was measured in length and width using Fiji ImageJ, with the mean of both representing the diameter of each sphere. Volume of spheres was determined using the formula:

$$V = \frac{4}{3} * \pi * \left(\frac{sphere\ diameter}{2}\right)^2 \quad (6)$$

The number of spheres was calculated by counting each sphere of all six representative images for each condition. For total cell mass calculation, mean of sphere volume was multiplied with the mean of sphere number. According to Weiswald and colleagues, spheres with a diameter of ≥ 20 µm were considered for further evaluation [17]. For the analysis of the influence of ATRA on BKZ-2 and BKZ-3 in monolayer, 3000 cells per 100 µL CSC medium containing 10% FCS were seeded in a 0.1% gelatin coated 96 well-plate. Additionally, 1000, 2500, 5000, 7500, and 10,000 cells per 100 µL medium were seeded in a 96 well for a standard curve. After adherence of the cells, cell viability was measured for the standard curve and ATRA was applied as described above. After 5 days of treatment, cell viability was measured and cell count was quantified using the standard curve. Each treatment condition was performed in triplicates. For the immunocytochemical staining of cleaved caspase 3 after ATRA-treatment, 1.5×10^4 cells per 500 µL CSC medium containing 10% FCS were seeded in a 24 well on top of etched cover slips. After adherence, cells were treated with different ATRA concentrations as well as DMSO as control for five days. Afterwards, cleaved caspase 3 immunocytochemical staining was performed as described above.

4.5. Real-Time PCR

RNA isolation of cultivated cell populations was done using the NucleoSpin® RNA Plus kit (Machery-Nagel, Düren, Germany) according to the manufacturers instruction. Quality and concentration of RNA were assessed via Nanodrop ultraviolet spectrophotometry. Copy DNA (cDNA) synthesis was performed using 1 µg of RNA and the First Strand cDNA Synthesis Kit (Thermo Fisher Scientific). For the synthesis, random hexamer primers were used. qPCR were performed in triplicates using 2 × qPCR SyGreen Mix (PCR Biosystems, London, UK), according to the manufacturer's instructions, and assayed with the Eco48 (PCRmax, Stone, Staffordshire, UK). Used primers (Sigma Aldrich) are listed in Table 1. Isolation of the genomic DNA for the analysis of gene copy number of *NMYC* and *MYC* was done using QUIamp® DNA Mini Kit (Qiagen, Hilden, Germany) according to the manufacturer's guidelines. Quantification of gene copy number was performed in triplicates using Platinum SYBR Green qPCR Super-Mix UDG (Invitrogen, Thermo Fisher Scientific), according to the manufacturers guidelines, and assayed with a Rotor Gene 6000 (Qiagen). Each gene assay included: (1) a no-template control, (2) 10 ng of calibrator human genomic DNA of MSCs (Lonza, Basel, Switzerland), and (3) 10 ng of tumor DNA. Haploid copy number was determined according to De Preter et al. [99].

Table 1. Primer sequences for quantitative polymerase chain reaction.

Target	Sequence 5′-3′
CD44 antigen (*CD44*)	CTACAAGCACAATCCAGGCAA
Rev-*CD44*	GCATTGGATGGCTGGTATGA
Programed death ligand 1 (*PDL1*)	CCCAGTTCTGCGCAGCTT
Rev-*PDL1*	ACCGTGACAGTAAATGCGTTC
Programed death ligand 2 (*PDL2*)	TCCAACTTGGCTGCTTCACA
Rev-*PDL2*	CCACAGGTTCAGATAGCACTGT
Prominin-1 (*CD133*)	AACAGTTTGCCCCCAGGAAA
Rev-*CD133*	GAAGGACTCGTTGCTGGTGA
Epithelial cell adhesion molecule (*EPCAM*)	GCTGGCCGTAAACTGCTTTG
Rev-*EPCAM*	ACATTTGGCAGCCAGCTTTG
N-myc proto-oncogene (*NMYC*) *(genomic)*	CGCAAAAGCCACCTCTCATTA
Rev-*NMYC (genomic)*	TCCAGCAGATGCCACATAAGG
Octamer-binding transcription factor 4 (*OCT4*)	CGAAAGAGAAAGCGAACCAG
Rev-*OCT4*	GCCGGTTACAGAACCACACT
Myc proto-oncogene (*MYC*) *(genomic)*	AAAAGTGGGCGGCTGGATAC
Rev-*MYC (genomic)*	AGGGATGGGAGGAAACGCTA
SRY-box transcription factor 2 (*SOX2*)	GGCACTTTGCACTGGAACTT
Rev-*SOX2*	AGGCTGCTGGTTTTCCACTA
Twist family bHLH transcription factor 1 (*TWIST*)	GTCCGCAGTCTTACGAGGAG
Rev-*TWIST*	CCAGCTTGAGGGTCTGAATC
Snail family transcriptional repressor 1 (*SNAIL*)	CCCAATCGGAAGCCTAACTA
Rev-*SNAIL*	GGACAGAGTCCCAGATGAGC
Snail family transcriptional repressor 2 (*SLUG*)	TCGGACCCACACATTACCTT
Rev-*SLUG*	TTGGAGCAGTTTTTGCACTG
Actin beta	TCCCTGGAGAAGAGCTACGA
Rev-Actin beta	AGCACTGTGTTGGCGTACAG
Eukaryotic translation elongation factor 2 (*EEF2*)	AGGTCGGTTCTACGCCTTTG
Rev-*EEF2*	TTCCCACAAGGCACATCCTC
Syndecan 4 *(genomic)*	CAGGGTCTGGGAGCCAAGT
Rev-Syndecan 4 *(genomic)*	GCACAGTGCTGGACATTGACA
Glyceraldehyde-3-phosphate dehydrogenase *(genomic)*	AGACTGGCTCTTAAAAAGTGCAGG
Rev-Glyceraldehyde-3-phosphate dehydrogenase *(genomic)*	TGCTGTAGCCAAATTCGTTGTC

4.6. MYC Inhibitor Treatment

To analyze the influence of the proto-oncogenes *MYC* and *NMYC*, cells were treated with different concentrations of the MYC and NMYC inhibitor KJ-Pyr-9 (Merck) and cell viability assays using Orangu^{TM} were performed in triplicates according to the manufacturers guidelines. For this, cells were seeded in 0.1% gelatin coated 96 well-plates in the amount of 1000, 2500, 5000, 7500 and 10,000 cells per 100 µL CSC medium containing 10% FCS for a standard curve and in the amount of 3000 cells per 100 µL CSC medium containing 10% FCS for the treatment. After adherence of the cells, cell viability was measured for the standard curve and treatment was started applying KJ-Pyr-9 in the concentrations of 10 µM, 20 µM, 40 µM, and 60 µM, as well as DMSO as control to the CSC medium supplemented with 10% FCS. After 5 days of treatment, cell viability was measured, and cell count was quantified using the standard curve. Survival rate was calculated by normalizing each cell count to the mean of controls for BKZ-2 and BKZ-3. For the immunocytochemical staining of cleaved caspase 3 after KJ-Pyr-9-treatment, 1.5×10^4 cells per 500 µL CSC medium containing 10% FCS were seeded in a 24 well on top of etched cover slips. After adherence, cells were treated with 10 µM, 20 µM, 40 µM or 60 µM of KJ-Pyr-9 or DMSO as a control for five days. Afterwards, cleaved caspase 3 immunocytochemical staining was performed as described above.

4.7. Flow Cytometry

To determine the ALDH-activity, BKZ-2 and BKZ-3 were pre-cultured as an explant culture as described above. After harvesting, using trypsin, cells were analyzed with the ALDEFLUOR™ Kit (STEMCELL Technologies Inc., Vancouver, BC, Canada) according to the manufacturer's instructions by flow cytometry on a Gallios flow-cytometer (Beckman Coulter Life Sciences). Dead cells were excluded by Propidium Iodide (Sigma Aldrich) co-staining and spectral overlap was compensated using samples of the K562 cell line (DSMZ-German Collection of Microorganisms and Cell Cultures), which also served as positive control. BKZ-2 and BKZ-3 cells were analyzed in parallel to yield comparable results.

4.8. Statistical Analysis

Data were raised at least in triplicates and statistically analyzed by using Prism V5.01 software (GraphPad Software, Inc., San Diego, CA, USA). Test for normality was performed by use of D'Agnostino & Pearson omnibus normality test. Student's *t*-test, non-parametric Kruskal–Wallis analysis of variance (ANOVA) and Dunn's Multiple Comparison post-hoc test or non-parametric Mann–Whitney-test were performed to assess differences between multiple groups. A significance value of $p \leq 0.05$ was considered as statistically significant. The data are presented as the means ± standard error of the mean (SEM).

5. Conclusions

In summary, we isolated the two novel colorectal cancer cell lines BKZ-2 and BKZ-3, originating from a rare rectal neuroendocrine carcinoma and a colorectal AC, respectively, both containing a subpopulation with potential stem-like properties. Thus, BKZ-2 and BKZ-3 represent excellent new in vitro models to study colorectal cancer in cellular systems. Higher expression of CD133 and CD44 of both cell populations and a higher number of formed spheres in comparison to well-established colon carcinoma cell lines HT-29 and HCT-116 validated the existence of a subpopulation with potential stem cell-like phenotype. Moreover, initial characterization revealed a gene copy number gain of the proto-oncogene *NMYC* for both cell lines. Indirect inhibition of MYC/NMYC activity with ATRA led to decreased sphere volume and total cell mass for BKZ-2, although not for BKZ-3, which is probably caused by its effect on proliferation. Inhibition of the protein–protein interaction of MYC and NMYC with MAX utilizing KJ-Pyr-9 exhibited a significant reduction in the survival rate of both cell lines by the induction of apoptosis. Consequently, the blockage of these interactions may serve as a possible treatment strategy for colorectal cancer cell lines with increased *NMYC* copy number. However, differences in phenotype and the modulation of proliferation subsequent to ATRA-treatment, respectively, underline the complexity of signaling pathways involved in tumorigenesis and CSC maintenance of the different subclasses of colorectal cancer cells warranting further studies on this relevant topic.

Supplementary Materials: The following are available online at http://www.mdpi.com/2072-6694/12/9/2582/s1, Figure S1: Expression of neuronal and neural crest related proteins in BKZ-2 and BKZ-3 cells, Figure S2: Immunocytochemical staining of adult human dermal fibroblasts (HDF) as negative control for confocal laser scanning microscopy, Figure S3: BKZ-2 and BKZ-3 are highly positive for cancer stem cell-markers prominin-1 (CD133) and CD44 antigen (CD44), Figure S4: All-trans retinoic acid (ATRA)-treatment reduces proliferation of BKZ-2 cells, but does not affect BKZ-3.

Author Contributions: Conceptualization, B.K. and C.K.; Data curation, J.S.a.E., B.A.W., J.H., C.F., L.W., B.K., and C.K.; Formal analysis, J.S.a.E. and B.A.W.; Funding acquisition, J.S.a.E., B.K., and C.K.; Investigation, J.S.a.E., B.A.W., J.H., and J.S.; Project administration, B.K. and C.K.; Supervision, B.K. and C.K.; Visualization, J.S.a.E., B.A.W., and M.K.; Writing—original draft, J.S.a.E., B.A.W., J.H., C.F., L.W., B.K., and C.K.; Writing—review & editing, J.S.a.E., B.A.W., J.H., J.S., C.F., L.W., M.K., B.K., and C.K. All authors have read and agreed to the published version of the manuscript.

Funding: This research was funded in part by the University of Bielefeld. Beatrice Ariane Windmöller is funded by an internal grant of the Bethel Foundation, Bielefeld, Germany.

Acknowledgments: The excellent technical assistance of Angela Kralemann-Köhler, Elke Redecker, Claudia Rose and Ulrike Hormel is gratefully acknowledged. The authors thank Isabel Faust for kindly providing adult human dermal fibroblasts. The authors acknowledge support for the publication costs by the Deutsche Forschungsgemeinschaft and the Open Access Publication Fund of Bielefeld University.

Conflicts of Interest: The authors declare no conflict of interest.

References

1. Bray, F.; Ferlay, J.; Soerjomataram, I.; Siegel, R.L.; Torre, L.A.; Jemal, A. Global cancer statistics 2018: GLOBOCAN estimates of incidence and mortality worldwide for 36 cancers in 185 countries. *CA Cancer J. Clin.* **2018**, *68*, 394–424. [CrossRef]
2. Centelles, J.J. General aspects of colorectal cancer. *ISRN Oncol.* **2012**, *2012*, 139268. [CrossRef]
3. Munro, M.J.; Wickremesekera, S.K.; Peng, L.; Tan, S.T.; Itinteang, T. Cancer stem cells in colorectal cancer: A review. *J. Clin. Pathol.* **2018**, *71*, 110–116. [CrossRef] [PubMed]
4. Kim, J.J.; Park, S.S.; Lee, T.-G.; Lee, H.-C.; Lee, S.-J. Large Cell Neuroendocrine Carcinoma of the Colon with Carcinomatosis Peritonei. *Ann. Coloproctol.* **2018**, *34*, 222–225. [CrossRef] [PubMed]
5. Saclarides, T.J.; Szeluga, D.; Staren, E.D. Neuroendocrine cancers of the colon and rectum. Results of a ten-year experience. *Dis. Colon Rectum* **1994**, *37*, 635–642. [CrossRef] [PubMed]
6. Abbasian, M.; Mousavi, E.; Arab-Bafrani, Z.; Sahebkar, A. The most reliable surface marker for the identification of colorectal cancer stem-like cells: A systematic review and meta-analysis. *J. Cell. Physiol.* **2019**, *234*, 8192–8202. [CrossRef]
7. Takahashi, Y.; Onda, M.; Tanaka, N.; Seya, T. Establishment and characterization of two new rectal neuroendocrine cell carcinoma cell lines. *Digestion* **2000**, *62*, 262–270. [CrossRef]
8. Pfragner, R.; Behmel, A.; Höger, H.; Beham, A.; Ingolic, E.; Stelzer, I.; Svejda, B.; Moser, V.A.; Obenauf, A.C.; Siegl, V.; et al. Establishment and characterization of three novel cell lines—P-STS, L-STS, H-STS—Derived from a human metastatic midgut carcinoid. *Anticancer Res.* **2009**, *29*, 1951–1961.
9. Krieg, A.; Mersch, S.; Boeck, I.; Dizdar, L.; Weihe, E.; Hilal, Z.; Krausch, M.; Möhlendick, B.; Topp, S.A.; Piekorz, R.P.; et al. New model for gastroenteropancreatic large-cell neuroendocrine carcinoma: Establishment of two clinically relevant cell lines. *PLoS ONE* **2014**, *9*, e88713. [CrossRef]
10. Dizdar, L.; Drusenheimer, J.; Werner, T.A.; Möhlendick, B.; Schütte, S.C.; Esposito, I.; Filler, T.J.; Knoefel, W.T.; Krieg, A. Establishment and Characterization of a Novel Cell Line Derived from a Small Cell Neuroendocrine Carcinoma of the Anal Canal. *Neuroendocrinology* **2018**, *107*, 246–256. [CrossRef]
11. Yanagihara, K.; Kubo, T.; Mihara, K.; Kuwata, T.; Ochiai, A.; Seyama, T.; Yokozaki, H. Establishment of a novel cell line from a rare human duodenal poorly differentiated neuroendocrine carcinoma. *Oncotarget* **2018**, *9*, 36503–36514. [CrossRef]
12. Gock, M.; Mullins, C.S.; Harnack, C.; Prall, F.; Ramer, R.; Göder, A.; Krämer, O.H.; Klar, E.; Linnebacher, M. Establishment, functional and genetic characterization of a colon derived large cell neuroendocrine carcinoma cell line. *World J. Gastroenterol.* **2018**, *24*, 3749–3759. [CrossRef]
13. Vlashi, E.; Pajonk, F. Cancer Stem Cells, Cancer Cell Plasticity and Radiation Therapy. *Semin. Cancer Biol.* **2014**, *31*, 28–35. [CrossRef]
14. Kaltschmidt, C.; Banz-Jansen, C.; Benhidjeb, T.; Beshay, M.; Förster, C.; Greiner, J.; Hamelmann, E.; Jorch, N.; Mertzlufft, F.; Pfitzenmaier, J.; et al. A Role for NF-κB in Organ Specific Cancer and Cancer Stem Cells. *Cancers* **2019**, *11*, 655. [CrossRef]
15. Ishiguro, T.; Ohata, H.; Sato, A.; Yamawaki, K.; Enomoto, T.; Okamoto, K. Tumor-derived spheroids: Relevance to cancer stem cells and clinical applications. *Cancer Sci.* **2017**, *108*, 283–289. [CrossRef]
16. Ohata, H.; Ishiguro, T.; Aihara, Y.; Sato, A.; Sakai, H.; Sekine, S.; Taniguchi, H.; Akasu, T.; Fujita, S.; Nakagama, H.; et al. Induction of the stem-like cell regulator CD44 by Rho kinase inhibition contributes to the maintenance of colon cancer-initiating cells. *Cancer Res.* **2012**, *72*, 5101–5110. [CrossRef]
17. Weiswald, L.-B.; Richon, S.; Massonnet, G.; Guinebretière, J.-M.; Vacher, S.; Laurendeau, I.; Cottu, P.; Marangoni, E.; Nemati, F.; Validire, P.; et al. A short-term colorectal cancer sphere culture as a relevant tool for human cancer biology investigation. *Br. J. Cancer* **2013**, *108*, 1720–1731. [CrossRef]
18. Zhang, H.-L.; Wang, P.; Lu, M.-Z.; Zhang, S.-D.; Zheng, L. c-Myc maintains the self-renewal and chemoresistance properties of colon cancer stem cells. *Oncol. Lett.* **2019**, *17*, 4487–4493. [CrossRef]

19. Humphries, H.N.; Wickremesekera, S.K.; Marsh, R.W.; Brasch, H.D.; Mehrotra, S.; Tan, S.T.; Itinteang, T. Characterization of Cancer Stem Cells in Colon Adenocarcinoma Metastasis to the Liver. *Front. Surg.* **2017**, *4*, 76. [CrossRef] [PubMed]
20. Elbadawy, M.; Usui, T.; Yamawaki, H.; Sasaki, K. Emerging Roles of C-Myc in Cancer Stem Cell-Related Signaling and Resistance to Cancer Chemotherapy: A Potential Therapeutic Target against Colorectal Cancer. *Int. J. Mol. Sci.* **2019**, *20*, 2340. [CrossRef] [PubMed]
21. Berger, A.; Brady, N.J.; Bareja, R.; Robinson, B.; Conteduca, V.; Augello, M.A.; Puca, L.; Ahmed, A.; Dardenne, E.; Lu, X.; et al. N-Myc-mediated epigenetic reprogramming drives lineage plasticity in advanced prostate cancer. *J. Clin. Investig.* **2019**, *130*, 3924–3940. [CrossRef] [PubMed]
22. Kim, H.-Y.; Kim, Y.-M.; Hong, S. Astaxanthin suppresses the metastasis of colon cancer by inhibiting the MYC-mediated downregulation of microRNA-29a-3p and microRNA-200a. *Sci. Rep.* **2019**, *9*, 9457. [CrossRef] [PubMed]
23. Zhou, B.P.; Hung, M.-C. Wnt, hedgehog and snail: Sister pathways that control by GSK-3beta and beta-Trcp in the regulation of metastasis. *Cell Cycle* **2005**, *4*, 772–776. [CrossRef] [PubMed]
24. Thiery, J.P.; Sleeman, J.P. Complex networks orchestrate epithelial-mesenchymal transitions. *Nat. Rev. Mol. Cell Biol.* **2006**, *7*, 131–142. [CrossRef]
25. Xu, F.; Li, S.; Zhang, J.; Wang, L.; Wu, X.; Wang, J.; Huang, Q.; Lai, M. Cancer Stemness, Immune Cells, and Epithelial-Mesenchymal Transition Cooperatively Predict Prognosis in Colorectal Carcinoma. *Clin. Colorectal Cancer* **2018**, *17*, e579–e592. [CrossRef]
26. Kong, H.; Liu, X.; Yang, L.; Qi, K.; Zhang, H.; Zhang, J.; Huang, Z.; Wang, H. All-trans retinoic acid enhances bystander effect of suicide gene therapy in the treatment of breast cancer. *Oncol. Rep.* **2016**, *35*, 1868–1874. [CrossRef]
27. Otsuka, K.; Sasada, M.; Iyoda, T.; Nohara, Y.; Sakai, S.; Asayama, T.; Suenaga, Y.; Yokoi, S.; Higami, Y.; Kodama, H.; et al. Combining peptide TNIIIA2 with all-trans retinoic acid accelerates N-Myc protein degradation and neuronal differentiation in MYCN-amplified neuroblastoma cells. *Am. J. Cancer Res.* **2019**, *9*, 434–448.
28. Karsy, M.; Albert, L.; Tobias, M.E.; Murali, R.; Jhanwar-Uniyal, M. All-trans retinoic acid modulates cancer stem cells of glioblastoma multiforme in an MAPK-dependent manner. *Anticancer Res.* **2010**, *30*, 4915–4920.
29. Modarai, S.R.; Gupta, A.; Opdenaker, L.M.; Kowash, R.; Masters, G.; Viswanathan, V.; Zhang, T.; Fields, J.Z.; Boman, B.M. The anti-cancer effect of retinoic acid signaling in CRC occurs via decreased growth of ALDH+ colon cancer stem cells and increased differentiation of stem cells. *Oncotarget* **2018**, *9*, 34658–34669. [CrossRef]
30. Gianni', M.; Boldetti, A.; Guarnaccia, V.; Rambaldi, A.; Parrella, E.; Raska, I.; Rochette-Egly, C.; Del Sal, G.; Rustighi, A.; Terao, M.; et al. Inhibition of the peptidyl-prolyl-isomerase Pin1 enhances the responses of acute myeloid leukemia cells to retinoic acid via stabilization of RARalpha and PML-RARalpha. *Cancer Res.* **2009**, *69*, 1016–1026. [CrossRef]
31. Shi, G.; Zheng, X.; Wu, X.; Wang, S.; Wang, Y.; Xing, F. All-trans retinoic acid reverses epithelial-mesenchymal transition in paclitaxel-resistant cells by inhibiting nuclear factor kappa B and upregulating gap junctions. *Cancer Sci.* **2019**, *110*, 379–388. [CrossRef] [PubMed]
32. Leng, Z.; Xia, Q.; Chen, J.; Li, Y.; Xu, J.; Zhao, E.; Zheng, H.; Ai, W.; Dong, J. Lgr5+CD44+EpCAM+ Strictly Defines Cancer Stem Cells in Human Colorectal Cancer. *Cell. Physiol. Biochem.* **2018**, *46*, 860–872. [CrossRef] [PubMed]
33. Zhou, Y.; Xia, L.; Wang, H.; Oyang, L.; Su, M.; Liu, Q.; Lin, J.; Tan, S.; Tian, Y.; Liao, Q.; et al. Cancer stem cells in progression of colorectal cancer. *Oncotarget* **2017**, *9*, 33403–33415. [CrossRef] [PubMed]
34. Mia-Jan, K.; Munkhdelger, J.; Lee, M.-R.; Ji, S.-Y.; Kang, T.Y.; Choi, E.; Cho, M.-Y. Expression of CD133 in neuroendocrine neoplasms of the digestive tract: A detailed immunohistochemical analysis. *Tohoku J. Exp. Med.* **2013**, *229*, 301–309. [CrossRef] [PubMed]
35. Shinji, S.; Sasaki, N.; Yamada, T.; Koizumi, M.; Ohta, R.; Matsuda, A.; Yokoyama, Y.; Takahashi, G.; Hotta, M.; Hara, K.; et al. Establishment and characterization of a novel neuroendocrine carcinoma cell line derived from a human ascending colon tumor. *Cancer Sci.* **2019**, *110*, 3708–3717. [CrossRef]
36. Lee, Y.-J.; Wu, C.-C.; Li, J.-W.; Ou, C.-C.; Hsu, S.-C.; Tseng, H.-H.; Kao, M.-C.; Liu, J.-Y. A rational approach for cancer stem-like cell isolation and characterization using CD44 and prominin-1(CD133) as selection markers. *Oncotarget* **2016**, *7*, 78499–78515. [CrossRef]

37. Jang, J.-W.; Song, Y.; Kim, S.-H.; Kim, J.; Seo, H.R. Potential mechanisms of CD133 in cancer stem cells. *Life Sci.* **2017**, *184*, 25–29. [CrossRef]
38. Liou, G.-Y. CD133 as a regulator of cancer metastasis through the cancer stem cells. *Int. J. Biochem. Cell Biol.* **2019**, *106*, 1–7. [CrossRef]
39. Todaro, M.; Francipane, M.G.; Medema, J.P.; Stassi, G. Colon cancer stem cells: Promise of targeted therapy. *Gastroenterology* **2010**, *138*, 2151–2162. [CrossRef]
40. Kazama, S.; Kishikawa, J.; Kiyomatsu, T.; Kawai, K.; Nozawa, H.; Ishihara, S.; Watanabe, T. Expression of the stem cell marker CD133 is related to tumor development in colorectal carcinogenesis. *Asian J. Surg.* **2018**, *41*, 274–278. [CrossRef]
41. Prochazka, L.; Tesarik, R.; Turanek, J. Regulation of alternative splicing of CD44 in cancer. *Cell. Signal.* **2014**, *26*, 2234–2239. [CrossRef] [PubMed]
42. Yan, Y.; Zuo, X.; Wei, D. Concise Review: Emerging Role of CD44 in Cancer Stem Cells: A Promising Biomarker and Therapeutic Target. *Stem Cells Transl. Med.* **2015**, *4*, 1033–1043. [CrossRef] [PubMed]
43. Neradil, J.; Veselska, R. Nestin as a marker of cancer stem cells. *Cancer Sci.* **2015**, *106*, 803–811. [CrossRef] [PubMed]
44. Wang, P.; Suo, Z.; Wang, M.; Høifødt, H.K.; Fodstad, O.; Gaudernack, G.; Kvalheim, G. In vitro and in vivo properties of CD133 expressing cells from human lung cancer cell lines. *Exp. Hematol. Oncol.* **2013**, *2*, 16. [CrossRef] [PubMed]
45. Wang, Y.; Zhou, L.; Qing, Q.; Li, Y.; Li, L.; Dong, X.; Xiao, B. Gene expression profile of cancer stem-like cells in the SW480 colon adenocarcinoma cell line. *Oncol. Rep.* **2019**, *42*, 386–398. [CrossRef]
46. Moore, N.; Houghton, J.; Lyle, S. Slow-cycling therapy-resistant cancer cells. *Stem Cells Dev.* **2012**, *21*, 1822–1830. [CrossRef]
47. Barbato, L.; Bocchetti, M.; Di Biase, A.; Regad, T. Cancer Stem Cells and Targeting Strategies. *Cells* **2019**, *8*, 926. [CrossRef]
48. Bläker, H.; Alwers, E.; Arnold, A.; Herpel, E.; Tagscherer, K.E.; Roth, W.; Jansen, L.; Walter, V.; Kloor, M.; Chang-Claude, J.; et al. The Association Between Mutations in BRAF and Colorectal Cancer-Specific Survival Depends on Microsatellite Status and Tumor Stage. *Clin. Gastroenterol. Hepatol.* **2019**, *17*, 455–462.e6. [CrossRef]
49. Davies, H.; Bignell, G.R.; Cox, C.; Stephens, P.; Edkins, S.; Clegg, S.; Teague, J.; Woffendin, H.; Garnett, M.J.; Bottomley, W.; et al. Mutations of the BRAF gene in human cancer. *Nature* **2002**, *417*, 949–954. [CrossRef]
50. Mas, L.; Bachet, J.-B.; Taly, V.; Bouché, O.; Taieb, J.; Cohen, R.; Meurisse, A.; Normand, C.; Gornet, J.-M.; Artru, P.; et al. BRAF Mutation Status in Circulating Tumor DNA from Patients with Metastatic Colorectal Cancer: Extended Mutation Analysis from the AGEO RASANC Study. *Cancers* **2019**, *11*, 998. [CrossRef]
51. Beumer, J.; Clevers, H. Regulation and plasticity of intestinal stem cells during homeostasis and regeneration. *Development* **2016**, *143*, 3639–3649. [CrossRef] [PubMed]
52. He, S.; Zhou, H.; Zhu, X.; Hu, S.; Fei, M.; Wan, D.; Gu, W.; Yang, X.; Shi, D.; Zhou, J.; et al. Expression of Lgr5, a marker of intestinal stem cells, in colorectal cancer and its clinicopathological significance. *Biomed. Pharmacother.* **2014**, *68*, 507–513. [CrossRef] [PubMed]
53. Uchida, H.; Yamazaki, K.; Fukuma, M.; Yamada, T.; Hayashida, T.; Hasegawa, H.; Kitajima, M.; Kitagawa, Y.; Sakamoto, M. Overexpression of leucine-rich repeat-containing G protein-coupled receptor 5 in colorectal cancer. *Cancer Sci.* **2010**, *101*, 1731–1737. [CrossRef] [PubMed]
54. Fumagalli, A.; Oost, K.C.; Kester, L.; Morgner, J.; Bornes, L.; Bruens, L.; Spaargaren, L.; Azkanaz, M.; Schelfhorst, T.; Beerling, E.; et al. Plasticity of Lgr5-Negative Cancer Cells Drives Metastasis in Colorectal Cancer. *Cell Stem Cell* **2020**, *26*, 569–578.e7. [CrossRef]
55. Trzpis, M.; McLaughlin, P.M.J.; de Leij, L.M.F.H.; Harmsen, M.C. Epithelial cell adhesion molecule: More than a carcinoma marker and adhesion molecule. *Am. J. Pathol.* **2007**, *171*, 386–395. [CrossRef]
56. Maetzel, D.; Denzel, S.; Mack, B.; Canis, M.; Went, P.; Benk, M.; Kieu, C.; Papior, P.; Baeuerle, P.A.; Munz, M.; et al. Nuclear signalling by tumour-associated antigen EpCAM. *Nat. Cell Biol.* **2009**, *11*, 162–171. [CrossRef]
57. Raffel, A.; Eisenberger, C.F.; Cupisti, K.; Schott, M.; Baldus, S.E.; Hoffmann, I.; Aydin, F.; Knoefel, W.T.; Stoecklein, N.H. Increased EpCAM expression in malignant insulinoma: Potential clinical implications. *Eur. J. Endocrinol.* **2010**, *162*, 391–398. [CrossRef]

58. Zheng, J.; Xu, L.; Pan, Y.; Yu, S.; Wang, H.; Kennedy, D.; Zhang, Y. Sox2 modulates motility and enhances progression of colorectal cancer via the Rho-ROCK signaling pathway. *Oncotarget* **2017**, *8*, 98635–98645. [CrossRef]
59. Yang, T.; Fang, S.; Zhang, H.-X.; Xu, L.-X.; Zhang, Z.-Q.; Yuan, K.-T.; Xue, C.-L.; Yu, H.-L.; Zhang, S.; Li, Y.-F.; et al. N-3 PUFAs have antiproliferative and apoptotic effects on human colorectal cancer stem-like cells in vitro. *J. Nutr. Biochem.* **2013**, *24*, 744–753. [CrossRef]
60. Han, X.; Fang, X.; Lou, X.; Hua, D.; Ding, W.; Foltz, G.; Hood, L.; Yuan, Y.; Lin, B. Silencing SOX2 induced mesenchymal-epithelial transition and its expression predicts liver and lymph node metastasis of CRC patients. *PLoS ONE* **2012**, *7*, e41335. [CrossRef]
61. Krejčí, E.; Kodet, O.; Szabo, P.; Borský, J.; Smetana, K.; Grim, M.; Dvořánková, B. In vitro differences of neonatal and later postnatal keratinocytes and dermal fibroblasts. *Physiol. Res.* **2015**, *64*, 561–569. [CrossRef]
62. Wiedenmann, B.; Franke, W.W.; Kuhn, C.; Moll, R.; Gould, V.E. Synaptophysin: A marker protein for neuroendocrine cells and neoplasms. *Proc. Natl. Acad. Sci. USA* **1986**, *83*, 3500–3504. [CrossRef] [PubMed]
63. Windmöller, B.A.; Greiner, J.F.W.; Förster, C.; Wilkens, L.; Mertzlufft, F.; Am Schulte Esch, J.; Kaltschmidt, B.; Kaltschmidt, C.; Beshay, M. A typical carcinoid of the lung—A case report with pathological correlation and propagation of the cancer stem cell line BKZ1 with synaptophysin expression. *Medicine* **2019**, *98*, e18174. [CrossRef] [PubMed]
64. Tian, T.; Li, X.; Hua, Z.; Ma, J.; Liu, Z.; Chen, H.; Cui, Z. S100A1 promotes cell proliferation and migration and is associated with lymph node metastasis in ovarian cancer. *Discov. Med.* **2017**, *23*, 235–245.
65. Ohata, H.; Shiokawa, D.; Obata, Y.; Sato, A.; Sakai, H.; Fukami, M.; Hara, W.; Taniguchi, H.; Ono, M.; Nakagama, H.; et al. NOX1-Dependent mTORC1 Activation via S100A9 Oxidation in Cancer Stem-like Cells Leads to Colon Cancer Progression. *Cell Rep.* **2019**, *28*, 1282–1295.e8. [CrossRef] [PubMed]
66. El Mestikawy, S.; Wallén-Mackenzie, A.; Fortin, G.M.; Descarries, L.; Trudeau, L.-E. From glutamate co-release to vesicular synergy: Vesicular glutamate transporters. *Nat. Rev. Neurosci.* **2011**, *12*, 204–216. [CrossRef]
67. Nilubol, N.; Freedman, E.M.; Quezado, M.M.; Patel, D.; Kebebew, E. Pancreatic Neuroendocrine Tumor Secreting Vasoactive Intestinal Peptide and Dopamine With Pulmonary Emboli: A Case Report. *J. Clin. Endocrinol. Metab.* **2016**, *101*, 3564–3567. [CrossRef]
68. Min, N.; Joh, T.H.; Kim, K.S.; Peng, C.; Son, J.H. 5′ Upstream DNA sequence of the rat tyrosine hydroxylase gene directs high-level and tissue-specific expression to catecholaminergic neurons in the central nervous system of transgenic mice. *Mol. Brain Res.* **1994**, *27*, 281–289. [CrossRef]
69. Conteduca, V.; Aieta, M.; Amadori, D.; de Giorgi, U. Neuroendocrine differentiation in prostate cancer: Current and emerging therapy strategies. *Crit. Rev. Oncol. Hematol.* **2014**, *92*, 11–24. [CrossRef]
70. Soundararajan, R.; Paranjape, A.N.; Maity, S.; Aparicio, A.; Mani, S.A. EMT, Stemness and Tumor Plasticity in Aggressive Variant Neuroendocrine Prostate Cancers. *Biochim. Biophys. Acta Rev. Cancer* **2018**, *1870*, 229–238. [CrossRef]
71. Mei, W.; Lin, X.; Kapoor, A.; Gu, Y.; Zhao, K.; Tang, D. The Contributions of Prostate Cancer Stem Cells in Prostate Cancer Initiation and Metastasis. *Cancers* **2019**, *11*, 434. [CrossRef] [PubMed]
72. Ikezono, Y.; Koga, H.; Akiba, J.; Abe, M.; Yoshida, T.; Wada, F.; Nakamura, T.; Iwamoto, H.; Masuda, A.; Sakaue, T.; et al. Pancreatic Neuroendocrine Tumors and EMT Behavior Are Driven by the CSC Marker DCLK1. *Mol. Cancer Res.* **2017**, *15*, 744–752. [CrossRef] [PubMed]
73. He, X.; Chen, Z.; Jia, M.; Zhao, X. Downregulated E-cadherin expression indicates worse prognosis in Asian patients with colorectal cancer: Evidence from meta-analysis. *PLoS ONE* **2013**, *8*, e70858. [CrossRef] [PubMed]
74. Kroepil, F.; Fluegen, G.; Totikov, Z.; Baldus, S.E.; Vay, C.; Schauer, M.; Topp, S.A.; Esch, J.S.A.; Knoefel, W.T.; Stoecklein, N.H. Down-Regulation of CDH1 Is Associated with Expression of SNAI1 in Colorectal Adenomas. *PLoS ONE* **2012**, *7*. [CrossRef]
75. Cui, J.; Gong, M.; He, Y.; Li, Q.; He, T.; Bi, Y. All-trans retinoic acid inhibits proliferation, migration, invasion and induces differentiation of hepa1-6 cells through reversing EMT in vitro. *Int. J. Oncol.* **2016**, *48*, 349–357. [CrossRef]
76. Lim, Y.C.; Kang, H.J.; Kim, Y.S.; Choi, E.C. All-trans-retinoic acid inhibits growth of head and neck cancer stem cells by suppression of Wnt/β-catenin pathway. *Eur. J. Cancer* **2012**, *48*, 3310–3318. [CrossRef]

77. Friedman, M.D.; Jeevan, D.S.; Tobias, M.; Murali, R.; Jhanwar-Uniyal, M. Targeting cancer stem cells in glioblastoma multiforme using mTOR inhibitors and the differentiating agent all-trans retinoic acid. *Oncol. Rep.* **2013**, *30*, 1645–1650. [CrossRef]
78. Nguyen, P.H.; Giraud, J.; Staedel, C.; Chambonnier, L.; Dubus, P.; Chevret, E.; Bœuf, H.; Gauthereau, X.; Rousseau, B.; Fevre, M.; et al. All-trans retinoic acid targets gastric cancer stem cells and inhibits patient-derived gastric carcinoma tumor growth. *Oncogene* **2016**, *35*, 5619–5628. [CrossRef]
79. Sun, D.-F.; Gao, Z.-H.; Liu, H.-P.; Yuan, Y.; Qu, X.-J. Sphingosine 1-phosphate antagonizes the effect of all-trans retinoic acid (ATRA) in a human colon cancer cell line by modulation of RARβ expression. *Cancer Lett.* **2012**, *319*, 182–189. [CrossRef]
80. Shi, W.-N.; Cui, S.-X.; Song, Z.-Y.; Wang, S.-Q.; Sun, S.-Y.; Yu, X.-F.; Li, Y.; Zhang, Y.-H.; Gao, Z.-H.; Qu, X.-J. Overexpression of SphK2 contributes to ATRA resistance in colon cancer through rapid degradation of cytoplasmic RXRα by K48/K63-linked polyubiquitination. *Oncotarget* **2017**, *8*, 39605–39617. [CrossRef]
81. Huang, E.H.; Hynes, M.J.; Zhang, T.; Ginestier, C.; Dontu, G.; Appelman, H.; Fields, J.Z.; Wicha, M.S.; Boman, B.M. Aldehyde dehydrogenase 1 is a marker for normal and malignant human colonic stem cells (SC) and tracks SC overpopulation during colon tumorigenesis. *Cancer Res.* **2009**, *69*, 3382–3389. [CrossRef] [PubMed]
82. Kim, D.; Choi, B.-H.; Ryoo, I.-G.; Kwak, M.-K. High NRF2 level mediates cancer stem cell-like properties of aldehyde dehydrogenase (ALDH)-high ovarian cancer cells: Inhibitory role of all-trans retinoic acid in ALDH/NRF2 signaling. *Cell Death Dis.* **2018**, *9*, 896. [CrossRef] [PubMed]
83. Farrell, A.S.; Pelz, C.; Wang, X.; Daniel, C.J.; Wang, Z.; Su, Y.; Janghorban, M.; Zhang, X.; Morgan, C.; Impey, S.; et al. Pin1 regulates the dynamics of c-Myc DNA binding to facilitate target gene regulation and oncogenesis. *Mol. Cell. Biol.* **2013**, *33*, 2930–2949. [CrossRef]
84. Wei, S.; Kozono, S.; Kats, L.; Nechama, M.; Li, W.; Guarnerio, J.; Luo, M.; You, M.-H.; Yao, Y.; Kondo, A.; et al. Active Pin1 is a key target of all-trans retinoic acid in acute promyelocytic leukemia and breast cancer. *Nat. Med.* **2015**, *21*, 457–466. [CrossRef] [PubMed]
85. Yang, D.; Luo, W.; Wang, J.; Zheng, M.; Liao, X.-H.; Zhang, N.; Lu, W.; Wang, L.; Chen, A.-Z.; Wu, W.-G.; et al. A novel controlled release formulation of the Pin1 inhibitor ATRA to improve liver cancer therapy by simultaneously blocking multiple cancer pathways. *J. Control. Release* **2018**, *269*, 405–422. [CrossRef] [PubMed]
86. Ciriello, G.; Miller, M.L.; Aksoy, B.A.; Senbabaoglu, Y.; Schultz, N.; Sander, C. Emerging landscape of oncogenic signatures across human cancers. *Nat. Genet.* **2013**, *45*, 1127–1133. [CrossRef]
87. Dang, C.V. MYC on the Path to Cancer. *Cell* **2012**, *149*, 22–35. [CrossRef]
88. Lee, K.S.; Kwak, Y.; Nam, K.H.; Kim, D.-W.; Kang, S.-B.; Choe, G.; Kim, W.H.; Lee, H.S. c-MYC Copy-Number Gain Is an Independent Prognostic Factor in Patients with Colorectal Cancer. *PLoS ONE* **2015**, *10*, e0139727. [CrossRef]
89. Dardenne, E.; Beltran, H.; Benelli, M.; Gayvert, K.; Berger, A.; Puca, L.; Cyrta, J.; Sboner, A.; Noorzad, Z.; MacDonald, T.; et al. N-Myc Induces an EZH2-Mediated Transcriptional Program Driving Neuroendocrine Prostate Cancer. *Cancer Cell* **2016**, *30*, 563–577. [CrossRef]
90. Lee, J.K.; Phillips, J.W.; Smith, B.A.; Park, J.W.; Stoyanova, T.; McCaffrey, E.F.; Baertsch, R.; Sokolov, A.; Meyerowitz, J.G.; Mathis, C.; et al. N-Myc Drives Neuroendocrine Prostate Cancer Initiated from Human Prostate Epithelial Cells. *Cancer Cell* **2016**, *29*, 536–547. [CrossRef]
91. Casey, S.C.; Tong, L.; Li, Y.; Do, R.; Walz, S.; Fitzgerald, K.N.; Gouw, A.M.; Baylot, V.; Gütgemann, I.; Eilers, M.; et al. MYC regulates the antitumor immune response through CD47 and PD-L1. *Science* **2016**, *352*, 227–231. [CrossRef] [PubMed]
92. Noman, M.Z.; Janji, B.; Abdou, A.; Hasmim, M.; Terry, S.; Tan, T.Z.; Mami-Chouaib, F.; Thiery, J.P.; Chouaib, S. The immune checkpoint ligand PD-L1 is upregulated in EMT-activated human breast cancer cells by a mechanism involving ZEB-1 and miR-200. *Oncoimmunology* **2017**, *6*, e1263412. [CrossRef] [PubMed]
93. Wang, H.B.; Yao, H.; Li, C.S.; Liang, L.X.; Zhang, Y.; Chen, Y.X.; Fang, J.-Y.; Xu, J. Rise of PD-L1 expression during metastasis of colorectal cancer: Implications for immunotherapy. *J. Dig. Dis.* **2017**, *18*, 574–581. [CrossRef] [PubMed]
94. Wang, Y.; Hu, J.; Wang, Y.A.; Ye, W.; Zhang, X.; Ju, H.; Xu, D.; Liu, L.; Ye, D.; Zhang, L.; et al. EGFR activation induced Snail-dependent EMT and myc-dependent PD-L1 in human salivary adenoid cystic carcinoma cells. *Cell Cycle* **2018**, *17*, 1457–1470. [CrossRef]

95. Guo, P.-D.; Sun, Z.-W.; Lai, H.-J.; Yang, J.; Wu, P.-P.; Guo, Y.-D.; Sun, J. Clinicopathological analysis of PD-L2 expression in colorectal cancer. *OncoTargets Ther.* **2018**, *11*, 7635–7642. [CrossRef]
96. Hart, J.R.; Garner, A.L.; Yu, J.; Ito, Y.; Sun, M.; Ueno, L.; Rhee, J.-K.; Baksh, M.M.; Stefan, E.; Hartl, M.; et al. Inhibitor of MYC identified in a Kröhnke pyridine library. *Proc. Natl. Acad. Sci. USA* **2014**, *111*, 12556–12561. [CrossRef]
97. Schindelin, J.; Arganda-Carreras, I.; Frise, E.; Kaynig, V.; Longair, M.; Pietzsch, T.; Preibisch, S.; Rueden, C.; Saalfeld, S.; Schmid, B.; et al. Fiji: An open-source platform for biological-image analysis. *Nat. Methods* **2012**, *9*, 676–682. [CrossRef]
98. O'Malley, D.P.; Yang, Y.; Boisot, S.; Sudarsanam, S.; Wang, J.-F.; Chizhevsky, V.; Zhao, G.; Arain, S.; Weiss, L.M. Immunohistochemical detection of PD-L1 among diverse human neoplasms in a reference laboratory: Observations based upon 62,896 cases. *Mod. Pathol.* **2019**, *32*, 929–942. [CrossRef]
99. De Preter, K.; Speleman, F.; Combaret, V.; Lunec, J.; Laureys, G.; Eussen, B.H.J.; Francotte, N.; Board, J.; Pearson, A.D.J.; de Paepe, A.; et al. Quantification of MYCN, DDX1, and NAG gene copy number in neuroblastoma using a real-time quantitative PCR assay. *Mod. Pathol.* **2002**, *15*, 159–166. [CrossRef]

Original Research Article

“Nanopore Sequencing Reveals Global Transcriptome Signatures of Mitochondrial and Ribosomal Gene Expressions in Various Human Cancer Stem-like Cell Populations”

Kaya E. Witte*, Oliver Hertel*, **Beatrice A. Windmöller**, Laureen P. Helweg, Anna L. Höving, Cornelius Knabbe, Tobias Busche, Johannes F. W. Greiner, Jörn Kalinowski, Thomas Noll, Fritz Mertzlufft, Morris Beshay, Jesco Pfitzenmaier, Barbara Kaltschmidt, Christian Kaltschmidt, Constanze Banz-Jansen* and Matthias Simon*
(*: equal contribution)

Cancers (Basel). 2021 Mar; 13(5): 1136.

cancers

MDPI

Article

Nanopore Sequencing Reveals Global Transcriptome Signatures of Mitochondrial and Ribosomal Gene Expressions in Various Human Cancer Stem-like Cell Populations

Kaya E. Witte [1,2,*,†], Oliver Hertel [3,4,†], Beatrice A. Windmöller [1,2], Laureen P. Helweg [1,2], Anna L. Höving [1,5], Cornelius Knabbe [2,5], Tobias Busche [4], Johannes F. W. Greiner [1,2], Jörn Kalinowski [4], Thomas Noll [3,4], Fritz Mertzlufft [2,6], Morris Beshay [2,7], Jesco Pfitzenmaier [2,8], Barbara Kaltschmidt [1,2,9], Christian Kaltschmidt [1,2], Constanze Banz-Jansen [2,10,‡] and Matthias Simon [2,11,‡]

1 Department of Cell Biology, Faculty of Biology, University of Bielefeld, Universitätsstrasse 25, 33699 Bielefeld, Germany; Beatrice.windmoeller@uni-bielefeld.de (B.A.W.); l.helweg@uni-bielefeld.de (L.P.H.); Anna.hoeving@uni-bielefeld.de (A.L.H.); Johannes.greiner@uni-bielefeld.de (J.F.W.G.); Barbara.kaltschmidt@uni-bielefeld.de (B.K.); C.Kaltschmidt@uni-bielefeld.de (C.K.)

2 Forschungsverbund BioMedizin Bielefeld, OWL (FBMB e.V.), Maraweg 21, 33699 Bielefeld, Germany; cknabbe@hdz-nrw.de (C.K.); fritz.mertzlufft@evkb.de (F.M.); Morris.Beshay@evkb.de (M.B.); Jesco.Pfitzenmaier@evkb.de (J.P.); Constanze.Banz-Jansen@evkb.de (C.B.-J.); Matthias.Simon@evkb.de (M.S.)

3 Department of Cell Culture Technology, Faculty of Technology, University of Bielefeld, Universitätsstrasse 25, 33699 Bielefeld, Germany; oliver.hertel@uni-bielefeld.de (O.H.); Thomas.Noll@uni-bielefeld.de (T.N.)

4 Center for Biotechnology-CeBiTec, University of Bielefeld, Universitätsstrasse 27, 33699 Bielefeld, Germany; tbusche@cebitec.uni-bielefeld.de (T.B.); joern@cebitec.uni-bielefeld.de (J.K.)

5 Heart and Diabetes Centre NRW, Institute for Laboratory and Transfusion Medicine, Ruhr-University Bochum, 32545 Bad Oeynhausen, Germany

6 Scientific Director of the Protestant Hospital of Bethel Foundation, University Medical School OWL at Bielefeld, Bielefeld University, Campus Bielefeld-Bethel, Maraweg 21, 33699 Bielefeld, Germany

7 Department for Thoracic Surgery and Pneumology, Protestant Hospital of Bethel Foundation, University Medical School OWL at Bielefeld, Bielefeld University, Campus Bielefeld-Bethel, Burgsteig 13, 33699 Bielefeld, Germany

8 Department of Urology and Center for Computer-Assisted and Robotic Urology, Protestant Hospital of Bethel Foundation, University Medical School OWL at Bielefeld, Bielefeld University, Campus Bielefeld-Bethel, Burgsteig 13, 33699 Bielefeld, Germany

9 Molecular Neurobiology, Faculty of Biology, Bielefeld University, Universitätsstrasse 25, 33699 Bielefeld, Germany

10 Department of Gynecology and Obstetrics, and Perinatal Center, Protestant Hospital of Bethel Foundation, University Medical School OWL at Bielefeld, Bielefeld University, Campus Bielefeld-Bethel, Burgsteig 13, 33699 Bielefeld, Germany

11 Department of Neurosurgery and Epilepsy Surgery, Protestant Hospital of Bethel Foundation, University Medical School OWL at Bielefeld, Bielefeld University, Campus Bielefeld-Bethel, Burgsteig 13, 33699 Bielefeld, Germany

* Correspondence: Kaya.friedrich@uni-bielefeld.de; Tel.: +49-521-106-5629

† Authors contributed equally as co-first authors.

‡ Authors contributed equally as co-last authors.

Simple Summary: Cancer is the leading cause of death in the industrialized world. In particular, so-called cancer stem cells (CSCs) play a crucial role in disease progression, as they are known to contribute to tumor growth and metastasis. Thus, CSCs are heavily investigated in a broad range of cancers. Nevertheless, global transcriptomic profiling of CSC populations derived from different tumor types is rare. We established three CSC populations from tumors in the uterus, brain, lung, and prostate and assessed their global transcriptomes using nanopore full-length cDNA sequencing, a new technique to assess insights into global gene profile. We observed common expression in all CSCs for distinct genes encoding proteins for organelles, such as ribosomes, mitochondria, and proteasomes. Additionally, we detected high expressions of inflammation- and immunity-related genes. Conclusively, we observed high similarities between all CSCs independent of their tumor of origin, which may build the basis for identifying novel therapeutic strategies targeting CSCs.

check for updates

Citation: Witte, K.E.; Hertel, O.; Windmöller, B.A.; Helweg, L.P.; Höving, A.L.; Knabbe, C.; Busche, T.; Greiner, J.F.W.; Kalinowski, J.; Noll, T.; et al. Nanopore Sequencing Reveals Global Transcriptome Signatures of Mitochondrial and Ribosomal Gene Expressions in Various Human Cancer Stem-like Cell Populations. *Cancers* **2021**, *13*, 1136. https://doi.org/10.3390/cancers13051136

Academic Editor: Shihori Tanabe

Received: 29 January 2021
Accepted: 4 March 2021
Published: 6 March 2021

Publisher's Note: MDPI stays neutral with regard to jurisdictional claims in published maps and institutional affiliations.

Abstract: Cancer stem cells (CSCs) are crucial mediators of tumor growth, metastasis, therapy resistance, and recurrence in a broad variety of human cancers. Although their biology is increasingly investigated within the distinct types of cancer, direct comparisons of CSCs from different tumor types allowing comprehensive mechanistic insights are rarely assessed. In the present study, we isolated CSCs from endometrioid carcinomas, glioblastoma multiforme as well as adenocarcinomas of lung and prostate and assessed their global transcriptomes using full-length cDNA nanopore sequencing. Despite the expression of common CSC markers, principal component analysis showed a distinct separation of the CSC populations into three clusters independent of the specific type of tumor. However, GO-term and KEGG pathway enrichment analysis revealed upregulated genes related to ribosomal biosynthesis, the mitochondrion, oxidative phosphorylation, and glycolytic pathways, as well as the proteasome, suggesting a great extent of metabolic flexibility in CSCs. Interestingly, the GO term "NF-kB binding" was likewise found to be elevated in all investigated CSC populations. In summary, we here provide evidence for high global transcriptional similarities between CSCs from various tumors, which particularly share upregulated gene expression associated with mitochondrial and ribosomal activity. Our findings may build the basis for identifying novel therapeutic strategies targeting CSCs.

Keywords: cancer stem cells; endometrioid carcinoma; glioblastoma multiforme; lung adenocarcinoma; prostate adenocarcinoma; nanopore sequencing; mitochondrion; ribosome

1. Introduction

Cancer stem cells (CSCs) are increasingly noticed to initiate tumor growth and to drive metastasis and tumor recurrence in a broad range of human cancers (reviewed in [1]). Within the highly heterogeneous tumor cell mass, CSCs represent only a small subpopulation [2] (reviewed in [3]), but possess stem-like properties like self-renewal, asymmetric division and multi-lineage differentiation [4–7] (reviewed in [1]). Moreover, CSCs remain hidden in the body of the patients until their reactivation by various stimuli leads to the regeneration of the tumor or to the formation of metastasis [8]. These characteristics facilitate the role of CSCs as major drivers of tumor formation and progression. From a therapeutic point of view, their quiescent-like state makes CSCs highly resistant to chemotherapeutic agents, while the low expression of major histocompatibility class I molecules enables the escape from immune surveillance by cytotoxic T-cells [9–11]. To gain a deeper understanding of CSC biology and potential treatment options, global transcriptional profiling has become a state-of-the-art tool during the recent years [12]. However, direct comparisons of CSCs from different tumor types are rarely assessed, although these may allow the identification of comprehensive mechanisms present in CSCs independent to the type of the tumor. In the present study, we isolated CSCs from endometrioid carcinomas, glioblastoma multiforme, as well as adenocarcinomas of lung and prostate, and assessed their global transcriptomes by nanopore RNA sequencing (RNA-Seq) to identify such potential common regulators and mechanisms.

Endometrial cancer is one of the most common sex-specific malignant diseases in women worldwide. Annually, about 320,000 women are diagnosed with endometrial cancer. Especially in high-income countries, the incidence of endometrial cancer is high, at 5.9% [13]. Major risk factors are obesity, physical inactivity, and elevated estrogen levels in postmenopausal women [14,15]. In Europe and North America, endometrial cancer is the most frequent cancer of the female genital tract. However, it is mainly presented with postmenopausal bleeding and therefore in most cases diagnosed at an early stage. Nevertheless, it is more and more emphasized that a small subpopulation of tumor stem-like cells with clonogenic, self-renewing, differentiating and tumorigenic properties are responsible for the production of endometrial carcinoma cells [4]. Additionally, endometrial CSCs seem to play a role in chemoresistance of endometrial carcinomas, as increased

expression of CSC markers were shown to enrich resistance to cisplatin, placlitaxel and doxorubicin [16].

Being the most common primary brain tumor, glioblastoma multiforme (GBM) possesses a high cellular heterogeneity and aggressiveness accompanied by an extensive invasiveness and inevitable recurrence, resulting in an average survival time of less than 15 months [6,17–19]. As a description of the cellular composition, GBM tumors contain a relatively rare glioblastoma stem-like cell (GSC) population, which is able to self-renew and repopulate the whole tumor building [20]. GSCs can be found within the tumor infiltrating zone and therefore contribute prominently to a subsequent tumor recurrence [21]. On the contrary, differentiated GBM cells are considered as the main contributor to the tumor mass development [20,22–26]. In a therapeutic context, Happold and coworkers analyzed GSCs and described NF-κB RELA as a positive regulator of O6-methylguanine-DNA methyltransferase (MGMT) [27]. Of note, *MGMT* promoter hypermethylation has proven an important predictive biomarker for benefit from alkylating chemotherapy as well as a powerful prognostic factor in gliomas [28,29].

Lung cancer is the leading cause of cancer-related deaths worldwide. According to its histological differentiation, it is classified into small-cell lung cancer and non-small cell lung cancer (NSCLC), which is the most frequent form with an incidence of about 80% [30]. In the last few years, target therapy or immune therapy has been gaining popularity. Nevertheless, the overall prognosis of NSCLC is bad, with a five-year survival rate of only 15% [31]. A meta-analysis evaluating the effect of CSC markers on the clinicopathological characteristics of lung cancer revealed a significant association with poor differentiation and metastasis [32]. Accordingly, CSCs were reported to be responsible for therapy resistance and tumor growth as well as metastasis in lung cancer [5]. Moreover, lung cancer stem-like cells (LCSCs) were shown to be regulated by NF-κB [33], as already mentioned for GSCs.

Prostate cancer (PCa) is the most common sex-specific cancer within industrialized countries as well as the second leading cause of cancer deaths (10%) in men [34]. PCas are described as having an epithelial origin and an almost exclusive occurrence as an acinar adenocarcinoma [35]. PCa mainly occurs in the elderly, from the age of at least 65 years, and can be detected using prostate-specific antigen-testing, enabling early stage detection [36]. The overall mortality is only reduced by performing a radically prostatectomy [37]. Relating to further therapeutic options, luminal epithelial stem cells could be revealed as the origin of PCa via lineage tracing in mice [38]. In context with CSCs, prostate tumor spheres, originating from prostate cancer stem-like cells (PCSCs), were also shown to express a constitutive NF-κB signaling and inherent increased IL-6 levels [39].

Here, we established cultures of CSCs and analyzed three of each cancer type via RNA-Seq on global transcriptome level. We used the recently developed nanopore sequencing technology (reviewed in [40]) and a protocol for generating full length cDNA to identify common regulators and mechanisms present in CSCs independent to the tumor origin.

2. Materials and Methods

2.1. Cancer Stem-like Cell Population Establishment and Cultivation

Cancer tissue samples used to isolate CSCs were obtained during surgical resection and were kindly provided by the Forschungsverbund BioMedizin Bielefeld/OWL (FBMB e.V.) at the Protestant Hospital of Bethel Foundation (Bielefeld, Germany) after assuring routine histopathological analysis. Primary tumor samples were collected from each tumor type, including three endometrioid carcinomas, three glioblastomas, and three adenocarcinomas of the lung and prostate, respectively. Informed consent according to local and international guidelines was signed by all patients and further experimental procedures were ethically approved (Ethics committee Münster, Germany, 2017-522-f-S).

Samples were transferred into ice-cold Dulbecco's phosphate buffered saline (PBS; Sigma Aldrich, Munich, Germany) and for further processing transported to the University of Bielefeld. Tumor tissue was mechanically disintegrated followed by enzymatic digestion with collagenase for 2 h at 37 °C as described previously [41,42]. The minced tissue was cul-

tured on gelatin (bovine skin-derived, type B; Sigma Aldrich)-coated culture dishes in CSC-selective medium composed of Dulbecco's modified Eagle's medium/Ham's F-12 (Sigma Aldrich) with the addition of 2 mM L-glutamine (Sigma Aldrich), penicillin/streptomycin (100 µg/mL; Sigma Aldrich), epidermal growth factor (EGF; 20 ng/mL; MiltenyiBiotec, Bergisch Gladbach, Germany), basic fibroblast growth factor-2 (bFGF-2; 40 ng/mL; Miltenyi Biotec), B27 supplement (Gibco, Thermo Fisher Scientific, Bremen, Germany) and 10% FCS (Sigma Aldrich). Enrichment of CSCs was achieved via serial trypsin treatment, as described by Walia et al. and Morata-Tarifa et al. [43,44]. Briefly, cells isolated by explant culture (passage 0) were washed with PBS and subsequently treated for 5 min with trypsin (Sigma Aldrich). Detached cells were transferred into a new gelatin pre-coated culture dish. Trypsinization and transfer of the cells were repeated every 48 to 72 h, at least for three cycles to assure stem-like characteristics in adherently grown and fibroblast-shaped cancer cells. For cultivation of free-floating spheres, CSC populations from endometrioid carcinoma and glioblastoma multiforme were cultured without the addition of serum for several days in regular growth medium supplemented with 4 µg/mL heparin (Sigma Aldrich).

2.2. Immunocytochemistry

For immunocytochemical staining of adherent CSC populations, cells were seeded at the top of sterilized coverslips with 15,000-30,000 cells per 4 cm^2 in 24-well plates with 0.5 mL growth medium and cultured initially for 48 to 72 h until cells reached 70–80% confluency. CSCs were fixed for 10 min with 4% para-formaldehyde in PBS. Blocking of free binding sides and permeabilization were performed with PBT solution, including 0.02% Triton-X-100 (Sigma Aldrich) and 5% goat serum (DIANOVA, Hamburg Germany) in PBS for 30 min. Next, three washing steps with PBS were performed as well as an incubation with primary antibodies for 1 h at room temperature (RT). Used antibodies for this study: anti-CD44 (1:400; 156-3C11; Cell Signaling, Frankfurt am Main, Germany), anti-CD133 (1:100; NB120-16518; NovusBio, Bio-Techne, Wiesbaden-Nordenstadt, Germany), anti-Nestin (1:200; MAB5326; Merck) and anti-MYC (10 µg/mL; Y69; Abcam, Cambridge, UK). After further washing steps, secondary fluorochrome-conjugated antibodies (Alexa Fluor 555 and -488 dyes; 1:300; goat anti-mouse and goat anti-rabbit; Life Technologies) were applied for 1 h at RT, protected from light. Nuclear staining were performed by using 4′,6-diamidino-2-phenylindole (DAPI; 1 µg/mL; Sigma Aldrich) for 10 min. Before CSC populations were embedded in Mowiol 4-88 (Carl Roth GmbH, Karlsruhe, Germany) upside down on the top of microscope slides, another washing step was performed. For fluorescence imaging, a confocal laser-scanning microscope (LSM 780; Carl Zeiss, Jena, Germany) was used.

For immunostaining of CSC spheres, free-floating cultured cells were fixed in 4% para-formaldehyde for 2 h, were further embedded in paraffin and sectionalized in 4 µm sections. Resulting slices were deparaffinized and rehydrated with xylol (Sigma Aldrich) as well as via ethanol in different steps. After reconditioning of the epitope with citrate buffer (pH 6), slices were washed in PBS and blocking of free binding sides were performed via incubation with 0.02% Triton-X 100, 10% appropriative serum and 1% bovine serum albumin (Sigma Aldrich) also in PBS for at least 2 h at RT. Next, incubation with primary antibodies was performed over night at 4 °C by using: anti-CD44 (1:50), anti-CD133 (1:100) and anti-MYC (10 µg/mL). Slices were washed three times with PBS and incubated for 1 h at RT with the Alexa Fluor 555 and −488 secondary fluorochrome-conjugated antibodies (1:300). Nuclear staining by using DAPI (1 µg/mL) as well as fluorescence imaging were processed equally to immunocytochemistry of adherently cultured CSCs.

2.3. RNA Isolation and Sequencing

RNA from 1 × 10^6 cultured CSCs of each population and cancer type were isolated by using the NucleoSpin® RNA Plus kit (Macherey-Nagel, Düren, Germany) according to manufacturer's guidelines. Quality and concentration of isolated RNAs were assessed

via nanodrop ultraviolet spectrophotometry. Total RNA samples with RNA Integrity Numbers (RIN) > 9.5 were used to convert full-length RNA molecules that are both capped and polyadenylated to cDNA using the TeloPrime Full-Length cDNA Amplification Kit V2 (Lexogen, Vienna, Austria). Amplified full length cDNAs were then used to prepare Oxford Nanopore Technologies (ONT) compatible libraries using the Ligation Sequencing Kit LSK109 with the Native Barcoding Kit NBD104 (ONT, Oxford, UK), which were run on three R9.4 flowcells on the ONT system GridION. Base calling and demultiplexing were performed using Guppy v3.1.5.

2.4. Preprocessing and Genome Alignment

Fastq files containing reads that passed the quality filtering were concatenated according to their barcodes from each flowcell. Since the three flowcells showed high correlation on gene count level, technical triplicates were merged accordingly. Sequencing adapters were trimmed using porechop v0.2.4 [45]. Trimming was checked using FastQC v0.11.9 [46]. Trimmed reads were aligned to the human RefSeq genome GRCh38.p13 [47,48] using minimap 2 [49] with the arguments -ax splice -p 0.99. Alignment files were converted to bam format using samtools v1.10.2 [50]. The bam files were quality checked using AlignQC v2.0.5 [51] samtools v1.10.2 [50]. As the alignments showed up to 15% trans-chimeric reads, which most likely resulted from the library preparation, those reads were removed from the alignments. Therefore, the chimera.bed file from the AlignQC output were converted to exclusion lists. Bam files were sorted using samtools v1.10.2 [50] and filtered using the FilterSamReads module of Picard Toolkit (http://broadinstitute.github.io/picard/ (accessed on 6 March 2020)) with the exclusion lists and the arguments –FILTER excludeReadList –SORT_ORDER. Mismatches and small indels were corrected using TranscriptClean [52] with the human RefSeq genome GRCh38.p13 [47]. These high-quality alignments were used as input for the estimation of gene abundances.

2.5. Gene Abundance Estimation and Enrichment Analysis

Mapped reads were assigned to genes and counted by the featureCounts module of the R/Bioconductor [53] package Rsubread v2.0.1 [54] with the arguments countMultiMappings = TRUE, fraction = TRUE, isLongRead = TRUE. The gtf file of the human RefSeq genome GRCh38.p13 [47] was used as external annotation. From genes with multiple integrations but the same exon structure, only one was retained, because they shared the same multimapping reads. These raw counts were grouped by the CSC populations and preprocessed using the R/Bioconductor package edgeR v3.28.1. [55,56]. Lowly expressed genes were filtered using the filterByExpr function with default arguments. Normalization factors were calculated using the trimmed mean of M-values method [57]. Differentially expressed genes (DEGs) were identified by an ANOVA-like testing using the generalized linear models with the quasi-likelihood F-test (glmQLFTest). The threshold of DEGs was set as p value < 0.05. Principle component analysis (PCA) was conducted using the R/Bioconductor package PCAtools v1.2.0 [58]. Heatmaps were created using the heatmap.2 function of the R package gplots v3.1.1 [59]. Correlation analysis was conducted using the R package Hmisc package [60]. Functional enrichment of GO-terms of genes expressed in all 12 CSC populations were calculated using the PANTHER classification system [61], while the DAVID database [62,63] served for calculating functional enriched KEGG pathways. Significantly (modified Fisher Exact p-value; $p < 0.05$) enriched GO-terms and pathways were visualized with Prism software (GraphPad Software, San Diego, CA, USA).

3. Results

3.1. Correlative Analysis of Characteristic Markers in Cancer Stem-like Cells from Endometrioid Carcinomas, Glioblastoma Multiforme, Lung- and Prostate Adenocarcinomas

In this study, 12 different CSC populations from four different carcinoma types were established. Carcinoma types included three endometrial carcinomas, three glioblastomas as well as three adenocarcinomas of the lung and the prostate, respectively. All female

donors of the endometrial cancer stem-like cell populations (ECSCs) suffered from endometrioid carcinomas of the corpus uteri ranging WHO grade I-II and were aged between 72 and 86 years. Donors of GSCs were two males (42 and 69 years old) and one female (60 years old), all revealing glioblastoma multiforme. Glioblastomas of the donors of GSCs_a and GSCs_c revealed no mutation for the isocitrate dehydrogenase (NADP(+)) 1 (*IDH1*), whereas in the glioblastoma of the donor of GSCs_b *IDH1* was mutated. Additionally, *MGMT* promoter methylation status differed between the three donors, as glioblastomas of the donors of GSCs_a and GSCs_b depicted *MGMT* promoter methylation in contrast to the glioblastoma of donor GSCs_c. LCSC populations were derived from three relatively young female patients (aged between 49 and 61 years) all diseased with adenocarcinomas. Analysis of clinically relevant mutations revealed an epidermal growth factor receptor (*EGFR*) mutation for the donor of LCSCs_a as well as tumor tissue of the donor of LCSCs_c showed mutations in the genes for the KRAS proto-oncogene (*KRAS*) and serine/threonine kinase 11 (*STK11*). The three PCSCs were isolated from male patients aged between 57 and 72 years all suffering from acinar adenocarcinomas with WHO grade II, III and V (Table 1).

Table 1. Cell population-specific donor information.

Donor of Cell Population	Tumor Typing/Characterization	WHO Grade	Sex	Age
ECSCs_a	Endometrioid carcinoma of the corpus uteri	GII	female	72
ECSCs_b	Endometrioid carcinoma of the corpus uteri	GI	female	83
ECSCs_c	Endometrioid carcinoma of the corpus uteri with invasion of the outer half of the myometrium and invasion of the cervix uteri	GII	female	86
GSCs_a	Primary glioblastoma multiforme, *IDH1* wildtype with *MGMT* promoter methylation	GIV	female	60
GSCs_b	Secondary glioblastoma multiforme, *IDH1* mutation with *MGMT* promoter methylation	GIV	male	42
GSCs_c	Primary glioblastoma multiforme, *IDH1* wildtype without *MGMT* promoter methylation	GIV	male	69
LCSCs_a	Highly metastatic adenocarcinoma of the lung, *EGFR* mutation	n.a.	female	50
LCSCs_b	Multifocal adenocarcinoma of the lung	GII	female	61
LCSCs_c	Adenocarcinoma of the lung, *KRAS* and *STK11* mutation	GII	female	49
PCSCs_a	Acinar adenocarcinoma	GIII	male	71
PCSCs_b	Acinar adenocarcinoma	GII	male	57
PCSCs_c	Locally advanced acinar adenocarcinoma	GV	male	72

All cancer populations were cultured as adherently growing cells within stem cell-selective media after passing serial trypsin treatment, for enrichment of the respective CSC-population. Here, we used chemically defined medium containing EGF and bFGF-2, in accordance with the isolation of colorectal cancer stem-like cells as well as of adult human stem cells from the nasal cavity and the heart auricle [42,64–67]. In contrast with the successful isolation of human stem cells from the nasal cavity as free-floating spheres [64,65], adoption of the reported isolation process for human CSCs from solid tumors resulted in an unsatisfactory low culture efficacy and low growth rates. Therefore, we utilized an alternative method to enrich primary isolated CSCs, namely via differential trypsinization [42,44]. In accordance with a range of previous studies, we obtained trypsin-sensitive CSC populations with low attachment capability by culturing with 10% FCS [42–44,66,67]. Representative images of one of the successfully isolated CSC populations derived from endometrioid carcinomas, glioblastomas, lung and prostate adenocarcinomas revealed similar morphology independently of the origin of parental tumor tissues (Figure 1B–E). In accordance with the observations by Walia et al. and Elble et al., cultured CSCs depicted a fibroblast-like and spindle-shaped morphology after selection with differential trypsin treatment [43]. To confirm the stem-like phenotype of isolated CSC populations, we determined the presence of characteristic CSC markers on protein level using immunocytochemistry. Notably, high levels of CD44, CD133, Nestin and MYC protein were detectable in adherently grown CSC populations from all tumor types as well as in spheres derived from ECSC_b and GSC_c (Figures S1 and S2 and Figure 2). Immunocytochemistry further revealed co-expressions of CD44 and CD133 as well as Nestin in isolated CSCs, independently to the tumor origin (Figure 2A and Figures S2 and S3). The proto-oncogene MYC was also detectable on protein level independent to the parental tumor tissue, particularly

with a nuclear localization (Figure 2B and Figure S4). As an internal negative control and evaluation of the unique stem-like characteristics of isolated CSCs, human dermal fibroblasts (HDFs) were additionally immunocytochemically stained for CD44, CD133, Nestin and MYC. Here, HDFs showed no signs of CSC markers on protein level (Figure S5), emphasizing the CSC-like character of our isolated cell populations.

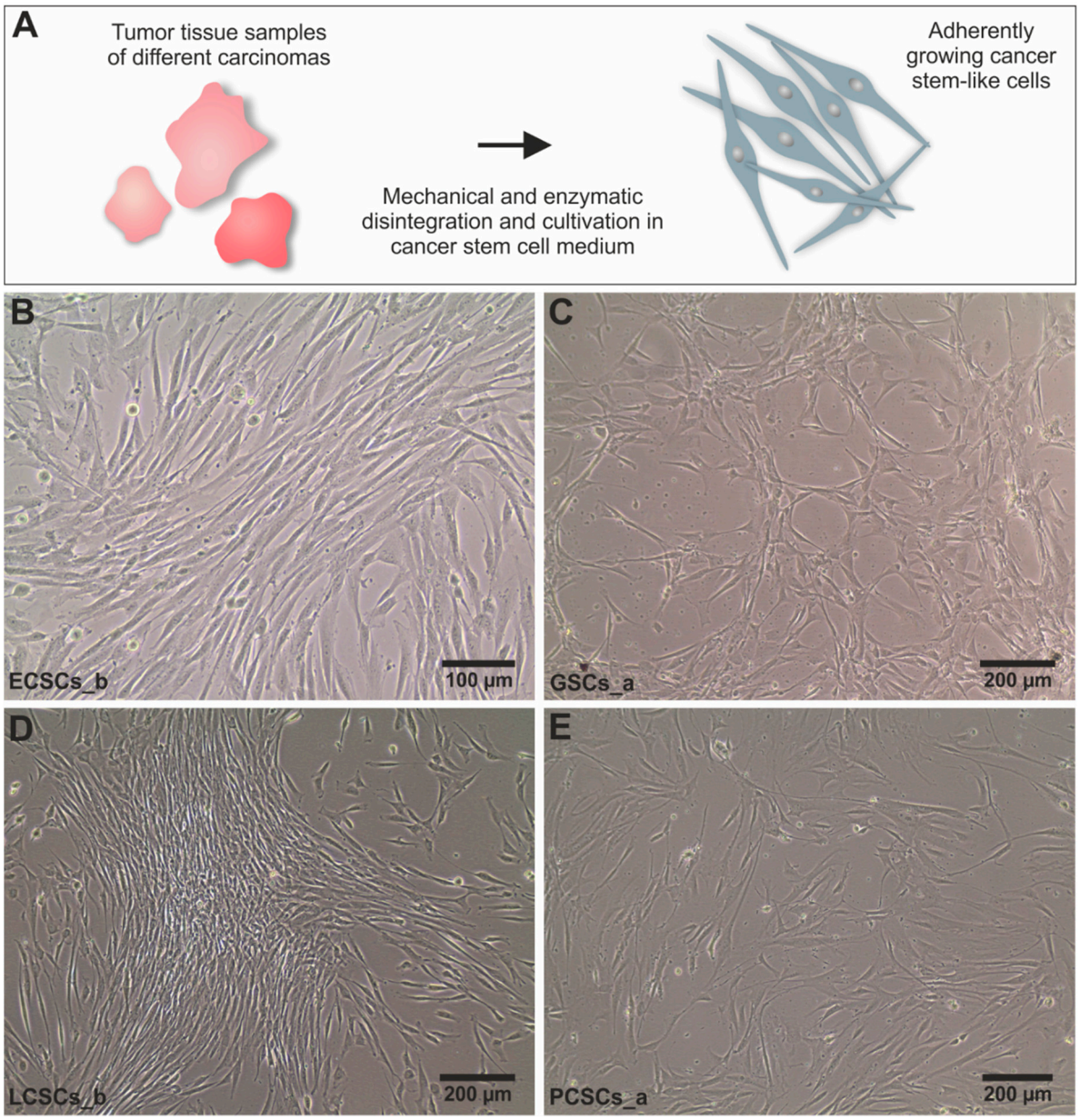

Figure 1. Isolation of cancer stem-like cell populations of four different types of carcinomas. (**A**) Schematic illustration of the isolation of cancer-stem-like cells out of primary tumor tissue. Representative pictures of adherently grown primary cancer stem-like cells derived from parental tumor tissue of (**B**) endometrial cancer stem-like cells b (ECSCs_b), (**C**) glioblastoma stem-like cells a (GSCs_a), (**D**) lung cancer stem-like cells b (LCSCs_b) and (**E**) prostate cancer stem-like cells a (PCSCs_a).

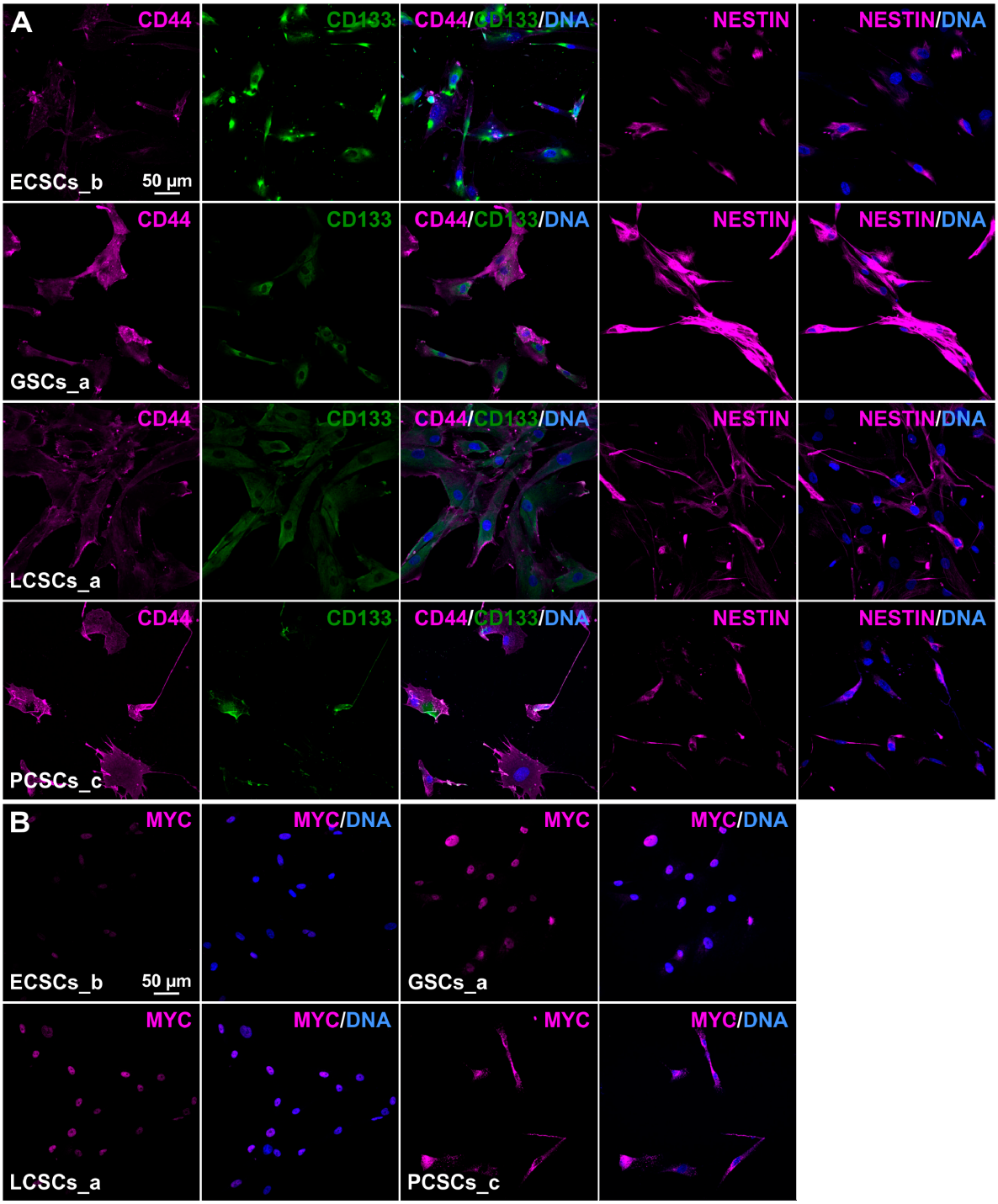

Figure 2. Immunocytochemistry of adherently grown cancer stem-like cell populations. (**A**) Representative immunostainings of co-expressed cancer stem cell (CSC) markers CD44/CD133 as well as Nestin, localized within the cytoplasm. (**B**) Exemplary depicted MYC expressions from one of each CSC population showed high frequencies of nuclear localizations of the analyzed protein. DAPI served in all cases for nuclear counterstaining.

For in-depth analysis of the gene expression of the 12 isolated CSC populations nanopore cDNA sequencing was used. Full-length cDNA sequencing was conducted using three R9.4 flowcells on the ONT system GridION. Only reads that passed the default quality criteria of the Guppy basecaller were further investigated. All sequencing runs yielded 10,627,235 reads (11.2 Gbp of sequence) with a mean read length of 1056 bp and a mean quality score of 21.3. Reads were aligned to the human genome (hg38) using minimap2 [49].

We observed a read alignment rate of 99.2% and an error rate of 7.3%, which was reduced to 0.69% using TranscriptClean [52] for correction. To check the reproducibility of gene counts between the technical triplicates, fastq files from the different flowcells were preprocessed, mapped, corrected, and quantified separately. Subsequent analysis showed strong correlation between respective flowcells (mean Spearman correlation coefficient $\rho = 0.94$). All datasets were processed similarly and gene expression of specific CSC markers was investigated firstly. CSC marker *CD44* was ubiquitously expressed in all 12 CSC populations. Analysis of the co-expression of *CD44* with further CSC markers revealed expression of MYC proto-oncogene (*MYC*) in all CSC populations, except for ECSCs_c. Here, especially LCSCs_a and GSCs_c showed high expression of *MYC* (Figure 3A). Further quantification depicted *Nestin* expression in LCSCs_a, _c, PCSCs_a, _c as well as in GSCs_a and ECSCs_b (Figure 3B). Pluripotency marker Kruppel-like factor 4 (*KLF4*) and aldehyde dehydrogenase 1 (*ALDH1*) were only expressed in three of 12 CSC populations each, as *KLF4* was only observable in GSCs_b, _c and PCSCs_c and *ALDH1* in LCSCs_b, _c as well as in PCSCs_c (Figure 3C,D). In CSC populations PCSCs_a and GSCs_b, expression of epithelial cell adhesion molecule (*EPCAM*) was detectable (Figure 3E). Additionally, PCSCs_c and ECSCs_b expressed ATP binding cassette subfamily G member 2 (*ABCG2*) (Figure 3F). On the contrary, we did not observe any expression of CSC markers Prominin-1 (*CD133*), SRY-box transcription factor 2 (*SOX2*), POU class 5 homeobox 1 (*OCT4*) and MYCN proto-oncogene in the here analyzed CSCs cultivated and sequenced as described above. In summary, all isolated CSC populations expressed the CSC marker *CD44*. Expression of further CSC markers was more heterogeneous, except for the expression level of *MYC*, which could be detected in 11 of 12 CSC populations. *Nestin*, *KLF4*, *ALDH1*, *EPCAM* as well as *ABCG2* expression was incongruous, with no clear relation to the four different parental tumor groups.

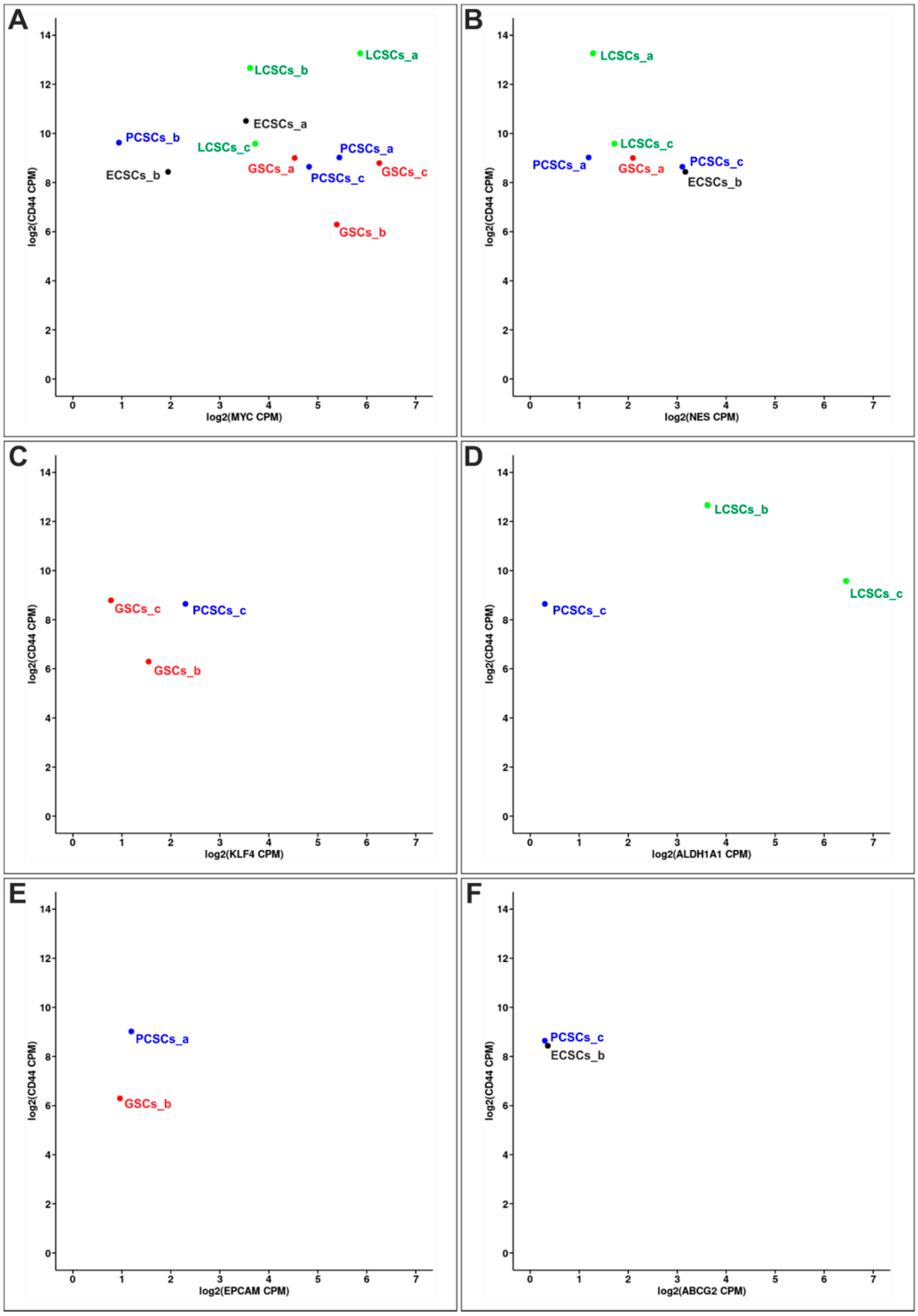

Figure 3. Correlated expression of CD44 with various other cancer stem cell (CSC) markers in different CSC populations. For each analysis, biological replicates depicted the mean of merged technical triplicates. (**A**) All CSC populations expressed CSC marker *CD44* and MYC proto-oncogene (*MYC*), except for endometrial cancer stem-like cell population c (ECSCs_c), which only expressed *CD44*. (**B**) CSC marker *Nestin* was expressed in lung cancer stem-like cells (LCSCs)_a and _c, prostate cancer stem-like cells (PCSCs)_a and _c as well as in glioblastoma stem-like cells (GSCs)_a and ECSCs_b. (**C**) Pluripotency marker Kruppel like factor 4 (*KLF4*) was expressed in GSCs_b, GSCs_c and in PCSCs_c as well as (**D**) aldehyde dehydrogenase 1 (*ALDH1*) could be detected in LCSCs_b, LCSCs_c and PCSCs_c. (**E**) Epithelial cell adhesion molecule (*EPCAM*) was only observed in PCSCs_a and GSCs_b. (**F**) Expression of the ATP binding cassette subfamily G member 2 (*ABCG2*) gene could only be detected in PCSCs_c and ECSCs_b.

3.2. Global Gene Expression Analysis of Cancer Stem-like Cell Populations Reveals Distinct Clusters

After analysis of the expression of known CSC markers, global gene expression of the 12 isolated CSC populations was investigated. Similarly, processed datasets were used for PCA, revealing three dominant clusters among the 12 populations (Figure 4). Here, cluster one comprises all three ECSC populations and PCSCs_b. However, variances between the populations could be seen within this cluster, too. Second and biggest cluster consisted of all LCSC populations, the two remaining PCSC populations and two GSC populations. Within this cluster, LCSCs_a and LCSCs_b revealed less variances in comparison to LCSCs_c, which was clustered next to GSCs_a and GSCs_c. GSCs_b clustered independently, with the highest variance of PC1 between the group of LCSCs_a and LCSCs_b, in comparison with GSCs_b. PC2 differed with a variance of 23.73% with the greatest variation between ECSCs_c and GSCs_b (Figure 4).

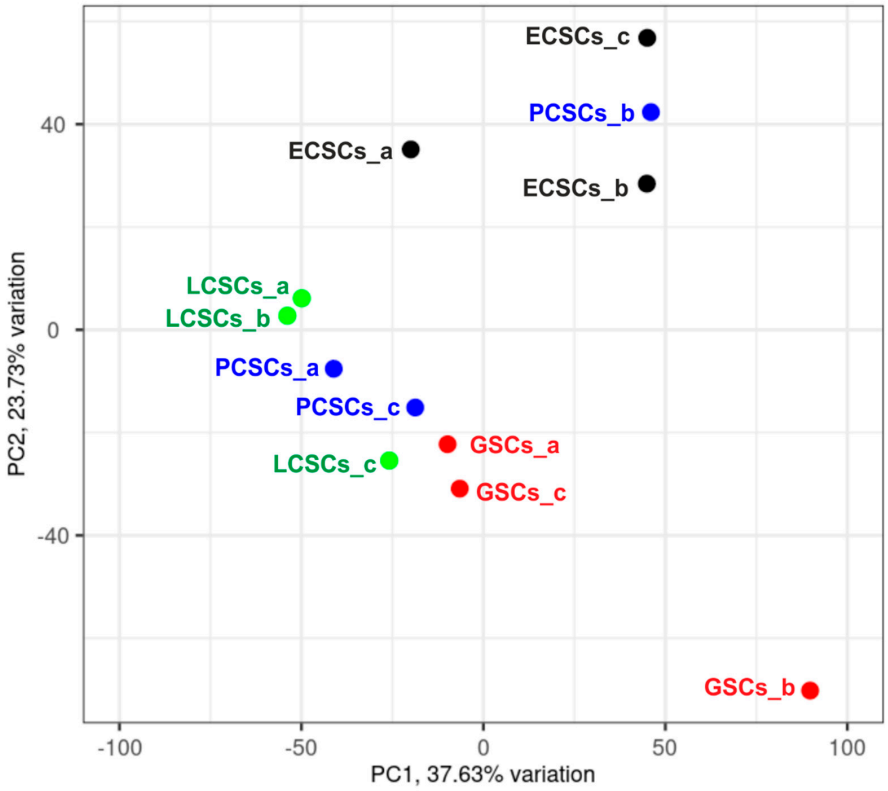

Figure 4. Comparison of gene expression profiles from different primary cancer stem-like cell (CSC) populations. Principal component analysis reveals two predominant clusters of CSCs, independently of the parental tumor types. Within the first cluster all three endometrial cancer stem-like cells (ECSCs) are present and one of the three prostate cancer stem-like cell (PCSCs) populations. The second cluster comprises the two remaining PCSCs, all three lung cancer-derived stem-like cell populations (LCSCs) as well as glioblastoma stem-like cells a (GSCs_a) and GSCs_c. The population of GSCs_b clustered independently.

The large variance between the different CSC populations as well as patient-specific variations within the four distinct groups of endometrioid carcinomas, glioblastomas, and adenocarcinomas of lung and prostate, were also visible in a hierarchical clustered heatmap of the 200 top expressed genes (for all detected genes see Figure S6). Distribution of up- and down-regulated genes of the top 200 expressed genes followed the Gaussian distribution (Figure 5, for the 200 top expressed genes, which were not significantly regulated see Figure S7). Notably, tumor type-specific clustering was not observable. However, cross-group clustering emerged with GSCs_a, GSCs_c, LCSCs_c, and PCSCs_c forming one pattern. A second pattern could be seen for PCSCs_a, ECSCs_a, LCSCs_a and LCSCs_b.

Further, ECSCs_b, PCSCs_b and ECSCs_c seemed to build one cluster-group (Figure 5). GSCs_b clustered independently, as already shown within the PCA (Figures 4 and 5). Of note, major histocompatibility complex class I A (*HLA-A*), major histocompatibility complex class I B (*HLA-B*) and interleukin 1 beta (*IL1B*) were detected in the top 200 expressed genes among the CSC populations.

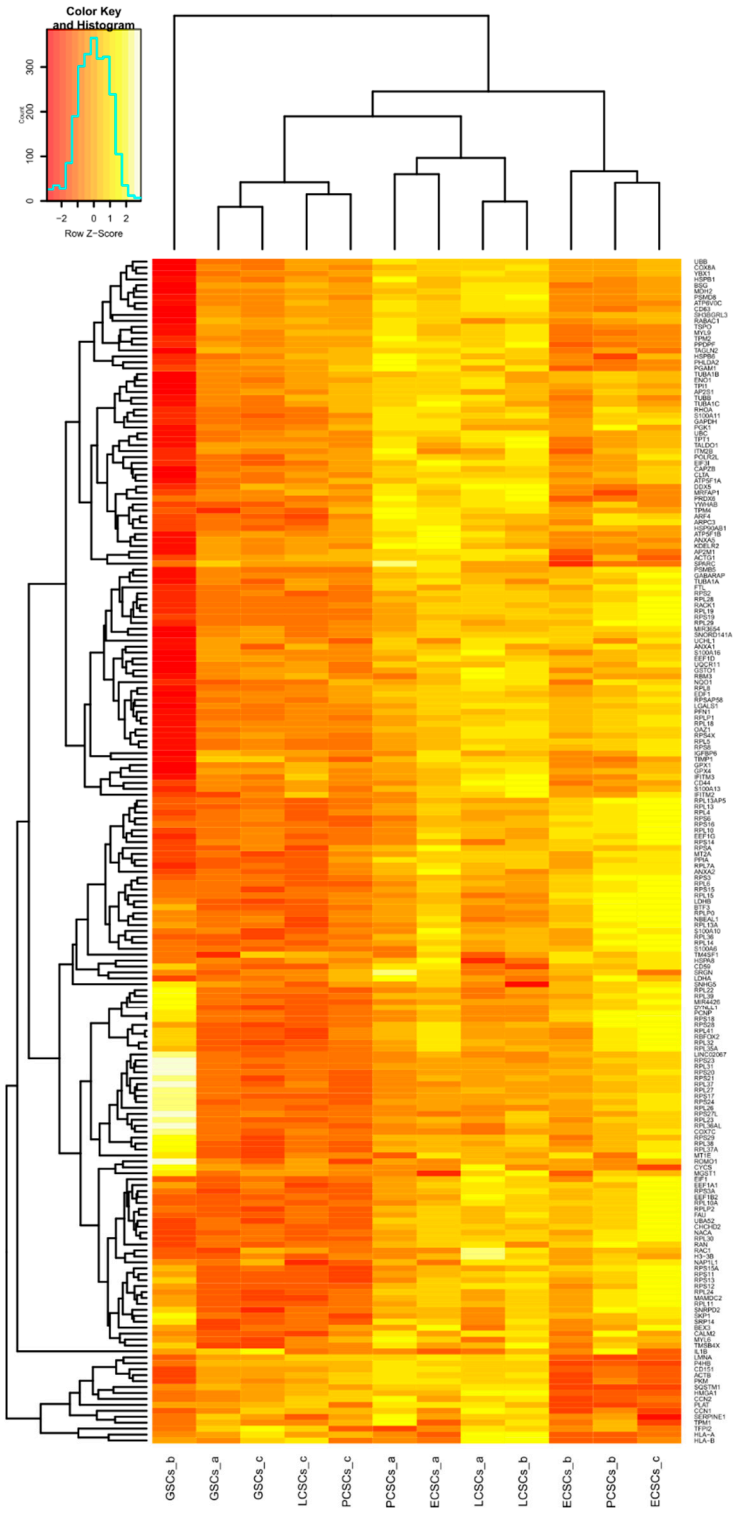

Figure 5. Hierarchically clustered heatmap of the 200 top expressed logarithmic gene counts within all 12 cancer stem-like cell (CSC) populations. RNA samples of different CSCs are arranged according to their corresponding expression profiles.

Next to the general clustering, it has been noticed that especially genes involved in ribosome biosynthesis have occurred more frequently (Figure 6A,B). Here, 20 different genes encoding for ribosomal proteins that are components of the 60S subunit can be found. Further, 14 genes involved in the protein synthesis of the 40S subunit of the ribosome are clustered under the 200 top expressed genes. Nevertheless, expression levels of genes relevant for the ribosome biosynthesis differed between the 12 CSC populations. Particularly striking was the high expression of diverse genes encoding for components of the 40S and 60S subunit in GSCs_b (Figure 6B). Additionally, PCSCs_b and ECSCs_c revealed high expression of ribosomal biosynthesis associated genes (Figure 6A). Among the enriched genes relevant for ribosome biosynthesis, we found distinct genes been highly expressed in GSCs_b (Figure 6A), while PCSCs_b and ECSCs_c showed other genes upregulated for ribosome biosynthesis (Figure 6B). As already shown within the dot plots, CSC marker *CD44* was ubiquitously expressed in all 12 CSC populations. Nevertheless, differences between the populations could be seen with LCSCs_a and LCSCs_b, revealing the highest expression (Figure 6A). Conspicuously, three genes of the S100 family are comprised within the top expressed genes among the 12 CSC populations, including *S100A13*, *S100A10* and *S100A6* (Figure 6A).

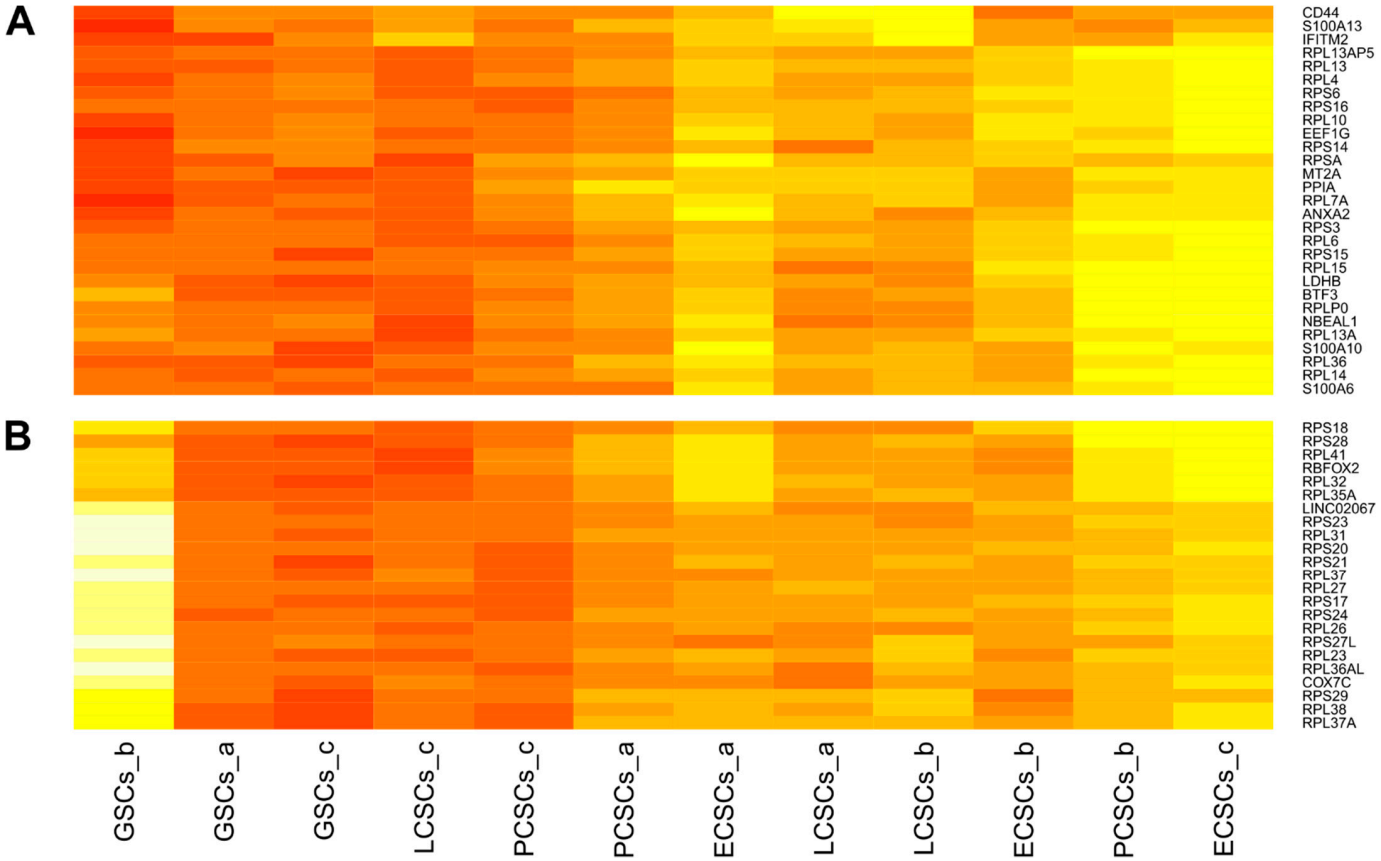

Figure 6. Two extracts of the hierarchically clustered heatmap of the 200 top expressed genes within all 12 cancer stem-like cell (CSC) populations. (**A**) Expressions of ribosomal biosynthesis associated genes were upregulated in endometrioid cancer stem-like cells c (ECSCs_c) and in prostate cancer stem-like cells b (PCSCs_b). Genes encoding for the S100 family were significantly expressed in all CSCs. (**B**) Expression levels of further genes relevant for ribosome biosynthesis differed between analyzed CSC populations, whereas glioblastoma stem-like cells b (GSCs_b) depicted the highest levels of genes responsible for the 40S and 60S subunit.

3.3. KEGG Pathway and GO-Term Analysis Reveal Broad Similarities between the Cancer Stem-like Cell Populations

For an unbiased detailed analysis of the transcriptomic profiles of the 12 CSC populations, we performed a KEGG pathway analysis (Figure 7, Table S1). Here, five of the top enriched pathways were significantly overrepresented in all CSC populations and plotted together ($p < 0.05$). Next to the gene pathway responsible for "Ribosome", which owns the strongest significance ($p = 1.9 \times 10^{-41}$), also "Oxidative phosphorylation" ($p = 0.013$) and "Non-alcoholic fatty liver disease" ($p = 0.015$) displayed highly enriched pathways. Surprisingly, two unexpected signaling pathways were also significantly overrepresented, namely the genes associated with "Parkinson's disease" ($p = 0.004$) and "Alzheimer's disease" ($p = 0.005$).

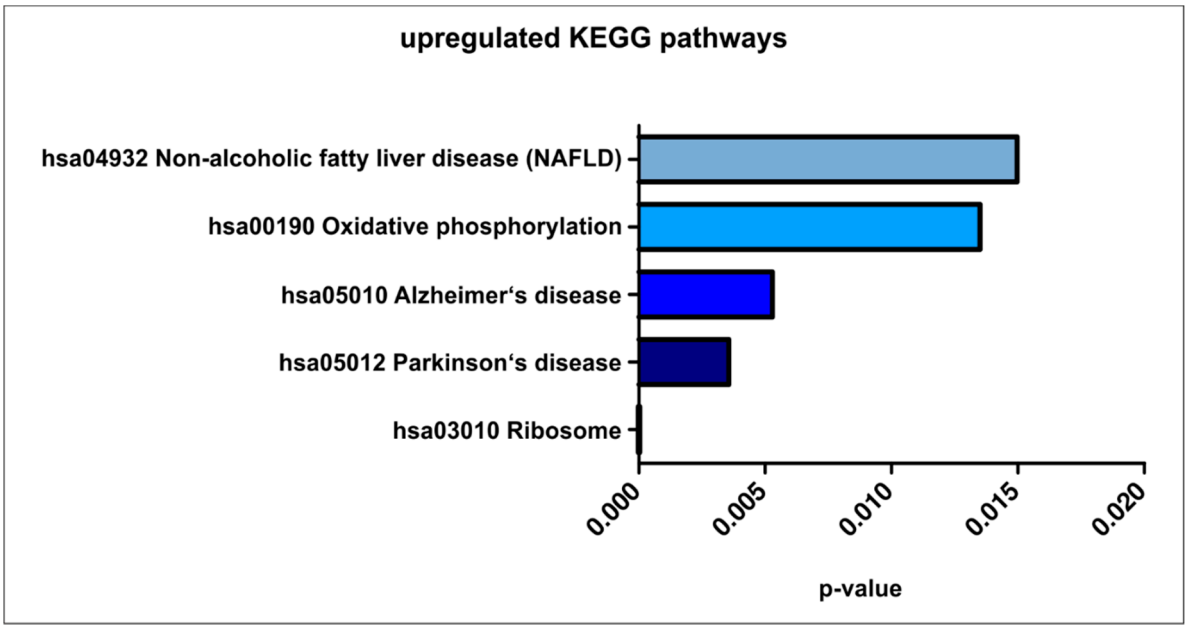

Figure 7. Top five upregulated KEGG pathways within the 12 investigated primary cancer stem-like cell populations ($p < 0.05$).

We further conducted GO-term enrichment analysis for a more specific insight into similarly upregulated terms from biological processes, cellular components and molecular functions (Figure 8). For enriched GO-terms relating to biological processes, the top ten terms were depicted in accordance with their fold enrichments (Figure 8A, Table S2). Here, genes involved in the glycolytic pathways (fructose and glycose) were highly enriched (see "methylglyoxal metabolic process"). Further, GO-terms "formation of cytoplasmic translation initiation complex" fitting to the enriched genes in ribosomal biosynthesis and "protein deneddylation" involved in ubiquitin-mediated proteasomal degradation were upregulated. Accordingly, GO-terms relating to the cellular components (Figure 8B, Table S3) showed six-fold upregulated genes involved in "translation preinitiation complex", "proteasome core complex, alpha-subunit complex" and "cytosolic large ribosomal subunit". Ribosome associated GO-terms were likewise found among the terms related to molecular function, such as "7S RNA binding", "5S rRNA binding" and "structural constituent of ribosome". Further, genes related to "peroxiredoxin activity" were highest enriched (Figure 8C). Additionally, "NF-κB binding" was found to be upregulated in all CSC populations (Table S4).

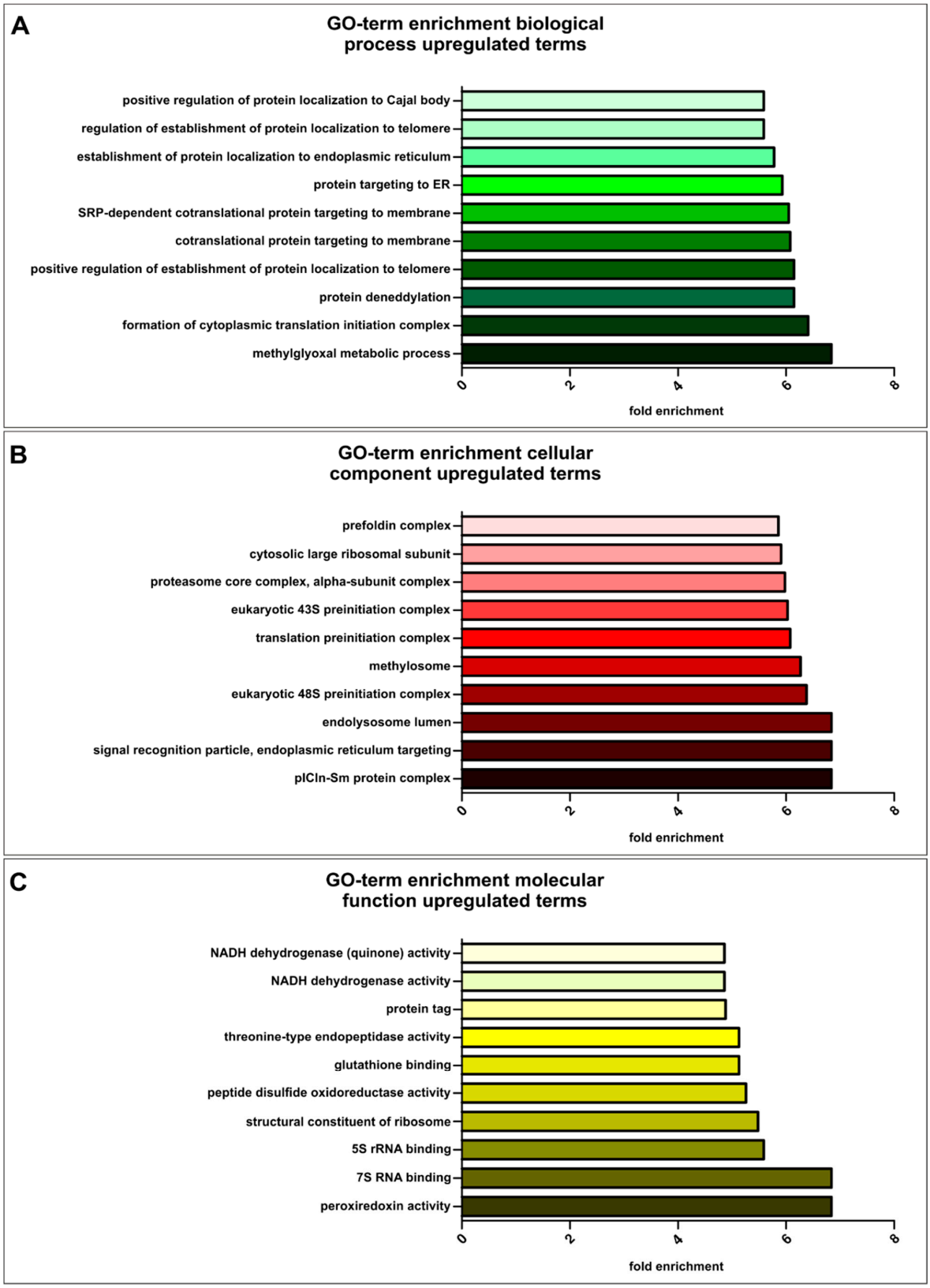

Figure 8. Gene ontology (GO)-term enrichment analysis of all 12 cancer stem-like cell populations, including all populations of endometrial-, glioblastoma-, lung- and prostate cancer stem-like cells, respectively. (**A**) Visualization of the top ten fold enriched GO-terms involved in biological processes ($p < 2.00 \times 10^{-3}$). (**B**) Top ten of the fold enriched GO-terms concerning cellular components ($p < 1.38 \times 10^{-3}$). **(C)** Representation of fold enriched GO-terms associated with molecular functions ($p < 2.65 \times 10^{-4}$).

4. Discussion

In the present study, we report for the first time global transcriptional differences and similarities of CSCs from various tumors including glioblastoma multiforme, non-small cell lung carcinoma, endometrial carcinoma, and prostate carcinoma. We found the transcripts of all investigated CSC-populations to share significantly upregulated genes associated with the mitochondrion, proteasome, and ribosome (Figure 9).

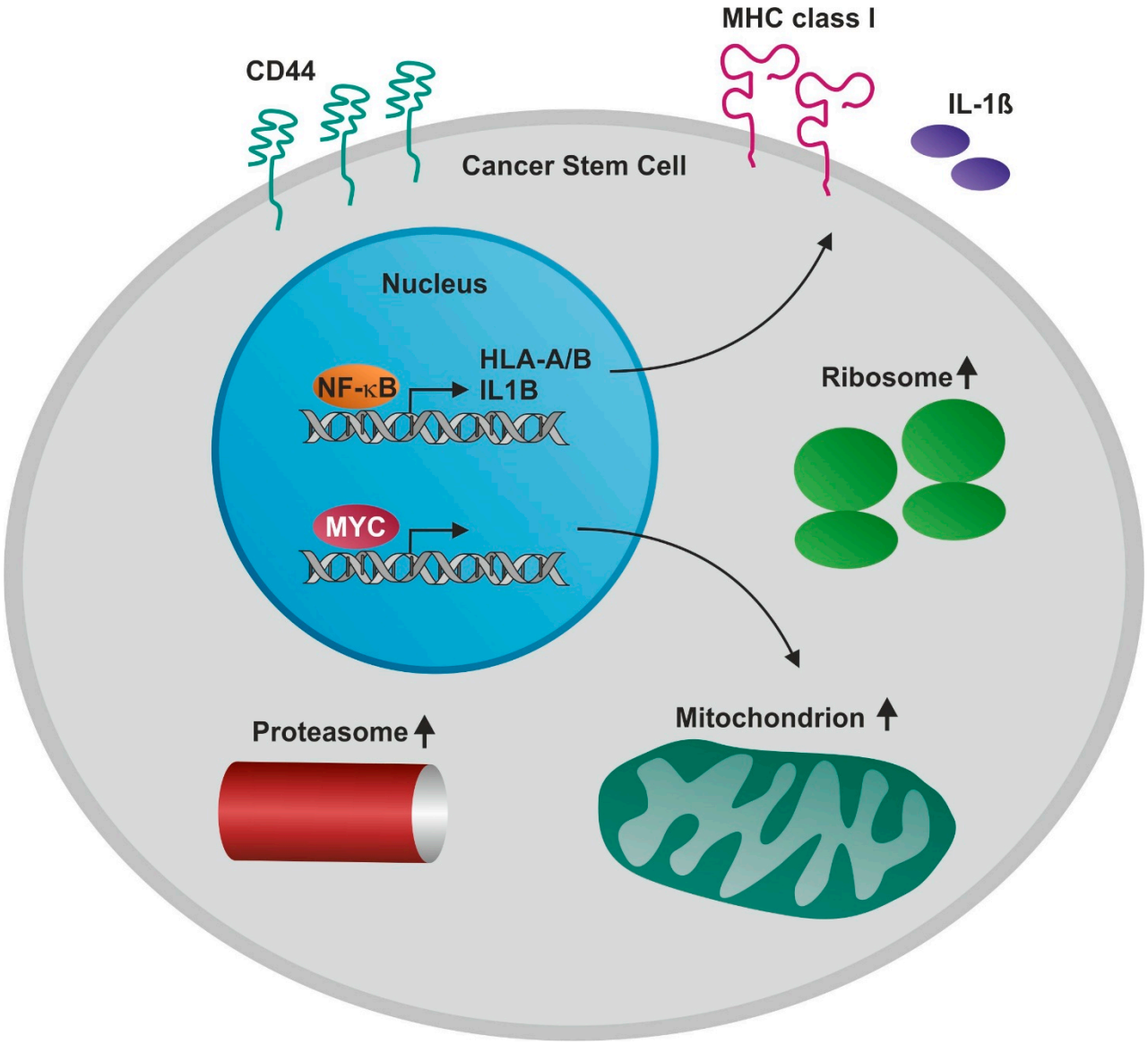

Figure 9. Schematic view on biological processes with enriched genes in CD44-positive cancer stem-like cells (CSCs) from glioblastoma, lung, endometrial and prostate cancer. Genes associated with the mitochondrion, proteasome, ribosome as well as *NF-κB* and *MYC* genes were highly enriched in all CSC populations.

In 1924, Otto Warburg and co-workers published a seminal paper on aerobic glycolysis in rat tumor cells and sections derived from human tumors [68]. The Warburg effect described an increased rate of glucose fermentation leading to lactic acid by tumor cells, even under aerobic conditions [69]. Eight-seven years later, the Warburg effect was included in the list of general hallmarks of cancer. Tumor cells are able to reprogram the energy metabolism to aerobic glycolysis independent to mitochondrial function to produce adenosine triphosphate (ATP) [70]. However, a tumor is increasingly recognized to consist of a highly heterogeneous cell mass, with the rare cell type of CSCs driving metastasis, in-

vasiveness, therapeutic resistance and recurrence of the tumor (reviewed in [71]). Here, we determined the global transcriptomes of CSCs propagated in vitro. Extending the findings of Warburg, these cells seem to have high metabolic plasticity and might use mitochondria for oxidative phosphorylation. In this line, gene enrichment analysis of the genes expressed in CSCs in comparison to the human genome showed a more than five-fold enrichment of expressed genes involved in mitochondria and oxidative phosphorylation. Accordingly, the amount of metabolic flexibility allowing the switch from oxidative phosphorylation to aerobic glycolysis was reported for CSCs (reviewed in [72]). In particular, a recent study investigated whether the metabolic state (especially the Warburg effect) of GSCs differs from the bulk of the tumor cells with a newly developed imaging system [73]. Vlashi and coworkers reported that monolayer cultures of GSCs produce about 20% less ATP than neurosphere cultures. Of note, another study showed high expressions of CD133 and Nestin in cultured GSC spheres but not in non-sphere GSC monolayers, cultured in 10% FBS [74]. In our study, we detected no difference in the expression of CSC markers in sphere cultures in comparison to adherently grown CSC populations. This might be due to a different experimental strategy used here, as we selected CSCs by differential trypsinization and cultured adherent populations with 10% serum supplemented with B27, bFGF-2 and EGF. Using specific inhibitors for oxidative phosphorylation and aerobic glycolysis, the authors suggested that ATP in both monolayer and neurosphere cultures was mainly produced by glycolysis and oxidative phosphorylation. Inhibition of glycolysis could be compensated through increased oxidative phosphorylation and vice versa. However, the authors conclude that the GSC-metabolism mainly relies on oxidative phosphorylation, which is in line to the here observed enrichment in genes involved in mitochondria and oxidative phosphorylation. Of note, mutations in *IDH1* and *IDH2* genes were shown to reprogram the metabolism of cancer cells to produce the onco-metabolite D-2-hydroxyglutarate and cells with mutations might be additionally dependent on lactate (see for review [75]). In our analysis, CSCs from a secondary GBM showing an *IDH1* mutation (see Figure 4, GSCs_b) did not cluster with the other analyzed GBM-derived CSCs without *IDH1* mutation because of significant changes in global gene expression.

Otto Warburg had many important contributions to biochemistry, such as the discovery of the 'oxygen-transferring ferment of respiration' (cytochrome-c oxidase complex), leading to him receiving the Nobel Prize in physiology or medicine, 1931. We found expressed genes enriched, which might be important for oxidative phosphorylation in mitochondria, such as NADH dehydrogenase activity, proton-transporting ATP synthase activity and cytochrome-c oxidase activity. Since respiratory chain activity leads to constant production of the reactive oxygen intermediate (ROS) it might not be surprising to find enrichment of genes, which code for antioxidant activity such as peroxiredoxin activity, glutathione binding and glutathione peroxidase activity. Some of the ROS produced might result in NF-κB binding. Other organelles containing enriched genes include ribosomes and 26 proteasomes. Indeed, oxidative phosphorylation in mitochondria have been identified as hallmark of CSC metabolism (reviewed in [76]). We also analyzed the expression of general CSC markers (Figure S7). Of special interest might be our recent observation of MYC, as a potential regulator of survival in colon carcinoma-specific CSCs (see [42]). In our study, we could detect MYC expressions in each investigated CSC population. Furthermore, published cancer surface markers CD44 and CD59, as well as the insulin-like growth factor binding protein 2 (IGFBP2), were expressed in all analyzed CSCs. In this context, Chen and Ding demonstrated gradually increased CD59 expression levels in different breast- and lung parental cancer cell lines and further observed that the absence of CD59 resulted in a completely suppression of tumorigenesis in vivo [77]. These results were investigated within sphere cultures, whereas we also detected CD59 within our adherently cultured CSC populations, further substantiating stem-like characteristics in our CSC models. Next, gene expressions for ribosomal proteins like *RPLP1*, *RPS27L*, *RPL14* and *RPL21* as well as the nuclear encoded and mitochondrial localized protein *COX8A* were detected after transcriptomic analysis. Finally, genes involved in cell cycle regulation and tumor growth

like *CDK16*, *CDC20* and the Ras homologue enriched in brain (*RHEB)* were ubiquitously expressed in our established CSCs. In this context, RHEB is commonly known to function in human carcinogenesis [78]. In more detail, Tian and co-workers reported the inhibition of cell proliferation and initiation of apoptosis in colorectal cancer cells via silencing of the *RHEB* gene [79].

We have previously shown that the guanine exchange factor (GEF) pleckstrin homology and RhoGEF domain containing G5 (*PLEKHG5*) plays an essential role in the formation of autolysosomes in glioblastoma cells and induces the transcription factor NF-κB [80]. However, in the present dataset we could not detect any expression of *PLEKHG5*. With respect to a recently proposed role of NF-κB in cancer and CSCs (reviewed in [1,81]), we searched for evidence of activated NF-κB in this transcriptome dataset. We detected highly enriched genes involved in the GO-term "NF-κB binding". However, out of all five DNA-binding subunits, only the expression of *RELA* in all CSC samples was detectable. Furthermore, expression of interleukin 6 and tumor necrosis factor-alpha was not detectable in CSCs, whereas we observed NF-κB target gene expression of *IL1B*, *HLA-A* as well as *HLA-B* in all CSC population. We therefore conclude that further experiments might be necessary to provide conclusive data on the role of NF-κB in CSCs.

We further demonstrate high amounts of ribosome-associated gene expressions in CSCs independent of the tumor type. These data suggest a mechanism of ribosome-enrichment for oxidative phosphorylation in CSCs. On the mechanistic level, RNA polymerase III (Pol III) may transcribe the ribosomal 5S rRNA and the 5.8S, 18S as well as 28S rRNAs are known to arise from the processing of a common precursor rRNA (47S) transcribed by the Pol I. Accordingly, altered ribosome components were discussed to play a significant role in CSCs [82]. There is additional evidence that ribosome biosynthesis and protein synthesis might be directed by transcription factor *MYC* (reviewed in [83]). Proteasome-related transcription was enriched by more than a factor of six in CSCs, although investigations with fluorogenic proteasome substrates suggest a low activity of proteasomal protein degradation in CSCs of breast cancer and glioma [84].

Limitations: on a technical level, this study relies on in vitro protein and transcriptomic data generated with newly developed nanopore sequencing. Although we generally achieved full-length transcript data using this technology, read depth is not as high as in standard Illumina approaches, but seems to be sufficiently sensitive to detect differences and similarities between CSC populations. However, due to the performed read depth, we cannot exclude the possibility of missing low abundant transcripts as transcription factors.

5. Conclusions

From our transcriptomic analysis, we conclude that the here used CSC populations could be divided into three clusters independent of the parental tumor. Nevertheless, we detected conserved expressions of the CSC markers CD44, Nestin, and MYC on mRNA and protein level as well as transcriptional expression of *CD59*. Moreover, GO-term and KEGG pathway enrichment analysis revealed upregulated genes related to ribosomal biosynthesis, the mitochondrion, oxidative phosphorylation, and glycolytic pathways as well as to the proteasome, suggesting the great extent of metabolic flexibility in CSCs. Taken together, transcriptomic analysis might pave the way for future pathway-directed therapies such as targeting mitochondria and 80S ribosomes, together with the already established proteasome. However, further in vitro and in vivo studies are necessary to overcome potential limitations of the study and for specific target discovery.

Supplementary Materials: The following are available online at https://www.mdpi.com/2072-6694/13/5/1136/s1, Figure S1: Immunocytochemical stainings of cultured cancer stem-like cells from one population of endometrioid cancer and glioblastoma multiforme, grown as spheres, Figure S2: Co-expressions of CD44/CD133 in cancer stem-like cell populations after immunocytochemistry, Figure S3: Nestin protein expressions of adherently grown cancer stem-like cell populations, detected via immunocytochemical stainings, Figure S4: MYC immunocytochemistry of adherently cultured cancer stem-like cell populations, Figure S5: Immunostaining of CD44/CD133, Nestin and MYC in

cultured adult human dermal fibroblasts (HDFs) as biological negative control to primary isolated cancer stem-like cell populations., Figure S6: Heatmap of all normalized gene counts detected by nanopore sequencing, Figure S7: Heatmap of the 200 top expressed, not significantly regulated genes detected via nanopore sequencing, Table S1: KEGG pathway analysis, Table S2: GO-term enrichment in biological processes, Table S3: GO-term enrichment in cellular components, Table S4: GO-term enrichment of molecular functions.

Author Contributions: Conceptualization, B.K., C.K. (Christian Kaltschmidt), C.B.-J. and M.S.; Data curation, K.E.W., O.H., B.A.W., A.L.H., C.K. (Cornelius Knabbe), T.B., J.F.W.G., J.K., T.N., F.M., M.B., J.P., B.K., C.K. (Christian Kaltschmidt), C.B.-J. and M.S.; formal analysis, K.E.W., O.H. and B.A.W.; funding acquisition, J.K., B.K. and C.K. (Christian Kaltschmidt); investigation, K.E.W., O.H., B.A.W., L.P.H., A.L.H. and T.B.; project administration, B.K. and C.K. (Christian Kaltschmidt); supervision, B.K., C.K. (Christian Kaltschmidt), C.B.-J. and M.S.; visualization, K.E.W., O.H., B.A.W. and J.F.W.G. writing—original draft, K.E.W., O.H., B.A.W., A.L.H., C.K. (Cornelius Knabbe), T.B., J.F.W.G., J.K., T.N., F.M., M.B., J.P., B.K., C.K. (Christian Kaltschmidt), C.B.-J. and M.S.; writing—review and editing, K.E.W., O.H., B.A.W., L.P.H., A.L.H., C.K. (Cornelius Knabbe), T.B., J.F.W.G., J.K., T.N., F.M., M.B., J.P., B.K., C.K. (Christian Kaltschmidt), C.B.-J. and M.S. All authors have read and agreed to the published version of the manuscript.

Funding: This research was funded in part by the University of Bielefeld. Kaya Elisa Witte, Beatrice Ariane Windmöller and Laureen Patricia Helweg are funded by an internal grant of the Bethel Foundation, Bielefeld, Germany. The authors gratefully acknowledge support by the "European Regional Development Fund (EFRE)" through project "Cluster Industrial Biotechnology (CLIB) Kompetenzzentrum Biotechnologie (CKB)" (34.EFRE-0300095/1703FI04) for Oliver Hertel, Tobias Busche and Jörn Kalinowski.

Institutional Review Board Statement: The study was conducted according to the guidelines of the Declaration of Helsinki, and approved by the Institutional Review Board (or Ethics Committee) of Ethics committee Münster, Germany (2017-522-f-S, 27.07.2018).

Informed Consent Statement: Informed consent was obtained from all subjects involved in the study.

Data Availability Statement: The transcriptomic data are available via NCBI BioProject PRJNA697831.

Acknowledgments: The authors appreciate the excellent help during sample preparation by Christine Förster, Institute of Pathology, KRH Hospital Nordstadt, affiliated with the Protestant Hospital of Bethel Foundation. We thank Christian Rückert for support with raw data upload to NCBI. Further, the technical work of Angela Kralemann-Köhler, Claudia Rose and Ulrike Hormel is gratefully acknowledged. The authors acknowledge support for the publication costs by the Deutsche Forschungsgemeinschaft and the Open Access Publication Fund of Bielefeld University.

Conflicts of Interest: The authors declare no conflict of interest. The funders had no role in the design of the study; in the collection, analyses, or interpretation of data; in the writing of the manuscript, or in the decision to publish the results.

References

1. Kaltschmidt, C.; Banz-Jansen, C.; Benhidjeb, T.; Beshay, M.; Förster, C.; Greiner, J.; Hamelmann, E.; Jorch, N.; Mertzlufft, F.; Pfitzenmaier, J.; et al. A Role for NF-κB in Organ Specific Cancer and Cancer Stem Cells. *Cancers* **2019**, *11*, 655. [CrossRef]
2. Lapidot, T.; Sirard, C.; Vormoor, J.; Murdoch, B.; Hoang, T.; Caceres-Cortes, J.; Minden, M.; Paterson, B.; Caligiuri, M.A.; Dick, J.E. A cell initiating human acute myeloid leukaemia after transplantation into SCID mice. *Nature* **1994**, *367*, 645–648. [CrossRef] [PubMed]
3. Meacham, C.E.; Morrison, S.J. Tumour heterogeneity and cancer cell plasticity. *Nature* **2013**, *501*, 328–337. [CrossRef]
4. Hubbard, S.A.; Friel, A.M.; Kumar, B.; Zhang, L.; Rueda, B.R.; Gargett, C.E. Evidence for cancer stem cells in human endometrial carcinoma. *Cancer Res.* **2009**, *69*, 8241–8248. [CrossRef] [PubMed]
5. Eramo, A.; Lotti, F.; Sette, G.; Pilozzi, E.; Biffoni, M.; Di Virgilio, A.; Conticello, C.; Ruco, L.; Peschle, C.; de Maria, R. Identification and expansion of the tumorigenic lung cancer stem cell population. *Cell Death Differ.* **2008**, *15*, 504–514. [CrossRef]
6. Bayin, N.S.; Modrek, A.S.; Placantonakis, D.G. Glioblastoma stem cells: Molecular characteristics and therapeutic implications. *World J. Stem Cells* **2014**, *6*, 230–238. [CrossRef]
7. Kasper, S. Exploring the origins of the normal prostate and prostate cancer stem cell. *Stem Cell Rev.* **2008**, *4*, 193–201. [CrossRef]
8. Sultan, M.; Coyle, K.M.; Vidovic, D.; Thomas, M.L.; Gujar, S.; Marcato, P. Hide-and-seek: The interplay between cancer stem cells and the immune system. *Carcinogenesis* **2017**, *38*, 107–118. [CrossRef] [PubMed]

9. Marsden, C.G.; Wright, M.J.; Pochampally, R.; Rowan, B.G. Breast tumor-initiating cells isolated from patient core biopsies for study of hormone action. *Methods Mol. Biol.* **2009**, *590*, 363–375. [CrossRef] [PubMed]
10. Singh, S.K.; Clarke, I.D.; Terasaki, M.; Bonn, V.E.; Hawkins, C.; Squire, J.; Dirks, P.B. Identification of a cancer stem cell in human brain tumors. *Cancer Res.* **2003**, *63*, 5821–5828. [PubMed]
11. Di Tomaso, T.; Mazzoleni, S.; Wang, E.; Sovena, G.; Clavenna, D.; Franzin, A.; Mortini, P.; Ferrone, S.; Doglioni, C.; Marincola, F.M.; et al. Immunobiological characterization of cancer stem cells isolated from glioblastoma patients. *Clin. Cancer Res.* **2010**, *16*, 800–813. [CrossRef] [PubMed]
12. Li, X.; Larsson, P.; Ljuslinder, I.; Öhlund, D.; Myte, R.; Löfgren-Burström, A.; Zingmark, C.; Ling, A.; Edin, S.; Palmqvist, R. Ex Vivo Organoid Cultures Reveal the Importance of the Tumor Microenvironment for Maintenance of Colorectal Cancer Stem Cells. *Cancers* **2020**, *12*, 923. [CrossRef]
13. Torre, L.A.; Bray, F.; Siegel, R.L.; Ferlay, J.; Lortet-Tieulent, J.; Jemal, A. Global cancer statistics, 2012. *CA Cancer J. Clin.* **2015**, *65*, 87–108. [CrossRef] [PubMed]
14. Renehan, A.G.; Roberts, D.L.; Dive, C. Obesity and cancer: Pathophysiological and biological mechanisms. *Arch. Physiol. Biochem.* **2008**, *114*, 71–83. [CrossRef]
15. Nevadunsky, N.S.; van Arsdale, A.; Strickler, H.D.; Moadel, A.; Kaur, G.; Levitt, J.; Girda, E.; Goldfinger, M.; Goldberg, G.L.; Einstein, M.H. Obesity and age at diagnosis of endometrial cancer. *Obstet. Gynecol.* **2014**, *124*, 300–306. [CrossRef] [PubMed]
16. Ding, D.-C.; Liu, H.-W.; Chang, Y.-H.; Chu, T.-Y. Expression of CD133 in endometrial cancer cells and its implications. *J. Cancer* **2017**, *8*, 2142–2153. [CrossRef] [PubMed]
17. Desai, R.; Suryadevara, C.M.; Batich, K.A.; Farber, S.H.; Sanchez-Perez, L.; Sampson, J.H. Emerging immunotherapies for glioblastoma. *Expert Opin. Emerg. Drugs* **2016**, *21*, 133–145. [CrossRef] [PubMed]
18. Delgado-López, P.D.; Corrales-García, E.M. Survival in glioblastoma: A review on the impact of treatment modalities. *Clin. Transl. Oncol.* **2016**, *18*, 1062–1071. [CrossRef] [PubMed]
19. Almeida, N.D.; Klein, A.L.; Hogan, E.A.; Terhaar, S.J.; Kedda, J.; Uppal, P.; Sack, K.; Keidar, M.; Sherman, J.H. Cold Atmospheric Plasma as an Adjunct to Immunotherapy for Glioblastoma Multiforme. *World Neurosurg.* **2019**, *130*, 369–376. [CrossRef]
20. Lathia, J.D.; Mack, S.C.; Mulkearns-Hubert, E.E.; Valentim, C.L.L.; Rich, J.N. Cancer stem cells in glioblastoma. *Genes Dev.* **2015**, *29*, 1203–1217. [CrossRef]
21. Glas, M.; Rath, B.H.; Simon, M.; Reinartz, R.; Schramme, A.; Trageser, D.; Eisenreich, R.; Leinhaas, A.; Keller, M.; Schildhaus, H.-U.; et al. Residual tumor cells are unique cellular targets in glioblastoma. *Ann. Neurol.* **2010**, *68*, 264–269. [CrossRef]
22. Schneider, M.; Ströbele, S.; Nonnenmacher, L.; Siegelin, M.D.; Tepper, M.; Stroh, S.; Hasslacher, S.; Enzenmüller, S.; Strauss, G.; Baumann, B.; et al. A paired comparison between glioblastoma "stem cells" and differentiated cells. *Int. J. Cancer* **2016**, *138*, 1709–1718. [CrossRef] [PubMed]
23. Bonavia, R.; Inda, M.-d.-M.; Cavenee, W.; Furnari, F. Heterogeneity Maintenance in Glioblastoma: A social network. *Cancer Res.* **2011**, *71*, 4055–4060. [CrossRef] [PubMed]
24. Yan, K.; Yang, K.; Rich, J.N. The Evolving Landscape of Brain Tumor Cancer Stem Cells. *Curr. Opin. Neurol.* **2013**, *26*, 701–707. [CrossRef] [PubMed]
25. Suvà, M.L.; Rheinbay, E.; Gillespie, S.M.; Patel, A.P.; Wakimoto, H.; Rabkin, S.D.; Riggi, N.; Chi, A.S.; Cahill, D.P.; Nahed, B.V.; et al. Reconstructing and reprogramming the tumor-propagating potential of glioblastoma stem-like cells. *Cell* **2014**, *157*, 580–594. [CrossRef] [PubMed]
26. Seymour, T.; Nowak, A.; Kakulas, F. Targeting Aggressive Cancer Stem Cells in Glioblastoma. *Front. Oncol.* **2015**, *5*. [CrossRef] [PubMed]
27. Happold, C.; Stojcheva, N.; Silginer, M.; Weiss, T.; Roth, P.; Reifenberger, G.; Weller, M. Transcriptional control of O6 -methylguanine DNA methyltransferase expression and temozolomide resistance in glioblastoma. *J. Neurochem.* **2018**, *144*, 780–790. [CrossRef]
28. Stupp, R.; Mason, W.P.; van den Bent, M.J.; Weller, M.; Fisher, B.; Taphoorn, M.J.; Belanger, K.; Brandes, A.A.; Marosi, C.; Bogdahn, U.; et al. Radiotherapy plus concomitant and adjuvant temozolomide for glioblastoma. *N. Engl. J. Med.* **2005**, *352*. [CrossRef]
29. Hegi, M.E.; Diserens, A.-C.; Gorlia, T.; Hamou, M.-F.; de Tribolet, N.; Weller, M.; Kros, J.M.; Hainfellner, J.A.; Mason, W.; Mariani, L.; et al. MGMT gene silencing and benefit from temozolomide in glioblastoma. *N. Engl. J. Med.* **2005**, *352*, 997–1003. [CrossRef]
30. Ruiz-Ceja, K.A.; Chirino, Y.I. Current FDA-approved treatments for non-small cell lung cancer and potential biomarkers for its detection. *Biomed. Pharmacother.* **2017**, *90*, 24–37. [CrossRef]
31. Schild, S.E.; Tan, A.D.; Wampfler, J.A.; Ross, H.J.; Yang, P.; Sloan, J.A. A new scoring system for predicting survival in patients with non-small cell lung cancer. *Cancer Med.* **2015**, *4*, 1334–1343. [CrossRef] [PubMed]
32. Tan, Y.; Chen, B.; Xu, W.; Zhao, W.; Wu, J. Clinicopathological significance of CD133 in lung cancer: A meta-analysis. *Mol. Clin. Oncol.* **2014**, *2*, 111–115. [CrossRef] [PubMed]
33. Zakaria, N.; Yusoff, N.M.; Zakaria, Z.; Lim, M.N.; Baharuddin, P.J.N.; Fakiruddin, K.S.; Yahaya, B. Human non-small cell lung cancer expresses putative cancer stem cell markers and exhibits the transcriptomic profile of multipotent cells. *BMC Cancer* **2015**, *15*, 84. [CrossRef] [PubMed]
34. Siegel, R.L.; Miller, K.D.; Jemal, A. Cancer statistics, 2019. *CA Cancer J. Clin.* **2019**, *69*, 7–34. [CrossRef]
35. Li, J.; Wang, Z. The pathology of unusual subtypes of prostate cancer. *Chin. J. Cancer Res.* **2016**, *28*, 130–143. [CrossRef]

36. Schröder, F.H.; Hugosson, J.; Roobol, M.J.; Tammela, T.L.J.; Zappa, M.; Nelen, V.; Kwiatkowski, M.; Lujan, M.; Määttänen, L.; Lilja, H.; et al. Screening and prostate cancer mortality: Results of the European Randomised Study of Screening for Prostate Cancer (ERSPC) at 13 years of follow-up. *Lancet* **2014**, *384*, 2027–2035. [CrossRef]
37. Bill-Axelson, A.; Holmberg, L.; Garmo, H.; Taari, K.; Busch, C.; Nordling, S.; Häggman, M.; Andersson, S.-O.; Andrén, O.; Steineck, G.; et al. Radical Prostatectomy or Watchful Waiting in Prostate Cancer—29-Year Follow-up. *N. Engl. J. Med.* **2018**, *379*, 2319–2329. [CrossRef] [PubMed]
38. Wang, X.; Kruithof-de Julio, M.; Economides, K.D.; Walker, D.; Yu, H.; Halili, M.V.; Hu, Y.-P.; Price, S.M.; Abate-Shen, C.; Shen, M.M. A luminal epithelial stem cell that is a cell of origin for prostate cancer. *Nature* **2009**, *461*, 495–500. [CrossRef]
39. Rajasekhar, V.K.; Studer, L.; Gerald, W.; Socci, N.D.; Scher, H.I. Tumour-initiating stem-like cells in human prostate cancer exhibit increased NF-κB signalling. *Nat. Commun.* **2011**, *2*, 162. [CrossRef] [PubMed]
40. Cao, Y.; Li, W.; Chu, X.; Wu, K.; Liu, H.; Liu, D. Research progress and application of nanopore sequencing technology. *Sheng Wu Gong Cheng Xue Bao* **2020**, *36*, 811–819. [CrossRef]
41. Windmöller, B.A.; Greiner, J.F.W.; Förster, C.; Wilkens, L.; Mertzlufft, F.; Am Schulte Esch, J.; Kaltschmidt, B.; Kaltschmidt, C.; Beshay, M. A typical carcinoid of the lung—A case report with pathological correlation and propagation of the cancer stem cell line BKZ1 with synaptophysin expression. *Medicine* **2019**, *98*, e18174. [CrossRef] [PubMed]
42. Schulte am Esch, J.; Windmöller, B.A.; Hanewinkel, J.; Storm, J.; Förster, C.; Wilkens, L.; Krüger, M.; Kaltschmidt, B.; Kaltschmidt, C. Isolation and Characterization of Two Novel Colorectal Cancer Cell Lines, Containing a Subpopulation with Potential Stem-like Properties: Treatment Options by MYC/NMYC Inhibition. *Cancers* **2020**, *12*, 2582. [CrossRef]
43. Walia, V.; Elble, R.C. Enrichment for breast cancer cells with stem/progenitor properties by differential adhesion. *Stem Cells Dev.* **2010**, *19*, 1175–1182. [CrossRef] [PubMed]
44. Morata-Tarifa, C.; Jiménez, G.; García, M.A.; Entrena, J.M.; Griñán-Lisón, C.; Aguilera, M.; Picon-Ruiz, M.; Marchal, J.A. Low adherent cancer cell subpopulations are enriched in tumorigenic and metastatic epithelial-to-mesenchymal transition-induced cancer stem-like cells. *Sci. Rep.* **2016**, *6*, 18772. [CrossRef] [PubMed]
45. Wick, R.R.; Judd, L.M.; Gorrie, C.L.; Holt, K.E. Completing bacterial genome assemblies with multiplex MinION sequencing. *Microb. Genom.* **2017**, *3*, e000132. [CrossRef] [PubMed]
46. Andrews, S. *FastQC: A Quality Control Tool for High Throughput Sequence Data*; Bioinformatics; Babraham: Cambridge, UK, 2010.
47. Schneider, V.A.; Graves-Lindsay, T.; Howe, K.; Bouk, N.; Chen, H.-C.; Kitts, P.A.; Murphy, T.D.; Pruitt, K.D.; Thibaud-Nissen, F.; Albracht, D.; et al. Evaluation of GRCh38 and de novo haploid genome assemblies demonstrates the enduring quality of the reference assembly. *Genome Res.* **2017**, *27*, 849–864. [CrossRef] [PubMed]
48. O'Leary, N.A.; Wright, M.W.; Brister, J.R.; Ciufo, S.; Haddad, D.; McVeigh, R.; Rajput, B.; Robbertse, B.; Smith-White, B.; Ako-Adjei, D.; et al. Reference sequence (RefSeq) database at NCBI: Current status, taxonomic expansion, and functional annotation. *Nucleic Acids Res.* **2016**, *44*, D733–D745. [CrossRef] [PubMed]
49. Li, H. Minimap2: Pairwise alignment for nucleotide sequences. *Bioinformatics* **2018**, *34*, 3094–3100. [CrossRef] [PubMed]
50. Li, H.; Handsaker, B.; Wysoker, A.; Fennell, T.; Ruan, J.; Homer, N.; Marth, G.; Abecasis, G.; Durbin, R. The Sequence Alignment/Map format and SAMtools. *Bioinformatics* **2009**, *25*, 2078–2079. [CrossRef]
51. Weirather, J.L.; de Cesare, M.; Wang, Y.; Piazza, P.; Sebastiano, V.; Wang, X.-J.; Buck, D.; Au, K.F. Comprehensive comparison of Pacific Biosciences and Oxford Nanopore Technologies and their applications to transcriptome analysis. *F1000Research* **2017**, *6*, 100. [CrossRef] [PubMed]
52. Wyman, D.; Mortazavi, A. TranscriptClean: Variant-aware correction of indels, mismatches and splice junctions in long-read transcripts. *Bioinformatics* **2018**, *35*, 340–342. [CrossRef]
53. Huber, W.; Carey, V.J.; Gentleman, R.; Anders, S.; Carlson, M.; Carvalho, B.S.; Bravo, H.C.; Davis, S.; Gatto, L.; Girke, T.; et al. Orchestrating high-throughput genomic analysis with Bioconductor. *Nat. Methods* **2015**, *12*, 115–121. [CrossRef]
54. Liao, Y.; Smyth, G.K.; Shi, W. The R package Rsubread is easier, faster, cheaper and better for alignment and quantification of RNA sequencing reads. *Nucleic Acids Res.* **2019**, *47*, e47. [CrossRef] [PubMed]
55. Robinson, M.D.; McCarthy, D.J.; Smyth, G.K. edgeR: A Bioconductor package for differential expression analysis of digital gene expression data. *Bioinformatics* **2010**, *26*, 139–140. [CrossRef] [PubMed]
56. McCarthy, D.J.; Chen, Y.; Smyth, G.K. Differential expression analysis of multifactor RNA-Seq experiments with respect to biological variation. *Nucleic Acids Res.* **2012**, *40*, 4288–4297. [CrossRef] [PubMed]
57. Robinson, M.D.; Oshlack, A. A scaling normalization method for differential expression analysis of RNA-seq data. *Genome Biol.* **2010**, *11*, R25. [CrossRef] [PubMed]
58. Blighe, K. *PCAtools: Everything Principal Components Analysis: Everything Principal Components Analysis*; PCAtools: London, UK, 2019.
59. Warnes, G.; Bolker, B.; Bonebakker, L.; Gentleman, R.; Huber, W.; Liaw, A.; Lumley, T.; Maechler, M.; Magnusson, A.; Moeller, S.; et al. *gplots: Various R Programming Tools for Plotting Data*, R Package Version 3.0.1.1. Available online: https://cran.r-project.org/web/packages/gplots/gplots.pdf (accessed on 6 March 2021).
60. Harrell Frank, E., Jr. With Contributions from Dupont, Charles and Many Others. *Hmisc: Harrell Miscellaneous*, R Package Version. Available online: https://cran.r-project.org/web/packages/Hmisc/Hmisc.pdf (accessed on 6 March 2021).

61. Mi, H.; Ebert, D.; Muruganujan, A.; Mills, C.; Albou, L.-P.; Mushayamaha, T.; Thomas, P.D. PANTHER version 16: A revised family classification, tree-based classification tool, enhancer regions and extensive API. *Nucleic Acids Res.* **2021**, *49*, D394–D403. [CrossRef] [PubMed]
62. Huang, D.W.; Sherman, B.T.; Lempicki, R.A. Systematic and integrative analysis of large gene lists using DAVID bioinformatics resources. *Nat. Protoc.* **2009**, *4*, 44–57. [CrossRef] [PubMed]
63. Huang, D.W.; Sherman, B.T.; Lempicki, R.A. Bioinformatics enrichment tools: Paths toward the comprehensive functional analysis of large gene lists. *Nucleic Acids Res.* **2009**, *37*, 1–13. [CrossRef]
64. Greiner, J.F.W.; Hauser, S.; Widera, D.; Müller, J.; Qunneis, F.; Zander, C.; Martin, I.; Mallah, J.; Schuetzmann, D.; Prante, C.; et al. Efficient animal-serum free 3D cultivation method for adult human neural crest-derived stem cell therapeutics. *Eur. Cells Mater.* **2011**, *22*, 403–419. [CrossRef]
65. Hauser, S.; Widera, D.; Qunneis, F.; Müller, J.; Zander, C.; Greiner, J.; Strauss, C.; Lüningschrör, P.; Heimann, P.; Schwarze, H.; et al. Isolation of novel multipotent neural crest-derived stem cells from adult human inferior turbinate. *Stem Cells Dev.* **2012**, *21*, 742–756. [CrossRef] [PubMed]
66. Höving, A.L.; Schmidt, K.E.; Merten, M.; Hamidi, J.; Rott, A.-K.; Faust, I.; Greiner, J.F.W.; Gummert, J.; Kaltschmidt, B.; Kaltschmidt, C.; et al. Blood Serum Stimulates p38-Mediated Proliferation and Changes in Global Gene Expression of Adult Human Cardiac Stem Cells. *Cells* **2020**, *9*, 1472. [CrossRef] [PubMed]
67. Höving, A.L.; Sielemann, K.; Greiner, J.F.W.; Kaltschmidt, B.; Knabbe, C.; Kaltschmidt, C. Transcriptome Analysis Reveals High Similarities between Adult Human Cardiac Stem Cells and Neural Crest-Derived Stem Cells. *Biology* **2020**, *9*, 435. [CrossRef] [PubMed]
68. Warburg, O.; Posener, K.; Negelein, E. Über den Stoffwechsel der Carcinomzelle. *Biochem. Zeitschr.* **1924**, *152*, 309–344. [CrossRef]
69. Warburg, O. On respiratory impairment in cancer cells. *Science* **1956**, *124*, 269–270. [PubMed]
70. Hanahan, D.; Weinberg, R.A. Hallmarks of cancer: The next generation. *Cell* **2011**, *144*, 646–674. [CrossRef] [PubMed]
71. Zhao, Y.; Dong, Q.; Li, J.; Zhang, K.; Qin, J.; Zhao, J.; Sun, Q.; Wang, Z.; Wartmann, T.; Jauch, K.W.; et al. Targeting cancer stem cells and their niche: Perspectives for future therapeutic targets and strategies. *Semin. Cancer Biol.* **2018**, *53*, 139–155. [CrossRef] [PubMed]
72. García-Heredia, J.M.; Carnero, A. Role of Mitochondria in Cancer Stem Cell Resistance. *Cells* **2020**, *9*, 1693. [CrossRef] [PubMed]
73. Vlashi, E.; Lagadec, C.; Vergnes, L.; Matsutani, T.; Masui, K.; Poulou, M.; Popescu, R.; Della Donna, L.; Evers, P.; Dekmezian, C.; et al. Metabolic state of glioma stem cells and nontumorigenic cells. *Proc. Natl. Acad. Sci. USA* **2011**, *108*, 16062–16067. [CrossRef] [PubMed]
74. Yuan, X.; Curtin, J.; Xiong, Y.; Liu, G.; Waschsmann-Hogiu, S.; Farkas, D.L.; Black, K.L.; Yu, J.S. Isolation of cancer stem cells from adult glioblastoma multiforme. *Oncogene* **2004**, *23*, 9392–9400. [CrossRef] [PubMed]
75. Dang, L.; Yen, K.; Attar, E.C. IDH mutations in cancer and progress toward development of targeted therapeutics. *Ann. Oncol.* **2016**, *27*, 599–608. [CrossRef] [PubMed]
76. Sancho, P.; Barneda, D.; Heeschen, C. Hallmarks of cancer stem cell metabolism. *Br. J. Cancer* **2016**, *114*, 1305–1312. [CrossRef] [PubMed]
77. Chen, J.; Ding, P.; Li, L.; Gu, H.; Zhang, X.; Zhang, L.; Wang, N.; Gan, L.; Wang, Q.; Zhang, W.; et al. CD59 Regulation by SOX2 Is Required for Epithelial Cancer Stem Cells to Evade Complement Surveillance. *Stem Cell Rep.* **2017**, *8*, 140–151. [CrossRef]
78. Lu, Z.H.; Shvartsman, M.B.; Lee, A.Y.; Shao, J.M.; Murray, M.M.; Kladney, R.D.; Fan, D.; Krajewski, S.; Chiang, G.G.; Mills, G.B.; et al. Mammalian target of rapamycin activator RHEB is frequently overexpressed in human carcinomas and is critical and sufficient for skin epithelial carcinogenesis. *Cancer Res.* **2010**, *70*, 3287–3298. [CrossRef]
79. Tian, Y.; Shen, L.; Li, F.; Yang, J.; Wan, X.; Ouyang, M. Silencing of RHEB inhibits cell proliferation and promotes apoptosis in colorectal cancer cells via inhibition of the mTOR signaling pathway. *J. Cell. Physiol.* **2020**, *235*, 442–453. [CrossRef] [PubMed]
80. Witte, K.E.; Slotta, C.; Lütkemeyer, M.; Kitke, A.; Coras, R.; Simon, M.; Kaltschmidt, C.; Kaltschmidt, B. PLEKHG5 regulates autophagy, survival and MGMT expression in U251-MG glioblastoma cells. *Sci. Rep.* **2020**, *10*, 21858. [CrossRef]
81. Kaltschmidt, B.; Greiner, J.F.W.; Kadhim, H.M.; Kaltschmidt, C. Subunit-Specific Role of NF-κB in Cancer. *Biomedicines* **2018**, *6*, 44. [CrossRef] [PubMed]
82. Bastide, A.; David, A. The ribosome, (slow) beating heart of cancer (stem) cell. *Oncogenesis* **2018**, *7*, 34. [CrossRef] [PubMed]
83. Van Riggelen, J.; Yetil, A.; Felsher, D.W. MYC as a regulator of ribosome biogenesis and protein synthesis. *Nat. Rev. Cancer* **2010**, *10*, 301–309. [CrossRef] [PubMed]
84. Vlashi, E.; Kim, K.; Lagadec, C.; Della Donna, L.; McDonald, J.T.; Eghbali, M.; Sayre, J.W.; Stefani, E.; McBride, W.; Pajonk, F. In vivo imaging, tracking, and targeting of cancer stem cells. *J. Natl. Cancer Inst.* **2009**, *101*, 350–359. [CrossRef]

Original Research Article

“Novel primary human Cancer Stem-like Cell Populations from Non-small Cell Lung Cancer: Inhibition of Cell Survival by targeting NF-κB- and MYC-Signaling”

Beatrice A. Windmöller*, Morris Beshay*, Laureen P. Helweg, Clara Flottmann, Miriam Beermann, Christine Förster, Ludwig Wilkens, Johannes F. W. Greiner, Christian Kaltschmidt and Barbara Kaltschmidt

(*: equal contribution)

Cells. 2021 Apr 27; 10(5): 1024.

cells

MDPI

Article

Novel Primary Human Cancer Stem-Like Cell Populations from Non-Small Cell Lung Cancer: Inhibition of Cell Survival by Targeting NF-κB and MYC Signaling

Beatrice A. Windmöller [1,2,*,†], Morris Beshay [2,3,†], Laureen P. Helweg [1,2], Clara Flottmann [1], Miriam Beermann [1], Christine Förster [2,4], Ludwig Wilkens [2,4], Johannes F. W. Greiner [1,2], Christian Kaltschmidt [1,2,†] and Barbara Kaltschmidt [1,2,5,†]

1 Department of Cell Biology, University of Bielefeld, Universitätsstrasse 25, 33615 Bielefeld, Germany; L.Helweg@uni-bielefeld.de (L.P.H.); Clara.Raeker@uni-bielefeld.de (C.F.); miriam.beermann@student.uni-luebeck.de (M.B.); Johannes.greiner@uni-bielefeld.de (J.F.W.G.); C.Kaltschmidt@uni-bielefeld.de (C.K.); barbara.kaltschmidt@uni-bielefeld.de (B.K.)
2 Forschungsverbund BioMedizin Bielefeld/OWL FBMB e. V., Maraweg 21, 33617 Bielefeld, Germany; morris.beshay@evkb.de (M.B.); christine.foerster@krh.eu (C.F.); ludwig.wilkens@krh.eu (L.W.)
3 Department of General Thoracic Surgery, Protestant Hospital of Bethel Foundation, Burgsteig 13, 33617 Bielefeld, Germany
4 Institute of Pathology, KRH Hospital Nordstadt, Haltenhoffstrasse 41, affiliated with the Protestant Hospital of Bethel Foundation, 30167 Hannover, Germany
5 Molecular Neurobiology, Bielefeld University, Universitätsstrasse 25, 33615 Bielefeld, Germany
* Correspondence: Beatrice.windmoeller@uni-bielefeld.de; Tel.: +49-0521-106-5629
† Authors contributed equally as Co-First and Co-Last Authors.

Abstract: There is growing evidence that cancer stem cells (CSCs), a small subpopulation of self-renewal cancer cells, are responsible for tumor growth, treatment resistance, and cancer relapse and are thus of enormous clinical interest. Here, we aimed to isolate new CSC-like cells derived from human primary non-small cell lung cancer (NSCLC) specimens and to analyze the influence of different inhibitors of NF-κB and MYC signaling on cell survival. CSC-like cells were established from three squamous cell carcinomas (SCC) and three adenocarcinomas (AC) of the lung and were shown to express common CSC markers such as Prominin-1, CD44-antigen, and Nestin. Further, cells gave rise to spherical cancer organoids. Inhibition of MYC and NF-κB signaling using KJ-Pyr-9, dexamethasone, and pyrrolidinedithiocarbamate resulted in significant reductions in cell survival for SCC- and AC-derived cells. However, inhibition of the protein–protein interaction of MYC/NMYC proto-oncogenes with Myc-associated factor X (MAX) using KJ-Pyr-9 revealed the most promising survival-decreasing effects. Next to the establishment of six novel in vitro models for studying NSCLC-derived CSC-like populations, the presented investigations might provide new insights into potential novel therapies targeting NF-κB/MYC to improve clinical outcomes in NSCLC patients. Nevertheless, the full picture of downstream signaling still remains elusive.

Keywords: cancer stem cell-like cells; squamous cell carcinoma; adenocarcinoma; NSCLC; MYC; NF-κB

Citation: Windmöller, B.A.; Beshay, M.; Helweg, L.P.; Flottmann, C.; Beermann, M.; Förster, C.; Wilkens, L.; Greiner, J.F.W.; Kaltschmidt, C.; Kaltschmidt, B. Novel Primary Human Cancer Stem-Like Cell Populations from Non-Small Cell Lung Cancer: Inhibition of Cell Survival by Targeting NF-κB and MYC Signaling. *Cells* **2021**, *10*, 1024. https://doi.org/10.3390/cells10051024

Academic Editor: Alexander E. Kalyuzhny

Received: 15 February 2021
Accepted: 23 April 2021
Published: 27 April 2021

1. Introduction

Lung cancer is the leading cause of cancer death worldwide and can be broadly classified into two types: small cell lung cancers (SCLC) and non-small cell lung cancers (NSCLC) [1,2]. The most common type of lung cancer is NSCLC, which accounts for approximately 80–85% of all lung cancer cases and can be divided into adenocarcinoma (AC, 40%), squamous cell carcinoma (SCC, 25–30%), and large cell carcinoma (5–10%) [3,4]. Even if NSCLC is less aggressive than SCLC and death rates for lung cancer in general dropped by 48% from 1990 to 2016 among males and by 23% from 2002 to 2016 among females, NSCLC prognosis is still poor, with an age-standardized 5-year net survival of

approximately 19% [1]. This poor prognosis is mainly caused by cancer aggressiveness and therapy resistance, which is increased by genetic and phenotypic heterogeneity of lung cancer cells [5].

There is growing evidence that a small subpopulation of cancer cells with stem cell characteristics, so-called cancer stem cells (CSCs), are responsible for tumor growth, therapy resistance, and recurrence, as well as metastasis, probably by remodeling the process of epithelial–mesenchymal transition (EMT) in lung cancer [6] (reviewed in [7,8]). Thus, CSCs are of enormous clinical interest and human in vitro models are extremely important to gather more insights into molecular regulators of lung cancer. Next to the formation of spherical cancer organoids [9], lung cancer stem cells (LCSCs) can be identified using different markers such as cell surface glycoproteins Prominin-1 (CD133) and CD44-antigen (CD44) [10–12]. These CSCs markers are linked to increased chemoresistance and poor prognosis as well as reduced overall survival in patients with lung cancer [12–14]. Other important regulators of CSC characteristics are members of the MYC transcription factor family, consisting of L-, N-, and C-MYC (further referred as MYC within this manuscript). Within a recent pan-cancer study, Schaub and coworkers identified MYC family members amplified in up to 33% of all lung adenocarcinomas [15]. Furthermore, MYC amplification was described as a poor prognostic marker of early stage adenocarcinomas of the lung [16] as well as MYC gain determined by fluorescence in situ hybridization was shown to be an independent poor prognostic factor for disease-free survival and overall survival in lung adenocarcinomas [17]. Concerning LCSCs, suppression of Myc proto-oncogene (MYC) signaling was shown to reduce viability, self-renewal, and invasion capacity of LCSC-like cells derived from A549 cells [18]. Accordingly, the LCSC phenotype of H460 and H292 cells was shown to be impaired by the suppression of MYC via the Src-STAT3 pathway [19]. Despite these promising findings, the role of MYC signaling in primary human LCSCs still remains unknown.

Next to the re-regulation of diverse stemness associated genes, transcriptomic profiling revealed a significant involvement of the transcription factor nuclear factor kappa-light-chain-enhancer of B cells (NF-κB) in regulating LCSC populations [10]. NF-κB signaling is vital for a broad range of cellular processes including proliferation, differentiation, apoptosis, immune response, angiogenesis, and inflammation [20,21]. Moreover, NF-κB activation is associated with cancer development, pathogenesis, abnormal cell proliferation and differentiation, enhanced metastasis, and treatment resistance in several tumors [22–26]. A meta-analysis further indicated that higher NF-κB expression in NSCLC cells is associated with shorter overall survival of NSCLC patients and is closely correlated with tumor stage, lymph node metastasis, and 5-year overall survival [27].

In the present study, we established three primary SCC-derived lung cancer cell populations named BKZ-4, BKZ-5, and BKZ-6, as well as three primary AC-derived lung cancer cell populations named BKZ-7, BKZ-8, and BKZ-9. All isolated NSCLC cell populations were enriched for a subset of cells with markers of stemness and were able to form spherical cancer organoids. Application of the NF-κB inhibitors dexamethasone and pyrrolidinedithiocarbamate (PDTC) significantly decreased cell survival of AC- and SCC-derived cells, while the NF-κB inhibitor lenalidomide did not impair cell survival. Notably, exposure of AC- and SCC-derived CSCs to the small molecule KJ-Pyr-9, which inhibits the protein–protein interaction of MYC/N-myc proto-oncogene (NMYC) with Myc-associated factor X (MAX) [28], resulted in the strongest decrease in cell survival.

2. Materials and Methods

2.1. Lung Cancer Stem Cell-like Cell Population Establishment and Cell Culture

The cancer tissue samples used to isolate lung cancer stem cell-like cells were obtained during surgical resection and were kindly provided by the Forschungsverbund BioMedizin Bielefeld/OWL FBMB e. V. (Bielefeld, Germany) at the Protestant Hospital of Bethel Foundation (Bielefeld, Germany) after assuring routine histopathological analysis. Informed consent according to local and international guidelines was signed by all patients.

All further experimental procedures were ethically approved (Ethics Committee Münster, Germany, 2017-522-f-S).

To obtain tumor material for the isolation of primary cells, we collected a cubic sample from each tumor type and transferred to ice-cold Dulbecco's phosphate-buffered saline (Sigma Aldrich, München, Germany). The specimen was washed 10 times with ice-cold PBS, mechanically disintegrated into 1–2 mm pieces, and enzymatically digested with Collagenase for 2 h at 37 °C as previously described [29]. The minced tissue was cultivated in cancer stem cell medium comprising Dulbecco's modified Eagle's medium/Ham's F-12 (Sigma Aldrich, München, Germany) with the addition of 2 mM L-glutamine (Sigma Aldrich), penicillin/streptomycin (100 µg/mL; Sigma Aldrich, München, Germany), epidermal growth factor (EGF) (20 ng/mL; Miltenyi Biotec, Bergisch Gladbach, Germany), basic fibroblast growth factor (FGF-2) (40 ng/mL; Miltenyi Biotec, Bergisch Gladbach), B27 supplement (Gibco, Thermo Fisher Scientific, Bremen, Germany), and 10% fetal calf serum (FCS) (Sigma Aldrich, München, Germany) in T75 culture flasks coated with 0.1% gelatin from bovine skin (type B; Sigma Aldrich, München, Germany). Adult human dermal fibroblasts (HDFs) (Genlantis, San Diego, CA, USA) and the well-established lung adenocarcinoma-derived cell line LXF-289 [30] (DSMZ, Braunschweig, Germany) were cultured in Dulbecco's modified Eagle's medium-high glucose (Sigma Aldrich, München, Germany) with 10% FCS, 2 mM L-glutamine, and penicillin/streptomycin (100 µg/mL). All cells were cultured at 37 °C and 5% CO_2 in a humidified incubator. Adherent cells were harvested with 0.05% Trypsin–EDTA solution (0.5 mg/mL; Sigma Aldrich, München, Germany). BKZ populations and LXF-289 cells were kept in culture for 1 week before experiments were conducted as well as only confluent cells were passaged. For sphere formation, 0.5×10^6 cells were cultured in CSC medium supplemented with 4 µg/mL heparin (Sigma Aldrich, München, Germany) in low adhesion T25 culture flask.

Population doubling times were determined using the Orangu Cell Counting Solution (Cell Guidance Systems, Cambridge, UK) and were performed nine times per cell population according to the manufacturers guidelines. For the standard curve, 1000, 2500, 5000, 7500, and 10,000 cells per 100 µL medium supplemented with 10% FCS were seeded in a 0.1% gelatin coated 96 well-plate. To determine the doubling time, we seeded 3000 cells per 100 µL medium supplemented with 10% FCS in a 0.1% gelatin-coated 96-well plate and cultivated for 72 h. Cell viability was measured and cell count was quantified using the respective standard curve. Growth rate and populations doubling times were determined by the following equations:

$$growth\ rate = \frac{\ln(xt) - \ln(x0)}{t - t0} \quad (1)$$

$$population\ doubling\ time = \frac{\ln(2)}{growth\ rate} \quad (2)$$

2.2. Immunocytochemistry

For immunocytochemical staining, pre-cultured BZK-4, BZK-5, BZK-6, BZK-7, BZK-8, BZK-9, LXF-289 cells, and HDFs were harvested and 1.5×10^4 cells per 500 µL medium supplemented with 10% FCS were seeded on etched cover slips in a 24-well plate. When 80% confluency was reached, cells were fixed with 4% phosphate-buffered paraformaldehyde (lab-made) for 15 min at room temperature (RT). After three washing steps with 1 × PBS, cells were blocked and permeabilized using 0.02% Triton-X 100 (Sigma Aldrich) with 5% goat serum (Dianova, Hamburg, Germany) for 30 min at RT followed by incubation with the primary antibody for 1 h at RT. Antibodies used were anti-CD44 (1:400; 156-3C11; Cell Signaling, Frankfurt am Main, Germany), anti-CD133 (1:100; NB120-16518; NovusBio, Bio-Techne, Wiesbaden-Nordenstadt, Germany), anti-Nestin (1:200; MAB5326; Millipore, Merck, Darmstadt, Germany), anti-MYC (0.1 µg/mL; Y69; Abcam), anti-NMYC (2.5 µg/mL; NCM II 100; Abcam), anti-RelA (1:400; Cell Signaling), anti-RelB (1:100; Cell Signaling), and anti-cRel (1:100; Cell Signaling). Afterwards, secondary fluorochrome-

conjugated antibodies (1:300; goat anti-mouse Alexa 555, goat anti-rabbit Alexa 555, goat anti-mouse Alexa 488; Life Technologies, Thermo Fisher Scientific) were incubated for 1 h at RT in the dark, followed by nuclear counterstaining with 4′,6-diamidino-2-phenylindole (DAPI; 1 µg/mL; Sigma Aldrich) for 10 min at RT. Fluorescence imaging was conducted using a confocal laser scanning microscope (LSM 780; Carl Zeiss, Jena, Germany) and analyzed using ZEN software from the same provider or Fiji ImageJ [31]. For the quantification of the amount of CD133/CD44 positive cells, the percentage of CD133/CD44 double-positive cells was conducted for at least five images per cell population.

For immunocytochemical staining of spheres, spheres were harvested at 300× *g* for 10 min, fixated in 4% PFA for two hours, and washed with water for 15 min. Afterwards, spheres were incubated in 50% isopropanol for 45 min, 75% isopropanol for 1 h, 90% isopropanol for 1 h, and finally 100% for 1 h and 15 min. In the final step, 100% isopropanol was changed after 1 h. Between each step, the spheres were harvested at 300× *g* for 10 min. After isopropanol vaporized, spheres were overnight embedded in paraffin (Sigma Aldrich) and centrifuged at 450× *g* for 10 min. Paraffin-embedded sections were washed twice in xylol for 10 min followed by 100% ethanol for 10 min. Thereafter, sections were rehydrated by 5 min washing steps in 90% ethanol, followed by 80% ethanol and 70% ethanol. Epitope retrieval was performed by boiling the slides in 0.01 M citrate buffer, pH 6.0 (lab made), for 20 min. After cooling down for at least 30 min at RT, the slides were washed twice with 0.02% Triton-X 100. Afterwards, slides were blocked and permeabilized using 0.02% Triton-X 100 with 10% goat serum and 1% bovine serum albumin for 2 h at RT. Anti-CD133 (1:100; NB120-16518; NovusBio), anti-CD44 (1:400; 156-3C11; Cell Signaling), anti-MYC (5 µg/mL; Y69, Abcam), and anti-NMYC (5 µg/mL; NCM II 100; Abcam) first antibodies were diluted in blocking solution and incubated over night at 4 °C. After three washing steps with PBS, secondary fluorochrome-conjugated antibodies (1:300; goat anti-mouse Alexa 555, goat anti-rabbit Alexa 555; Life Technologies) were applied and incubated for 1 h at RT in the dark. After three washing steps with PBS, nuclear counterstaining was performed using DAPI (1 µg/mL) for 10 min at RT. Fluorescence imaging was performed using a confocal laser scanning microscope (LSM 780; Carl Zeiss) and analyzed using Fiji ImageJ.

To determine the nuclear size of the cells, we analyzed five randomized images of immunocytochemically stained cells for each cell population. The area of each nucleus was defined in the DAPI channel and was measured using ImageJ. The size of the nuclei were clustered into three groups: (1) $\leq$100 µm^2, (2) $\geq$100 to $\leq$200 µm^2, and (3) $\geq$200 µm^2.

For the tumor necrosis factor α (TNF-α) treatment, 2 × 10^4 cells were seeded in 500 µL CSC medium supplemented with 10% FCS on etched cover slips. After 1 day of cultivation, medium was replaced with CSC medium supplemented with 10% FCS and 10 ng/mL TNFα (Miltenyi Biotec). Subsequent to the incubation for 10, 30, and 60 min, cells were each washed with 1 × PBS and fixated with 4% PFA for 15 min. As control, cells were incubated in CSC medium supplemented with 10% FCS without TNF-α for 60 min. After fixation, cells were washed with 1 × PBS and immunocytochemically stained for RelA as described above. To quantify the fluorescence intensity (FI) in the nuclei, we took five randomized pictures for each time point and cell population. The area of each nucleus was defined in the DAPI channel using ImageJ and the average nuclear fluorescence intensity of the respective protein channel was measured by overlay. The fluorescence intensities of all nuclei with an area value of $\geq$30 µm^2 were included in the quantification. The fold change of the nuclear fluorescence intensity was calculated according to the following equation:

$$\text{fold change } = \frac{FI_{ex} - FI_{min}}{FI_{max} - FI_{min}} * 100 \quad (3)$$

The ratio of nuclear to total fluorescence intensity (N/T ratio) was calculated according to Kelley and Paschal [32]. To measure the total fluorescence intensity, we placed a ring measuring 1,098,159 µm^2 around the nucleus of the cell, and the average fluorescence intensity

was determined. The average nuclear fluorescence intensity was measured as described above, and the ratio of nuclear to total fluorescence intensity was calculated accordingly.

For the immunocytochemical staining of MYC after KJ-Pyr-9-treatment, 1.5×10^4 cells per 500 µL CSC medium containing 10% FCS were seeded in a 24 well on top of etched cover slips. After adherence (4–6 h), cells were treated with 10 µM and 20 µM of KJ-Pyr-9 or dimethyl sulfoxide (DMSO) as a control for 24 h. Afterwards, immunocytochemical staining against MYC was performed and nuclear fluorescence intensity was measured as described above. For the immunocytochemical staining of RelA after PDTC-treatment, 1.5×10^4 cells per 500 µL CSC medium containing 10% FCS were seeded in a 24 well on top of etched cover slips. After adherence (4–6 h), cells were treated with/without 100 µM PDTC for 24 h. Thereafter, immunocytochemical staining against RelA was conducted and ratio of nuclear to total fluorescence intensity was measured as described above.

2.3. Western Blot

For preparation of whole cell lysates, 10^6 cells were lysed in 0.1 M Tris, 3 mM EDTA, and 1% SDS. For each cell population, 20 µg protein was used and separated by SDS-PAGE followed by the transfer to a PVDF membrane (Carl Roth GmbH, Karlsruhe, Germany). After the membrane was washed with 0.05% Tween-20 (VWR International GmbH, Darmstadt, Germany) in PBS (lab-made) for 10 min three times, the membrane was blocked using PBS containing 0.05% Tween-20 and 5% milk powder (Carl Roth GmbH) followed by probing with primary antibodies anti-MYC (1:1000, Y69, Abcam), anti-NMYC (1:50, NCM II 100; Abcam), and anti β-Actin (1:1000, 13E5, Cell Signaling) overnight at 4 °C. After three washing steps, the secondary horseradish peroxidase-conjugated antibody (anti-rabbit or anti-mouse, 1:4000, DIANOVA) was applied for 1 h at RT. Then, the membrane was washed again three times using PBS containing 0.05% Tween-20 with an additional washing step in 10 mM Tris-HCl (pH 7.5). Subsequent to the development, we used enhanced chemiluminescence with a solution containing 1 mL of Solution A (50 mg Luminol; Sigma-Aldrich in 200 mL 0.1 M Tris-HCl), 0.3 µL 30% H_2O_2, and 100 µL Solution B (11 mg Coumarin acid; Sigma-Aldrich in 10 mL DMSO) on a radiographic film (Super RX-N, FUJIFILM, Düsseldorf, Germany). The protein amounts were normalized to their related β-actin signals and quantified using ImageJ and Prism V5.01 software.

2.4. Senescence Assay

To measure the number of senescent cells, we seeded 5×10^4 cells per 2 mL CSC medium supplemented with 10% FCS in a 0.1% gelatin-coated 6 well-plate. After adherence (4–6 h), cells were each treated with 20 µM KJ-Pyr-9, 100 µM PDTC, and DMSO as a control for 24 h. Then, activity of senescence-associated β-galactosidase was measured according to Debacq-Chainiaux and colleagues [33]. Briefly, cells were washed with PBS and fixated with 3% PFA; then, the staining solution containing 1 mg/mL X-Gal (Carl Roth GmbH) was added. Incubation overnight at 37 °C led to final staining, which could be visualized by phase contrast microscopy. For each condition and each cell line, three pictures were taken and analyzed, and percentage of senescent cells was calculated accordingly.

2.5. Quantitaive Polymerase Chain Reaction

For the analysis of gene copy number of NMYC and MYC, we isolated genomic DNA using the QUIamp DNA Mini Kit (Qiagen, Hilden, Germany) according to the manufacturer's guidelines. Gene copy number was quantified using the Platinum SYBR Green qPCR Super-Mix UDG (Invitrogen, Thermo Fisher Scientific) according to the manufacturer's guidelines. Each copy number quantification was performed in triplicate and was assayed with a Rotor Gene 600 (Qiagen). The gene assays each included a no-template control, 10 ng of calibrator human genomic DNA (Sigma Aldrich), and 10 ng of CSC DNA. Haploid copy number was determined according to De Preter et al. [34].

For the analysis of MYC target genes under the influence of KJ-Pyr-9, we seeded 7.5×10^4 BKZ-6, BKZ-8, and LXF-289 cells in a 6-well plate. After 1 day of cultivation, cells

were treated with 20 µM KJ-Pyr-9 for 24 h. Thereafter, cells were harvested using a cell scrapper, and RNA was isolated using the NucleoSpin RNA Kit (Macherey-Nagel, Düren, Germany) according to the manufacturer's guidelines. Quality and concentration of RNA were assessed via Nanodrop ultraviolet spectrophotometry. Copy DNA (cDNA) synthesis was performed using 250 ng of RNA and the First Strand cDNA Synthesis Kit (Thermo Fisher Scientific). For the synthesis, random hexamer primers were used. Quantitative polymerase chain reaction was performed in triplicates using the qPCRBIO Sygreen-Mix (PCR Biosystems, London, UK) according to the manufacturer's guidelines and assayed with a Rotor Gene 6000 (Qiagen). Used primers (Sigma Aldrich) are listed in Table 1.

Table 1. Primer sequences for quantitative polymerase chain reaction.

Target Gene	Sequence 5′–3′
NMYC (genomic)	CGCAAAAGCCACCTCTCATTA
Rev-*NMYC* (genomic)	TCCAGCAGATGCCACATAAGG
MYC (genomic)	AAAAGTGGGCGGCTGGATAC
Rev-*MYC* (genomic)	AGGGATGGGAGGAAACGCTA
Syndecan 4 (genomic)	CAGGGTCTGGGAGCCAAGT
Rev-Syndecan 4 (genomic)	GCACAGTGCTGGACATTGACA
Glyceraldehyde-3-phosphate dehydrogenase (*GAPDH*) (genomic)	AGACTGGCTCTTAAAAAGTGCAGG
Rev-*GAPDH* (genomic)	TGCTGTAGCCAAATTCGTTGTC
Beta-actin (*ACTB*)	CTTCGCGGGCGACGAT
Rev-*ACTB*	CCACATAGGAATCCTTCTGACC
Cyclin D1 (*CCND1*)	ATGCCAACCTCCTCAACGAC
Rev-*CCND1*	TCTGTTCCTCGCAGACCTCC
Cyclin D3 (*CCND3*)	ACTGGCACTGAAGTGGACTG
Rev-*CCND3*	GGGCTACAGGTGTATGGCTG
Lactate dehydrogenase A (*LDHA*)	CTTGACCTACGTGGCTTGGA
Rev-*LDHA*	CCAGCCTTTCCCCCATTAGG
Ribosomal protein L5 (*RPL5*)	CAGCGTATGCACACGAACTG
Rev-*RPL5*	ACCTATTGAGAAGCCTGCGG
Ribosomal protein L14 (*RPL14*)	TTGGACCTCATGCCGGAAAA
Rev-*RPL14*	GCACTGTGCGGAAACTTGAG
Ribosomal protein L28 (*RPL28*)	CTCTTTCCGTCTCAGGTCGC
Rev-*RPL28*	TCTTGCGGTGAATCAGTCCG
Ribosomal protein P1 (*RPLP1*)	TGAAAACTGCACTGGGGTGG
Rev-*RPLP1*	AGGGTAAATACCCAGGAGGCT
GAPDH	CATGAGAAGTATGACAACAGCCT
Rev-GAPDH	AGTCCTTCCACGATACCAAAGT
MYC	GGCACTTTGCACTGGAACTT
Rev-*MYC*	AGGCTGCTGGTTTTCCACTA

2.6. Inhibitor Treatments

To analyze the influence of the proto-oncogenes MYC and NMYC as well as transcription factor NF-kB, we treated cells with MYC/NMYC inhibitor KJ-Pyr-9 (Merck) and/or dexamethasone (Dexa; Sigma Aldrich), lenalidomide (Sigma Aldrich), and PDTC (Sigma Aldrich). Cell viability was assayed using Orangu Cell Counting Solution (Cell Guidance Systems) and were performed in triplicates according to the manufacturer's instructions. For the standard curve, 1000, 2500, 5000, 7500, and 10,000 cells and for the treatment of 3000 cells per 100 µL respective medium supplemented with 10% FCS were seeded in a 0.1% gelatin-coated 96 well-plate. After adherence of the cells (4–6 h), cell viability was measured for the standard curve and treatment was started by applying the respective inhibitor combinations. KJ-Pyr-9 was applied in the concentrations of 1, 5, 10, and 20 µM, and DMSO was used as control. Lenalidomide was used in concentrations of 30, 100, and 300 µM, and DMSO was applied as solvent control [35,36]. For the co-treatment, 10 ng/mL TNF-α, 100 µM PDTC [37,38], and 300 µM Dexa [39,40] were applied in the following conditions: (1) TNF-α, (2) TNF-α + Dexa, (3) TNF-α + PDTC, (4) TNF-α + Dexa + PDTC, (5) Dexa, (6) PDTC, (7) Dexa + PDTC. Each condition was tested with and without 10 µM

KJ-Pyr-9 as well as solvent controls were carried along. After 5 days of treatment, cell viability was measured using again Orangu Cell Counting Solution (Cell Guidance Systems), and cell count was quantified using the respective standard curve. Relative survival rate was calculated by normalizing each cell count to the mean of controls for the respective cell population. Additionally, the half maximal inhibitory concentrations (IC_{50}) of KJ-Pyr-9 were calculated from the log(concentration) versus normalized survival rate non-linear regression fit using Prism V5.01 software (GraphPad Software, Inc., San Diego, CA, USA).

2.7. Statistical Analysis

Data were raised at least in triplicate and were statistically analyzed using the Prism V5.01 software (GraphPad Software, Inc., San Diego, CA, USA). Test for normality was conducted using D'Agnostino and Pearson omnibus normality test. To evaluate differences between multiple groups, we performed unpaired *t*-test or the non-parametric Mann–Whitney test. A significance value of $p \leq 0.05$ was considered as statistically significant. The data are presented as means ± standard error of the mean (SEM).

3. Results

3.1. Squamous Cell Carcinoma- and Adenocarcinoma-Derived Cells Depicted Stemness-like Phenotype

In this study, we aimed for the isolation of LCSC-like cells from various NSCLC tumors. Therefore, tumor material from six NSCLC patients was sampled and used for the establishment of adherently growing cells as well as cancer spheroids. Cell populations BKZ-4, BKZ-5, and BKZ-6 were isolated from male donors aged 67, 79, and 74, respectively, all suffering under squamous cell carcinomas GII (Supplementary Figure S1A–C, Table S1). The source of BKZ-7, BKZ-8, and BKZ-9 were female patients depicting invasive adenocarcinomas of the lung (Supplementary Figure S1D–F, Table S1). Analysis of clinically relevant mutations of donors of BKZ-7, -8, and -9, which were inoperable, revealed an epidermal growth factor receptor (*EGFR*) mutation for the tumor tissue of the donor of BKZ-7, with no mutation for KRAS proto-oncogene (*KRAS*), B-Raf proto-oncogene (*BRAF*), or serine/threonine kinase 11 (*STK11*). Donor of BKZ-8 did not reveal any therapeutic relevant mutation, while the tumor material of BKZ-9 donor showed mutations in the *KRAS* gene and in *STK11* (Table S2).

Using chemically defined media, we successfully cultivated adherently growing cells with the addition of FCS as well as cancer organoids in the form of free-floating spheres in serum-free media for all six donors (Figure 1A–L). Cells cultured in 2D on the surface of tissue culture plates depicted an elongated spindle form morphology, with no obvious difference in cells derived from SCC (Figure 1A–C) in comparison to cells from AC (Figure 1G–I). Moreover, quantification of nuclear sizes revealed heterogeneity for all six populations (Supplementary Figure S2). All cell populations formed cancer organoid-like structures in serum-free media with sizes up to 100 µm (Figure 1D–F,J–L). Measurements of the population doubling time (Equations (1) and (2)) of SCC-derived cells depicted BKZ-4 as the slowest, with a mean population doubling time of 27.90 h (±0.17), whereas BKZ-6 had a doubling time of 19.56 h (±0.14) (Figure 1M). Similarly, the AC group consisted of slowly proliferating cells, such as BKZ-7, with a mean population doubling time of 35.20 h (±0.62), and those showing fast proliferation such as BKZ-8 with a population doubling of 18.76 h (±0.23) (Figure 1N).

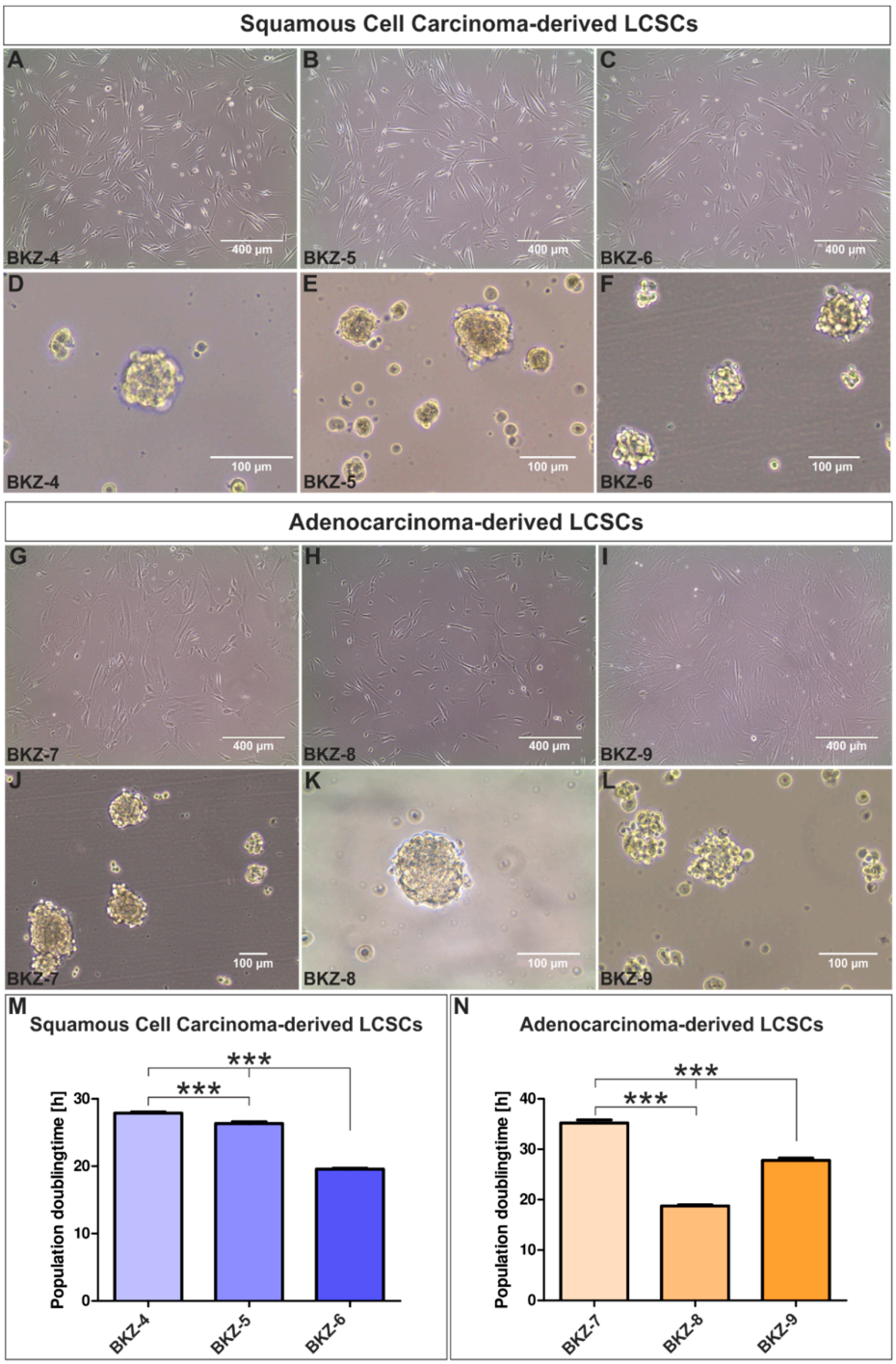

Figure 1. Successful isolation of squamous cell carcinoma (SCC)-derived lung cancer stem cell (LCSC)-like cell populations: (**A**) BKZ-4, (**B**) BKZ-5, and (**C**) BKZ-6. (**D–F**) Serum-free cultivation of the isolated cell populations led to the formation of free-floating cancer organoids for all three SCC-derived cell populations. Isolated adenocarcinoma (AC)-derived lung cancer stem cell-like cell populations could be also grown as (**G–I**) adherent culture as well as (**J–L**) sphere culture. (**M**) Analysis of the population doubling times of the adherent SCC-LCSCs revealed a higher population doubling time for BKZ-4 in comparison to BKZ-5 and BKZ-6, with BKZ-6 revealing the lowest doubling time. (**N**) Quantification of the population doubling times for the different AC-LCSC depicted a significantly higher population for BKZ-7 in comparison to BKZ-8 and BKZ-9. Further, population doubling time of BKZ-9 was significantly higher when compared to BKZ-8. Unpaired *t*-test ($p \leq 0.05$). $n = 9$, *** $p \leq 0.001$. Mean ± SEM (standard error of the mean).

Next, we analyzed the presence of known CSC markers CD133, CD44, and Nestin on protein level and detected robust expression of CD133 and CD44 in SCC cell populations BKZ-4 (100% double-positive cells, Figure 2A) and BKZ-5 (99.13% double-positive cells, Figure 2C). Expression of CD133 and CD44 was lower but still well recognizable in BKZ-6 (100% double-positive cells Figure 2E). High expression of CD133 and CD44 was likewise observable in all three AC-derived cell populations of BKZ-7 (100% double-positive cells, Figure 2G), BKZ-8 (100% double-positive cells, Figure 2I), and BKZ-9 (99.75% double-positive cells, Figure 2K). Further, all SCC- and AC-derived cell populations likewise showed robust levels of Nestin protein (Figure 2B,D,F,H,J,L). Immunocytochemical staining of the respective CSC markers in the well-established lung adenocarcinoma-derived cell line LXF-289 revealed no expression for cancer stem cell markers CD133 and Nestin and only low expression of CD44 in comparison to LCSC-like cells (Figure 2M,N). As no expression for CD133 could be detected the percentage of CD133/CD44 double-positive cells was zero for LXF-289 cell line. Representative immunocytochemical staining for CD133 and CD44 also revealed strong expression in NSCLC-derived spheroids, as exemplarily shown in BKZ-5-derived spheres (Supplementary Figure S3). HDFs additionally served as biological negative control for immunocytochemical stainings of CSC markers (Supplementary Figure S4).

3.2. Tumor Necrosis Factor-α Stimulation Activated NF-κB RelA in Squamous Cell Carcinoma- and Adenocarcinoma-Derived Lung Cancer Stem Cell-like Cells

Since NF-κB directs pathways linking cancer with inflammation, we analyzed expression of transactivating NF-κB subunits c-Rel, RelB, and RelA in CSC-like cells. All subunits were expressed in our established SCC- and AC-derived LCSC-like cell populations, with NF-κB RelA showing the most robust protein levels compared to RelB and cRel (Supplementary Figures S5 and S6). As NF-κB RelA was predominantly located within the cytoplasm of all six LCSC-like cells, translocation in the nucleus and thus activation of RelA was stimulated using TNF-α. Immunocytochemical analysis of the nuclear fluorescence intensity of RelA revealed its nuclear translocation in SCC-derived cells (Figure 3A–D) as well as in AC-derived cell populations (Figure 3F–I) after exposure to TNF-α. Quantification of the fold change of nuclear fluorescence intensity of all three SCC-derived cell populations showed a significant increase after only 10 min TNF-α exposure compared to the control (Equation (3), Figure 3E). Moreover, fold change of nuclear fluorescence intensity of RelA significantly increased with longer TNF-α incubation time (Figure 3E). Statistical analysis of the fold change of nuclear RelA in AC-derived cell populations showed a significant increase after TNF-α-stimulation longer than 30 min compared to the control, with a time-dependent increase from 10 min to 30 min (Figure 3J). Further analysis of the ratio of the fluorescence intensity of nuclear RelA to total RelA depicted a shift from predominantly cytoplasmic RelA with basal nuclear expression in the control towards a solely nuclear expression after 60 min of TNF-α exposure for SCC- and AC-derived cells (Supplementary Figure S7).

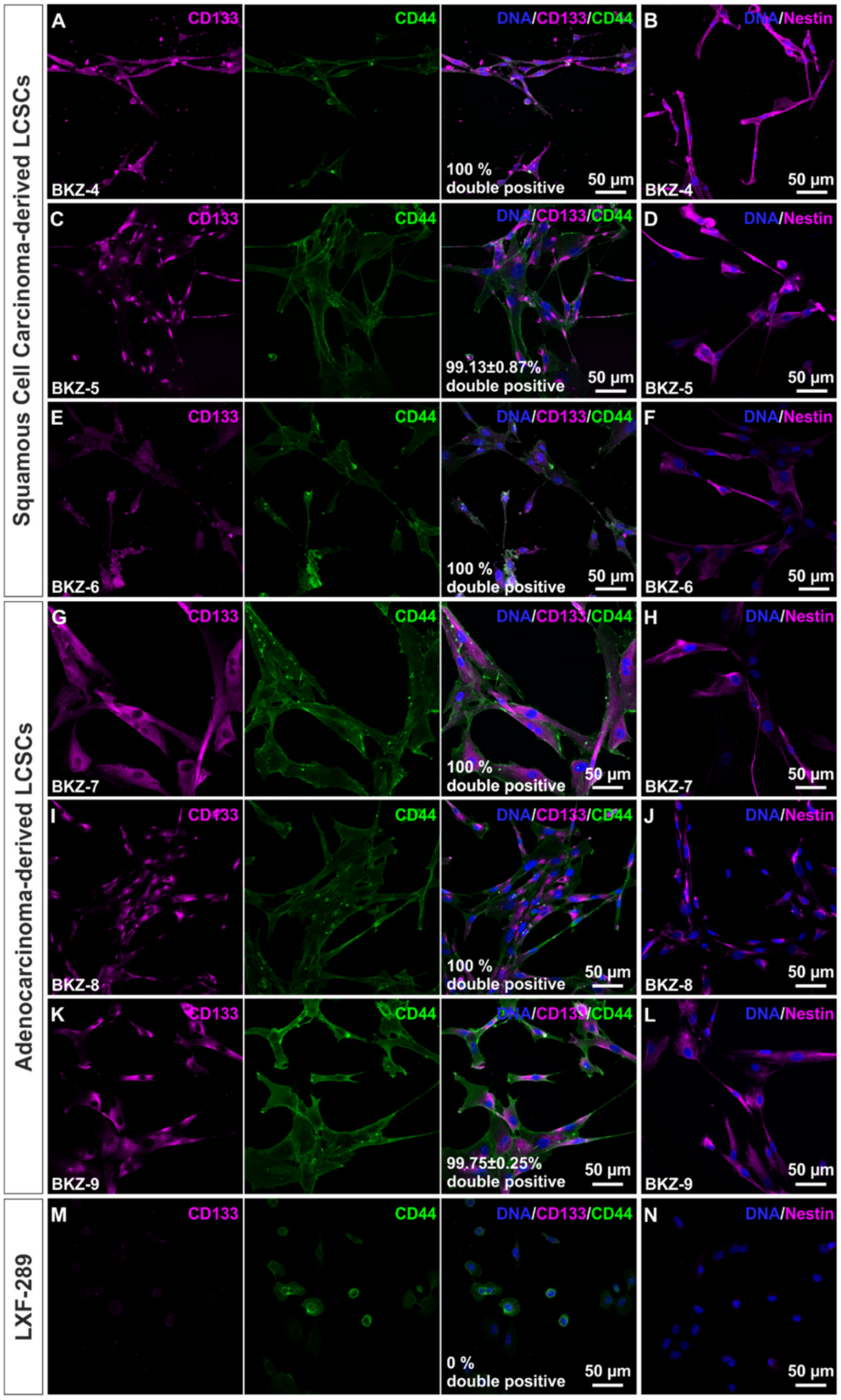

Figure 2. Isolated squamous cell carcinoma-derived and adenocarcinoma-derived lung cancer stem cell-like cells express higher amounts of cancer stem cell markers CD133, CD44, and Nestin in comparison to lung adenocarcinoma-derived cell line LXF-289. Immunocytochemistry revealed the presence of cancer stem cell markers CD133 and CD44 as well as the stem cell marker Nestin on protein level in (**A**–**F**) BKZ-4, BKZ-5, and BKZ-6 as well as (**G**–**L**) BKZ-7, BKZ-8, and BKZ-9. (**M**,**N**) Well-established lung adenocarcinoma-derived cell line LXF-289 did not express CD133 and Nestin and only express CD44 in low amounts in comparison to BKZ populations.

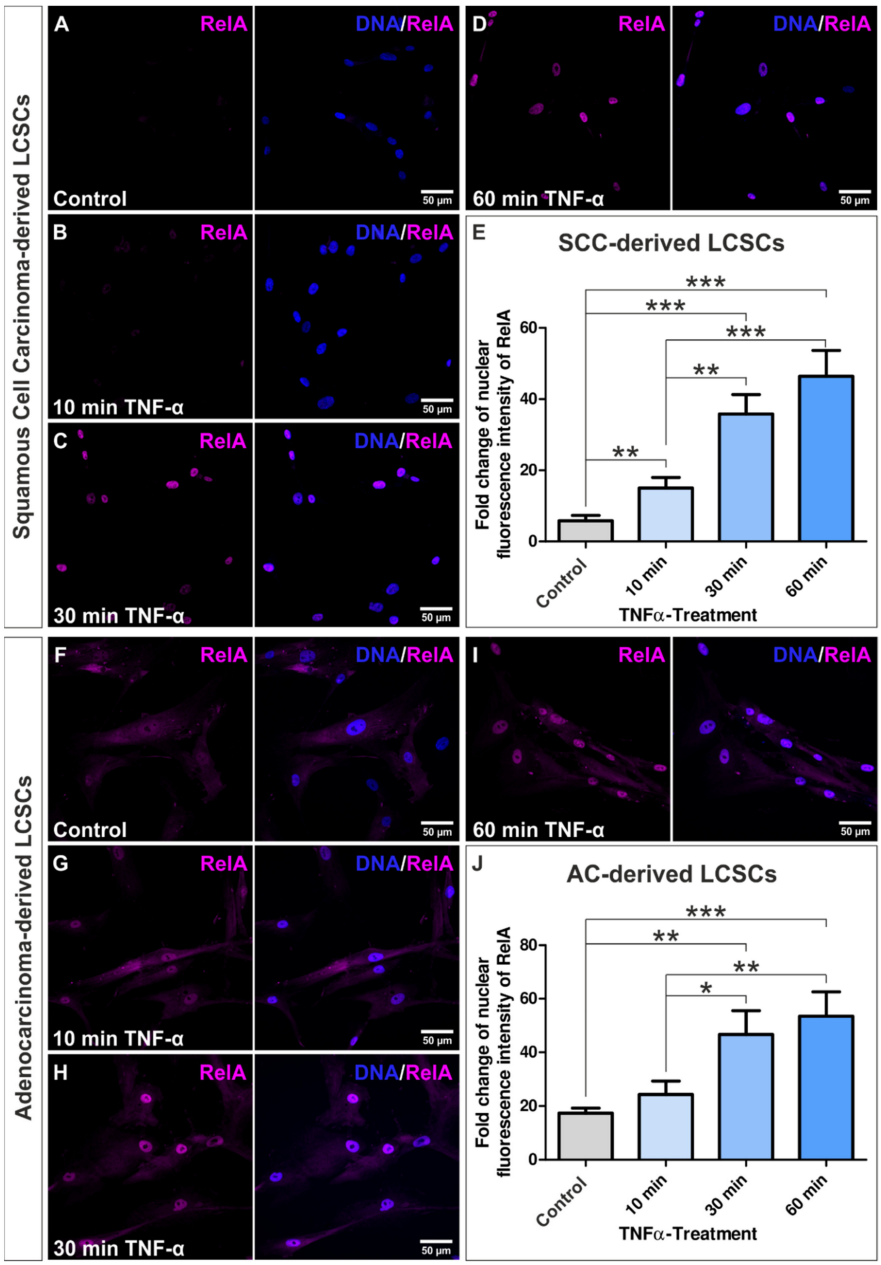

Figure 3. Tumor necrosis factor α (TNF-α) stimulation of non-small cell lung cancer-derived lung cancer stem cell (LCSC)-like cells activated NF-κB subunit RelA. Representative pictures of immunocytochemical staining for RelA of (**A**) untreated squamous cell carcinoma-derived BKZ-5 cells (control) and BKZ-5 cells after stimulation with TNF-α for (**B**) 10 min, (**C**) 30 min, and (**D**) 60 min. (**E**) Merged quantification of immunocytochemical assays for BKZ-4, BKZ-5, and BKZ-6 revealed a statistically significant increase of the fold change of nuclear fluorescence intensity after stimulation with TNF-α for all four time points in comparison to the control. Moreover, fold change of nuclear fluorescence intensity significantly increased with stimulation time. Accordingly, TNF-α stimulation activated NF-κB subunit RelA within adenocarcinoma (AC)-derived LCSC-like cells BKZ-7, BKZ-8, and BKZ-9. (**F**–**I**) Representative pictures of the immunocytochemical staining of RelA for AC-derived BKZ-7. (**J**) Quantification of nuclear fluorescence intensity of RelA after TNF-α stimulation for BKZ-7, BKZ-8, and BKZ-9 showed a statistically significant increase of the fold change of nuclear fluorescence intensity after stimulation with TNF-α for all four time points in comparison to the control. Unpaired *t*-test ($p \leq 0.05$). $n = 3$, * $p \leq 0.05$, ** $p \leq 0.01$, *** $p \leq 0.001$. Mean ± SEM (standard error of the mean).

3.3. Inhibition of MYC and NMYC in Squamous Cell Carcinoma- and Adenocarcinoma-Derived Lung Cancer Stem Cell-like Cells Significantly Impaired Cell Survival

The MYC family members are tightly regulated transcription factors that are responsible for the coordination of cell growth and proliferation and are thus commonly deregulated in a wide range of cancers. Immunocytochemical analysis of MYC showed nuclear localization in BKZ-4 as well as BKZ-6, with BKZ-5 only depicting slight nuclear localized MYC (Figure 4A,C,E). Next to MYC, NMYC protein was robustly expressed in all cell populations, even though expression was predominantly cytoplasmatic (Figure 4B,D,F). Analyzing MYC protein in AC-derived cells depicted nuclear protein expression in BKZ-7 and BKZ-8, but only a slight expression in BKZ-9 (Figure 4G,I,K). Of note, all three AC-cell populations were shown to robustly express mainly cytosolic NMYC (Figure 4H,J,L). Immunocytochemical analysis of the MYC and NMYC expression of the well-established lung adenocarcinoma cell line LXF-289 revealed similar expressions for MYC and a slightly lower amount NMYC in comparison to BKZ populations (Figure 4M–N). Additionally, representative immunocytochemical stainings for MYC and NMYC depicted conserved protein expression in spheroids, as exemplarily shown in BKZ-5-derived spheres (Supplementary Figure S8). Further analysis concerning MYC and NMYC protein levels using Western blot from whole-cell lysates revealed expressions within all BKZ cell populations and LXF-289 cells for MYC and NMYC, respectively (Supplementary Figure S9A). However, BKZ populations revealed additional signals for NMYC in comparison to LXF-289, possibly suggesting the presence of further isoforms of this protein in LCSC-like cells. Additionally, quantification of the relative expression levels revealed higher expression of MYC and NMYC for most of the BKZ populations in comparison to LXF-289 cells, with only BKZ-4 revealing less MYC protein. Still, some BKZ populations at least depicted up to 15-fold NMYC and 2.2-fold MYC expression. In general, NMYC expression levels varied more in AC-derived BKZ populations than in SCC-derived cells, which depicted generally lower level of NMYC. Contrarily, MYC levels varied more in SCC-derived BKZ populations in comparison to AC-derived BKZ populations (Supplementary Figure S9B). Additional investigation of the haploid copy number of MYC and NMYC of all six cell populations revealed a normal copy number (Supplementary Figure S10).

On the basis of the consistent expression of MYC and NMYC in all NSCLC-derived cells, we examined the influence of the small molecule KJ-Pyr-9, an inhibitor of the protein–protein interaction of MYC/NMYC with MAX. Usage of KJ-Pyr-9 doses higher than 5 µM significantly decreased survival rates for BKZ-4, BKZ-5, and BKZ-6. However, for BKZ-6, even a concentration of 1 µM KJ-Pyr-9 impaired survival. Treatment with 10 µM KJ-Pyr-9 led to a significant decrease of the survival rates of BKZ-4 with 72.42% (±8.43), BKZ-5 with 80.01% (±1.4), and BKZ-6 with 70.23% (±4.62). Nevertheless, especially the treatment with 20 µM KJ-Pyr-9 showed a potential therapeutically relevant effect on survival of BKZ-4, -5, and -6, as survival rates were impaired to 4.92% (±0.16), 3.58% (±0.32), and 3.09% (±0.19), respectively (Figure 5A–C). Statistical analysis of merged data of all three SCC populations showed a highly significant effect of KJ-Pyr-9 values greater than 5 µM on cell survival, even though only 20 µM of KJ-Pyr-9-treatment led a reduction of more than 95% survival (Figure 5G). Calculation of the half maximal inhibitory concentration (IC_{50}) of KJ-Pyr-9 revealed IC_{50} values of 10.33 µM for BKZ-4, 11.40 µM for BKZ-5, and 11.48 µM for BKZ-6 (Figure 5J). In accordance with SCC-derived cells, KJ-Pyr-9-treatment of AC-derived cells showed similar results. Nevertheless, for AC-derived cells, only concentrations greater than 10 µM KJ-Pyr-9 revealed a significant effect on cell survival compared to control. Again, usage of 20 µM KJ-Pyr-9 reduced cell survival significantly for BKZ-7 to 5.98% (±0.93), BKZ-8 to 2.02% (±0.33), and BKZ-9 to 3.36% (±0.28) (Figure 5D–F). Analysis of the merged data of all three AC-derived LCSC-like cells showed significant reductions of cell survival after the exposure to KJ-Pyr-9 concentrations greater than 10 µM with survival of 88.38% (±4.11). However, only application of 20 µM KJ-Pyr-9 impaired cell survival in a highly significant way, with final survival of only 3.79% (±0.65) (Figure 5H). Analysis of the half maximal inhibitory concentration (IC_{50}) of KJ-Pyr-9 depicted IC_{50} values of 10.89 µM for BKZ-7, 11.57 µM for BKZ-8, and 11.08 µM for BKZ-9 (Figure 5K). Investigation of the influence of KJ-Pyr-9 on LXF-289 cells revealed significant reductions in cell survival after exposure to 10 µM KJ-Pyr-9 with 69.78%

(±3.62) and 20 µM KJ-Pyr-9 with 9.877 (±4.94) survival left (Figure 5I). Calculated IC_{50} was 10.64 µM (Figure 5L). Interestingly, 24 h treatment of NSCLC-derived cell populations with 10 or 20 µM KJ-Pyr-9 led to heterogeneous nuclear localization of MYC for SCC- and AC-derived cell populations (Supplementary Figure S11).

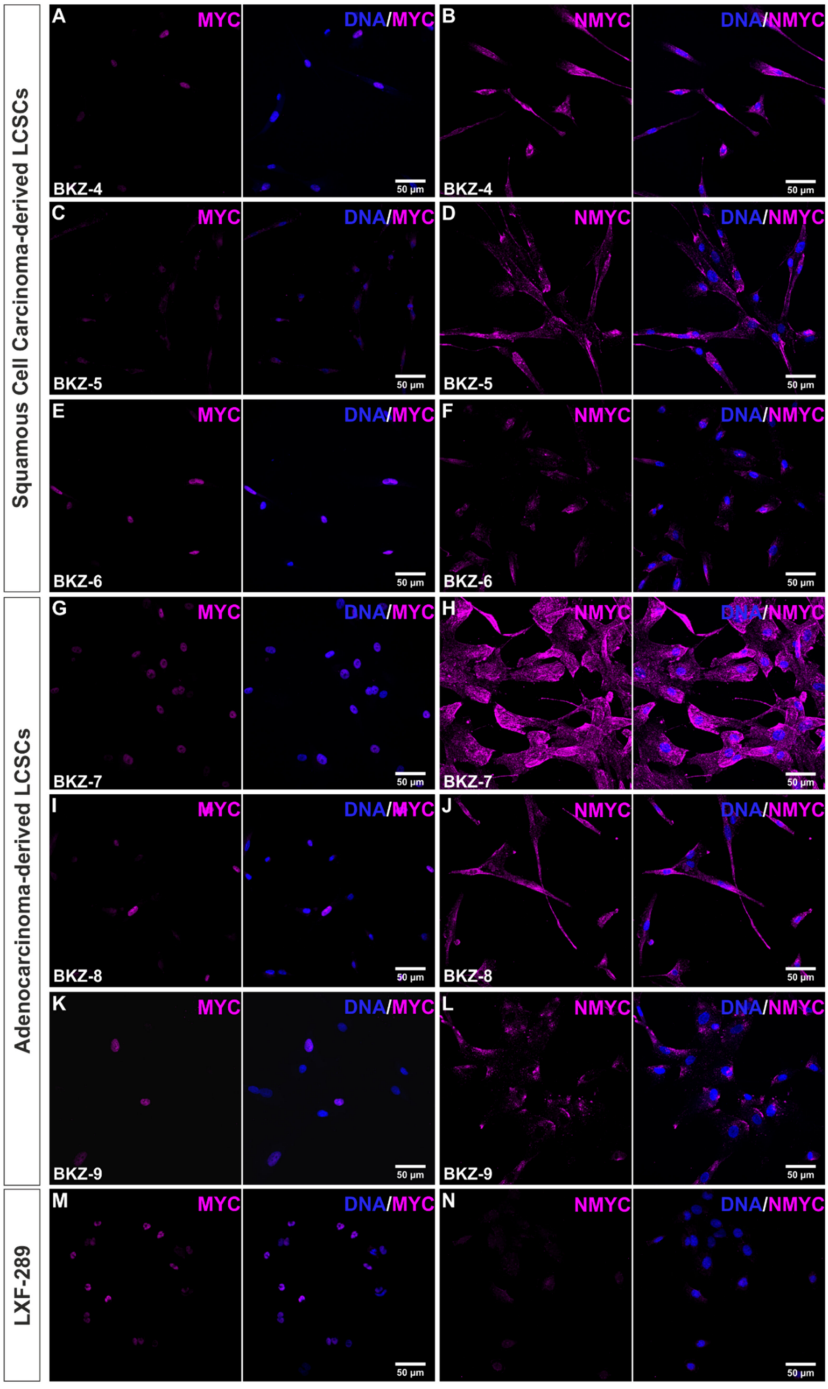

Figure 4. Squamous cell carcinoma- and adenocarcinoma-derived lung cancer stem cell-like cells all expressed myc proto-oncogene (MYC) and N-myc proto-oncogene (NMYC) at the protein level. Analysis of the protein expression of the oncogenes via immunocytochemical staining depicted a nuclear expression of (**A**,**C**,**E**,**G**,**I**,**K**) MYC and a predominantly cytosolic expression of (**B**,**D**,**F**,**H**,**J**,**L**) NMYC for all cell populations. Immunocytochemical analysis of the well-established lung adenocarcinoma-derived cell line LXF-289 depicted nuclear (**M**) MYC expression, as well as slight cytosolic expression of (**N**) NMYC.

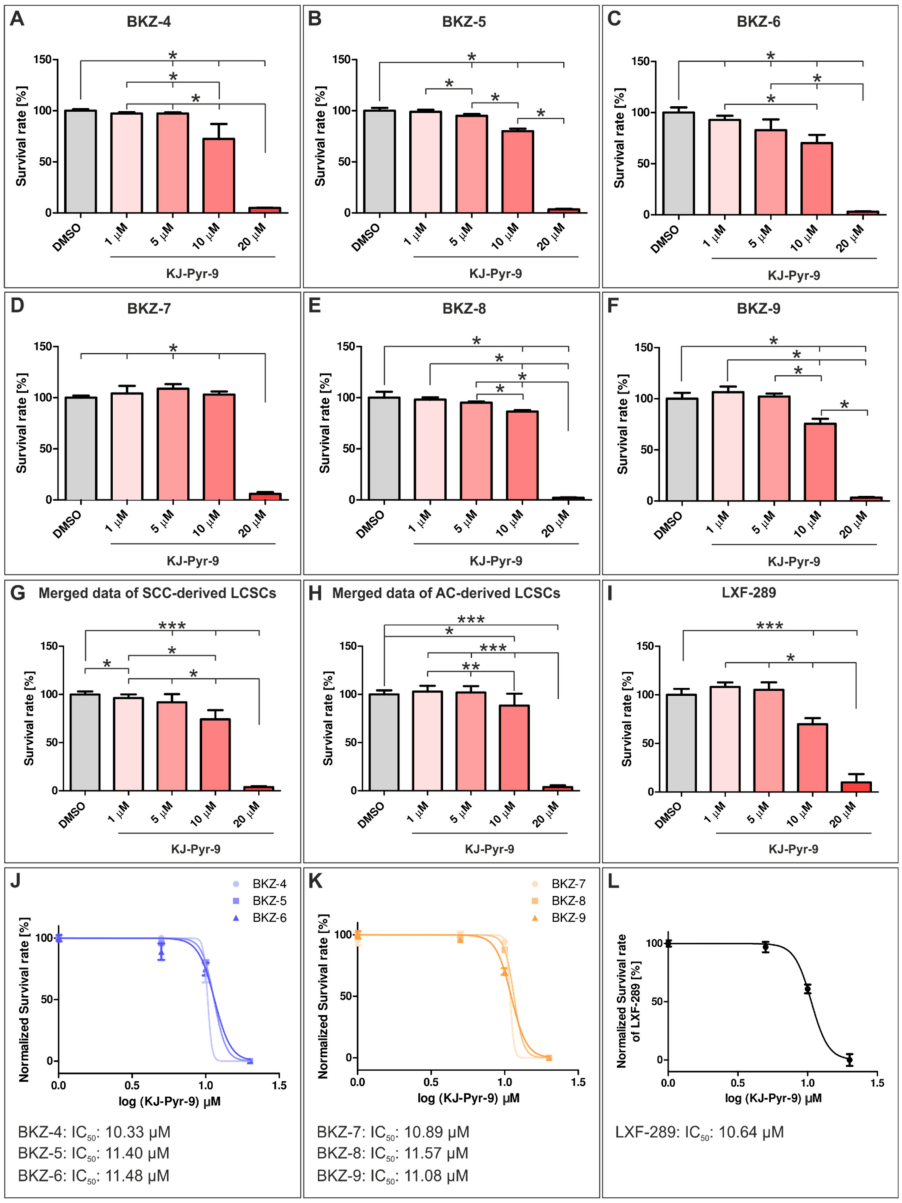

Figure 5. Inhibition of myc proto-oncogene (MYC) and N-myc proto-oncogene (NMYC) protein interaction with Myc-associated factor X significantly decreased survival of squamous cell carcinoma (SCC)- and adenocarcinoma (AC)-derived lung cancer stem cell (LCSC)-like cells. Metabolism was measured using Orangu, and cell count was determined by using a standard curve. Quantification of the normalized survival rate of SCC-derived (**A**) BKZ-4, (**B**) BKZ-5, and (**C**) BKZ-6 showed a significantly decreased survival after exposure to values greater than 5 µM of the MYC/NMYC inhibitor KJ-Pyr-9 in comparison to the control. Calculation of the normalized survival rate for AC-derived (**D**) BKZ-7, (**E**) BKZ-8, and (**F**) BKZ-9 showed a significantly decreased survival after exposure to 20 µM of KJ-Pyr-9 in comparison to the control. However, BKZ-8 and BKZ-9 seemed to be more sensitive in comparison to BKZ-7 as they also revealed a significantly decreased survival after the treatment with 10 µM KJ-Pyr-9. (**G**) Merged data of SCC-derived LCSC-like cells showed a significantly reduced survival after treatment with KJ-Pyr-9, with values higher than 5 µM for and (**J**) half maximal inhibitory concentration (IC_{50}) values between 10.33 and 11.48 µM. (**H**) Quantification of merged data of AC-derived LCSC-like cell populations showed significantly reduced survival upon KJ-Pyr-9 values higher than 10 µM. (**K**) IC_{50} values ranged between 10.89 µM and 11.57 µM KJ-Pyr-9 for AC-derived LCSC-like cells. (**I**) Quantification of the survival of lung adenocarcinoma cell line LXF-289 showed significantly reduced survival after exposure to 10 µM KJ-Pyr-9 with an (**L**) IC_{50} of 10.64 µM. Non-parametric Mann–Whitney test (**A**–**G**,**I**, $p \leq 0.05$). Unpaired *t*-test (**H**, $p \leq 0.05$). $n = 3$, * $p \leq 0.05$, ** $p \leq 0.01$, *** $p \leq 0.001$. Mean ± SEM (standard error of the mean).

Analysis of potential target genes of MYC involved in the KJ-Pyr-9-induced survival decrease revealed a decrease of cyclin D1 (*CCND1*) after 24 h treatment with 20 µM KJ-Pyr-9 for BKZ-6 and BKZ-8 as representative cell populations for squamous cell carcinoma- and adenocarcinoma-derived LCSC-like cells. Additionally, BKZ-8 exhibited significantly reduced mRNA expression levels of ribosomal protein lateral stalk subunit P1 (*RPLP1*) and ribosomal protein L28 (*RPL28*), both involved in ribosomal biosynthesis. Not regulated in LCSC-like cells but regulated in the lung adenocarcinoma cell line LXF-289 were lactate dehydrogenase A (*LDHA*) and *MYC* mRNA expressions, as *LDHA* was significantly reduced and *MYC* significantly increased after KJ-Pyr-9 application (Figure 6). Further tested but not regulated MYC target genes were cyclin D3 (*CCND3*), ribosomal protein L5 (*RPL5*), and ribosomal protein L14 (*RPL14*) (Supplementary Figure S12). Additional analysis of the number of senescent cells after treatment with 20 µM KJ-Pyr-9 for 24 h led to a significant increase in SCC-derived senescent cells, but not in AC-derived senescent cells (Supplementary Figure S13).

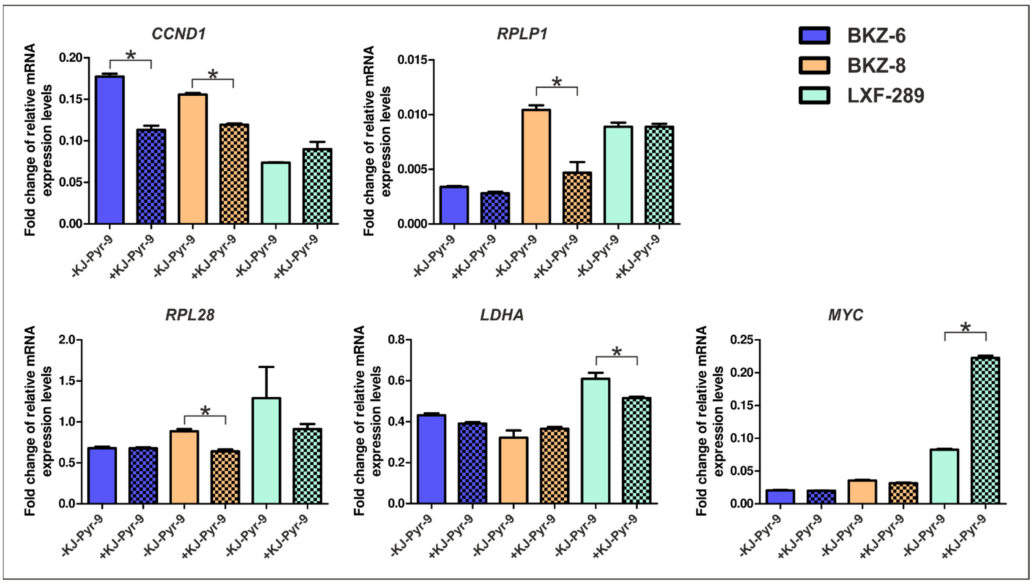

Figure 6. Myc proto-oncogene (MYC)-regulated target genes in lung cancer stem cell (LCSC)-like cells. Quantitative polymerase chain reaction of different target genes of MYC revealed a significant reduction of Cyclin D1 (*CCND1*) after the application of 20 µM KJ-Pyr-9 for BKZ-6 and BKZ-8 as representative cell populations for squamous cell carcinoma- and adenocarcinoma-derived LCSC-like cells. Further, BKZ-8 exhibited significantly reduced mRNA expressions of ribosomal protein lateral stalk subunit P1 (*RPLP1*) and ribosomal protein L28 (*RPL28*). Additionally, lung adenocarcinoma cell line LXF-289 showed a significantly decreased mRNA level of lactate dehydrogenase A (*LDHA*) and a significantly increase in *MYC* expression after KJ-Pyr-9 treatment. Non-parametric Mann–Whitney-test ($p \leq 0.05$). $n = 3$, * $p \leq 0.05$. Mean ± SEM (standard error of the mean).

3.4. Inhibition of NF-κB Signaling Decreased Survival of Squamous Cell Carcinoma- and Adenocarcinoma-Derived Lung Cancer Stem Cell-like Cells

Next to the influence of MYC/NMYC inhibition, we investigated NSCLC-derived cell survival after inhibition of NF-κB signaling utilizing dexamethasone and PDTC. Additionally, the influence of possible synergistic effects on the impairment of cell survival was determined by utilizing different combinations of these inhibitors with TNF-α and KJ-Pyr-9. Here, treatment with dexamethasone (300 µM) and PDTC (100 µM) led to significant reductions of SCC- and AC-derived cell survival (Figure 7A,B). On the contrary, application of the NF-κB inhibitor lenalidomide only slightly impaired cell survival of SCC-derived cells with nearly no effect on AC-derived LCSC-like cells (Supplementary Figure S14). PDTC-treatment in SCC-derived LCSC-like cells led to a significantly elevated reduction with only 14.60% (±2.17) cell survival left in comparison to dexamethasone

with 27.17% (±5.17) survival (Figure 7A). This effect was not detectable for AC-derived LCSC-like cells, as 26.24% (±5.12) survival was observable after dexamethasone treatment and still 24.16% (±6.04) survival after the exposure to PDTC (Figure 7B). No additional effect on survival reduction of NSCLC-derived cells was detectable after application of dexamethasone and PDTC, even though a tendency could be seen for AC-derived LCSC-like cells (Figure 7A,B). In addition, treatment of SCC- and AC-derived LCSC-like cells with PDTC resulted in a significant increase in senescence in comparison to the control (Supplementary Figure S13). Interestingly, nuclear RelA localization was only slightly affected by PDTC-treatment for 24 h, although a tendency showing a decrease in the ratio of nuclear RelA to total RelA was observable after exposure of LCSC-like cells to PDTC compared to control (Supplementary Figure S15).

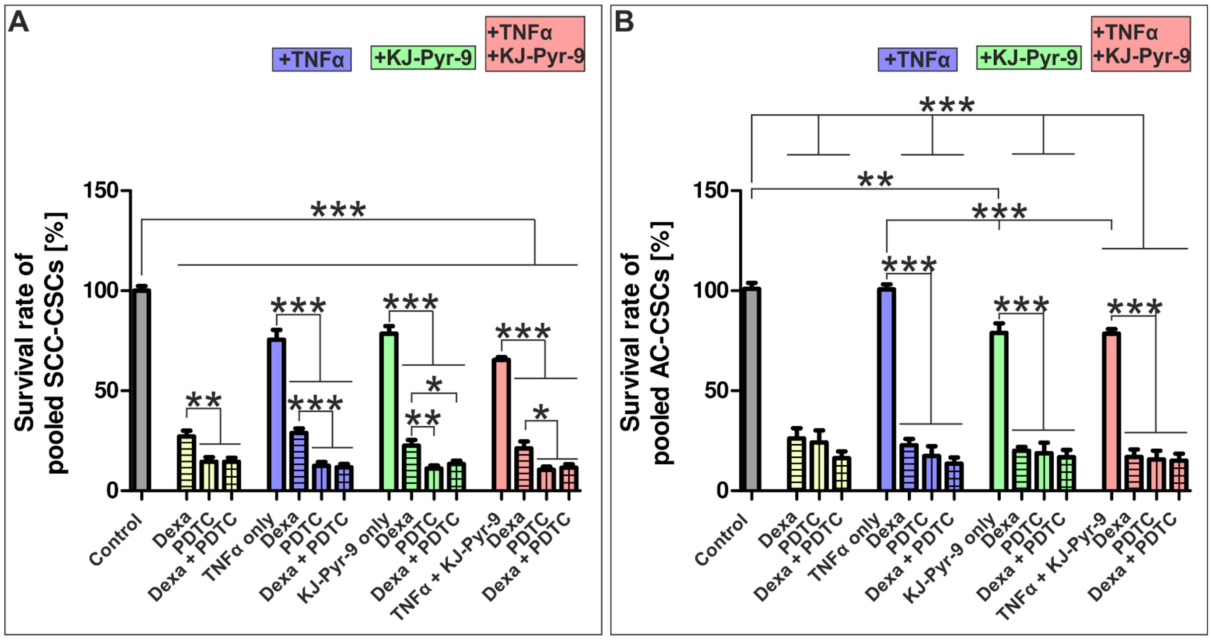

Figure 7. Co-inhibition of MYC and NF-κB signaling did not synergistically affect survival of NSCLC-derived LCSC-like cells. To analyze possible synergistic effects of MYC and NF-κB signaling inhibition on cell survival, we treated cells with dexamethasone (Dexa; 300 µM), PDTC (100 µM), TNF-α (10 ng/mL), and KJ-Pyr-9 (10 µM), and cellular viability was analyzed using Orangu. (**A**) Statistical analysis of normalized survival rates of SCC-derived LCSC-like cells revealed a significantly reduced survival upon all treatment combinations but did not show any synergistically effect of the different reagents. There was no difference in cell survival upon the usages of dexamethasone and PDTC in combination with TNF-α, KJ-Pyr-9, or TNF-α with KJ-Pyr-9 together. (**B**) Quantification of the normalized AC-derived cell survival also revealed no synergistical effect of inhibition of MYC and NF-κB signaling. However, TNF-α alone did not influence cell survival of AC-derived cells in contrast to SCC-derived ones. Unpaired *t*-test ($p \leq 0.05$). $n = 3$, * $p \leq 0.05$, ** $p \leq 0.01$, *** $p \leq 0.001$. Mean ± SEM (standard error of the mean).

Analysis of the influence of TNF-α (10 ng/mL) on NSCLC-derived LCSC-like cells exhibited a survival-decreasing effect only on SCC-derived LCSC-like cells (75.51% (±4.92) survival), but no effect for AC-derived cells. Nevertheless, no synergistic depletion of cellular survival of NSCLC-derived LCSC-like cells was detectable by co-treatments using TNF-α with dexamethasone and/or PDTC together. Accordingly, combined MYC/NMYC and NF-κB inhibition using 10 µM KJ-Pyr-9 with dexamethasone and/or PDTC did not result in synergistic reductions in survival of NSCLC-derived LCSC-like cells. Of note, MYC/NMYC inhibition using only 10 µM KJ-Pyr-9 alone decreased survival of SCC- and AC-derived LCSC-like cells significantly. The use of TNF-α, KJ-Pyr-9, dexamethasone, and PDTC in parallel did not impair NSCLC-derived LCSC-like cell survival synergistically (Figure 7A,B). In summary, the inhibition of MYC/NMYC signaling using KJ-Pyr-9 as well

as the inhibition of NF-κB signaling utilizing dexamethasone or PDTC significantly reduced survival of SCC- and AC-derived LCSC-like cells with no synergistic effects (Table 2).

Table 2. Survival rates of squamous cell carcinoma (SCC)- and adenocarcinoma (AD)-derived lung cancer stem cell (LCSC)-like cells after the application of different NF-κB inhibitors and the MYC inhibitor KJ-Pyr-9.

Treatment	Concentration	Target	Survival Rate of SCC-Derived LCSC-Like Cells	Survival Rate of AD-Derived LCSC-Like Cells
KJ-Pyr-9	1 µM	MYC	96.35% (±1.23)	103.0% (±1.99)
KJ-Pyr-9	5 µM	MYC	91.77% (±2.86)	102.1% (±2.16)
KJ-Pyr-9	10 µM	MYC	74.22% (±3.17)	88.38% (±4.11)
KJ-Pyr-9	20 µM	MYC	3.86% (±0.30)	3.80% (±0.65)
PDTC [1]	100 µM	NF-κB	14.60% (±2.17)	24.16% (±6.04)
Dexa [2]	300 µM	NF-κB	27.17% (±5.17)	26.24% (±5.12)
PDTC + Dexa	100 µM/300 µM	NF-κB	14.61% (±1.91)	16.33% (±3.29)
KJ-Pyr-9 + PDTC	10 µM/100 µM	MYC/NF-κB	11.18% (±1.48)	18.84% (±5.25)
KJ-Pyr-9 + Dexa	10 µM/300 µM	MYC/NF-κB	22.53% (±2.95)	20.09% (±1.90)
KJ-Pyr-9 + PDTC + Dexa	10 µM/100 µM/300 µM	MYC/NF-κB	13.40% (±1.60)	16.84% (±3.61)

[1] PDTC = pyrrolidinedithiocarbamate; [2] Dexa = dexamethasone.

4. Discussion

In this study, we present six novel LCSC-like cell populations derived from three SCC and three AC of the lung as promising in vitro models for LCSC-like cells. Usage of low doses of the MYC signaling inhibitor KJ-Pyr-9 led to a significant depletion in survival of SCC- as well as AC-derived LCSC-like cells, representing the impairment of protein–protein interaction of MYC/NMYC, with MAX as a promising target in treating NCSLC, particularly by engaging MYC high-expressing LCSC. One possibly relevant MYC target gene, which we detected to be regulated by KJ-Pyr-9, was cyclin D1. Nevertheless, the whole picture of the underlying working mechanism still remains elusive.

Cancer stem cells are defined by the expression of a set of different markers such as CD133 [41], CD44 [42], and Nestin [43]. In primary NSCLC cell lines, Chen and colleagues demonstrated that $CD133^+$ cells displayed higher ability for self-renewal and tumor initiation, as well as higher resistance to chemotherapy in comparison to $CD133^-$ cells [44]. This in vivo tumorigenicity and the correlation of the expression of stemness-related genes of $CD133^+$ cells was confirmed additionally by Tirino and Huang [45,46]. Further, CD44 expression was shown to correlate with stem cell-like properties such as chemotherapy resistance, enhanced spheroid formation and tumor-initiating capacities [47,48]. Moreover, CD44 expression was demonstrated to be linked to drug resistance [49], NSCLC occurrence, and metastasis [50,51]. Double-positive $CD133^+/CD44^+$ primary AC-derived lung cancer cells revealed higher colony formation units than $CD133^-/CD44^-$ ones. Further, Wang and colleagues depicted that IL6 pretreatment of $CD133^+/CD44^+$ cells assisted in entering into the cell cycle in quiescent lung cancer stem cells and significantly increased chemosensitivity [52]. Nestin initially served as stem cell marker especially for the central nervous system [53], although its role as CSC marker became more prominent in recent years. Regarding NSCLC, a knockdown of Nestin protein using short hairpin RNA not only decreased proliferation but also affected migration, invasion, and sphere formation of AC-derived cells [54]. This stands in accordance with Liu and coworkers, who indicated that a CRISPR/Cas9-mediated knockout of Nestin led to reduced proliferation, invasion, and colony formation of H1299 and A549 cell lines [55]. Even though, some studies of NSCLC-derived cancer stem cells exist, most of them are based on sorted well-established cell lines and not on primary ones. Thus, the herein presented co-expression of CSC markers CD133 and CD44, as well as the expression of Nestin in the novel BKZ-4, -5, -6, -7, -8, and -9 cell populations, strongly suggests their LCSC-like character and represents these as promising new in vitro models for studying NSCLC-derived stem cells. Additionally, immunocytochemical investigation of the well-established lung adenocarcinoma cell line LXF-289 revealed no expression for CD133 and Nestin and lower expression of CD44, underpinning the presence of a CSC phenotype in the here-presented BKZ cell populations.

Tumor spheroid formation of all six BKZ cell populations further substantiated LCSC properties, as cell populations with tumor-sphere-forming-properties are constantly shown to form tumors in xenograft models of LCSC-like cells [56].

Myc family members are key regulators of cell proliferation, self-renewal, and differentiation and are known to play an important role in tumor initiation and progression [57]. Recently, we reported a significant survival-decreasing effect in primary human colon cancer stem-like cells by the inhibition of MYC signaling using KJ-Pyr-9 [29]. While KJ-Pyr-9 is a small molecule with highest activity in MYC inhibition, it is interesting to note that recent efforts in drug development led to new derivates with similar activity but higher solubility and better stability [58]. Regarding NSCLC, the working group around Tao reported that viability, self-renewal, and invasion of A549-derived LCSC-like cells was decreased by affecting MYC signaling [18]. Targeting MYC also enhanced chemotherapeutic efficacy of cisplatin in NSCLC cells [59]. In accordance with these results, we here observed a high protein amount of MYC and NMYC in all six NSCLC-derived LCSC-like cells, further underlining their stem-like characteristics. Notably, inhibition of MYC by application of 20 µM small molecule KJ-Pyr-9 [28] resulted in strong inhibition of cell survival in LCSC-like cells, while concentration of up to 10 µM KJ-Pyr-9 led to a slight yet significant decrease in survival. Calculation of the half maximal inhibitory concentrations (IC_{50}) revealed IC_{50} values between 10.33 and 11.57 µM KJ-Pyr-9 for the here-established LCSC-like cells. Accordingly, recombinant MYC–MAX–DNA interaction was reported to be inhibited with an IC_{50} of approximately 10 and 30 µM [28,60]. On the contrary, KJ-Pyr-9 was described to have no effect on MYC–MAX in an SPR assay up to 10 µM, with the reason for this discrepancy being unclear [61]. Investigation of lung adenocarcinoma cell line LXF-289 revealed similar results concerning the influence of MYC inhibition on cell survival, suggesting a conserved working mechanism on lung adenocarcinoma cells with MYC expression. Nevertheless, MYC and NMYC expression of LXF-289 were principally lower in comparison to BKZ populations, except for BKZ-4 for MYC protein. Furthermore, LCSC-like cells revealed additional signals within the NMYC blot, suggesting the presence of further isoforms of this protein in LCSC-like cells in comparison to LXF-289. However, the characteristics and role of these possible new isoforms have to be investigated in future studies. To gain first insights into the working mechanism of KJ-Pyr-9-induced survival decrease in MYC expressing lung cancer cells, we tested for alterations in mRNA levels of several known MYC target genes, such as *CCND1*, *CCND3*, and *MYC* itself. Further, we recently published high expressions of genes involved in ribosomal biosynthesis in different CSC-like populations, including the here-presented BKZ-7, BKZ-8, and BKZ-9 (there referred to as LCSC_a, LCSC_b, and LCSC_c [62]). Here, we focused on known MYC target genes, such as *RPLP1*, *RPL5*, *RPL14*, *RPL28*, and *LDHA* [63–67]. Quantification revealed significant reductions in *CCND1* mRNA levels for the representative LCSC-like cell populations BKZ-6 and BKZ-8 after KJ-Pyr-9 application, possibly explaining the survival-decreasing effects. This stands in line with studies of Zhou et al. and Chen et al. that reported MYC-dependent cell cycle regulation in NSCLC cell lines [68,69]. Furthermore, *RPLP1* and *RPL28* expression in BKZ-8 was affected by KJ-Pyr-9 application, suggesting an involvement of MYC signaling in ribosomal biosynthesis of AC-derived LCSC-like cells, as already shown for several cancer types (reviewed in [70,71]). However, lung adenocarcinoma cell line LXF-289 and SCC-derived LCSC-like cell population BKZ-6 did not reveal differences in the investigated genes involved in ribosomal biosynthesis, highlighting a cell line-specific response. These variances could also be seen in the response of *LDHA*, as it was only downregulated in LXF-289 cells but not in BKZ-6 or BKZ-8. In pancreatic and prostate cancer, a correlation of MYC with LDHA expression was detected and linked to the regulation of aerobic glycolysis while promoting tumor progression and decreasing apoptosis [67,72]. Thus, downregulation of *LDHA* may be one cause for KJ-Pyr-9-mediated decrease in cell survival of LXF-289. Nevertheless, this effect could not be detected in the two representative BKZ populations, suggesting a difference between the here-established LCSC-like cells and the LXF-289 cell line. Further, the in 1995 established

lung adenocarcinoma-derived cell line LXF-289 [30] showed atypical effects upon MYC inhibition, as mRNA levels of the transcript were increased by KJ-Pyr-9 treatment. Generally, it is postulated that MYC creates a positive auto-regulatory circuit, which is essential for sustaining mutual high expression in tumor cells [73]. However, the data presented in this manuscript revealed a more complex mechanism involved in the regulation of MYC signaling, suggesting the need for large-scale target gene analysis to fully understand the signaling cascade. In conclusion, our observations strongly emphasized MYC inhibition as an auspicious therapy for treating NSCLC by targeting cyclin D1 expression in LCSC-like cells, while the whole underlying mechanism still remains unclear.

Next to MYC, NF-κB signaling is broadly described to be involved in multiple steps of lung carcinogenesis, to mediate therapy resistance [74], and to be active in lymph node metastasis [27], providing an important linkage between the pathogenesis of pulmonary inflammation and lung cancer [75]. Accordingly, the presence of NSCLC cells positive for NF-κB RelA was reported to be correlated with shorter overall survival time, suggesting RelA expression as a prognostic factor for NSCLC [27,76] (reviewed in [77]). Regarding its role in LCSCs, NF-κB was also reported to be highly associated with the CSC gene expression signature of NSCLC cells [10]. Depletion of NF-κB RelA utilizing the kinase inhibitor BMS-345541 effectively reduced stemness and EMT markers, self-renewal, and migratory properties of LCSCs [78], suggesting NF-κB as a promising target for CSC depletion in NSCLC (reviewed in [77]). Accordingly, we observed RelA protein in high amounts in SCC- and AC-derived LCSC-like cells and thus conclude that RelA expression seems to be a unifying factor of all NSCLC-derived cell populations described here. Application of TNF-α led to nuclear translocation and thus to the activation of RelA in all six LCSC-like cells. TNF-α-mediated signaling in NSCLC cell lines was shown to be favorable for cancer initiation, as TNF-α-induced NF-κB signaling led to the protection from cell death [79] and was shown to have a metastasis-promoting effect associated with tumor recurrence and drug resistance [80]. On the other hand, TNF-α expression was reported to be unfavorable as it was involved in necroptosis of NSCLC cells [81]. Additionally, there is a concept of pro-tumor inflammation being present in cancer [82]. Regarding NSCLC, anti-inflammatory therapy targeting the interleukin-1β innate immunity pathway was shown to significantly reduce lung cancer mortality [83]. In the present study, we investigated this concept of pro-inflammatory cytokines as growth factors for CSCs by using TNF-α, but could not detect any increase in cell number in comparison to control. Accordingly, analysis of cell survival after TNF-α-stimulation revealed no change in survival of AC-derived LCSC-like cells, but a significant reduction in survival of SCC-derived LCSC-like cells, reflecting differences in the dependence on TNF-α/NF-κB-mediated pathways between NSCLC-derived LCSC-like cells.

Inhibitors of pro-inflammatory signaling such as dexamethasone, lenalidomide, or PDTC are known to influence the production of cytokines and growth factors, which in turn enhances the immune response against tumor cells and inhibits tumor angiogenesis [84]. Even though proliferation of some NSCLC cell lines have been shown to be affected by lenalidomide [85], we here observed fivefold higher doses to marginally impair survival of NSCLC-derived LCSC-like cells in comparison to the study around Kim and colleagues [85]. This kind of lenalidomide resistance possibly highlights their enrichment for stem-like properties. Lenalidomide was shown to affect NF-kB-induced apoptosis by modulating the production of cytokines and growth factors such as TNF-α and insulin-like growth factor–1 [86], thus acting more upstream in comparison to PDTC and dexamethasone. Hence, the here-presented LCSC-like cells potentially evade the immunomodulatory effects of lenalidomide by a mechanism more downstream of the respective signaling pathway. Nevertheless, underlying mechanisms have to be clarified. Contrarily, application of the immunomodulatory synthetic glucocorticoid dexamethasone resulted in a more elevated reduction in cell survival of NSCLC-derived LCSC-like cells. Dexamethasone was shown to interfere with NF-κB activation and reduced TNF-α production [87,88]. In NSCLC cells it was shown to inhibit TGF-β1-induced migration as well as EMT via the

AKT/ERK signaling pathways [89], suggesting a modulatory effect on CSC properties. Nevertheless, dexamethasone is also suggested to impair chemotherapy efficacy, as co-administration was shown to decrease chemosensitivity in NSCLC xenograft models [90]. Next to dexamethasone, PDTC is commonly known to inhibit the IkBα degradation and p65 nuclear import [91], and was likewise shown to reduce survival of NSCLC-derived LCSC-like cells in the present study. Accordingly, Zhang and coworkers demonstrated that PDTC regulates metastasis of A549 cells in co-culture with lymphatic endothelial cells, possibly representing a link between NF-κB and the lymphocytic metastasis of NSCLC cells [92]. In this study, PDTC treatment was more effective in decreasing cell survival of SCC-derived LCSC-like cells in comparison to high doses of dexamethasone. However, this difference could not be detected in AC-derived LCSC-like cells, suggesting a more chemoresistant phenotype compared to SCC-derived cells. Two of three parental tissues of AC-derived LCSC-like cells revealed clinically relevant mutations, one for *EGFR* and one for *KRAS* and *STK11*, possibly explaining the observed reduction in sensitivity for PDTC. However, SCC-derived cells were not tested for potential mutations, as no clinical relevance was existent. Generally, co-treatment with PDTC and dexamethasone, and especially application of KJ-Pyr-9 seem to be more effective in targeting NSCLC-derived LCSC-like cells in comparison to various standard chemotherapeutics such as cisplatin, docetaxel, pemetrexed, paclitaxel or vinorelbine as investigated by Herreros-Pomares and colleagues. Those chemotherapeutics were shown to impair CSC survival only marginally with 83.5%, 86.9%, 76.2%, 68.2%, and 56.9% cells alive after treatment, respectively. More effective, but still not as effective as KJ-Pyr-9 and co-treatment with PDTC and dexamethasone, was salinomycin with 21.7% survival left [93] (Table 2). Salinomycin was already identified as highly active drug, reducing breast CSCs more than 100-fold in comparison to standard drug treatment with paclitaxel [94]. Further, it was shown to inhibit NF-κB activity in prostate cancer cells, which was reported by Ketola and coworkers [95]. Thus, we conclude that targeting of the NF-kB pathway with drugs such as PDTC or salinomycin might be a new route for post-surgical treatment of NSCLC. Nevertheless, MYC seems to also play a pivotal role, as its expression was also impaired by salinomycin [95]. Interestingly, PDTC was reported to induce cytotoxic effects against SCLC cells by suppressing MYC expression and inducing S phase arrest [96], suggesting a role of PDTC in MYC modulation in NSCLC cells. Still, direct inhibition of MYC/NMYC using low doses of KJ-Pyr-9 was shown to be more effective than PDTC-treatment for both SCC- and AC-derived LCSC-like cells. Additionally, no synergistic effect of the inhibition of NF-κB and MYC signaling was detectable in NSCLC-derived LCSC-like cells, suggesting either inhibition of MYC signaling or NF-κB signaling to inhibit survival of LCSCs without a cross-coupling between the two pathways.

In summary, we successfully isolated six novel NSCLC-derived lung cancer stem-like cells as promising in vitro models to further study CSC–driven tumor growth, treatment resistance, and cancer relapse. Expression of the prominent CSC markers CD133, CD44, and Nestin as well as successful formation of spherical cancer organoids confirmed a CSC-like phenotype. Additionally, all three AC- as well as SCC-derived LCSC-like cells expressed proto-oncogenes MYC and NMYC, further emphasizing their stem-like characteristics. Application of inhibitors of NF-κB and MYC signaling led to significant reductions in survival of both AC- and SCC-derived cells. Nevertheless, inhibition of MYC/NMYC using KJ-Pyr-9 was observed to impair LCSC-like cells most effectively, suggesting MYC signaling as a possible object for targeting LCSC. Even though MYC signaling could be identified to play a crucial role in LCSC-like survival, underlying mechanisms involved in this signaling pathway still remain unclear, and MYC-inhibiting drugs have to be clinically approved to be able to use them against NSCLC. In contrast, dexamethasone and the PDTC derivative zinc diethyldithiocarbamate are already in clinical use and thus more rapidly applicable against NSCLC. Overall, both signaling pathways are promising targets in NSCLC-derived LCSC-like cells, but molecular signaling needs further investigation.

Supplementary Materials: The following are available online at https://www.mdpi.com/article/10.3390/cells10051024/s1, Figure S1: Clinical imaging of the different donors of the six isolated lung cancer stem cell-like cell populations. Figure S2. SCC- and AC-derived LCSC-like cells were heterogeneous in size. Figure S3. BKZ-5-derived spheres expressed cancer stem cell markers Prominin-1 (CD133) and CD44-antigen (CD44). Figure S4. Immunocytochemical staining of cancer stem cell markers in adult human dermal fibroblasts (HDF). Figure S5. Squamous cell carcinoma-derived lung cancer stem cell-like cells BKZ-4, BKZ-5, and BKZ-6 all expressed NF-κB subunits RelA, RelB, and cRel. Figure S6. Adenocarcinoma-derived lung cancer stem cell-like cells all predominantly expressed NF-κB subunits RelA, RelB, and cRel. Figure S7. Stimulation with tumor necrosis factor α (TNF-α) shifted cytoplasmic NF-κB RelA into the nucleus of squamous cell carcinoma- and adenocarcinoma-derived lung cancer stem-like cells. Figure S8. BKZ-5-derived spheres expressed myc proto-oncogene (MYC) and slightly N-myc proto-oncogene (NMYC). Figure S9. Western blot analysis of the protein levels of NMYC and MYC within BKZ populations and LXF-289 cells. Figure S10. Squamous cell carcinoma (SCC)- and adenocarcinoma (AC)-derived LCSC-like cells all revealed a normal copy number for myc proto-oncogene (MYC) and N-myc proto-oncogene (NMYC). Figure S11. Treatment of non-small cell lung cancer-derived cell populations with KJ-Pyr-9 led to heterogeneous nuclear localization of myc proto-oncogene (MYC). Figure S12: Analysis of putative MYC-target genes in lung cancer stem cell (LCSC)-like cells. Figure S13. Pyrrolidinedithiocarbamate (PDTC) induced senescence in squamous cell carcinoma (SCC)- and adenocarcinoma (AC)-derived lung cancer stem cell-like cells. Figure S14. Inhibition of upstream pro-inflammatory signaling using lenalidomide only significantly decreased survival of squamous cell carcinoma (SCC)- not adenocarcinoma (AC)-derived lung cancer stem cell-like cells. Figure S15. Pyrrolidinedithiocarbamate (PDTC) treatment slightly decreased nuclear RelA of squamous cell carcinoma (SCC)- and adenocarcinoma (AC)-derived lung cancer stem cell-like cells. Table S1. Cell population-specific donor information. Table S2. Analysis of therapeutical relevant mutations.

Author Contributions: Conceptualization, C.K. and B.K.; data curation, B.A.W., M.B. (Morris Beshay), L.P.H., C.F. (Clara Flottmann), M.B. (Miriam Beermann), C.F. (Christine Förster), L.W., J.F.W.G., C.K., and B.K.; formal analysis, B.A.W. and J.F.W.G.; funding acquisition, M.B. (Morris Beshay), C.K., and B.K.; investigation, B.A.W., L.P.H., C.F. (Clara Flottmann), and M.B. (Miriam Beermann); project administration, C.K. and B.K.; supervision, C.K. and B.K.; visualization, B.A.W. and L.P.H.; writing—original draft, B.A.W., M.B. (Morris Beshay), L.P.H., C.F. (Clara Flottmann), M.B. (Miriam Beermann), C.F. (Christine Förster), L.W., J.F.W.G., C.K., and B.K.; writing—review and editing, B.A.W., M.B. (Morris Beshay), L.P.H., C.F. (Clara Flottmann), M.B. (Miriam Beermann), C.F. (Christine Förster), L.W., J.F.W.G., C.K., and B.K. All authors have read and agreed to the published version of the manuscript.

Funding: This research was funded in part by the University of Bielefeld. Beatrice Ariane Windmöller and Laureen Helweg are funded by an internal grant of the Bethel Foundation, Bielefeld, Germany.

Institutional Review Board Statement: The study was conducted according to the guidelines of the Declaration of Helsinki and approved by the Institutional Review Board (or Ethics Committee) of Ethics Committee Münster, Germany (2017-522-f-S, 27.07.2018).

Informed Consent Statement: Informed consent was obtained from all subjects involved in the study.

Acknowledgments: The excellent technical assistance of Angela Kralemann-Köhler, Claudia Rose, and Ulrike Hormel is gratefully acknowledged. The authors acknowledge support for the publication costs by the Deutsche Forschungsgemeinschaft and the Open Access Publication Fund of Bielefeld University.

Conflicts of Interest: The authors declare no conflict of interest. The funders had no role in the design of the study; in the collection, analyses, or interpretation of data; in the writing of the manuscript; or in the decision to publish the results.

References

1. Siegel, R.L.; Miller, K.D.; Jemal, A. Cancer statistics, 2019. *CA Cancer J. Clin.* **2019**, *69*, 7–34. [CrossRef] [PubMed]
2. Bray, F.; Ferlay, J.; Soerjomataram, I.; Siegel, R.L.; Torre, L.A.; Jemal, A. Global cancer statistics 2018: GLOBOCAN estimates of incidence and mortality worldwide for 36 cancers in 185 countries. *CA Cancer J. Clin.* **2018**, *68*, 394–424. [CrossRef] [PubMed]
3. Ruiz-Ceja, K.A.; Chirino, Y.I. Current FDA-approved treatments for non-small cell lung cancer and potential biomarkers for its detection. *Biomed. Pharmacother.* **2017**, *90*, 24–37. [CrossRef] [PubMed]

4. Zappa, C.; Mousa, S.A. Non-small cell lung cancer: Current treatment and future advances. *Transl. Lung Cancer Res.* **2016**, *5*, 288–300. [CrossRef] [PubMed]
5. De Sousa, V.M.L.; Carvalho, L. Heterogeneity in Lung Cancer. *Pathobiology* **2018**, *85*, 96–107. [CrossRef]
6. Eramo, A.; Lotti, F.; Sette, G.; Pilozzi, E.; Biffoni, M.; Di Virgilio, A.; Conticello, C.; Ruco, L.; Peschle, C.; De Maria, R. Identification and expansion of the tumorigenic lung cancer stem cell population. *Cell Death Differ.* **2007**, *15*, 504–514. [CrossRef]
7. Pardal, R.; Clarke, M.F.; Morrison, S.J. Applying the principles of stem-cell biology to cancer. *Nat. Rev. Cancer* **2003**, *3*, 895–902. [CrossRef]
8. Prabavathy, D.; Swarnalatha, Y.; Ramadoss, N. Lung cancer stem cells—origin, characteristics and therapy. *Stem Cell Investig.* **2018**, *5*, 6. [CrossRef]
9. Sun, F.-F.; Hu, Y.-H.; Xiong, L.-P.; Tu, X.-Y.; Zhao, J.-H.; Chen, S.-S.; Song, J.; Ye, X.-Q. Enhanced expression of stem cell markers and drug resistance in sphere-forming non-small cell lung cancer cells. *Int. J. Clin. Exp. Pathol.* **2015**, *8*, 6287–6300.
10. Zakaria, N.; Yusoff, N.M.; Zakaria, Z.; Lim, M.N.; Baharuddin, P.J.N.; Fakiruddin, K.S.; Yahaya, B. Human non-small cell lung cancer expresses putative cancer stem cell markers and exhibits the transcriptomic profile of multipotent cells. *BMC Cancer* **2015**, *15*, 1–16. [CrossRef]
11. Zhang, H.Z.; Lin, X.G.; Hua, P.; Wang, M.; Ao, X.; Xiong, L.H.; Wu, C.; Guo, J.J. The study of the tumor stem cell properties of CD133+CD44+ cells in the human lung adenocarcinoma cell line A549. *Cell. Mol. Biol.* **2010**, *56*, 1350–1358.
12. Maiuthed, A.; Chantarawong, W.; Chanvorachote, P. Lung Cancer Stem Cells and Cancer Stem Cell-targeting Natural Compounds. *Anticancer. Res.* **2018**, *38*, 3797–3809. [CrossRef]
13. Tan, Y.; Chen, B.; Xu, W.; Zhao, W.; Wu, J. Clinicopathological significance of CD133 in lung cancer: A meta-analysis. *Mol. Clin. Oncol.* **2014**, *2*, 111–115. [CrossRef]
14. Bertolini, G.; Roz, L.; Perego, P.; Tortoreto, M.; Fontanella, E.; Gatti, L.; Pratesi, G.; Fabbri, A.; Andriani, F.; Tinelli, S.; et al. Highly tumorigenic lung cancer CD133+ cells display stem-like features and are spared by cisplatin treatment. *Proc. Natl. Acad. Sci. USA* **2009**, *106*, 16281–16286. [CrossRef]
15. Schaub, F.X.; Dhankani, V.; Berger, A.C.; Trivedi, M.; Richardson, A.B.; Shaw, R.; Zhao, W.; Zhang, X.; Ventura, A.; Liu, Y.; et al. Pan-cancer Alterations of the MYC Oncogene and Its Proximal Network across the Cancer Genome Atlas. *Cell Syst.* **2018**, *6*, 282–300.e2. [CrossRef]
16. Iwakawa, R.; Kohno, T.; Kato, M.; Shiraishi, K.; Tsuta, K.; Noguchi, M.; Ogawa, S.; Yokota, J. MYC Amplification as a Prognostic Marker of Early-Stage Lung Adenocarcinoma Identified by Whole Genome Copy Number Analysis. *Clin. Cancer Res.* **2010**, *17*, 1481–1489. [CrossRef]
17. Seo, A.N.; Yang, J.M.; Kim, H.; Jheon, S.; Kim, K.; Lee, C.T.; Jin, Y.; Yun, S.; Chung, J.-H.; Paik, J.H. Clinicopathologic and prognostic significance of c-MYC copy number gain in lung adenocarcinomas. *Br. J. Cancer* **2014**, *110*, 2688–2699. [CrossRef]
18. Tao, X.; Yin, Y.; Lian, D.; Gu, H.; Chen, W.; Yang, L.; Yin, G.; Liu, P.; Li, L.; Wei, Y.; et al. Puerarin 6″-O-xyloside suppresses growth, self-renewal and invasion of lung cancer stem-like cells derived from A549 cells via regulating Akt/c-Myc signalling. *Clin. Exp. Pharmacol. Physiol.* **2020**, *47*, 1311–1319. [CrossRef]
19. Bhummaphan, N.; Petpiroon, N.; Prakhongcheep, O.; Sritularak, B.; Chanvorachote, P. Lusianthridin targeting of lung cancer stem cells via Src-STAT3 suppression. *Phytomedicine* **2019**, *62*, 152932. [CrossRef]
20. Lawrence, T. The Nuclear Factor NF- B Pathway in Inflammation. *Cold Spring Harb. Perspect. Biol.* **2009**, *1*, a001651. [CrossRef]
21. Kaltschmidt, B.; Kaltschmidt, C. NF- B in the Nervous System. *Cold Spring Harb. Perspect. Biol.* **2009**, *1*, a001271. [CrossRef]
22. Xia, L.; Tan, S.; Zhou, Y.; Lin, J.; Wang, H.; Oyang, L.; Tian, Y.; Liu, L.; Su, M.; Wang, H.; et al. Role of the NFκB-signaling pathway in cancer. *OncoTargets Ther.* **2018**, *11*, 2063–2073. [CrossRef]
23. Sau, A.; Lau, R.; Cabrita, M.A.; Nolan, E.; Crooks, P.A.; Visvader, J.E.; Pratt, M.C. Persistent Activation of NF-κB in BRCA1-Deficient Mammary Progenitors Drives Aberrant Proliferation and Accumulation of DNA Damage. *Cell Stem Cell* **2016**, *19*, 52–65. [CrossRef]
24. Forlani, G.; Abdallah, R.; Accolla, R.S.; Tosi, G. The Major Histocompatibility Complex Class II Transactivator CIITA Inhibits the Persistent Activation of NF-κB by the Human T Cell Lymphotropic Virus Type 1 Tax-1 Oncoprotein. *J. Virol.* **2016**, *90*, 3708–3721. [CrossRef]
25. Walther, W.; Kobelt, D.; Bauer, L.; Aumann, J.; Stein, U. Chemosensitization by diverging modulation by short-term and long-term TNF-? action on ABCB1 expression and NF-?B signaling in colon cancer. *Int. J. Oncol.* **2015**, *47*, 2276–2285. [CrossRef]
26. Kaltschmidt, B.; Greiner, J.F.W.; Kadhim, H.M.; Kaltschmidt, C. Subunit-Specific Role of NF-κB in Cancer. *Biomedicines* **2018**, *6*, 44. [CrossRef]
27. Gu, L.; Wang, Z.; Zuo, J.; Li, H.; Zha, L. Prognostic significance of NF-κB expression in non-small cell lung cancer: A meta-analysis. *PLoS ONE* **2018**, *13*, e0198223. [CrossRef]
28. Hart, J.R.; Garner, A.L.; Yu, J.; Ito, Y.; Sun, M.; Ueno, L.; Rhee, J.-K.; Baksh, M.M.; Stefan, E.; Hartl, M.; et al. Inhibitor of MYC identified in a Krohnke pyridine library. *Proc. Natl. Acad. Sci. USA* **2014**, *111*, 12556–12561. [CrossRef]
29. Esch, J.S.A.S.A.; Windmöller, B.A.; Hanewinkel, J.; Storm, J.; Förster, C.; Wilkens, L.; Krüger, M.; Kaltschmidt, B.; Kaltschmidt, C. Isolation and Characterization of Two Novel Colorectal Cancer Cell Lines, Containing a Subpopulation with Potential Stem-Like Properties: Treatment Options by MYC/NMYC Inhibition. *Cancers* **2020**, *12*, 2582. [CrossRef]
30. Stammler, G.; Pommerenke, E.; Mattern, J.; Volm, M. Effects of single doses of irradiation on the expression of resistance-related proteins in murine NIH 3T3 and human lung carcinoma cells. *Carcinogenesis* **1995**, *16*, 2051–2055. [CrossRef]

31. Schindelin, J.; Arganda-Carreras, I.; Frise, E.; Kaynig, V.; Longair, M.; Pietzsch, T.; Preibisch, S.; Rueden, C.; Saalfeld, S.; Schmid, B.; et al. Fiji: An open-source platform for biological-image analysis. *Nat. Methods* **2012**, *9*, 676–682. [CrossRef] [PubMed]
32. Kelley, J.B.; Paschal, B.M. Fluorescence-based quantification of nucleocytoplasmic transport. *Methods* **2019**, *157*, 106–114. [CrossRef] [PubMed]
33. Debacq-Chainiaux, F.; Erusalimsky, J.D.; Campisi, J.; Toussaint, O. Protocols to detect senescence-associated beta-galactosidase (SA-βgal) activity, a biomarker of senescent cells in culture and in vivo. *Nat. Protoc.* **2009**, *4*, 1798–1806. [CrossRef] [PubMed]
34. De Preter, K.; Speleman, F.; Combaret, V.; Lunec, J.; Laureys, G.; Eussen, B.H.; Francotte, N.; Board, J.; Pearson, A.D.; De Paepe, A.; et al. Quantification of MYCN, DDX1, and NAG Gene Copy Number in Neuroblastoma Using a Real-Time Quantitative PCR Assay. *Mod. Pathol.* **2002**, *15*, 159–166. [CrossRef]
35. Yin, L.; Wen, X.; Lai, Q.; Li, J.; Wang, X. Lenalidomide improvement of cisplatin antitumor efficacy on triple-negative breast cancer cells inï¿½vitro. *Oncol. Lett.* **2018**, *15*, 6469–6474. [CrossRef]
36. Lu, L.; Payvandi, F.; Wu, L.; Zhang, L.-H.; Hariri, R.J.; Man, H.-W.; Chen, R.S.; Muller, G.W.; Hughes, C.C.; Stirling, D.I.; et al. The anti-cancer drug lenalidomide inhibits angiogenesis and metastasis via multiple inhibitory effects on endothelial cell function in normoxic and hypoxic conditions. *Microvasc. Res.* **2009**, *77*, 78–86. [CrossRef]
37. Wang, C.; Gu, W.; Zhang, Y.; Ji, Y.; Wen, Y.; Xu, X. Nicotine promotes cervical carcinoma cell line HeLa migration and invasion by activating PI3k/Akt/NF-κB pathway in vitro. *Exp. Toxicol. Pathol.* **2017**, *69*, 402–407. [CrossRef]
38. Kanekura, T.; Higashi, Y.; Kanzaki, T. Inhibitory effects of 9-cis-retinoic acid and pyrrolidinedithiocarbamate on cyclooxygenase (COX)-2 expression and cell growth in human skin squamous carcinoma cells. *Cancer Lett.* **2000**, *161*, 177–183. [CrossRef]
39. He, J.; Zhou, J.; Yang, W.; Zhou, Q.; Liang, X.; Pang, X.; Li, J.; Pan, F.; Liang, H. Dexamethasone affects cell growth/apoptosis/chemosensitivity of colon cancer via glucocorticoid receptor α/NF-κB. *Oncotarget* **2017**, *8*, 67670–67683. [CrossRef]
40. Suzuki, S.; Okada, M.; Sanomachi, T.; Togashi, K.; Seino, S.; Sato, A.; Yamamoto, M.; Kitanaka, C. Therapeutic targeting of pancreatic cancer stem cells by dexamethasone modulation of the MKP-1–JNK axis. *J. Biol. Chem.* **2020**, *295*, 18328–18342. [CrossRef]
41. Behrooz, A.B.; Syahir, A.; Ahmad, S. CD133: Beyond a cancer stem cell biomarker. *J. Drug Target.* **2019**, *27*, 257–269. [CrossRef]
42. Yan, Y.; Zuo, X.; Wei, D. Concise Review: Emerging Role of CD44 in Cancer Stem Cells: A Promising Biomarker and Therapeutic Target. *STEM CELLS Transl. Med.* **2015**, *4*, 1033–1043. [CrossRef]
43. Neradil, J.; Veselska, R. Nestin as a marker of cancer stem cells. *Cancer Sci.* **2015**, *106*, 803–811. [CrossRef]
44. Chen, Y.-C.; Hsu, H.-S.; Chen, Y.-W.; Tsai, T.-H.; How, C.-K.; Wang, C.-Y.; Hung, S.-C.; Chang, Y.-L.; Tsai, M.-L.; Lee, Y.-Y.; et al. Oct-4 Expression Maintained Cancer Stem-Like Properties in Lung Cancer-Derived CD133-Positive Cells. *PLoS ONE* **2008**, *3*, e2637. [CrossRef]
45. Tirino, V.; Camerlingo, R.; Franco, R.; Malanga, D.; La Rocca, A.; Viglietto, G.; Rocco, G.; Pirozzi, G. The role of CD133 in the identification and characterisation of tumour-initiating cells in non-small-cell lung cancer. *Eur. J. Cardio-Thorac. Surg.* **2009**, *36*, 446–453. [CrossRef]
46. Huang, X.; Huang, J.; Leng, D.; Yang, S.; Yao, Q.; Sun, J.; Hu, J. Gefitinib-loaded DSPE-PEG2000 nanomicelles with CD133 aptamers target lung cancer stem cells. *World J. Surg. Oncol.* **2017**, *15*, 167. [CrossRef]
47. Leung, E.L.-H.; Fiscus, R.R.; Tung, J.W.; Tin, V.P.-C.; Cheng, L.C.; Sihoe, A.D.-L.; Fink, L.M.; Ma, Y.; Wong, M.P. Non-Small Cell Lung Cancer Cells Expressing CD44 Are Enriched for Stem Cell-Like Properties. *PLoS ONE* **2010**, *5*, e14062. [CrossRef]
48. Satar, N.A.; Fakiruddin, K.S.; Lim, M.N.; Mok, P.L.; Zakaria, N.; Fakharuzi, N.A.; Rahman, A.Z.A.; Zakaria, Z.; Yahaya, B.H.; Baharuddin, P. Novel triple-positive markers identified in human non-small cell lung cancer cell line with chemotherapy-resistant and putative cancer stem cell characteristics. *Oncol. Rep.* **2018**, *40*, 669–681. [CrossRef]
49. Liu, J.; Xiao, Z.; Wong, S.K.-M.; Tin, V.P.-C.; Ho, K.-Y.; Wang, J.; Sham, M.-H.; Wong, M.P. Lung cancer tumorigenicity and drug resistance are maintained through ALDHhiCD44hi tumor initiating cells. *Oncotarget* **2013**, *4*, 1698–1711. [CrossRef]
50. Liu, Y.; Qing, H.; Su, X.; Wang, C.; Li, Z.; Liu, S. Association of CD44 Gene Polymorphism with Survival of NSCLC and Risk of Bone Metastasis. *Med. Sci. Monit.* **2015**, *21*, 2694–2700. [CrossRef]
51. Li, G.; Gao, Y.; Cui, Y.; Zhang, T.; Cui, R.; Jiang, Y.; Shi, J. Overexpression of CD44 is associated with the occurrence and migration of non-small cell lung cancer. *Mol. Med. Rep.* **2016**, *14*, 3159–3167. [CrossRef]
52. Wang, X.; Zhao, X.; Shi, L.; Wu, Y.; Zhang, X.; Fan, Z.; Shen, B. IL6 pretreatment promotes chemosensitivity by eliminating quiescent cancer (stem) cells in lung adenocarcinoma. *Clin. Transl. Med.* **2020**, *10*, e217. [CrossRef]
53. Park, D.; Xiang, A.P.; Mao, F.F.; Zhang, L.; Di, C.-G.; Liu, X.-M.; Shao, Y.; Ma, B.-F.; Lee, J.-H.; Ha, K.-S.; et al. Nestin Is Required for the Proper Self-Renewal of Neural Stem Cells. *Stem Cells* **2010**, *28*, 2162–2171. [CrossRef]
54. Narita, K.; Matsuda, Y.; Seike, M.; Naito, Z.; Gemma, A.; Ishiwata, T. Nestin regulates proliferation, migration, invasion and stemness of lung adenocarcinoma. *Int. J. Oncol.* **2014**, *44*, 1118–1130. [CrossRef]
55. Liu, F.; Zhang, Y.; Lu, M.; Wang, C.; Li, Q.; Gao, Y.; Mu, D.; Cao, Y.; Li, M.; Meng, X. Nestin servers as a promising prog-nostic biomarker in non-small cell lung cancer. *Am. J. Transl. Res.* **2017**, *9*, 1392–1401.
56. Qiu, X.; Wang, Z.; Li, Y.; Miao, Y.; Ren, Y.; Luan, Y. Characterization of sphere-forming cells with stem-like properties from the small cell lung cancer cell line H446. *Cancer Lett.* **2012**, *323*, 161–170. [CrossRef]
57. Adhikary, S.; Eilers, M. Transcriptional regulation and transformation by Myc proteins. *Nat. Rev. Mol. Cell Biol.* **2005**, *6*, 635–645. [CrossRef]

58. Jacob, N.T.; Miranda, P.O.; Shirey, R.J.; Gautam, R.; Zhou, B.; Izquierdo, M.E.D.O.; Hixon, M.S.; Hart, J.R.; Ueno, L.; Vogt, P.K.; et al. Synthetic molecules for disruption of the MYC protein-protein interface. *Bioorganic Med. Chem.* **2018**, *26*, 4234–4239. [CrossRef]
59. Li, Q.-Q.; Xie, Y.-K.; Wu, Y.; Li, L.-L.; Liu, Y.; Miao, X.-B.; Liu, Q.-Z.; Yao, K.-T.; Xiao, G.-H. Sulforaphane inhibits cancer stem-like cell properties and cisplatin resistance through miR-214-mediated downregulation of c-MYC in non-small cell lung cancer. *Oncotarget* **2017**, *8*, 12067–12080. [CrossRef]
60. Choi, S.H.; Mahankali, M.; Lee, S.J.; Hull, M.; Petrassi, H.M.; Chatterjee, A.K.; Schultz, P.G.; Jones, K.A.; Shen, W. Targeted Disruption of Myc–Max Oncoprotein Complex by a Small Molecule. *ACS Chem. Biol.* **2017**, *12*, 2715–2719. [CrossRef]
61. Castell, A.; Yan, Q.; Fawkner, K.; Hydbring, P.; Zhang, F.; Verschut, V.; Franco, M.; Zakaria, S.M.; Bazzar, W.; Goodwin, J.; et al. A selective high affinity MYC-binding compound inhibits MYC:MAX interaction and MYC-dependent tumor cell proliferation. *Sci. Rep.* **2018**, *8*, 1–17. [CrossRef] [PubMed]
62. Witte, K.; Hertel, O.; Windmöller, B.; Helweg, L.; Höving, A.; Knabbe, C.; Busche, T.; Greiner, J.; Kalinowski, J.; Noll, T.; et al. Nanopore Sequencing Reveals Global Transcriptome Signatures of Mitochondrial and Ribosomal Gene Expressions in Various Human Cancer Stem-like Cell Populations. *Cancers* **2021**, *13*, 1136. [CrossRef] [PubMed]
63. Li, Z.; Van Calcar, S.; Qu, C.; Cavenee, W.K.; Zhang, M.Q.; Ren, B. A global transcriptional regulatory role for c-Myc in Burkitt's lymphoma cells. *Proc. Natl. Acad. Sci. USA* **2003**, *100*, 8164–8169. [CrossRef] [PubMed]
64. Fernandez, P.C.; Frank, S.R.; Wang, L.; Schroeder, M.; Liu, S.; Greene, J.; Cocito, A.; Amati, B. Genomic targets of the human c-Myc protein. *Genes Dev.* **2003**, *17*, 1115–1129. [CrossRef]
65. Schuhmacher, M.; Eick, D. Dose-dependent regulation of target gene expression and cell proliferation by c-Myc levels. *Transcription* **2013**, *4*, 192–197. [CrossRef]
66. Kim, J.; Lee, J.-H.; Iyer, V.R. Global Identification of Myc Target Genes Reveals Its Direct Role in Mitochondrial Biogenesis and Its E-Box Usage In Vivo. *PLoS ONE* **2008**, *3*, e1798. [CrossRef]
67. He, T.-L.; Zhang, Y.-J.; Jiang, H.; Li, X.-H.; Zhu, H.; Zheng, K.-L. The c-Myc–LDHA axis positively regulates aerobic glycolysis and promotes tumor progression in pancreatic cancer. *Med. Oncol.* **2015**, *32*, 1–8. [CrossRef]
68. Chen, S.; Gu, T.; Lu, Z.; Qiu, L.; Xiao, G.; Zhu, X.; Li, F.; Yu, H.; Li, G.; Liu, H. Roles of MYC-targeting long non-coding RNA MINCR in cell cycle regulation and apoptosis in non-small cell lung Cancer. *Respir. Res.* **2019**, *20*, 1–11. [CrossRef]
69. Zhou, L.; Wu, F.; Jin, W.; Yan, B.; Chen, X.; He, Y.; Yang, W.; Du, W.; Zhang, Q.; Guo, Y.; et al. Theabrownin Inhibits Cell Cycle Progression and Tumor Growth of Lung Carcinoma through c-myc-Related Mechanism. *Front. Pharmacol.* **2017**, *8*, 75. [CrossRef]
70. Van Riggelen, J.; Yetil, A.; Felsher, D.W. MYC as a regulator of ribosome biogenesis and protein synthesis. *Nat. Rev. Cancer* **2010**, *10*, 301–309. [CrossRef]
71. Destefanis, F.; Manara, V.; Bellosta, P. Myc as a Regulator of Ribosome Biogenesis and Cell Competition: A Link to Cancer. *Int. J. Mol. Sci.* **2020**, *21*, 4037. [CrossRef]
72. Liang, T.; Ye, X.; Yan, D.; Deng, C.; Li, Z.; Tian, B. FAM46B Promotes Apoptosis and Inhibits Glycolysis of Prostate Cancer Through Inhibition of the MYC-LDHA Axis. *OncoTargets Ther.* **2020**, *13*, 8771–8782. [CrossRef]
73. Yue, M.; Jiang, J.; Gao, P.; Liu, H.; Qing, G. Oncogenic MYC Activates a Feedforward Regulatory Loop Promoting Essential Amino Acid Metabolism and Tumorigenesis. *Cell Rep.* **2017**, *21*, 3819–3832. [CrossRef]
74. Batra, S.; Balamayooran, G.; Sahoo, M.K. Nuclear Factor-κB: A Key Regulator in Health and Disease of Lungs. *Arch. Immunol. Ther. Exp.* **2011**, *59*, 335–351. [CrossRef]
75. Chen, W.; Li, Z.; Bai, L.; Lin, Y. NF-kappaB, a mediator for lung carcinogenesis and a target for lung cancer preven-tion and therapy. *Front. Biosci.* **2011**, *16*, 1172–1185. [CrossRef]
76. Zhang, D.; Jin, X.; Wang, F.; Wang, S.; Deng, C.; Gao, Z.; Guo, C. Combined Prognostic Value of Both RelA and IκB-α Expression in Human Non–Small Cell Lung Cancer. *Ann. Surg. Oncol.* **2007**, *14*, 3581–3592. [CrossRef]
77. Kaltschmidt, C.; Banz-Jansen, C.; Benhidjeb, T.; Beshay, M.; Förster, C.; Greiner, J.; Hamelmann, E.; Jorch, N.; Mertzlufft, F.; Pfitzenmaier, J.; et al. A Role for NF-κB in Organ Specific Cancer and Cancer Stem Cells. *Cancers* **2019**, *11*, 655. [CrossRef]
78. Zakaria, N.; Yusoff, N.M.; Zakaria, Z.; Widera, D.; Yahaya, B.H. Inhibition of NF-κB Signaling Reduces the Stemness Characteristics of Lung Cancer Stem Cells. *Front. Oncol.* **2018**, *8*, 166. [CrossRef]
79. Gong, K.; Guo, G.; Gerber, D.E.; Gao, B.; Peyton, M.; Huang, C.; Minna, J.D.; Hatanpaa, K.J.; Kernstine, K.; Cai, L.; et al. TNF-driven adaptive response mediates resistance to EGFR inhibition in lung cancer. *J. Clin. Investig.* **2018**, *128*, 2500–2518. [CrossRef]
80. Shang, G.-S.; Liu, L.; Qin, Y.-W. IL-6 and TNF-α promote metastasis of lung cancer by inducing epithelial-mesenchymal transition. *Oncol. Lett.* **2017**, *13*, 4657–4660. [CrossRef]
81. Yu, W.-N.; Lai, Y.-J.; Ma, J.-W.; Ho, C.-T.; Hung, S.-W.; Chen, Y.-H.; Chen, C.-T.; Kao, J.-Y.; Way, T.-D. Citronellol Induces Necroptosis of Human Lung Cancer Cells via TNF-α Pathway and Reactive Oxygen Species Accumulation. *In Vivo* **2019**, *33*, 1193–1201. [CrossRef] [PubMed]
82. Taniguchi, K.; Karin, M. NF-κB, inflammation, immunity and cancer: Coming of age. *Nat. Rev. Immunol.* **2018**, *18*, 309–324. [CrossRef] [PubMed]
83. Ridker, P.M.; MacFadyen, J.G.; Thuren, T.; Everett, B.M.; Libby, P.; Glynn, R.J.; Lorenzatti, A.; Krum, H.; Varigos, J.; Siostrzonek, P.; et al. Effect of interleukin-1β inhibition with canakinumab on incident lung cancer in patients with atherosclerosis: Exploratory results from a randomised, double-blind, placebo-controlled trial. *Lancet* **2017**, *390*, 1833–1842. [CrossRef]
84. Teo, S.K. Properties of thalidomide and its analogues: Implications for anticancer therapy. *AAPS J.* **2005**, *7*, E14–E19. [CrossRef]

85. Kim, K.; An, S.; Cha, H.J.; Choi, Y.M.; Choi, S.J.; An, I.-S.; Lee, H.G.; Min, Y.H.; Lee, S.-J.; Bae, S. Lenalidomide induces apoptosis and alters gene expression in non-small cell lung cancer cells. *Oncol. Lett.* **2012**, *5*, 588–592. [CrossRef]
86. Mitsiades, N.; Mitsiades, C.S.; Poulaki, V.; Chauhan, D.; Richardson, P.G.; Hideshima, T.; Munshi, N.C.; Treon, S.P.; Anderson, K.C. Apoptotic signaling induced by immunomodulatory thalidomide analogs in human multiple myeloma cells: Therapeutic implications. *Blood* **2002**, *99*, 4525–4530. [CrossRef]
87. Crinelli, R.; Antonelli, A.; Bianchi, M.; Gentilini, L.; Scaramucci, S.; Magnani, M. Selective Inhibition of NF-kB Activation and TNF-α Production in Macrophages by Red Blood Cell-Mediated Delivery of Dexamethasone. *Blood Cells. Mol. Dis.* **2000**, *26*, 211–222. [CrossRef]
88. Chang, C.K.; Llanes, S.; Schumer, W. Effect of Dexamethasone on NF-kB Activation, Tumor Necrosis Factor Formation, and Glucose Dyshomeostasis in Septic Rats. *J. Surg. Res.* **1997**, *72*, 141–145. [CrossRef]
89. Zhang, D.; Zhang, Y.; Cai, Z.; Tu, Y.; Hu, Z. Dexamethasone and lenvatinib inhibit migration and invasion of non-small cell lung cancer by regulating EKR/AKT and VEGF signal pathways. *Exp. Ther. Med.* **2019**, *19*, 762–770. [CrossRef]
90. Ge, H.; Ke, J.; Xu, N.; Li, H.; Gong, J.; Li, X.; Song, Y.; Zhu, H.; Bai, C. Dexamethasone alleviates pemetrexed-induced senescence in Non-Small-Cell Lung Cancer. *Food Chem. Toxicol.* **2018**, *119*, 86–97. [CrossRef]
91. Herrmann, J.L.; Beham, A.W.; Sarkiss, M.; Chiao, P.J.; Rands, M.; Bruckheimer, E.M.; Brisbay, S.; McDonnell, T.J. Bcl-2 Suppresses Apoptosis Resulting from Disruption of the NF-κB Survival Pathway. *Exp. Cell Res.* **1997**, *237*, 101–109. [CrossRef]
92. Zhang, S.; Wang, H.; Xu, Z.; Bai, Y.; Xu, L. Lymphatic Metastasis of NSCLC Involves Chemotaxis Effects of Lymphatic Endothelial Cells through the CCR7–CCL21 Axis Modulated by TNF-α. *Genes* **2020**, *11*, 1309. [CrossRef]
93. Herreros-Pomares, A.; De-Maya-Girones, J.D.; Calabuig-Fariñas, S.; Lucas, R.; Martínez, A.; Pardo-Sánchez, J.M.; Alonso, S.; Blasco, A.; Guijarro, R.; Martorell, M.; et al. Lung tumorspheres reveal cancer stem cell-like properties and a score with prognostic impact in resected non-small-cell lung cancer. *Cell Death Dis.* **2019**, *10*, 1–14. [CrossRef]
94. Gupta, P.B.; Onder, T.T.; Jiang, G.; Tao, K.; Kuperwasser, C.; Weinberg, R.A.; Lander, E.S. Identification of Selective Inhibitors of Cancer Stem Cells by High-Throughput Screening. *Cell* **2009**, *138*, 645–659. [CrossRef]
95. Ketola, K.; Hilvo, M.; Hyötyläinen, T.; Vuoristo, A.; Ruskeepää, A.-L.; Orešič, M.; Kallioniemi, O.; Iljin, K. Salinomycin inhibits prostate cancer growth and migration via induction of oxidative stress. *Br. J. Cancer* **2012**, *106*, 99–106. [CrossRef]
96. Tahata, S.; Yuan, B.; Kikuchi, H.; Takagi, N.; Hirano, T.; Toyoda, H. Cytotoxic effects of pyrrolidine dithiocarbamate in small-cell lung cancer cells, alone and in combination with cisplatin. *Int. J. Oncol.* **2014**, *45*, 1749–1759. [CrossRef]

Original Research Article

“Diminishment of novel endometrial carcinoma-derived stem-like cells by targeting mitochondrial bioenergetics and MYC”

Beatrice A. Windmöller*, Laureen P. Helweg*, Leonie Burghardt, Jonathan Storm, Christine Förster, Ludwig Wilkens, Barbara Kaltschmidt, Constanze Banz-Jansen* and Christian Kaltschmidt*

(*: equal contribution)

Under review at Gynecologic Oncology

Diminishment of novel endometrial carcinoma-derived stem-like cells by targeting mitochondrial bioenergetics and MYC

Beatrice A. Windmöller[1,2,*,+], Laureen P. Helweg[1,2,+], Leonie Burghardt[1], Jonathan Storm[1,2], Christine Förster[2,3], Ludwig Wilkens[2,3], Barbara Kaltschmidt[1,2,4], Constanze Banz-Jansen[2,5,+], Christian Kaltschmidt[1,2,+]

[1] Department of Cell Biology, University of Bielefeld, Universitätsstrasse 25, Bielefeld, Germany; Beatrice.windmoeller@uni-bielefeld.de, L.Helweg@uni-bielefeld.de, leonie.burghardt@uni-bielefeld.de, jonathan.storm@uni-bielefeld.de, C.Kaltschmidt@uni-bielefeld.de

[2] Forschungsverbund BioMedizin Bielefeld/OWL FBMB e.V., Maraweg 21, Bielefeld, Germany

[3] Institute of Pathology, KRH Hospital Nordstadt, Haltenhoffstrasse 41, affiliated with the Protestant Hospital of Bethel Foundation, 30167 Hannover, Germany; christine.foerster@krh.eu, ludwig.wilkens@krh.eu

[4] Molecular Neurobiology, Bielefeld University, Universitätsstrasse 25, 33615 Bielefeld, Germany; barbara.kaltschmidt@uni-bielefeld.de

[5] Department of Gynecology and Obstetrics, and Perinatal Center, Protestant Hospital of Bethel Foundation, University Medical School OWL at Bielefeld, Bielefeld University, Campus Bielefeld-Bethel, Burgsteig 13, Bielefeld, Germany; Constanze.Banz-Jansen@evkb.de

* Correspondence: Beatrice A. Windmöller; University of Bielefeld, Universitätsstrasse 25, Bielefeld; Beatrice.windmoeller@uni-bielefeld.de; Tel.: +49-0521-106-5629

[+] Authors contributed equally as Co-First and Co-Last Authors

Abstract:

Objective: Cancer stem cells (CSC) are a small subpopulation of tumor cells harboring properties like self-renewal, multi-lineage differentiation, tumor reconstitution, drug resistance and invasiveness, making them key players in tumor relapse. Here, we developed new CSC models and analyzed molecular pathways involved in survival to identify targets for the establishment of novel therapies.

Methods: Endometrial carcinoma-derived stem-like cells (ECSCs) were isolated from carcinogenic gynecological tissue and subsequently analyzed regarding their expression of prominent CSC markers. Further, they were treated with MYC-signaling inhibitor KJ-Pyr-9, chemotherapeutic agent carboplatin and type II diabetes medication metformin.

Results: ECSC populations express common CSC markers like Prominin-1, CD44 antigen and Nestin and exhibit the ability to form free floating spheres. Inhibition of MYC-signaling and treatment with carboplatin as well as metformin significantly reduced cell survival of ECSC-like cells. Further, treatment with metformin significantly decreased the mitochondrial membrane potential of ECSC-like cells while the extracellular lactate concentration was increased.

Conclusions: The here established ECSC-like cell populations represent promising *in vitro* models to further study the contribution of ECSCs on endometrial carcinogenesis. Targeting MYC-signaling as well as mitochondrial bioenergetics has shown promising results in the diminishment of ECSCs, although molecular signaling pathways need further investigations.

Keywords: Cancer Stem Cells, Endometrial Cancer, primary Endometrial Cancer Stem Cells, MYC, metformin, mitochondria

1. Introduction

Endometrial carcinoma (EC) is the most common gynecological tumor and accounts for about 3% of worldwide mortality among women [1]. Main risk factors are obesity or diabetes mellitus, thus incidence rates are generally higher in high-income countries than in low- and middle-income countries [2]. Since 1983, EC has been broadly classified into two types, based on molecular profiling, histopathology and clinical behavior [3]: Type I endometrial cancer accounting for 70-80% of all ECs is typically less aggressive, estrogen-

related and highly to moderately differentiated with an endometrioid morphology. Type II endometrial cancer summarizes estrogen-independent non-endometrioid carcinomas [4]. ECs are usually diagnosed at an early stage due to symptoms like postmenopausal uterine bleeding and have a good prognosis with a 5-year survival rate of 81.1% [5]. With current cancer treatments, extensive and even complete cancer regression can be achieved, however this is often followed by relapse [6].

A key player driving tumor relapse is a small subpopulation of cells that harbor properties like self-renewal, multi-lineage differentiation, tumor reconstitution, drug resistance and invasiveness [7]. The presence of these so-called cancer stem cells (CSCs) has been assumed for several decades, as tumors recapitulate their corresponding tissue and hold a hierarchical organization with CSCs at the top. Endometrial carcinoma-derived stem-like cells (ECSCs) are commonly identified using specific cell surface markers like CD44-antigen (CD44) and Prominin-1 (CD133), as their expression is associated with tumorigenicity, invasiveness and metastasis [8–10]. Further, ECSCs were characterized by expressing stemness-related genes such as MYC, SOX2, OCT4, ABCG2 and Nestin [11]. Accordingly, increased expression of ALDH1, OCT4, SOX2 and MYC was reported in a $CD133^+$ cell subpopulation isolated from an endometrioid adenocarcinoma [12]. Consistently, downregulation of MYC in EC was shown to significantly reduce cell invasion as well as drug resistance [13]. In recent years, several studies investigated the metabolic plasticity of CSCs as they are able to switch between increased oxidative mitochondrial metabolism and anaerobic glycolysis [14]. Accordingly, high mitochondrial mass correlates with ALDH activity, tumor-initiating activity and chemoresistance of CSCs [15].

Within this study, we established three ECSC-like cell populations named BKZ-10, BKZ-11 and BKZ-12 expressing various stemness-related proteins and harboring the ability to form spherical cancer organoids. Inhibition of protein-protein interaction of MYC/NMYC with MYC-associated factor X (MAX) as well as the application of metformin

and carboplatin significantly decreased cell survival of ECSCs. Further, metformin treatment significantly reduced mitochondrial membrane potential, representing metformin as a promising drug targeting the mitochondrial metabolism of ECSCs.

2. Methods

2.1. Endometrial Cancer Stem-like Cell Establishment and Cell Culture

The cancer tissue samples used for the isolation of ECSCs were obtained during surgical resection after assuring routine histopathological analysis and kindly provided by the Forschungsverbund BioMedizin Bielefeld/OWL FBMB e. V. (Bielefeld, Germany) at the Protestant Hospital of Bethel Foundation (Bielefeld, Germany). Informed consent according to local and international guidelines was signed by all patients and further experimental procedures were ethically approved (Ethics committee Münster, Germany, 2017-522-f-S).

For the isolation of primary cells, a cubic tumor material sample measuring 5 mm was collected from each tumor and transferred to ice-cold Dulbecco's Phosphate Buffered Saline (PBS; Sigma-Aldrich, Munich, Germany), repeatedly washed with PBS, mechanically disintegrated and enzymatically digested with collagenase for 2h at 37°C as previously described [16–18]. The minced tissue was cultivated in CSC medium containing Dulbecco's Modified Eagle's medium/Ham's F-12 (Sigma-Aldrich), 2 mM L-Glutamin (Sigma-Aldrich), Penicillin/Streptomycin (100 µg/mL; Sigma-Aldrich), epidermal growth factor (EGF) (20 ng/mL; Miltenyi Biotec, Bergisch Gladbach, Germany), fibroblast growth factor 2 (FGF-2) (40 ng/mL; Miltenyi Biotec), B27 supplement (Gibco, Thermo Fisher Scientific, Bremen, Germany), supplemented with 10% fetal calf serum (FCS, Sigma-Aldrich) on T75-culture flasks coated with 0.1% gelatin from bovine skin (type-B; Sigma-

Aldrich). CSCs were enriched through serial trypsin treatment, as described by Walia and coworkers and Morata-Tarifa and colleagues [19,20]. Briefly, after washing with PBS, cells were treated with 0.05% Trypsin-EDTA solution (0.5 mg/mL; Sigma-Aldrich) for 5min and transferred onto a new gelatin-coated culture flask. To assure stem-like characteristics, trypsinization was repeated every 48 to 72h for at least three cycles. For sphere formation, $0.5x10^6$ cells were cultured in serum-free CSC medium supplemented with 4 µg/mL heparin (Sigma-Aldrich) in low adhesion culture flasks. All cells were cultured at 37°C and 5% CO_2 in a humidified incubator.

Population doubling times were determined using the Orangu™ Cell Counting Solution (Cell Guidance Systems, Cambridge, UK) according to the manufacturer's guidelines. As a standard curve, 1000, 2500, 5000, 7500 and 10000 cells and to determine the population doubling time 3000 cells per 100 µL CSC medium supplemented with 10% FCS were seeded in a 0.1% gelatin-coated 96 well-plate. After adherence, cell viability was measured for the standard curve and after 72h for the growing cells. Cell count was quantified using the respective standard curve, growth rate and populations doubling times were determined by the following equations:

$$growth\ rate = \frac{\ln(xt) - \ln(x0)}{t - t0} \quad (1)$$

$$population\ doubling\ time = \frac{\ln(2)}{growth\ rate} \quad (2).$$

To quantify the volume of spheres, at least five pictures were taken and every sphere was measured in length and width using Fiji ImageJ [21]. The volume of spheres was calculated according to the following equation:

$$V = \frac{4}{3} * \pi * (\frac{sphere\ diameter}{2})^3 \quad (3).$$

2.2. Immunocytochemistry

For immunocytochemical staining, pre-cultured cells were harvested and seeded on etched cover slips in a 24-well plate at a density of $1.5x10^4$ cells per 500 µL CSC medium supplemented with 10 % FCS. At 80% confluency, cells were fixated with 4% phosphate-buffered paraformaldehyde (lab-made) for 15min at room temperature (RT), washed with PBS, blocked/permeabilized using 0.02% Triton-X 100 (Sigma-Aldrich) with 5% goat serum (Dianova, Hamburg, Germany) for 30min at RT and incubated with the primary antibody for 1h at RT. Antibodies used were anti-CD44 (1:400; 156-3C11; Cell Signaling, Frankfurt am Main, Germany), anti-CD133 (1:100; NB120-16518; NovusBio, Bio-Techne, Wiesbaden-Nordenstadt, Germany), anti-Nestin (1:200; MAB5326; Sigma-Aldrich), anti-MYC (0,1 µg/mL; Y69; Abcam, Cambridge, UK), anti-NMYC (2,5 µg/mL; NCM II 100; Abcam), anti-Synaptophysin (1:250; MAB5258; Sigma-Aldrich) and anti-Slug (1:100; C19G7; Cell Signaling). Secondary fluorochrome-conjugated antibodies (1:300; goat anti-mouse Alexa 555, goat anti-rabbit Alexa 555, goat anti-mouse Alexa 488; Life Technologies, Thermo Fisher Scientific) were incubated for 1h at RT in the dark. Nuclear counterstaining was performed with 4',6-diamidino-2-phenylindole (1 µg/mL; Sigma-Aldrich) for 10min at RT. Fluorescence imaging was performed using a confocal laser scanning microscope (LSM 780; Carl Zeiss, Jena, Germany) and analyzed using ZEN software from the same provider or Fiji ImageJ [21].

Immunohistochemical stainings were performed at the Institute of Pathology of KRH Hospital Nordstadt (Hannover, Germany) using the automated immunohistochemistry and *in situ* hybridization platform Dako Omnis (DAKO, Agilent, Santa Clara, USA) according to the manufacturer's instructions. The used antibody was anti-PDL1 (22C3; DAKO, Agilent). For visualization, the EnVision FLEX, High pH (DAKO, Agilent) visualization system was

used according to the manufacturer's instructions. Analysis of the expression of PDL1 was done according to international standards [22]:

$$TPS = \frac{PDL1\ positive\ vital\ tumor\ cells}{PDL1\ positive+negative\ vital\ tumor\ cells} \quad (4)$$

$$CPS = \frac{PDL1\ positive\ vital\ tumor\ cells+lymphocytes+macrophages}{PDL1\ positive+negative\ vital\ tumor\ cells} * 100 \quad (5)$$

$$IC = \frac{PDL1\ positive\ lymphocytes+macrophages+dendritic\ cells+granulocytes}{tumor\ area} \quad (6).$$

2.3. Flow cytometry

Cultured cells were harvested and stained with anti-CD44 FITC (P-glycoprotein 1; 1:50; REA690; Miltenyi Biotec) anti-CD273 APC-Vio®770 (PDCD1-L2; 1:50; REA985; Miltenyi Biotec), anti-CD274 PE (PDCD1-L1; 1:10; MIH1; BD Biosciences, Heidelberg, Germany). Dead cells were excluded via Propidium Iodide (PI; 1µg/ml; Thermo Fisher Scientific). Analysis was performed using a Gallios Flow Cytometer and the Kaluza 1.0 software (both Beckman Coulter Life Sciences, Krefeld, Germany) using appropriate Fluorescence Minus One controls and automatic compensation. Unspecific binding was controlled for using appropriate isotype controls beforehand. Measurements of ALDH activities were performed utilizing the ALDEFLUOR™ Kit (STEMCELL Technologies, Vancouver, BC, Canada) according to the manufacturer's guidelines and PI (1µg/ml; Thermo Fisher Scientific) for dead-cell discrimination with the instrument and software mentioned above.

2.4. Inhibitor and Drug treatments

ECSCs were treated with the MYC/NMYC inhibitor KJ-Pyr-9 (Merck, Darmstadt, Germany), diabetes medication metformin (Merck) and chemotherapeutic agent

carboplatin (Sigma-Aldrich). Cell viability was assayed using Orangu™ Cell Counting Solution according to the manufacturer's instructions. For the standard curve, 1000, 2500, 5000, 7500 and 10000 cells and for the treatment 3000 cells per 100 µL CSC medium supplemented with 10% FCS were seeded in a 0.1% gelatin-coated 96 well-plate. After adherence, cell viability was measured for the standard curve and the treatment started by applying KJ-Pyr-9 in the concentrations of 10 µM, 20 µM, 40 µM and 60 µM, metformin in the concentrations of 1, 5, 10 and 20 mM and carboplatin in the concentrations of 50, 100 and 300 µM. After treatment with metformin and carboplatin for 72h and KJ-Pyr-9 for 96h, cell viability was measured and cell count quantified using the respective standard curve. Relative survival rates were determined by normalizing each cell count to the mean of controls for the respective cell population and the half maximal inhibitory concentration (IC_{50}) calculated from a log(concentration) versus normalized survival rate non-linear regression fit using Prism V5.01 software (GraphPad Software, Inc., San Diego, CA, USA).

2.5. Mitochondrial membrane potential assay and lactate concentration

To analyze the mitochondrial membrane potential and assess the lactate concentration, 3000 cells per 100 µL CSC medium supplemented with 10% FCS were seeded in a 0.1% gelatin-coated 96 well-plate and after adherence 10 and 20 mM metformin applied. After 72h, the mitochondrial membrane potential was assessed using the TMRE-Mitochondrial Membrane Potential Kit (Abcam) according to the manufacturer's instructions. Briefly, 20 µM FCCP was added to the respective control wells 10min prior to TMRE staining with 400 nM TMRE for 25 min. The medium was discarded, the cells were washed with 100 µL 0.2% BSA/PBS (Sigma-Aldrich), 100 µL 0.2% BSA/PBS was added to the cells and the fluorescence read at Ex525/Em580. To measure lactate concentration of the media of

ECSCs, 25 µL of the medium was applied on the Accutrend® Plus using the BM-Lactate test strips (Roche, Mannheim, Deutschland).

2.6. Statistical analysis

Data were raised at least in triplicated and statistically analyzed using the Prism V5.01 software (GraphPad Software, Inc., San Diego, CA, USA). Test for normality was conducted using D'Agostino & Pearson omnibus normality test. To evaluate differences between multiple groups, Student's t-test or non-parametric Mann–Whitney-test were performed. A significance value of $p \leq 0.05$ was considered as statistically significant. The data are presented as means ± standard error of the mean (SEM).

3. Results

3.1. Successful isolation of endometrial carcinoma-derived stem-like cells

In this study, we aimed to isolate cancer stem-like cells from carcinogenic endometrial tissues. Therefore, the samples were mechanically and enzymatically digested followed by cultivation in chemically defined CSC medium with added EGF and bFGF (Fig. 1A). Using serial trypsin treatment, we successfully cultivated adherently growing cells (Fig. 1B-D) with the addition of FCS as well as free floating spheres (Fig. 1E-G) in serum free media for all three donors. Isolated ECSC populations depicted an elongated spindle form morphology when cultured on 2D surfaces (Fig. 1B-D). Calculation of population doubling times revealed significant differences between each cell population. BKZ-10 depicted the highest population doubling time with 33.10h (± 0.65), which was slightly but significantly higher than the doubling time of BKZ-11 with a doubling time of 30.72h (± 0.76). BKZ12 proliferated significantly faster than the other two cell populations with an average

population doubling time of 18.69h (± 0.34) (Fig. 1H). Further, all cell populations were able to form organoid-like structures in the form of free-floating spheres with average sizes of 84255, 61164 and 149576 μm^3 for BKZ-10, BKZ-11 and BKZ-12, respectively (Fig. 1I).

To confirm the isolation of ECSC populations, the protein expression of established CSC markers like CD44, CD133 and Nestin was analyzed using immunocytochemistry and detected robust expression of each marker for all three ECSC populations (Fig. 2A-F). Additional analysis via flow cytometry revealed 100% CD44-positive cells for BKZ-10 and BKZ-12 (Fig. 2G, I) as well as 99.88% CD44-positive cells for BKZ-11 (Fig. 2H). Fluorescence minus One controls can be found in the supplement (Fig. S1 A-C). Further investigations of the expression of the epithelial-to-mesenchymal transition (EMT)-related transcription factor Slug and the neuroendocrine CSC marker Synaptophysin on protein level revealed a moderate expression of predominantly nuclear Slug and Synaptophysin for BKZ-10 (Fig. S2A-B). Expression of Slug in BKZ-11 was predominantly cytosolic, while Synaptophysin expression was predominantly nuclear (Fig. S2C-D). BKZ-12 expressed a high amount of predominantly nuclear Slug and Synaptophysin (Fig. S2E-F). Further analysis of ALDH activity of ECSCs revealed 6.13% ALDH high expressing BKZ-10 cells, 11.51% ALDH high expressing BKZ-11 cells and 11.06% ALDH high expressing BKZ-12 cells (Fig. S3).

3.2. Endometrial carcinoma-derived stem-like cells reveal immune-evasive characteristics

Histopathological examination of a bioptic sample retrieved from each parental tumor of the ECSC populations revealed immune checkpoint ligand programed death ligand 1 (PD-L1)-expressing cells in each sample. Analysis of PD-L1 expression was done according to international standards by calculating combined positive score (CPS), tumor

proportion score (TPS) and immune cell score (IC) (Formulas 4-6). Quantification revealed 0% PD-L1-positive vital tumor cells for the parental tissue of BKZ-10, but analyzing the percentage of PD-L1-positive lymphocytes, macrophages and non-necrotic tumor cells by calculating the CPS displayed a score of 5%. Quantifying PD-L1-positive lymphocytes, macrophages, dendritic cells and granulocytes per tumor area depicted an IC score of 2 (Fig. 3A). Similar to the parental tissue of BKZ-10, analysis of PD-L1 expression of the parental tissue of BKZ-11 revealed no PD-L1-positive vital tumor cells. However, the CPS score for this tissue was 1% and the IC score was 1 (Fig. 3B). Contrary to the first two ECs, the parental tissue of BKZ-12 depicted 20% PD-L1-positive vital tumor cells and a CPS score of 20% with an IC of 1 (Fig. 3C).

Additional analysis of the expression of both PD-L1 and PD-L2 in ECSCs using flow cytometry revealed 94.06% PD-L1-positive BKZ-10, 93.55% PD-L1-positive BKZ-11 and 93.35% PD-L1-positive BKZ-12 cells (Fig. 3D-F). Likewise, every ECSC-like cell population contained over 99% PD-L2-positive cells (Fig. 3G-I). Fluorescence minus One controls can be found in the supplement (Fig. S1 D-I).

3.3. Impairment of endometrial carcinoma-derived stem-like cells by targeting MYC

The proto-oncogenes MYC and NMYC are tightly regulated transcription factors and master regulators of various cellular processes. Analysis of MYC expression on protein level revealed nuclear expression of MYC for each cell population (Fig. 4A-C). Similarly, robust expression of NMYC was detected for each cell population, even though expression was predominantly cytosolic (Fig. 4D-F). To assess the influence of MYC and NMYC, cells were treated with an inhibitor of the protein-protein interaction of MYC/NMYC with MAX. Therefore, the small molecule KJ-Pyr-9 was applied and resulted in significantly decreased cell survival upon concentrations higher than 20 µM (Fig. 4G). Further, calculation of IC_{50}

values for each cell population revealed BKZ-11 as the most sensitive cell population, with an IC_{50} value of 14.25 µM, followed by BKZ-10 with an IC_{50} value of 17.49 µM. High proliferative BKZ-12 cells were the most resistant with an IC_{50} value of 19.01 µM (Fig. 4H).

3.4. Metformin targets the mitochondrial metabolism of endometrial carcinoma-derived stem-like cells

Next to the influence of MYC/NMYC inhibition, the effect of standard type 2 diabetes medication metformin and chemotherapeutic agent carboplatin was assessed in ECSC populations. Already the lowest tested concentration of each drug significantly reduced cell survival of ECSC populations (Fig. 5A). In general, both drugs affected cell survival of ECSC populations in a dose-dependent manner. Cells treated with 1 mM metformin showed a survival rate of 79.92% (± 2.47), while application of 5 and 10 mM led to survival rates of 62.47% (± 1.93) and 50.96% (± 4.26), respectively, and treatment with 20 mM depicted the most elevated survival decreasing effect with a survival rate of 15.65% (± 2.67) (Fig. 5A). Treatment with 50 µM carboplatin revealed an ECSC survival rate of 40.32% (± 5.96), 100 µM of 21.98% (± 5.13) and 300 µM of 7.61% (± 1.07) (Fig. 5A).

Calculation of IC_{50} for metformin depicted similar IC_{50} values for each cell population, as BKZ-10 depicted an IC_{50} value of 6.79 mM, BKZ-11 an IC_{50} value of 5.99 mM and BKZ-12 an IC_{50} value of 6.00 mM (Fig. 5B). The IC_{50} values for carboplatin were more heterogeneous, as highly proliferative BKZ-12 was more sensitive with an IC_{50} value of 16.41 µM than BKZ-10 and BKZ-11 with IC_{50} values of 46.79 µM and 49.24 µM, respectively (Fig. 5B). Even though carboplatin revealed the most effective survival-decreasing impact concerning the cumulated ECSC populations, metformin-mediated impairment was more consistent considering the different ECSC populations.

As metformin is known to modulate mitochondrial bioenergetics, we assessed the mitochondrial membrane potential of metformin-treated and untreated cells using the mitochondrial membrane potential detecting TMRE staining. Treatment with 10 and 20 mM metformin significantly reduced the mitochondrial membrane potential of ECSCs (Fig. 5C). Further, we measured the lactate concentration of the media of ECSCs, which was significantly enhanced after treatment with 10 mM metformin and significantly decreased after application of 20 mM metformin (Fig. 5D).

4. Discussion

Within this study, endometrial cancer-derived stem-like cell populations were successfully isolated and initially characterized as promising *in vitro* models to study ECSC-like cells. Treatment with the MYC-signaling inhibitor KJ-Pyr-9, diabetes medication metformin and chemotherapeutic agent carboplatin significantly reduced cell survival of ECSCs. However, MYC inhibition and the usage of metformin depicted more coherent survival decreasing effects, demonstrating these as promising therapeutics in EC.

CSCs are a small subpopulation of highly-tumorigenic cells that are characterized by the expression of markers like CD133, CD44 [9] and Nestin (reviewed in [23]). $CD133^+$ EC cells showed an aggressive proliferation potential, colony formation and migration ability as well as higher chemoresistance [12]. Further, $CD133^+$ ECSCs depicted an upregulation of CD44 [10], which is associated with infiltrating patterns and proliferation [8]. In addition to CD44, highly tumorigenic $CD133^+$ ECSCs were shown to express Nestin [11] and knockdown of Nestin inhibited cell growth, invasive potential and colony formation of EC cell lines while overepression enhanced their malignant phenotype [24]. Another recently studied CSC marker is the neuroedocrine marker Synaptophysin, whose expression was observed in CSCs derived from lung and colorectal cancer, as we recently published [16,25]. The here presented co-expression of CSC-markers CD133 and CD44 as well as Nestin and nuclear

Synaptophsin strongly indicates ECSC-like character and their potential as novel *in vitro* models to study EC-derived stem cells. The ability of all tested ECSC populations to form spheres further affirms their CSC-like phenotype, as ECSCs capable of forming sphere-like structures have an increased self-renewal and chemoresistance capacity as well as tumor initiating abilities in xenograft studies [10]. A study around Mori and coworkers revealed that ALDH-induced glycolysis mediates stemness and chemoresistance of EC-derived spheres [26]. However, the here isolated ECSC populations only exhibited $ALDH^{high}$ expressing cells at ranges between 6 and 11%. Accordingly, it was shown that breast CSCs balance between $CD24^{-}/CD44^{+}$-mesenchymal-like and $ALDH^{high}$ epithelial-like stem cell populations, enabling reversible EMT/MET transitions [27]. This concords with the here shown predominant expression of CD44 and the nuclear expression of a key EMT transcription factor namely Slug. In contrast to other obervations describing EMT transcription factor TWIST even as potential target for vaccination against CSCs, Slug was the predominant transcription factor in ECSCs (data not shown) [28]. EMT is a crucial process involved in embryonic development, which also contributes to cancer progression as cells gain stemness and chemoresistance as well as invasive characteristics (reviewed in [29]). Moreover, it has been suggested that CSCs arise from differentiated cancer cells through dedifferentiation mediated by EMT [30]. The here presented expression of Slug emphasizes the correlation of EMT, stemness and the expression of PD-L1, as EMT has been suggested to induce PD-L1 mediated immune evasion of CSCs [31]. Accordingly, flow cytometric analysis of the here isolated ECSC populations revealed over 93% positive PD-L1 and 99% PD-L2 expressing cells, substantiating the ability of ECSCs to evade immune surveillance. Next to EMT, MYC has been shown to contribute to immunosuppression by directly inducing PD-L1 expression, while downregulation of MYC led to immune cell infiltration (reviewed in [32]).

The MYC family consisting of MYC, NMYC and LMYC is a master regulator of various important cellular processes, thus playing a crucial role in tumorigenesis of various cancer types (reviewed in [33]). Expression of MYC was already observed in ECSC-like cells as well as EC-derived spheres [11,12,26], which concords with the here detected robust expression of MYC and NMYC. Depletion of MYC in EC cells has been shown to reverse Sal-like protein 4 (SALL4)-induced EMT, invasion and drug resistance [13]. Accordingly, we detected an EMT phenotype in the here presented MYC-expressing ECSC populations, too. Further, we recently published a significant survival-decreasing effect through MYC-signaling inhibition utilizing small molecule KJ-Pyr-9 [34] in primary human colon and lung CSCs [16,17]. Consistently, inhibition of MYC-signaling in the here established ECSC populations by application of KJ-Pyr-9 in concentrations greater than 10 µM significantly reduced cell survival. KJ-Pyr-9 has been shown to interfere with heterodimerization of MYC and MAX by directly interacting with MYC, therefore disrupting its transcriptional activity [34]. Calculation of the IC_{50} revealed values between 14.25 and 19.01 µM, which stands in line with recently reported IC_{50} values [17]. However, molecular signaling regarding KJ-Pyr-9 induced survival decrease needs further investigation to understand the underlying mechanism.

Next to KJ-Pyr-9, the effect of chemotherapeutic agent carboplatin and standard type 2 diabetes medication metformin on the here established ECSC populations was assessed. A promising effect of the already clinically used carboplatin in combination with paclitaxel was already shown in the treatment of advanced and recurrent EC [35]. Here, we demonstrate a significant survival decreasing effect of solely carboplatin on ECSCs. However, response was relatively heterogeneous with IC_{50} values differing between 16.41 µM for the highly proliferative BKZ-12 and 49.24 µM for BKZ-11. In line with carboplatin, application of metformin impaired ECSC survival significantly and coherently. Metformin has been shown to radiosensitize cancer cells and predominantly eradicate CSCs by

downregulation of genes like CD44 and EPCAM [36] or inhibition of EMT [37]. Notably, here calculated IC_{50} values around 6 mM are in accordance with reported IC_{50} values of 3.72 and 6.77 mM [38]. Further, metformin has been shown to inhibit cancer cell growth and induce apoptosis by suppressing mitochondrial-dependent biosynthetic activity [39]. Recently, we assessed global transcriptomes of CSCs derived from various tissues including the here established ECSC populations (there referred to as ECSC_a, ECSC_b and ECSC_c) and detected upregulation of genes associated with mitochondrial activity [18]. Application of metformin significantly impaired the mitochondrial membrane potential, highlighting the importance of mitochondrial respiration for ECSCs. As CSCs are able to switch to anaerobic glycolysis upon inhibition of mitochondrial metabolism [14], the increase of extracellular lactate concentration after application of 10 mM metformin of ECSCs suggests a flexible metabolism to some extent. Nevertheless, they initially seem to prefer energy production through mitochondrial respiration, in contrast to the Warburg effect described in cancer cells [40].

In summary, we successfully established three novel primary ECSC-like cell populations as promising *in vitro* models to study CSC-mediated endometrial carcinogenesis. CSC-like phenotype was confirmed by their expression of CD133, CD44, Nestin and Synaptophysin as well as sphere formation. Additionally, ECSCs exhibited ALDH activity and expressed EMT marker Slug as well as proto-oncogenes MYC and NMYC, further emphasizing stem-like properties. Inhibition of MYC-signaling as well as application of metformin and carboplatin led to a significant reduction of cell survival of ECSCs, while the usage of the MYC inhibitor and metformin acted more uniformly on the different ECSC populations. Inhibition of MYC-signaling at low doses of KJ-Pyr-9 led to similar survival rates as application of metformin and carboplatin at much higher concentrations. Further, metformin was shown to significantly decrease mitochondrial membrane potential and increase lactate concentration, indicating metabolic plasticity of ECSCs. Thus, targeting MYC-signaling and

mitochondrial bioenergetics represent promising novel treatment options for the treatment of EC affecting ECSCs.

Acknowledgement

This research was funded in part by the University of Bielefeld. Beatrice Ariane Windmöller, Laureen Patricia Helweg and Jonathan Storm are funded by an internal grant of the Bethel Foundation, Bielefeld, Germany. The excellent technical assistance of Claudia Rose and Ulrike Hormel is gratefully acknowledged.

Conflict of Interest

The authors declare no conflict of interest. The funders had no role in the design of the study; in the collection, analyses, or interpretation of data; in the writing of the manuscript; or in the decision to publish the results.

Author Contribution

Beatrice A. Windmöller: Data curation, Formal analysis, Investigation, Visualization, Writing—original draft, Writing—review & editing.

Laureen P. Helweg: Data curation, Formal analysis, Investigation, Visualization, Writing—original draft, Writing—review & editing.

Leonie Burghardt: Data curation, Investigation, Writing—original draft, Writing—review & editing.

Jonathan Storm: Data curation, Investigation, Writing—original draft, Writing—review & editing.

Christine Förster: Data curation, Writing—original draft, Writing—review & editing.

Ludwig Wilkens: Data curation, Writing—original draft, Writing—review & editing.

Barbara Kaltschmidt: Conceptualization, Data curation, Funding acquisition, Project administration, Supervision, Writing—original draft, Writing—review & editing.

Constanze Banz-Jansen: Data curation, Funding acquisition, Writing—original draft, Writing—review & editing.

Christian Kaltschmidt: Conceptualization, Data curation, Funding acquisition, Project administration, Supervision, Writing—original draft, Writing—review & editing.

References

[1] J. Ferlay, M. Colombet, I. Soerjomataram, T. Dyba, G. Randi, M. Bettio, A. Gavin, O. Visser, F. Bray, Cancer incidence and mortality patterns in Europe: Estimates for 40 countries and 25 major cancers in 2018, Eur. J. Cancer 103 (2018) 356–387. https://doi.org/10.1016/j.ejca.2018.07.005.

[2] L.A. Torre, F. Islami, R.L. Siegel, E.M. Ward, A. Jemal, Global Cancer in Women: Burden and Trends, Cancer Epidemiol Biomarkers Prev 26 (2017) 444–457. https://doi.org/10.1158/1055-9965.EPI-16-0858.

[3] J.V. Bokhman, Two pathogenetic types of endometrial carcinoma, Gynecologic Oncology 15 (1983) 10–17. https://doi.org/10.1016/0090-8258(83)90111-7.

[4] A. Di Cristofano, L.H. Ellenson, Endometrial carcinoma, Annu. Rev. Pathol. 2 (2007) 57–85. https://doi.org/10.1146/annurev.pathol.2.010506.091905.

[5] Cancer Stat Facts: Uterine Cancer (accessed June 1st, 2021).

[6] E. Vizza, G. Cutillo, V. Bruno, I. Sperduti, E. Mancini, E. Baiocco, B. Chiofalo, L. Cicchillitti, C. Certelli, A. Zampa, E. Piccione, G. Corrado, Pattern of recurrence in patients with endometrial cancer: A retrospective study, European Journal of Surgical Oncology 46 (2020) 1697–1702. https://doi.org/10.1016/j.ejso.2020.03.203.

[7] T. Ito, B. Zimdahl, T. Reya, aSIRTing control over cancer stem cells, Cancer Cell 21 (2012) 140–142. https://doi.org/10.1016/j.ccr.2012.01.014.

[8] J.Y. Park, D. Hong, J.Y. Park, Association between Morphological Patterns of Myometrial Invasion and Cancer Stem Cell Markers in Endometrial Endometrioid Carcinoma, Pathol. Oncol. Res. 25 (2019) 123–130. https://doi.org/10.1007/s12253-017-0320-5.

[9] S.S. Elbasateeny, A.A. Salem, W.A. Abdelsalam, R.A. Salem, Immunohistochemical expression of cancer stem cell related markers CD44 and CD133 in endometrial cancer, Pathol. Res. Pract. 212 (2016) 10–16. https://doi.org/10.1016/j.prp.2015.10.008.

[10] S. Rutella, G. Bonanno, A. Procoli, A. Mariotti, M. Corallo, M.G. Prisco, A. Eramo, C. Napoletano, D. Gallo, A. Perillo, M. Nuti, L. Pierelli, U. Testa, G. Scambia, G. Ferrandina, Cells with characteristics of cancer stem/progenitor cells express the CD133 antigen in human endometrial tumors, Clin. Cancer Res. 15 (2009) 4299–4311. https://doi.org/10.1158/1078-0432.CCR-08-1883.

[11] Y. Sun, T. Yoshida, M. Okabe, K. Zhou, F. Wang, C. Soko, S. Saito, T. Nikaido, Isolation of Stem-Like Cancer Cells in Primary Endometrial Cancer Using Cell Surface Markers CD133 and CXCR4, Transl. Oncol. 10 (2017) 976–987. https://doi.org/10.1016/j.tranon.2017.07.007.
[12] D.-C. Ding, H.-W. Liu, Y.-H. Chang, T.-Y. Chu, Expression of CD133 in endometrial cancer cells and its implications, J. Cancer 8 (2017) 2142–2153. https://doi.org/10.7150/jca.18869.
[13] L. Liu, J. Zhang, X. Yang, C. Fang, H. Xu, X. Xi, SALL4 as an Epithelial-Mesenchymal Transition and Drug Resistance Inducer through the Regulation of c-Myc in Endometrial Cancer, PLOS ONE 10 (2015) e0138515. https://doi.org/10.1371/journal.pone.0138515.
[14] B. Ozsvari, G. Bonuccelli, R. Sanchez-Alvarez, R. Foster, F. Sotgia, M.P. Lisanti, Targeting flavin-containing enzymes eliminates cancer stem cells (CSCs), by inhibiting mitochondrial respiration: Vitamin B2 (Riboflavin) in cancer therapy, Aging (Albany NY) 9 (2017) 2610–2628. https://doi.org/10.18632/aging.101351.
[15] G. Farnie, F. Sotgia, M.P. Lisanti, High mitochondrial mass identifies a sub-population of stem-like cancer cells that are chemo-resistant, Oncotarget 6 (2015) 30472–30486. https://doi.org/10.18632/oncotarget.5401.
[16] J.S. am Schulte Esch, B.A. Windmöller, J. Hanewinkel, J. Storm, C. Förster, L. Wilkens, M. Krüger, B. Kaltschmidt, C. Kaltschmidt, Isolation and Characterization of Two Novel Colorectal Cancer Cell Lines, Containing a Subpopulation with Potential Stem-Like Properties: Treatment Options by MYC/NMYC Inhibition, Cancers (Basel) 12 (2020). https://doi.org/10.3390/cancers12092582.
[17] B.A. Windmöller, M. Beshay, L.P. Helweg, C. Flottmann, M. Beermann, C. Förster, L. Wilkens, J.F.W. Greiner, C. Kaltschmidt, B. Kaltschmidt, Novel Primary Human Cancer Stem-Like Cell Populations from Non-Small Cell Lung Cancer: Inhibition of Cell Survival by Targeting NF-κB and MYC Signaling, Cells 10 (2021) 1024. https://doi.org/10.3390/cells10051024.
[18] K.E. Witte, O. Hertel, B.A. Windmöller, L.P. Helweg, A.L. Höving, C. Knabbe, T. Busche, J.F.W. Greiner, J. Kalinowski, T. Noll, F. Mertzlufft, M. Beshay, J. Pfitzenmaier, B. Kaltschmidt, C. Kaltschmidt, C. Banz-Jansen, M. Simon, Nanopore Sequencing Reveals Global Transcriptome Signatures of Mitochondrial and Ribosomal Gene Expressions in Various Human Cancer Stem-like Cell Populations, Cancers (Basel) 13 (2021). https://doi.org/10.3390/cancers13051136.
[19] V. Walia, R.C. Elble, Enrichment for breast cancer cells with stem/progenitor properties by differential adhesion, Stem Cells Dev. 19 (2010) 1175–1182. https://doi.org/10.1089/scd.2009.0430.
[20] C. Morata-Tarifa, G. Jiménez, M.A. García, J.M. Entrena, C. Griñán-Lisón, M. Aguilera, M. Picon-Ruiz, J.A. Marchal, Low adherent cancer cell subpopulations are enriched in tumorigenic and metastatic epithelial-to-mesenchymal transition-induced cancer stem-like cells, Sci. Rep. 6 (2016) 18772. https://doi.org/10.1038/srep18772.
[21] J. Schindelin, I. Arganda-Carreras, E. Frise, V. Kaynig, M. Longair, T. Pietzsch, S. Preibisch, C. Rueden, S. Saalfeld, B. Schmid, J.-Y. Tinevez, D.J. White, V. Hartenstein, K. Eliceiri, P. Tomancak, A. Cardona, Fiji: an open-source platform for biological-image analysis, Nat. Methods 9 (2012) 676–682. https://doi.org/10.1038/nmeth.2019.
[22] D.P. O'Malley, Y. Yang, S. Boisot, S. Sudarsanam, J.-F. Wang, V. Chizhevsky, G. Zhao, S. Arain, L.M. Weiss, Immunohistochemical detection of PD-L1 among diverse human neoplasms in a reference laboratory: observations based upon 62,896 cases, Mod. Pathol. 32 (2019) 929–942. https://doi.org/10.1038/s41379-019-0210-3.
[23] J. Neradil, R. Veselska, Nestin as a marker of cancer stem cells, Cancer Science 106 (2015) 803–811. https://doi.org/10.1111/cas.12691.

[24] A.A. Bokhari, T.M. Baker, B. Dorjbal, S. Waheed, C.M. Zahn, C.A. Hamilton, G.L. Maxwell, V. Syed, Nestin suppression attenuates invasive potential of endometrial cancer cells by downregulating TGF-β signaling pathway, Oncotarget 7 (2016) 69733–69748. https://doi.org/10.18632/oncotarget.11947.
[25] B.A. Windmöller, J.F.W. Greiner, C. Förster, L. Wilkens, F. Mertzlufft, J. Am Schulte Esch, B. Kaltschmidt, C. Kaltschmidt, M. Beshay, A typical carcinoid of the lung - a case report with pathological correlation and propagation of the cancer stem cell line BKZ1 with synaptophysin expression, Medicine (Baltimore) 98 (2019) e18174. https://doi.org/10.1097/MD.0000000000018174.
[26] Y. Mori, K. Yamawaki, T. Ishiguro, K. Yoshihara, H. Ueda, A. Sato, H. Ohata, Y. Yoshida, T. Minamino, K. Okamoto, T. Enomoto, ALDH-Dependent Glycolytic Activation Mediates Stemness and Paclitaxel Resistance in Patient-Derived Spheroid Models of Uterine Endometrial Cancer, Stem Cell Reports 13 (2019) 730–746. https://doi.org/10.1016/j.stemcr.2019.08.015.
[27] S. Liu, Y. Cong, D. Wang, Y. Sun, L. Deng, Y. Liu, R. Martin-Trevino, L. Shang, S.P. McDermott, M.D. Landis, S. Hong, A. Adams, R. D'Angelo, C. Ginestier, E. Charafe-Jauffret, S.G. Clouthier, D. Birnbaum, S.T. Wong, M. Zhan, J.C. Chang, M.S. Wicha, Breast cancer stem cells transition between epithelial and mesenchymal states reflective of their normal counterparts, Stem Cell Reports 2 (2014) 78–91. https://doi.org/10.1016/j.stemcr.2013.11.009.
[28] A.R. Kwilas, A. Ardiani, U. Dirmeier, C. Wottawah, J. Schlom, J.W. Hodge, A poxviral-based cancer vaccine the transcription factor twist inhibits primary tumor growth and metastases in a model of metastatic breast cancer and improves survival in a spontaneous prostate cancer model, Oncotarget 6 (2015) 28194–28210. https://doi.org/10.18632/oncotarget.4442.
[29] Y. Zhang, R.A. Weinberg, Epithelial-to-mesenchymal transition in cancer: complexity and opportunities, Front. Med. 12 (2018) 361–373. https://doi.org/10.1007/s11684-018-0656-6.
[30] S.A. Mani, W. Guo, M.-J. Liao, E.N. Eaton, A. Ayyanan, A.Y. Zhou, M. Brooks, F. Reinhard, C.C. Zhang, M. Shipitsin, L.L. Campbell, K. Polyak, C. Brisken, J. Yang, R.A. Weinberg, The epithelial-mesenchymal transition generates cells with properties of stem cells, Cell 133 (2008) 704–715. https://doi.org/10.1016/j.cell.2008.03.027.
[31] J.-M. Hsu, W. Xia, Y.-H. Hsu, L.-C. Chan, W.-H. Yu, J.-H. Cha, C.-T. Chen, H.-W. Liao, C.-W. Kuo, K.-H. Khoo, J.L. Hsu, C.-W. Li, S.-O. Lim, S.-S. Chang, Y.-C. Chen, G.-X. Ren, M.-C. Hung, STT3-dependent PD-L1 accumulation on cancer stem cells promotes immune evasion, Nat Commun 9 (2018) 1908. https://doi.org/10.1038/s41467-018-04313-6.
[32] D. Marinkovic, T. Marinkovic, The new role for an old guy: MYC as an immunoplayer, J. Cell. Physiol. 236 (2021) 3234–3243. https://doi.org/10.1002/jcp.30123.
[33] M. Eilers, R.N. Eisenman, Myc's broad reach, Genes Dev. 22 (2008) 2755–2766. https://doi.org/10.1101/gad.1712408.
[34] J.R. Hart, A.L. Garner, J. Yu, Y. Ito, M. Sun, L. Ueno, J.-K. Rhee, M.M. Baksh, E. Stefan, M. Hartl, K. Bister, P.K. Vogt, K.D. Janda, Inhibitor of MYC identified in a Kröhnke pyridine library, Proc. Natl. Acad. Sci. U. S. A. 111 (2014) 12556–12561. https://doi.org/10.1073/pnas.1319488111.
[35] T. Akram, P. Maseelall, J. Fanning, Carboplatin and paclitaxel for the treatment of advanced or recurrent endometrial cancer, Am. J. Obstet. Gynecol. 192 (2005) 1365–1367. https://doi.org/10.1016/j.ajog.2004.12.032.
[36] B. Bao, Z. Wang, S. Ali, A. Ahmad, A.S. Azmi, S.H. Sarkar, S. Banerjee, D. Kong, Y. Li, S. Thakur, F.H. Sarkar, Metformin inhibits cell proliferation, migration and invasion by attenuating CSC

function mediated by deregulating miRNAs in pancreatic cancer cells, Cancer Prev Res 5 (2012) 355–364. https://doi.org/10.1158/1940-6207.CAPR-11-0299.
[37] R. Zhang, P. Zhang, H. Wang, D. Hou, W. Li, G. Xiao, C. Li, Inhibitory effects of metformin at low concentration on epithelial-mesenchymal transition of CD44(+)CD117(+) ovarian cancer stem cells, Stem Cell Res Ther 6 (2015) 262. https://doi.org/10.1186/s13287-015-0249-0.
[38] S.J. Kitson, M. Rosser, D.P. Fischer, K.M. Marshall, R.B. Clarke, E.J. Crosbie, Targeting Endometrial Cancer Stem Cell Activity with Metformin Is Inhibited by Patient-Derived Adipocyte-Secreted Factors, Cancers (Basel) 11 (2019). https://doi.org/10.3390/cancers11050653.
[39] Z.-Y. Gao, Z. Liu, M.-H. Bi, J.-J. Zhang, Z.-Q. Han, X. Han, H.-Y. Wang, G.-P. Sun, H. Liu, Metformin induces apoptosis via a mitochondria-mediated pathway in human breast cancer cells in vitro, Exp. Ther. Med. 11 (2016) 1700–1706. https://doi.org/10.3892/etm.2016.3143.
[40] O. Warburg, F. Wind, E. Negelein, THE METABOLISM OF TUMORS IN THE BODY, J. Gen. Physiol. 8 (1927) 519–530. https://doi.org/10.1085/jgp.8.6.519.

Figures:

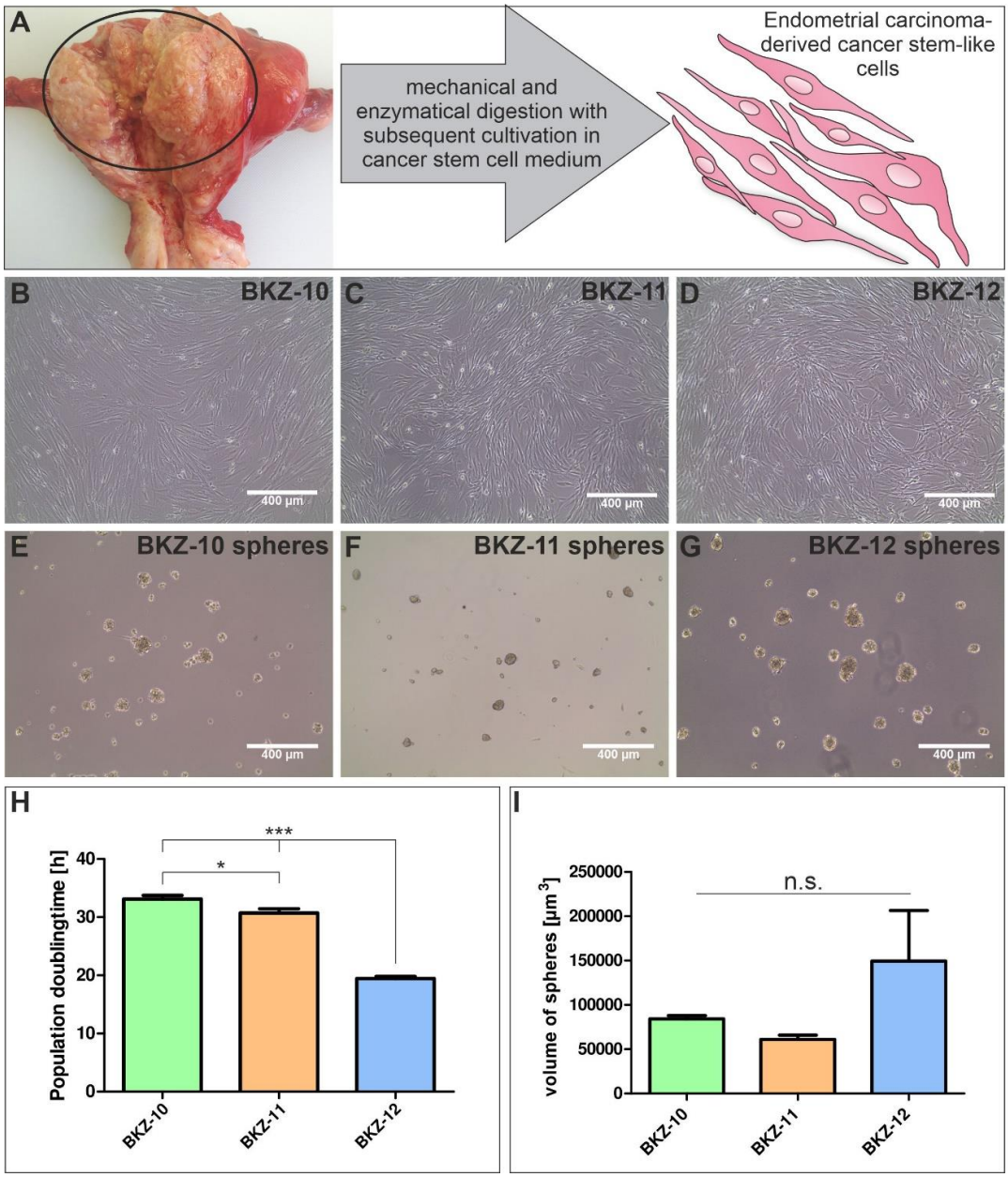

Figure 1: Establishment of endometrial carcinoma-derived stem-like cell populations. **(A)** For the isolation of endometrial carcinoma-derived stem-like cell populations, endometrial carcinoma tissue samples were obtained, mechanically and enzymatically digested and cultivated in cancer stem cell medium either supplemented with 10 % fetal calf serum leading to **(B/C/D)** adherent growing cells or 4 µg/mL heparin for **(E/F/G)** sphere formation.

(H) Quantification of population doubling time of BKZ-10, BKZ-11 and BKZ-12 revealed a significantly lower population doubling time for BKZ-12 in comparison to BKZ-10 and BKZ-11. Moreover, BKZ-10 exhibited a significantly higher population doubling time than BKZ-11. Quantification of the **(I)** volume of spheres showed a higher sphere volume for BKZ-12 in comparison to BKZ-10 and BKZ-11. Unpaired t-test ($p \leq 0.05$). n = 3, * $p \leq 0.05$, *** $p \leq 0.001$. Mean ± SEM (standard error of the mean).

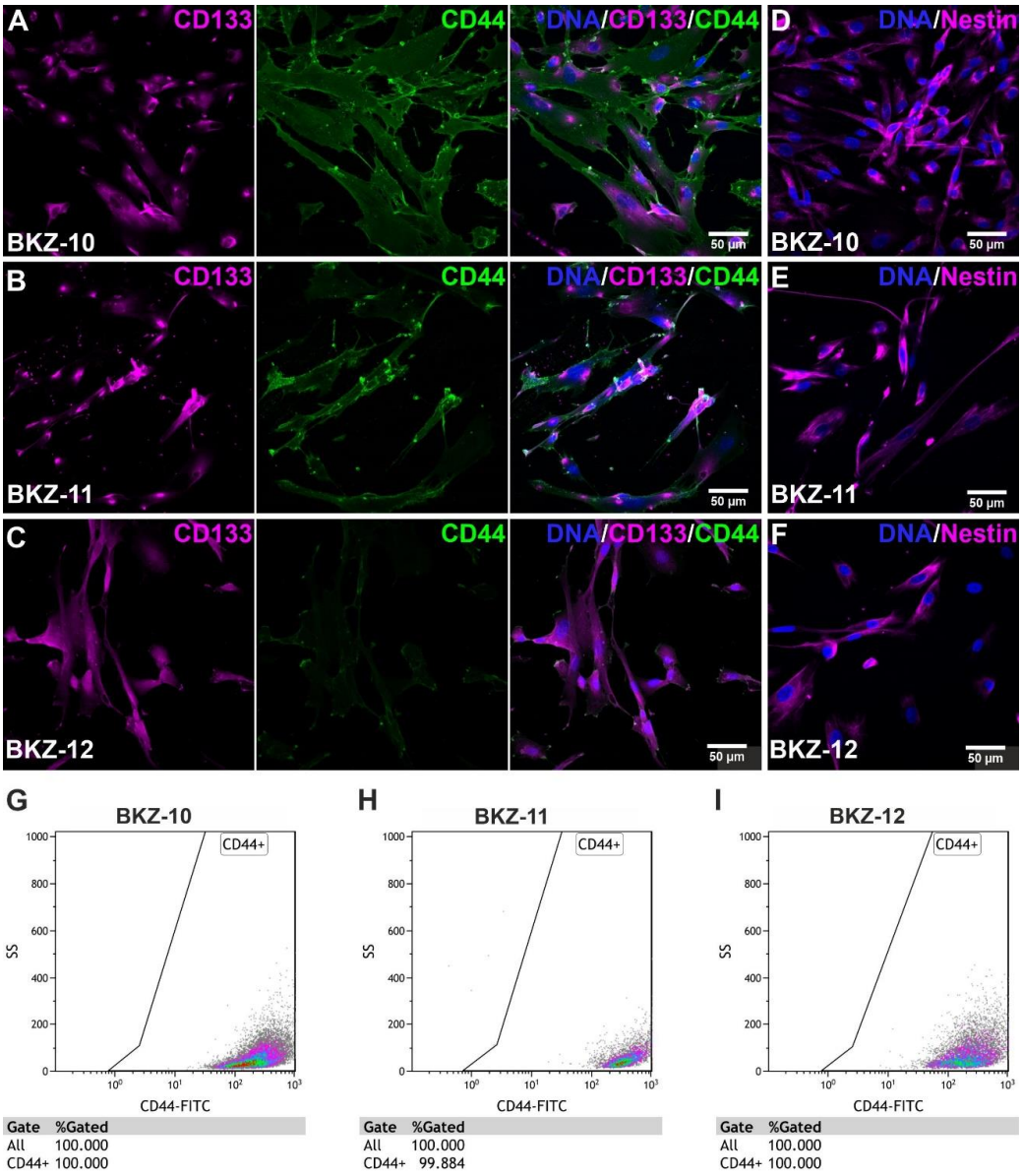

Figure 2: Isolated endometrial carcinoma-derived stem-like cell populations express cancer stem cell markers. Immunocytochemical staining revealed a high amount of cancer stem cell markers **(A/B/C)** Prominin-1 (CD133), CD44 antigen and **(D/E/F)** Nestin. Flow cytometric analysis of CD44 positive cells depicted 100% CD44 positive cells for **(G)** BKZ-10 as well as for **(I)** BKZ-12 and 99.884% CD44 positive cells for **(H)** BKZ-11.

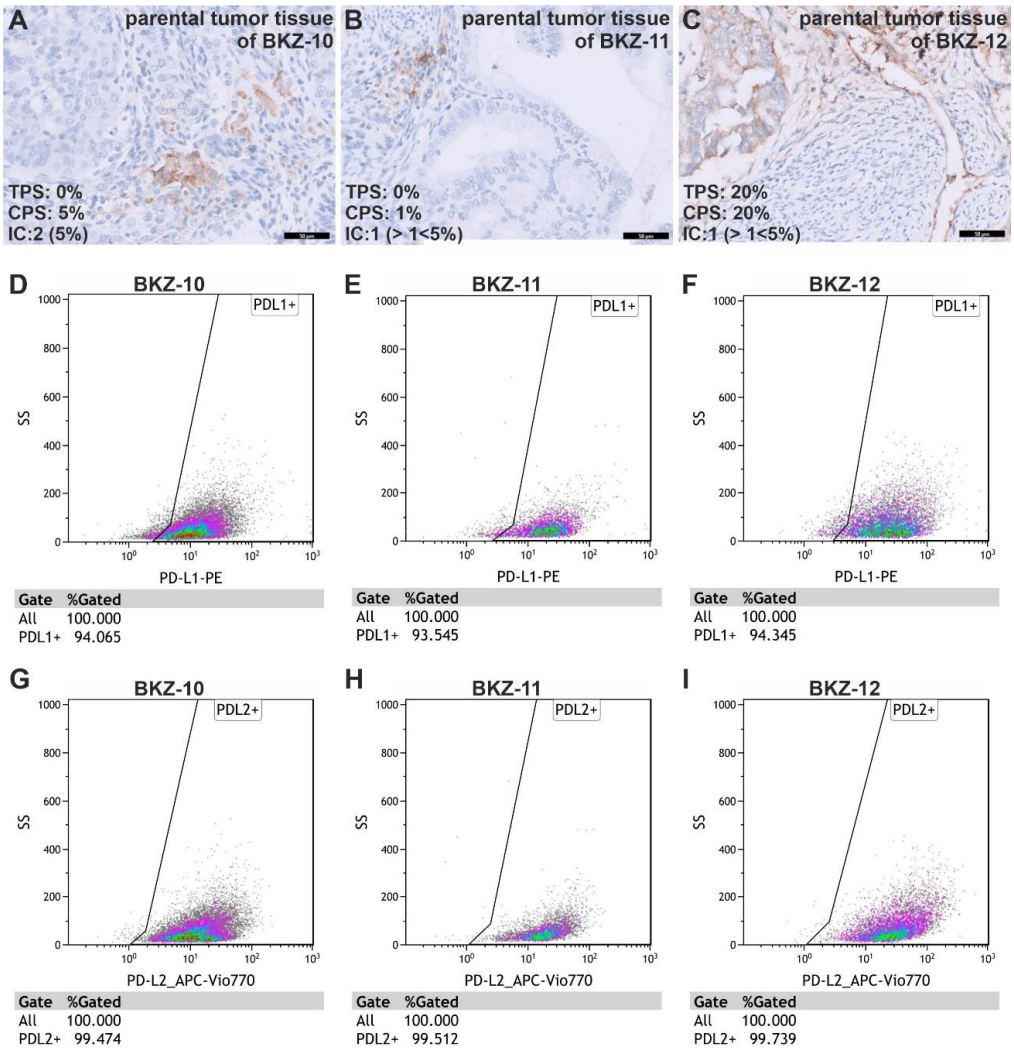

Figure 3: Isolated endometrial carcinoma-derived stem-like cell populations are enriched in PD-L1 and PD-L2 expression. **(A)** Immunohistochemical analysis of PD-L1 expression in the parental tissue of BKZ-10 revealed a tumor proportion score (TPS) of 0%, a combined positive score of 5% and an immune cell score (IC) of 2. **(B)** Analysis of PD-L1 expression in the parental tissue of BKZ-11 displayed a TPS of 0%, a CPS of 1% and an IC of 1. **(C)** For the parental tissue of BKZ-12, a TPS of 20%, a CPS of 20% and an IC of 1 was assessed. Analysis of PD-L1 **(D/E/F)** and PD-L2 **(G/H/I)** expression of endometrial carcinoma-derived cancer stem-like cell populations using flow cytometry revealed over 93 % PD-L1-positive and 99% PD-L2-positive cells.

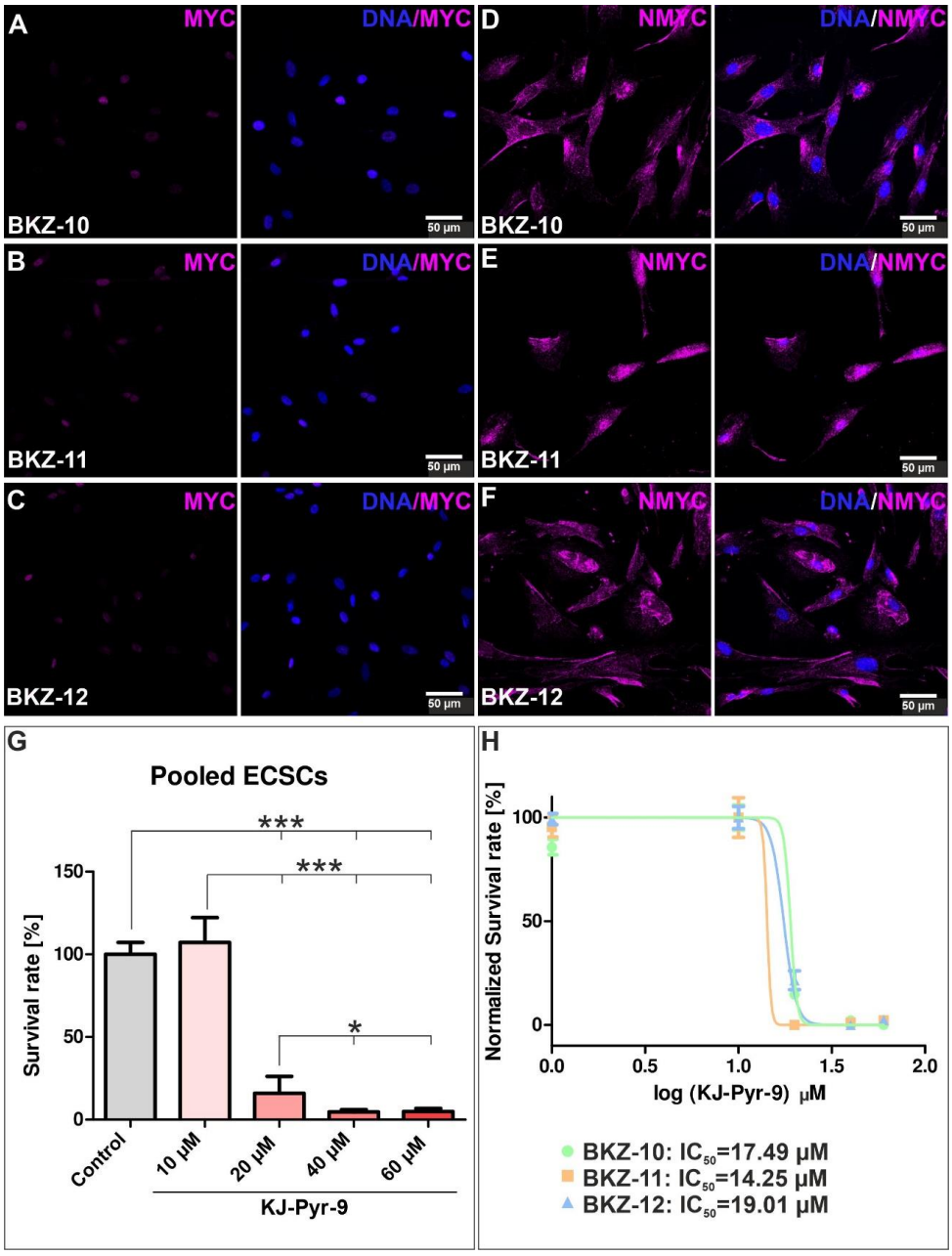

Figure 4: Inhibition of the MYC and NMYC protein interaction with MYC-associated factor X (MAX) decreases survival of endometrial carcinoma-derived stem-like cell populations. Immunocytochemical staining revealed **(A/B/C)** predominantly nuclear MYC expression as well as **(D/E/F)** cytosolic NMYC expression for all three ECSC-populations, respectively. To analyze the influence of the MYC/NMYC inhibitor KJ-Pyr-9, cells were treated with different concentrations or the respective control for 120 h. Subsequent, viability was measured using OranguTM (Cell Guidance Systems, Cambridge, UK) and cell count was determined by

using a standard curve. **(G)** Statistical analysis revealed a significantly impaired survival of ECSCs upon application of 20, 40 and 60 µM KJ-Pyr-9. **(H)** Analysis of the half maximal inhibitory concentration (IC50) revealed an IC50 value of 17.49 µM KJ-Pyr9 for BKZ-10, 14.25 µM KJ-Pyr9 for BKZ-11 and 19.01 µM KJ-Pyr9 for BKZ-12. Means±SEM (standard error of the mean) were statistically analyzed by a non-parametric Mann–Whitney-test (n=3, *$p \leq 0.05$, ***$p \leq 0.001$).

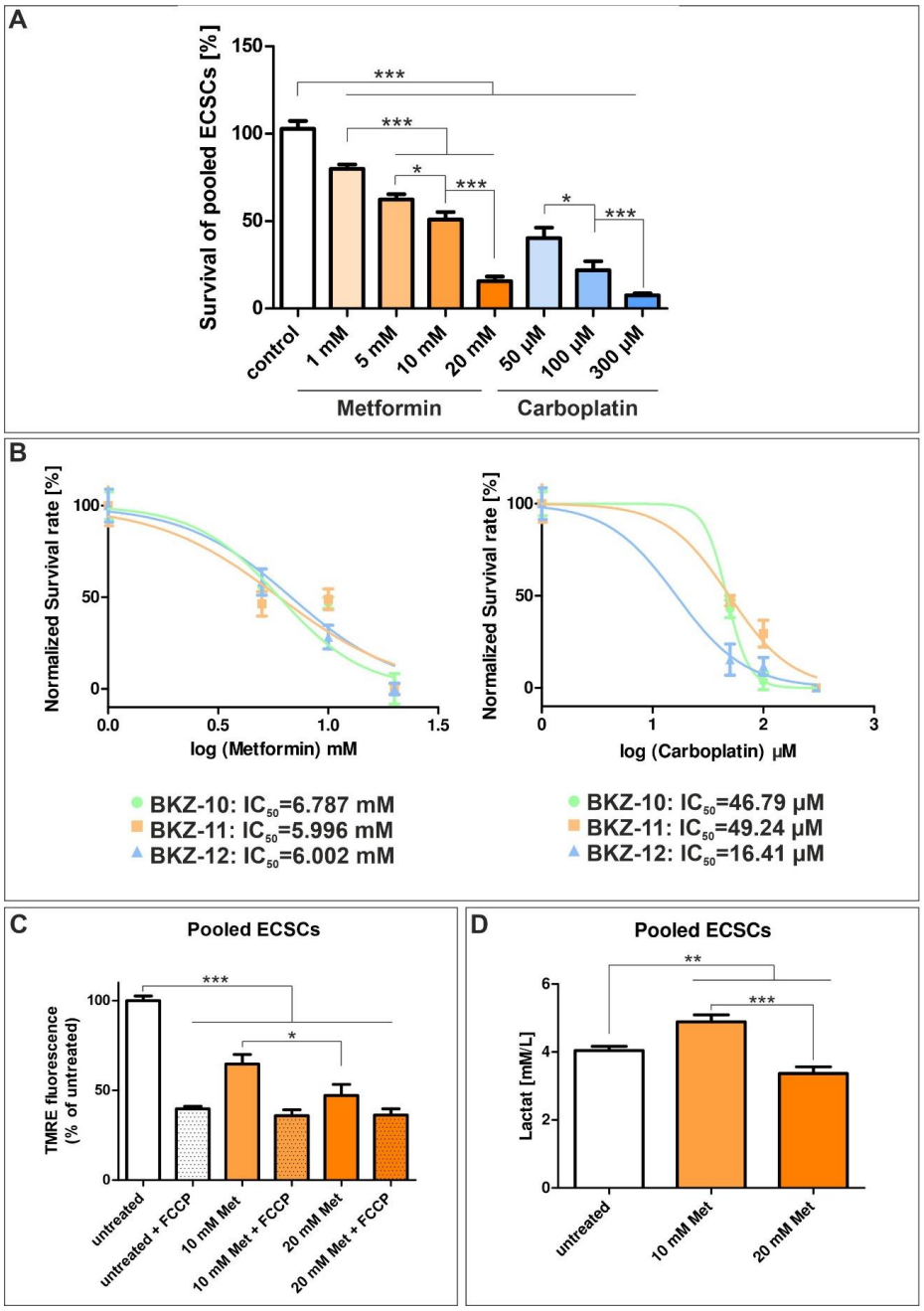

Figure 5: Treatment with metformin and carboplatin significantly decreases survival of endometrial carcinoma-derived stem-like cell populations. To analyze the influence of carboplatin and metformin, cells were treated with different concentrations of the reagents for 72h. Afterwards, cellular viability was measured using OranguTM (Cell Guidance Systems, Cambridge, UK) and cell count was determined by using the respective standard curve. **(A)** Statistical analysis of survival rates of pooled ECSCs revealed a significantly

decreased survival of ECSCs for every tested concentration of carboplatin and metformin in a dose-dependent manner. **(B)** Analysis of the half maximal inhibitory concentration (IC50) for carboplatin revealed an IC50 value of 46.79 µM for BKZ-10, 49.24 µM for BKZ-11 and 16.41 µM for BKZ-12. The IC50 value for metformin was assessed as 6.787 mM for BKZ-10, 5.996 mM for BKZ-11 and 6.002 mM for BKZ-12. **(C)** Membrane Potential of ECSCs was measured using TMRE, and the mitochondrial oxidative phosphorylation uncoupler FCCP was used as technical control. Treatment with 10 and 20 mM metformin significantly reduces the membrane potential of ECSCs in comparison to untreated cells. **(D)** The lactate concentration of the media of untreated and treated cells was determined using Accutrend® Plus, which revealed a significantly enhanced lactate concentration after treatment with 10 mM metformin and a significantly decreased concentration after treatment with 20 mM Metformin. Means±SEM (standard error of the mean) were statistically analyzed by an Unpaired t-test (n=3, *$p \leq 0.05$, ***$p \leq 0.001$).

Supplementary Figures:

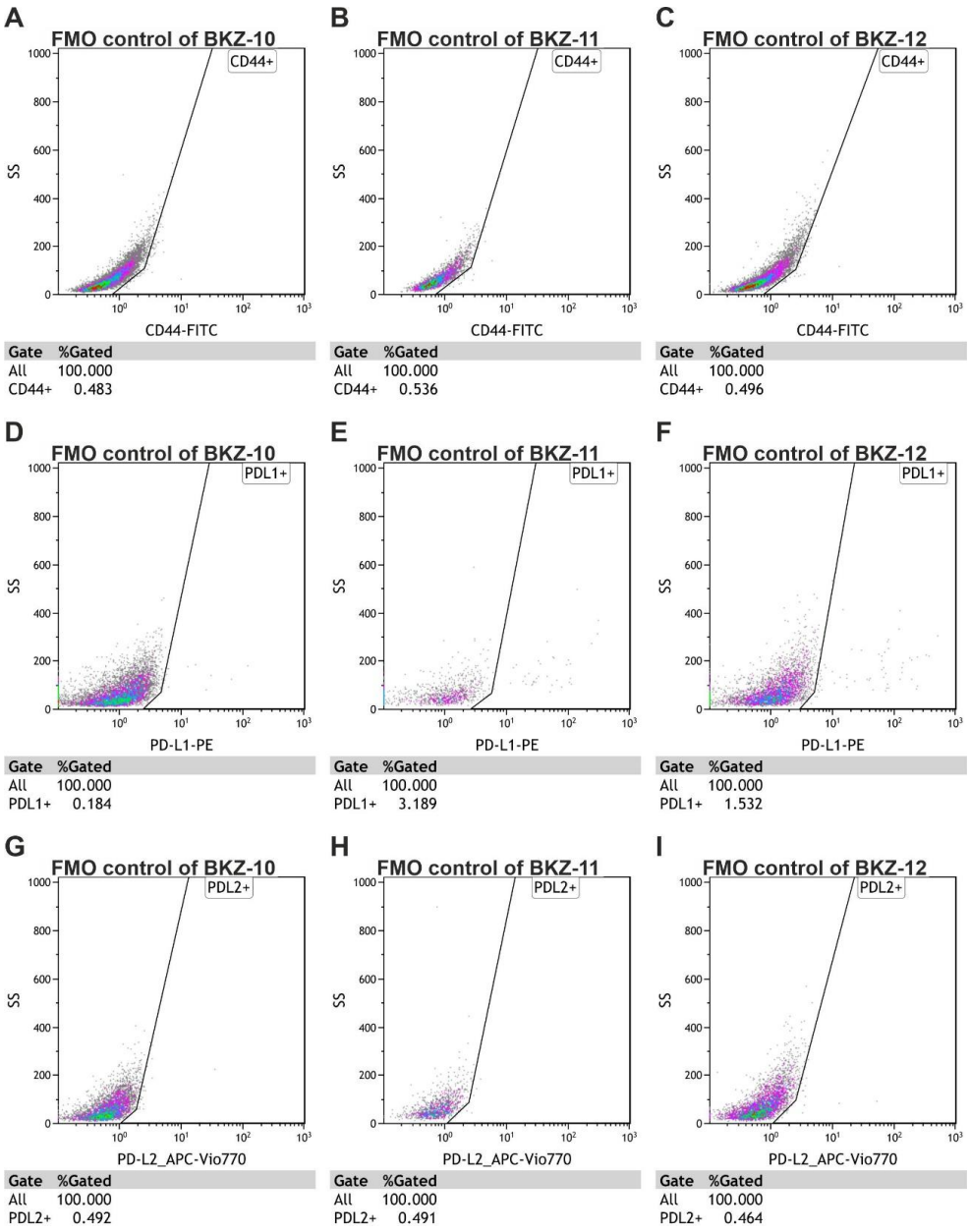

Figure S1: Fluorescence minus One controls for flow cytometric analysis. Fluorescence minus One (FMO) controls for flow cytometric analysis of **(A/B/C)** CD44-antigen expression, **(D/E/F)** programmed death ligand (PD-L) 1 expression and **(G/H/I)** PD-L2 expression.

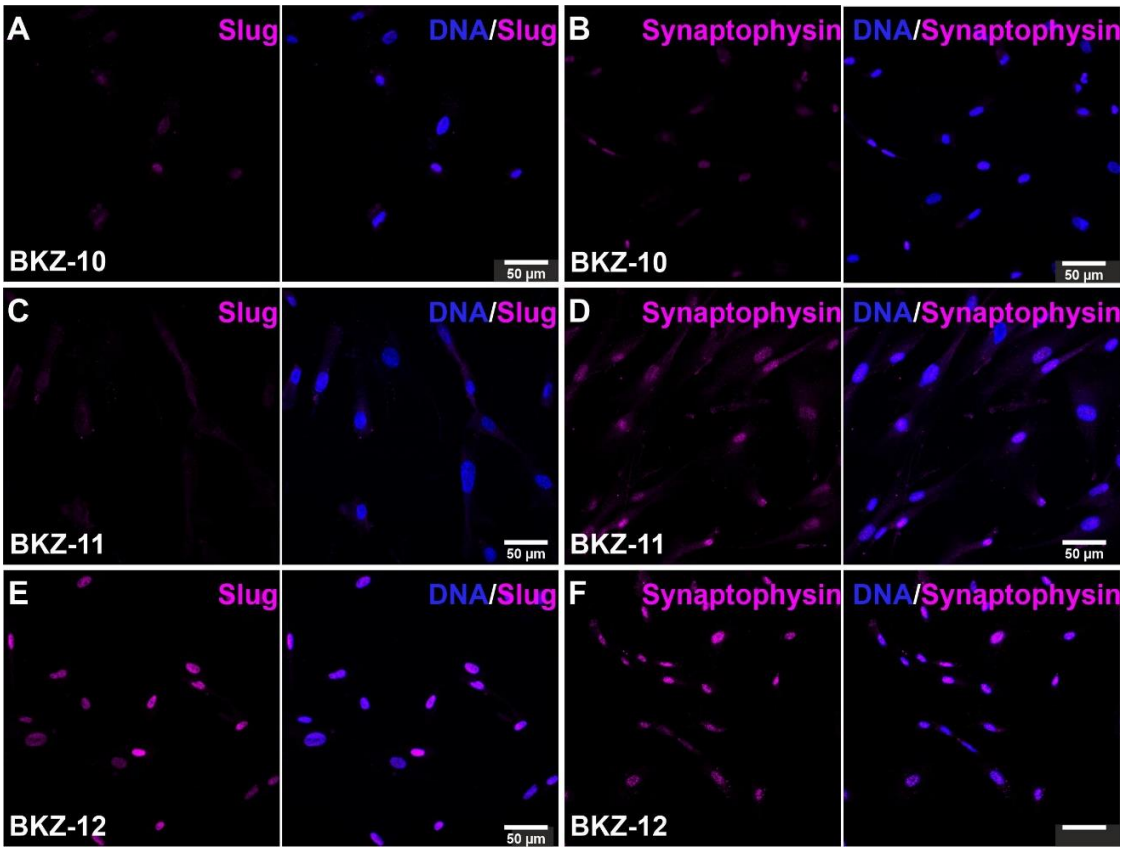

Figure S2: Endometrial carcinoma-derived stem-like cell populations express Slug and Synaptophysin. Immunocytochemical staining of Slug revealed a moderate nuclear protein expression in (A) BKZ-10 and (C) BKZ-11 as well as high nuclear expression in (E) BKZ-12. Expression of neuroendocrine and cancer stem cell marker Synaptophysin was slightly detected in (B) BKZ-10, moderately detected in (D) BKZ-11 and highly detected in (F) BKZ-12.

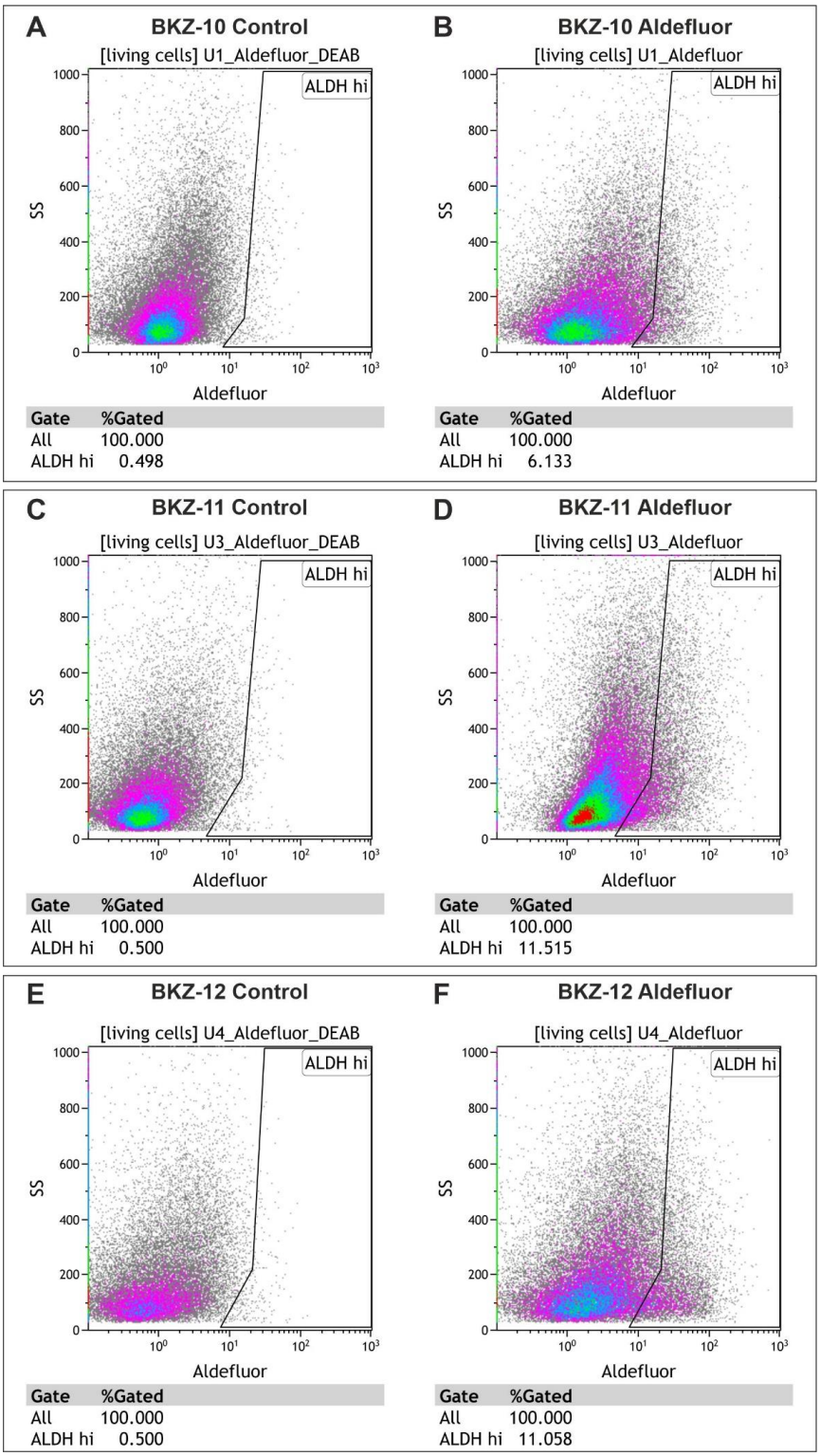

Figure S3: Established endometrial carcinoma-derived stem-like cell populations exhibit aldehyde dehydrogenase (ALDH) activity. Flow cytometric analysis of ALDH1 activity revealed (B) 6.133% ALDH high cells for BKZ-10, (D) 11.515% ALDH high cells for BKZ-11

and (F) 11.058% ALDH high cells for BKZ-12 in comparison to the respective control (A/C/E) with the specific ALDH inhibitor diethylaminobenzaldehyde (DEAB).